CONDENSATION AND SINGLE-PHASE HEAT TRANSFER COEFFICIENT AND FLOW REGIME VISUALIZATION IN MICROCHANNEL TUBES FOR HFC-134A

DISSERTATION

Presented in Partial Fulfillment of the Requirements for the Degree Doctor of Philosophy in the Graduate School of the Ohio State University

By

Wei-Wen William Wang, MS.

*****

The Ohio State University

1999

Dissertation Committee:

Professor Richard N. Christensen, Adviser

Professor Tunc Aldemir

Professor Terrence Conlisk

Professor Margaret Drake

Approved by

Richard N. Christensen

Adviser

Department of Mechanical Engineering

UMI Number: 9941453

UMI
300 North Zeeb Road
Ann Arbor, MI 48103

ABSTRACT

This dissertation is to document experimental, local condensation and single-phase heat transfer and flow data of the minute diameter, microchannel tube and to develop correlation methods for optimizing the design of horizontal-microchannel condensers. It is essential to collect local data as the condensation progresses through several different flow patterns, since as more liquid is formed, the mechanism conducting heat transfer and flow is also changing. Therefore, the identification of the flow pattern is as important as the thermal and dynamic data. The experimental results were compared with correlation and flow regime maps from literature. The experiment using refrigerant HFC-134a in flat, multi-port aluminum tubing with 1.46mm hydraulic diameter was conducted. The characteristic of single-phase friction can be described with the analytical solution of square channel. The Gnielinski correlation provided good prediction of single-phase turbulent flow heat transfer. Higher mass fluxes and qualities resulted in increased condensation heat transfer and were more effective in the shear-dominated annular flow. The effect of temperature gradient from wall to refrigerant attributed profoundly in the gravity-dominated wavy/slug flow. Two correlation based on different flow mechanisms were developed for specified flow regimes. Finally, an asymptotic correlation was successfully proposed to account for the entire data regardless of flow patterns.

Data taken from experiment and observations obtained from flow visualization, resulted in a better understanding of the physics in microchannel condensation, optimized designs in the microchannel condensers are now possible.

Dedicated to my beloved family

ACKNOWLEDGEMENTS

I wish to thank my advisor, Dr. Richard N. Christensen, for his dedication, financial support, and intellectual guidance, which made me through all these 5 years and finish this thesis.

I also want to convey my gratitude to Dr. Thomas D. Radcliff for his enthusiasm, patience, effort, and advisory.

I am grateful to Mr. Rodney Black for his effort to make this project more feasible.

This research was supported initially by a grant from the Ford Motor Company. Mr. Qun Liu and Dr. Arif Kan provided kindly assistance.

VITA

February 2, 1969 ....Born - Keelung, Taiwan

1991 .... B. S. Mechanical Engineering, National Chiao-Tung University.

1993 .... M. S. Mechanical Engineering, National Chiao-Tung University.

1995 - 1997 ....Graduate Research Associate, The Ohio State University.

FIELDS OF STUDY

Major Field: Mechanical Engineering

TABLE OF CONTENTS

LIST OF TABLES

LIST OF FIGURES

NOMENCLATURE

SYMBOLS		DEFINITION
a	constant	
a/b	aspect ratio	
a_l	constant of the Lockhart-Martinelli parameter	
a_v	constant of the Lockhart-Martinelli parameter	
A	area	
b	constant	
C	constant	
C_f	constant of friction	
Cp	constant pressure specific heat	
D_h	hydraulic diameter	
D_{le}	equivalent laminar diameter	
e	energy balance factor	
f	friction factor	
F	heat transfer multiplier	
F_{td}	Taitel-Dukler modified Froude number	$\sqrt{\frac{\rho_g}{\rho_l - \rho_g}} \frac{j_g}{\sqrt{Dg\cos\alpha}}$
Fr_{so}	Soliman modified Froude number	

g	gravitational acceleration
G	mass flux
Ga	Galileo number
h	heat transfer coefficient
$\bar{h}$	averaged heat transfer coefficient
h_{fg}	latent heat
h_l	height of the liquid level
i	enthalpy
I	current of electricity
j	superficial velocity
Ja	Jakob number
K	laminar friction constant
k	thermal conductivity
K_{td}	Taitel-Dukler parameter for stratified to wavy regime
L	length
L	liquid mass flow rate of the Baker's map
m	mass flow rate
n	constant
Nu	Nusselt number
P	pressure
P_{cr}	critical pressure
Pr	Prandtl number

Q	heat transfer rate	
R	thermal resistance	
Re	Reynolds number	
S	circumference	
Su	Suratman number	$\rho_v D\sigma / \mu_v^2$
T	temperature	
T_δ	dimensionless temperature difference across the liquid film	
T_{td}	Taitel-Dukler parameter for intermittent to dispersed bubble regime	
u	velocity	
$\tilde{u}_g$	vapor velocity / superficial vapor velocity	
$\tilde{u}_l$	vapor velocity / superficial vapor velocity	
U	overall heat transfer coefficient	
V	voltage of electricity	
We	Weber number	
x	quality	
X	Lockhert Martinelli parameter	
Xtt	turbulent turbulent Lockhert Martinelli parameter	
y^+	wall coordinate in the y direction	

GREEK LETTERS

α	void fraction
α	heat diffusivity

β	fraction of the circumference of the tube	
δ	liquid film thickness	
ε	eddy diffusivity	
ε	surface roughness	
φ	two-phase pressure drop multiplier	
η	efficiency	
λ	density correction factor for Baker's map	$\lambda = \sqrt{\frac{\rho_l}{62.3}\frac{\rho_v}{0.075}}$
μ	viscosity	
ρ	density	
σ	surface tension	
τ	shear stress	
Ψ	correction factor for Baker's map	$\Psi = \frac{73}{\sigma}\left[\mu_l\left(\frac{62.3}{\rho_l}\right)^2\right]^{\frac{1}{3}}$

SUBSCRIPT

a	air
acc	acceleration
anul	annular flow
e	exit
f	fluid
f	frictional

g	gas
h	thermal
i	inlet
l	liquid
o	outlet
r	refrigerant
sat	saturation
v	vapor
w	wall
wysg	wavy/slug flow

CHAPTER 1

INTRODUCTION

1.1 Background

It has been many decades since Du Pont started to manufacture chlorofluorocarbons (CFC) as refrigerants, cleaning solvents, and spread agents. In 1974, concern over the depletion of the stratospheric ozone layer began with the publication by Rowland and Molina [49]. Growing concerns over a decade resulted in the 1985 UNEP convention with 28 invitee countries to reach the stratospheric ozone layer protection agreement known as the Vienna Pact. This was followed by the Montreal Protocol in 1987, which called for a 50% reduction in CFC usage by 1998, but no phase out of hydrofluorocarbon (HCFC). However, the phase-out timetables were shortened domestically by the 1990 Clean Air Act and internationally by the 1990 London Convention. The Clean Air Act demanded total elimination of CFC usage by 1996 and no HCFC after 2015.

In the meantime, energy efficiency was gaining concerns and would be another issue. The National Appliance Energy Conservation Act (NAECA) of 1987 promulgated a wide range of increases in minimum energy efficiency standards for refrigerators, freezers, air conditioners, and heat pumps. For instance, a 25% increase in energy efficiency was mandated for the refrigerators.

Those two simultaneous regulatory decisions have and continued to have a profound impact on the heating, ventilating and air conditioning industry. In order to satisfy the requirement of higher energy efficiency while not damaging the ozone layer, both the new designs of the system components and the alternative refrigerants are being introduced and tested. As a result of making an effort to achieve these mandatory regulations, an experiment has been conducted in microchannel tubes with the new refrigerant HFC-134a (1,1,1,2 Tetrafluoroethane).

1.2 Overview of Microchannel tubes

The use of microchannel tubes for practical heat transfer assembly is made feasible by recent developments in aluminum extrusion and brazing processes. The condensers constructed with microchannel tubes are compact, lightweight, design-flexible, and provide improved thermal efficiency.

Figure 1.1 shows one single microchannel tube with louvered aluminum plate fins providing enhanced airside heat transfer. The microchannel tubes are aluminum extruded with a particular number of ports and specific geometry which is limited by the feasibility of extrusion tooling. The hydraulic diameter of a typical microchannel tube shown in the Figure 1.1, is only 1/5 to 1/20 of the tubing currently used in many round-tube plate-fin heat exchangers.

A completed microchannel conditioner is made of several microchannel tubes brazed to the headers on both ends, as shown on Figure 1.2. The refrigerant circulation is regulated by baffles inside the headers as a result of several passes with multiple tubes per passage.

Compared to the traditional round-tube with plate-fin condensers, microchannel condensers are more compact and thus lightweight for a specific heat transfer capacity and pressure drop. Consequently, both the face area and the system charge have been reduced. That is the reason why the microchannel condensers were first commercialized by auto industries. Compact face areas are favorable for designs to shape the front end more streamlined to improve the aerodynamics of the cars. Furthermore, the reduced refrigerant charge is environmental friendly and economically desirable. The relative mass production scales and short design cycles of the automobiles industry have made the implementation of the microchannel condenser possible. Meanwhile, more attention has been paid to stationary air-conditioning systems because of the system miniaturization and charge reduction.

1.3 Flow Visualization

The purpose of this research is to determine the heat transfer coefficient in microchannel tubes as a function of multiphase flow regimes. Although a cohesive theory for in-tube condensation has not yet been established, there is agreement in the literature that the mechanisms governing the condensation heat transfer and pressure drops are intimately linked with the prevailing two-phase flow regime. Thus, many studies have been made to predict the governing dimensionless parameters when specific flow regime transitions occur. Although some debates still exist, researchers have gained a general appreciation of flow regimes and the governing parameters in transition. Flow visualization will provide the spatial and temporal resolution of the multi-phase distribution in the minrochannel tubes and verify the local heat transfer measurements.

1.4 Objectives

The study described here represents an extensive effort to relate the heat transfer and pressure drop with flow regimes. With data taken from the experiment and observations obtained from flow visualization, a better understanding of microchannel condensation can be resolved. The followings are the tasks in pursuit:

(1) Review the literature pertaining to the performance of microchannel condensers, including studies of heat transfer, pressure drop, and multiphase flow regime predictions.

(2) Study both single-phase and condensation conditions while completing the experimental work.

(3) Analyze, verify and correlate collected data. Review the observed flow regimes and compare to several predictive methods. The relationship between the trends of data and flow regimes is discussed.

(4) Develop the heat transfer correlation for the microchannel tubes based on the physical observation and experimental data.

(5) Summarize results of the study and recommend work for the future research.

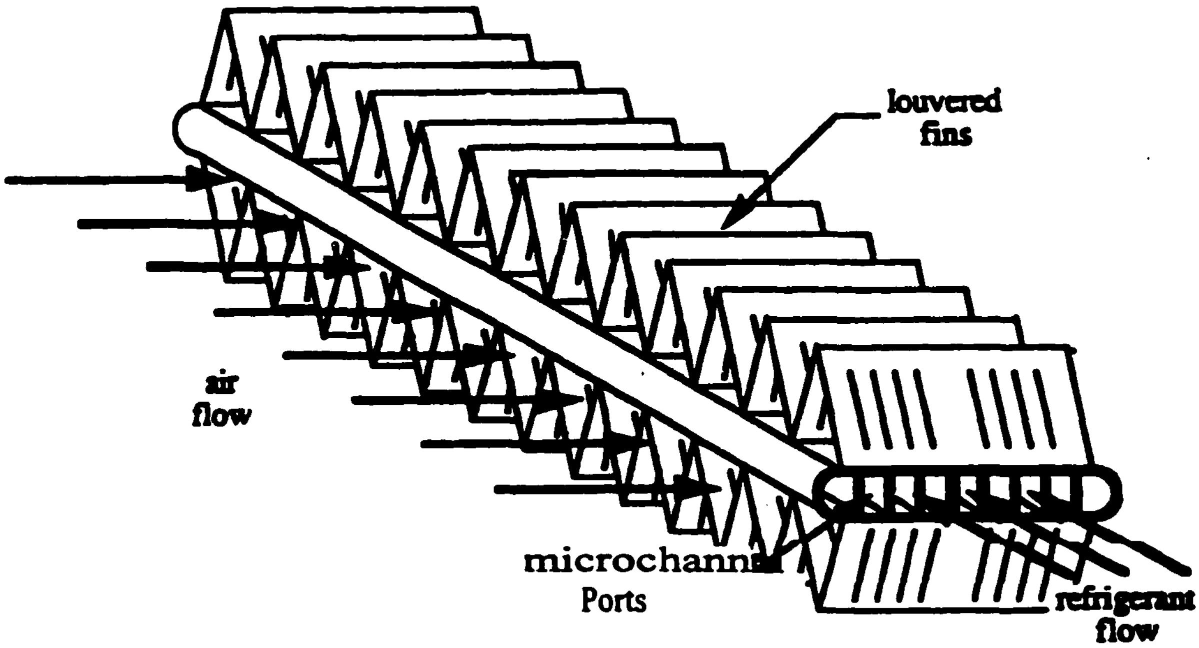

Figure 1.1 Single-tube Test Facility crossflow test section.

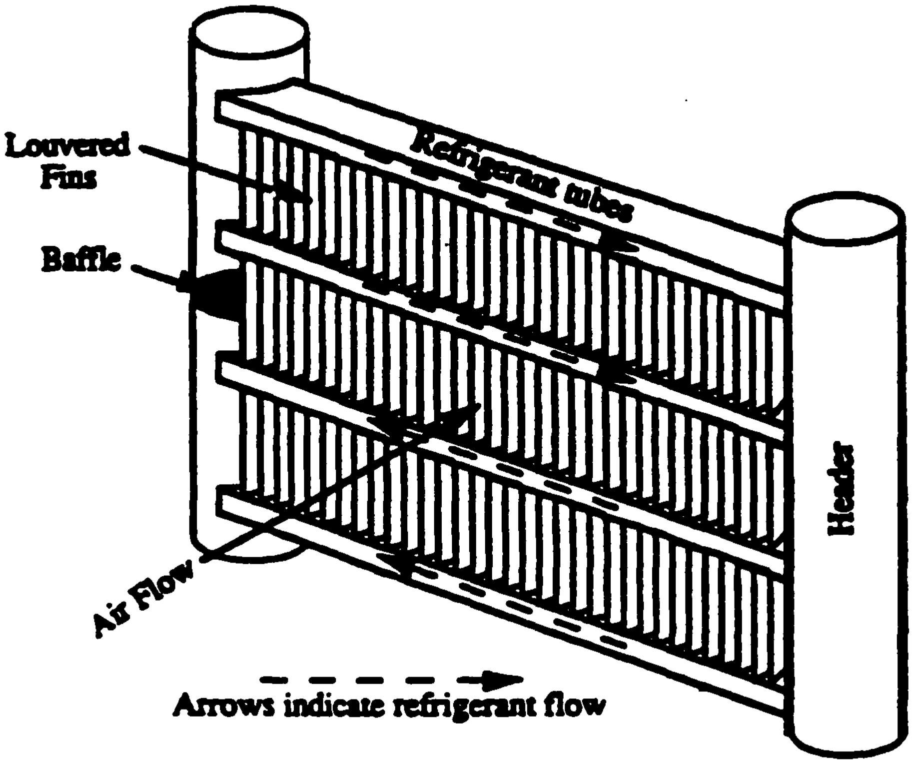

Figure 1.2 Example of a microchannel heat exchanger.

CHAPTER 2

LITERATURE REVIEW

There are numerous research efforts related to the present study. Some important aspects of development, from the past to the present state of the art, will now be discussed. The dimensionless groups discussed in this proposal are included in Section 2.1. Flow regime classification and mapping efforts by visualization are presented in Section 2.2. The abundant literature concerning pressure drop and heat transfer in either single-phase or two-phase condensation is discussed in Sections 2.3 and 2.4.

2.1 Dimensionless Groups

Table 2.1 lists some frequently used dimensionless groups and their definitions and interpretations.

2.2 Flow Regimes

The flow regime, or flow pattern, refers to the void distribution orientation of the liquid-vapor two-phase flow. Depending on the pressure, channel geometry, flow rates of both phases, and the orientation of the flow with respect to gravity, a variety of flow patterns can occur.

2.2.1 Classification

A compilation of the more typical liquid-vapor flow regimes in condensation processes is listed in Figure 2.1. The top group of the figure occur at high void fraction, $\alpha > 0.5$, and vice versa for the bottom group.

The top category, for $\alpha > 0.5$ includes five regimes: stratified, wavy, wavy-annular, annular, and annular-mist, corresponding to an increase in the vapor velocity. Due to a decrease in void fraction or an increase in the liquid inventory, the flow patterns at the bottom category change from slug to plug and finally to the bubbly flow.

(1) Stratified Flow

Stratified flow occurs at very low vapor velocities, so the interface remains smooth. The condensate forms at the top of the tube, is driven downward by gravity and collects in the bottom liquid pool.

(2) Wavy Flow

Wavy flow happens when the two-phase interface becomes Helmholtz unstable and stirs some surface waves as the vapor velocity builds up. The thickness of the liquid pool increases gradually.

(3) Wavy-Annular Flow

Some waves begin to build up around the circumference of the tube, as the vapor velocity increases, but the velocity is not great enough to always sustain an annular film.

(4) Annular Flow

The liquid continues to migrate from the bottom pool to the top with further increases in the vapor velocity until it forms an annular liquid film along the wall and a high-speed vapor core in the center.

(5) Annular-Mist flow

When the vapor velocity is sufficiently high, it may shear off the liquid film and carry liquid droplets. Hewitt and Roberts [34] suggested that in such an annular-dispersed flow regime, the droplets can gather in clouds forming an annular-mist regime. These droplets entrained in the vapor core by shearing can be de-entrained to replenish the annular liquid film.

(6) Slug Flow

When interfacial waves grow large enough in amplitude to fill the tube with liquid at some locations, the liquid forms slug flow. Some observers like Hubbard, Dukler [35] and Lin, Hanratty [41] showed that slug flow can create large pressure spikes due to the rapid deceleration of the vapor flow.

(7) Plug Flow

As condensation continues, vapor plugs are separated by liquid slugs and surrounded by the liquid film.

(8) Bubbly Flow

When turbulent fluctuations within the liquid eventually break the vapor plugs into smaller vapor bubbles which are dispersed into a continuous liquid phase, the bubbly flow regime is present.

2.2.2 Flow Regime Maps

The flow regimes have generally been related to the flow rate, slip ratio, quality, fluid properties and tube geometry which strongly influence the heat and momentum transfer. Transitions in flow regimes depicted on the maps provide the criteria for designers to predict the flow patterns.

Followings are various flow maps cited in the literature based on the data of regular-size round tubes.

(1) Baker Map

The Baker [6] map based on adiabatic, gas-liquid flows in 1 to 4 inches diameter round tubing, was the pioneer work is this field. As shown in Figure 2.2 with the liquid mass flow rate L, the coordinates are given by,

$$\frac{G}{\lambda} \tag{2.1}$$

$$\frac{L\lambda\Psi}{G} \tag{2.2}$$

(2) Mandhane Map

Based on 5935 data points, Mandhane et al. [43] developed a flow regime map by taking the superficial gas velocity as the abscissa and the superficial liquid velocity as the ordinate, as shown in Figure 2.3. The correlation was improved from 42% for the Baker map to 68%. However, the vapor density of the refrigerant is much larger than the air; therefore, there may be reveal some systematic problems with the Mandhane map.

(3) Taitel-Dukler map

There are five regimes on Taitel-Dukler [64] map, including stratified smooth, stratified-wavy, annular, intermittent (plug and slug), and dispersed bubble, as shown in Figure 2.4. Based on a mechanistic approach, Taitel and Dukler predicted some flow transitions from a smooth, stratified flow. With the schematic shown in Figure 2.5, the momentum equations for the liquid and vapor phases are,

$$-A_l(\frac{dp}{dz}) - \tau_{wl} S_l - \tau_i S_i = 0 \qquad (2.3)$$

$$-A_g(\frac{dp}{dz}) - \tau_{wg} S_g - \tau_i S_i = 0 \qquad (2.4)$$

Taitel and Dukler showed that the Lockhart-Martinelli parameter, X_{tt}, is a function of h_l, height of the liquid level.

$$X_{tt} = f(\tilde{h}_l) \qquad (2.5)$$

$$\tilde{h}_l = \frac{h_l}{D} \qquad (2.5.1)$$

From stratified to wavy flow, Taitel and Dulker hypothesized, based on the works of Jeffreys [37], [38], that a critical vapor velocity was exceeded so the pressure and shear forces could overcome the viscous dissipation in the wave. That is,

$$K_{td} = F_{td} \cdot \sqrt{\mathrm{Re}_l} \geq \frac{20}{\tilde{u}_g \sqrt{\tilde{u}_l}} \qquad (2.6)$$

$$F_{td} = \sqrt{\frac{\rho_g}{\rho_l - \rho_g}} \cdot \frac{GX}{\sqrt{Dg\cos\alpha \cdot \rho_g}} \qquad (2.6.1)$$

Based on a modification of the Kelvin-Helmholtz stability analysis, Taitel and Dukler predicted the transition from a stratified-wavy to intermittent or annular flow as follows,

$$F_{td}^{2} \cdot f(X_{tt}) \geq 1 \qquad (2.7)$$

$$f(X_{tt}) = \frac{\tilde{u}_g^{2} \sqrt{1 - (2\tilde{h}_l - 1)^2}}{(1 - \tilde{h}_l)^2 \cdot \tilde{A}_g} \qquad (2.7.1)$$

The possibilities of being an intermittent or an annular flow depend upon the liquid level or alternately $\tilde{h}_l$. For $\tilde{h}_l$< 0.5 or X_{tt}< 1.6, annular flow would be expected. On the other hand, an intermittent flow is expected for $\tilde{h}_l$>0.5 or X_{tt} >1.6.

The transition from intermittent to bubbly flow occurs when the large coalescing vapor bubbles of slug and plug flows are broken up and dispersed throughout the liquid. The authors suggested that a balance between buoyancy forces and turbulent fluctuations resulted in the transition.

$$T_{td}^{2} \geq \frac{8\tilde{A}_g(\tilde{u}_l\tilde{D}_l)^n}{\tilde{S}_i\tilde{u}_i^{2}} = f(X_{tt}) \tag{2.8}$$

$$T_{td} = \frac{-(dp/dz)_l}{(\rho_l-\rho_v)g\cos\alpha} = \frac{2a}{\mathrm{Re}_l^{\,n}}\cdot\frac{j_l}{gD\cos\alpha}\cdot\frac{1}{1-\rho_v/\rho_l} \tag{2.8.1}$$

(4) Breber Map

By verifying the Taitel and Dukler map with the horizontal tube condensation data, Breber et al. [9] simplified the map into four zones. By broadening the boundary between the annular and wavy regions to include a transition zone and shifting the boundary between the wavy and slug flow regions, some simplified criteria were proposed.

Zone I: Annular and mist annular

$j_g^{*} > 1.5, \ \ X < 1$

Zone II: Wavy and stratified

$j_g^{*} < 0.5, \ \ X < 1$

Zone III: Slug and plug

$j_g^{*} < 1.5, \ \ X > 1.5$

Zone IV: Bubbly

$j_g^{*} > 1.5, \ \ X > 1.5$

where $j_g^{*} = \dfrac{G\cdot x}{\sqrt{D\cdot g\cdot\rho_v(\rho_l-\rho_v)}}$

The resulting map is shown on Figure 2.6.

(5) Soliman Transitions

Two flow regime transitions for condensation, to and from annular flow regimes, were developed by Soliman [55], [56]. For the transition from wavy to annular flow, Soliman proposed the expressions for the Froude number:

$$Fr_{so} = 0.025 \cdot \mathrm{Re}_l^{1.59} \cdot \left(\frac{1 + 1.09 X_{tt}^{0.039}}{X_{tt}}\right)^{1.5} \cdot Ga^{-0.5}, \mathrm{Re}_l \le 1250 \qquad (2.9.1)$$

$$Fr_{so} = 1..26 \cdot \mathrm{Re}_l^{1.04} \cdot \left(\frac{1 + 1.09 X_{tt}^{0.039}}{X_{tt}}\right)^{1.5} \cdot Ga^{-0.5}, \mathrm{Re}_l > 1250 \qquad (2.9.2)$$

The transition was observed at $Fr_{so}=7$. For annular flow, $Fr_{so}>7$. For $Fr_{so}<7$, it is wavy flow. This result was confirmed by Dobson et al. [23] to be a transition indicator from wavy to wavy-annular flow.

Later, Soliman [57], [58] based on a modified Weber number,

$$We_{so} = 2.45 \frac{\mathrm{Re}_v^{0.64}}{Su_v^{0.3}(1 + 1.09 X_{tt}^{0.039})^{0.4}}, \mathrm{Re}_l \le 1250 \qquad (2.10.1)$$

$$We_{so} = 0.85 \left[\left(\frac{\mu_v}{\mu_l}\right)^2 \left(\frac{\rho_l}{\rho_v}\right)\right]^{-0.084} \frac{\mathrm{Re}_v^{0.79} X_{tt}^{0.157}}{Su_v^{0.3}(1 + 1.09 X_{tt}^{0.039})^{0.4}}, \mathrm{Re}_l > 1250 \qquad (2.10.2)$$

concluded that if $We_{so}<20$ then the pattern was annular flow, or it was a pure mist if $We_{so}>30$. Otherwise, annular-mist flow was for $20<We_{so}<30$.

2.3 Pressure Drop

2.3.1 Single-Phase

The pressure drop is important so that the designer can determine pump or compressor requirements. To determine the pressure drop, the definition of the Moody or Darcy friction factor is convenient to use,

$$f \equiv \frac{-(\frac{dP}{dx})\cdot D_h}{\frac{1}{2}\rho u_m^2} \tag{2.11}$$

In addition, the friction coefficient or the Fanning friction factor is defined as

$$C_f = \frac{\tau_w}{\frac{1}{2}\rho u_m^2} \tag{2.12}$$

Using the definition of τ_w, the Fanning factor is one fourth of the Darcy factor,

$$C_f = \frac{f}{4} \tag{2.13}$$

In fully developed flow inside the duct, Shah and London [50] pointed out that the velocity profile and the friction factor are invariant in the axial direction.

$$\frac{\Delta P}{\frac{1}{2}\rho u_m^2} = f\cdot\frac{L}{D_h} \tag{2.14}$$

However, in the entrance region, due to the developing velocity profile, the pressure drop is greater than that of fully developed flow. Therefore, Shah and Bhatti [51] used a pressure drop number, K_∞, to account for this effort as

$$\frac{\Delta P}{\frac{1}{2}\rho u_m^2} = f \cdot \frac{L}{D_h} + K_\infty \quad (2.15)$$

2.3.1.1 Laminar Flow

For fully developed laminar flow, the solution to the momentum equation yields

$$f = \frac{K_f}{\mathrm{Re}_{D_h}} \quad (2.16)$$

where $K_f = -\dfrac{8\frac{dP}{dx}a^2}{U\left[1+(a/b)\right]^2}$ (2.16.1)

and $U = -\dfrac{(\frac{dp}{dx})a^2}{3}\left[1-\dfrac{192}{\pi^5}\left(\dfrac{a}{b}\right)\sum_{n=1,3,...}^{\infty}\dfrac{1}{n^5}\tanh\left(\dfrac{n\pi b}{2a}\right)\right]$ (2.16.2)

for rectangular ducts. Resulting K_f are listed in Figure 2.7 for various rectangular duct geometries.

For the entrance regions of noncircular ducts, a graph by Shah and London [50] was developed from research.

2.3.1.2 Turbulent Flow

For a smooth circular tube with transitional regime flow, typically 2300<Re<4000, Churchill [19] derived

$$\frac{f_D}{8} = 7.1 \times 10^{-10} \cdot \mathrm{Re}^2 \quad (2.17)$$

On the other hand, Bhatti and Shah [51] suggested the Prandtl-Karmen-Nikuradse correlation for turbulent flow,

$$\frac{1}{\sqrt{f_D}} = 0.8686 \cdot \ln(\mathrm{Re}\sqrt{f_D}) - 0.9967 \qquad (2.18)$$

Accounting for the surface roughness, ε, Churchill [19] derived an equation for all regimes, including laminar, transition, and turbulent,

$$\frac{f_D}{8} = \left[\left(\frac{8}{\mathrm{Re}}\right)^{12} + \frac{1}{(A+B)^{\frac{3}{2}}}\right]^{\frac{1}{12}} \qquad (2.19)$$

where
$$A = \left\{2.457 \cdot \ln\left[\left(\frac{7}{\mathrm{Re}}\right)^{0.9} + \frac{0.27\varepsilon}{D}\right]\right\}^{16}$$
$$B = \left(\frac{37530}{\mathrm{Re}}\right)^{16}$$

In order to apply these correlation for circular tubes to noncircular ducts, the hydraulic diameter or other equivalent diameters were introduced. The use of the hydraulic diameter can be used, if there are not many sharp corners. Ahmed and Brundrett [3] introduced a diameter scale, D_{ic}, accounting for the diameters of the inscribed and circumscribed circles.

Based on the similarity between circular and rectangular tubes in laminar flow, Jones [39] proposed the laminar equivalent diameter, D_{le},

$$D_{le} = \frac{64}{K_f} \cdot D_h \qquad (2.20)$$

where K_f is the laminar friction constant listed in Figure 2.7. This idea was extended to other noncircular ducts by Obot [46]. The comparison of various diameters scales for some duct geometry is listed on Table 2.2.

2.3.2 Two-Phase Pressure Drop

The pressure gradient of a horizontal tube can be obtained by solving the momentum equation in the axial, z direction, of a one-dimensional channel,

$$\frac{\partial}{\partial t}(G_m A_z) + \frac{\partial}{\partial Z}\left(\frac{G_m^2 \cdot A_z}{\rho_m}\right) = -\frac{\partial}{\partial Z}(\rho A_z) - \int_{P_z} \tau_w dP_z \tag{2.21}$$

For steady flow in a constant area channel, Eq. (2.21) can be simplified to

$$-\frac{dP}{dZ} = \frac{d}{dZ}\left(\frac{G_m^2}{\rho_m}\right) + \frac{1}{A_z}\int_{P_z} \tau_w dP_z \tag{2.22}$$

The first term on the right hand side on Eq. (2-22) refers to the acceleration pressure drop for heated channels, and the second term is known as the friction pressure drop.

For the acceleration pressure drop,

$$\frac{G_m{}^2}{\rho_m} = \{\rho_v \alpha V_v^2\} + \{\rho_l (1-\alpha) V_l^2\} \tag{2.23}$$

and the flow quality can be given by

$$xG_m = \{\rho_v \alpha V_v\} \tag{2.24}$$

$$(1-x)G_m = \{\rho_l (1-\alpha) V_l\} \tag{2.25}$$

Thus, the acceleration pressure drop for radial uniform velocity of each phase in the channel can be written as

$$\frac{G_m^{\ 2}}{\rho_m} = \frac{x^2}{\{\rho_v \alpha\}} + \frac{(1-x)^2}{\{\rho_l (1-\alpha)\}} \tag{2.26}$$

Therefore, the acceleration pressure drop for a constant mass flux is

$$\left.\frac{dP}{dz}\right|_{acc} = G_m^{\ 2} \frac{d}{dz}\left[\frac{x^2}{\{\rho_v \alpha\}} + \frac{(1-x)^2}{\{\rho_l (1-\alpha)\}}\right] \tag{2.27}$$

$$= G_m^{\ 2} \frac{d}{dz}\left[\frac{x^2 v_v}{\{\alpha\}} + \frac{(1-x)^2 v_l}{\{(1-\alpha)\}}\right]$$

$$= G_m^{\ 2}\left[\frac{2x v_v}{\{\alpha\}} - \frac{2(1-x) v_l}{\{(1-\alpha)\}}\right]\frac{dx}{dz} + G_m^{\ 2}\left[-\frac{x^2 v_v}{\{\alpha\}^2} + \frac{(1-x)^2 v_l}{\{(1-\alpha)\}^2}\right]\frac{d\alpha}{dz} + G_m^{\ 2}\frac{x^2 v_v}{\{\alpha\}}\frac{\partial v_v}{\partial P}\frac{dP}{dz}$$

The friction pressure gradient can be expressed in a form similar to the single-phase flow,

$$\left.\frac{dP}{dZ}\right|_{fric} = \frac{1}{A_z}\int_{P_z} \tau_w dP_z = \frac{\tilde{\tau}_w P_w}{A_z} = \frac{4\tilde{\tau}_w}{D_h} = \frac{f_{TP}}{D_h}\left(\frac{G_m^2}{2\rho_m}\right) \tag{2.28}$$

Lockhart and Martinelli [42] proposed the two-phase multiplier relations the two-phase frictional pressure gradient to the single-phase one, by defining

$$\left.\frac{dP}{dZ}\right|_{fric}^{TP} \equiv \phi_{lo}^2\left(\frac{dP}{dZ}\right)_{fric}^{lo} \equiv \phi_l^2\left(\frac{dP}{dZ}\right)_{fric}^{l} \equiv \phi_{vo}^2\left(\frac{dP}{dZ}\right)_{fric}^{vo} \equiv \phi_v^2\left(\frac{dP}{dZ}\right)_{fric}^{v} \tag{2.29}$$

By definition, the single-phase friction pressure drop is

$$\left.\frac{dP}{dZ}\right|_{fric}^{l} = \frac{f_l}{D_h}\left[\frac{G_m^2(1-x)^2}{2\rho_l}\right] \tag{2.30.1}$$

and

$$\left.\frac{dP}{dZ}\right|_{fric}^{v} = \frac{f_v}{D_h}\left[\frac{G_m^2 x^2}{2\rho_v}\right] \tag{2.30.2}$$

Lockhart and Martinelli introduced the parameter, X, as

$$X^2 = \frac{\left.\frac{dP}{dZ}\right|_{fric}^{l}}{\left.\frac{dP}{dZ}\right|_{fric}^{v}} \tag{2.31}$$

Together with the relation between the friction factor, f, and the respective Reynolds number, Re,

$$f = \frac{a}{\mathrm{Re}^n} \tag{2.32}$$

where a is equal to 16, and n is 1 for the laminar flow. On the other hand, a is 0.046 and n is 0.2 for the turbulent regime.

The resulting Lockhart-Martinelli parameter, X , is given by,

$$X = \frac{a_l}{a_v}\frac{\mu_l^{n_l}}{\mu_v^{n_v}}\frac{\rho_v}{\rho_l}\frac{(1-x)^{2n_l}}{x^{2-n_v}} \tag{2.33}$$

All the combinations of the Lockhart-Martinelli parameter, $X_{liquid,vapor}$, follow,

$$X_{tt} = \left(\frac{\mu_l}{\mu_v}\right)^{0.1}\left(\frac{\rho_v}{\rho_l}\right)^{0.5}\left(\frac{1-x}{x}\right)^{0.9} \tag{2.34.1}$$

$$X_{lt} = 18.65\cdot\left(\frac{\mathrm{Re}_v^{0.1}}{\mathrm{Re}_l^{0.5}}\right)\left(\frac{\rho_v}{\rho_l}\right)^{0.5}\left(\frac{1-x}{x}\right) \tag{2.34.2}$$

$$X_{tl} = \frac{1}{18.65}\cdot\left(\frac{\mathrm{Re}_v^{0.5}}{\mathrm{Re}_l^{0.1}}\right)\left(\frac{\rho_v}{\rho_l}\right)^{0.5}\left(\frac{1-x}{x}\right) \tag{2.34.3}$$

$$X_{ll} = \left(\frac{\mu_l}{\mu_v}\right)^{0.5}\left(\frac{\rho_v}{\rho_l}\right)^{0.5}\left(\frac{1-x}{x}\right)^{0.9} \tag{2.34.4}$$

The curve relation between ϕ_l, ϕ_v , α and X presented by Lockhart and Martinelli were fitted by Chisholm [17],

$$\phi_l^2 = 1 + \frac{C}{X} + \frac{1}{X^2} \tag{2.35.1}$$

$$\phi_v^2 = 1 + CX + X^2 \tag{2.35.2}$$

$$1 - \alpha = \frac{X}{1 + CX + X^2} \tag{2.35.3}$$

where values of C are given on Table 2.3.

Later, the void fraction (α) correlation was fitted by Butterworth [10] as

$$\alpha = \frac{1}{1 + 0.28X^{0.71}} \tag{2.36}$$

2.4 Heat Transfer

2.4.1 Single-phase

2.4.1.1 Laminar flow

For fully developed laminar flow in a tube, applying the appropriate boundary conditions to the energy equations can solve the temperature profile. Combining Newton's law of cooling, the heat transfer coefficient and the Nusselt number can be obtained. Table 2.4 lists some Nusselt numbers for fully developed laminar flow in different duct cross sections.

For circular tubes with a thermal developing entry length and constant surface temperature conditions, Kays [40] presented an average Nusselt number correlation attributed to Hausen [33],

$$\overline{Nu}_D = 3.66 + \frac{0.0668 \cdot (D/L) \cdot \mathrm{Re} \cdot \mathrm{Pr}}{1 + 0.04 \cdot [(D/L) \cdot \mathrm{Re} \cdot \mathrm{Pr}]^{2/3}} \qquad (2.37)$$

For the combined thermal and velocity entry length, Sider and Tate [54] proposed,

$$\overline{Nu}_D = 1.86 \cdot [(D/L) \cdot \mathrm{Re} \cdot \mathrm{Pr}]^{1/3} \cdot \left(\frac{\mu}{\mu_w}\right)^{0.14} \qquad (2.38)$$

for $0.48 < \mathrm{Pr} < 16700$, $0.0044 < \left(\frac{\mu}{\mu_w}\right)^{0.14} < 9.75$

Shah and Bhatti [51] did the most extensively summarized work for various geometries and boundary conditions.

2.4.1.2 Turbulent flow

For fully developed turbulent flow in a circular tube, Colburn [21] used the Chilton-Colburn analogy,

$$\frac{C_f}{2} = \frac{f}{8} = \frac{Nu}{\mathrm{Re}\,\mathrm{Pr}} \mathrm{Pr}^{\frac{2}{3}}; \qquad (2.39)$$

substituting for the friction factor,

$$f = 0.184\,\mathrm{Re}^{-0.2} \qquad (2.40)$$

then, the Colburn equation is

$$Nu = 0.023\,\mathrm{Re}^{0.8}\,\mathrm{Pr}^{1/3} \qquad (2.41)$$

The Dittus-Boelter [22] equation is a revised and preferred version of the above result in Eq. (2.41),

$$Nu = 0.023\,\mathrm{Re}^{0.8}\,\mathrm{Pr}^{n} \quad \begin{array}{l} 0.7 \le \mathrm{Pr} \le 160 \\ \mathrm{Re} \ge 10000 \\ L/D \ge 10 \end{array} \tag{2.42}$$

where n=0.3 for cooling and n=0.4 for heating process.

Sider and Tate accounted for large property variations and obtained the following equation,

$$Nu = 0.027\,\mathrm{Re}^{0.8}\,\mathrm{Pr}^{1/3}\left(\frac{\mu}{\mu_w}\right)^{0.14} \tag{2.43}$$

Recently, Buyukalaca and Jackson [11] suggested the correlation,

$$n = 0.048 + 2.6 \cdot 10^{-6} \cdot \mathrm{Re} \tag{2.44}$$

to replace 0.14 in the equation (2.43).

Petukhov, Kirillov, and Popov [47] proposed the following correlation,

$$Nu = \frac{\frac{f}{8}\,\mathrm{Re}\,\mathrm{Pr}}{1.07 + 12.7\left(\frac{f}{8}\right)^{1/2}\left(\mathrm{Pr}^{2/3} - 1\right)} \tag{2.45}$$

where $f = (1.82 \log \mathrm{Re} - 1.64)^{-2}$ for $\begin{array}{l} 0.5 \le \mathrm{Pr} \le 2000 \\ 10000 < \mathrm{Re} \le 5 \cdot 10^{6} \end{array}$ (2.45.1)

which reduced the margin of error from 25 % for Sieder and Tate to less than 10 %.

Gnielinski [29] further modified the correlation for small Reynolds numbers,

$$Nu = \frac{\frac{f}{8}(\mathrm{Re}-1000)\,\mathrm{Pr}}{1+12.7(\frac{f}{8})^{1/2}(\mathrm{Pr}^{2/3}-1)} \tag{2.46}$$

where $f = (0.79 \cdot \ln \mathrm{Re} - 1.64)^{-2}$ (2.46.1)

for $2300 < \mathrm{Re} \leq 5 \cdot 10^{6}$ for smooth tubes.

Churchill [19] included all three regimes in one correlation,

$$Nu^{10} = Nu_l^{10} + \left\{ \frac{e^{\frac{2200-\mathrm{Re}}{365}}}{Nu_l^2} + \left[Nu_0 + \frac{0.079(\frac{f}{8})^{1/2}\mathrm{Re}\,\mathrm{Pr}}{(1+\mathrm{Pr}^{0.8})^{5/6}} \right]^{-2} \right\}^{-5} \tag{2.47}$$

where	$Nu_l = 3.657$	for constant wall temperature
	$Nu_l = 4.364$	for constant heat flux
and	$Nu_0 = 4.8$	for constant wall temperature
	$Nu_0 = 6.3$	for constant heat flux

For fully developed turbulent flow in noncircular ducts, the hydraulic diameter is commonly used as the characteristic length in the Reynolds and Nusselt numbers. However, length scales other than those discussed in the previous section were chosen by some researchers. Ahmeed and Brundrett [3] used D_{ic} as the alternative length scale.

As for the circular microchannel tubes, an improved version of the Gnielinski correlation, Equation (2.45), was introduced by Adams et al. [1] in the form,

$$Nu = Nu_{GN}(1+F) \tag{2.48}$$

$$\text{where } F = C \cdot \mathrm{Re} \cdot [1-(\frac{D}{D_0})^2] \qquad \text{for} \qquad \begin{array}{l} 1.53 \le \mathrm{Pr} \le 6.43 \\ 2600 \le \mathrm{Re} \le 23000 \\ 0.102mm \le D \le 1.09mm \end{array}$$

and $C = 7.6 \cdot 10^{-5}, D_0 = 1.164mm$.

2.4.2 Condensation

There are numerous studies of condensation including experimental work to observe the heat transfer and flow regime behavior of certain fluids, analytical efforts to model the processes, and some combinations of the two. In this study, the internal condensation is divided into groups based on different driving mechanisms.

2.4.2.1 Gravity-Driven Film Condensation

Condensation within the tube depends strongly on the velocity of the vapor flowing through the tube. For low vapor velocity regimes including stratified, wavy, and slug flows, the gravitational force is much stronger than the interfacial shear force. Therefore, a layer of condensate film forms on the upper portion of the tube and grows in thickness as it flows along the circumference into the bottom liquid pool.

Chato [15] developed a correlation of the averaged heat transfer coefficient, $\bar{h}$, based upon the analysis of the falling film condensation on a horizontal cylinder.

$$\bar{h} = 0.555\left[\frac{g\rho_l(\rho_l-\rho_v)k_l^3 h_{fg}}{\mu_l(T_{sat}-T_w)D}\right]^{1/4}, \text{ for } \mathrm{Re}_{v,i} = (\frac{\rho_v u_{m,i} D}{\mu_v})_i < 35000 \quad (2.49)$$

Jaster and Kosky [36] modified Chato's correlation by accounting for the pool depth variation with the pressure gradient,

$$\bar{h} = 0.728 \cdot \alpha^{3/4} \cdot \left[\frac{g\rho_l(\rho_l - \rho_v)k_l^3 h_{fg}'}{\mu_l (T_{sat} - T_w) D} \right]^{1/4} \tag{2.50}$$

where $\alpha = \left[1 + \frac{1-X}{X} (\frac{\rho_v}{\rho_l})^{\frac{2}{3}} \right]^{-1}$ (2.50.1)

Unlike the previous two studies, Rossan and Myers [48] also accounted for the heat transfer in the bottom pool,

$$h_{top} = 0.31 \cdot \mathrm{Re}_v^{\ 0.12} \cdot \left[\frac{g\rho_l(\rho_l - \rho_v)k_l^3 h_{fg}'}{\mu_l (T_{sat} - T_w) D} \right]^{1/4} \tag{2.51}$$

$$h_{bot} = 0.31 \cdot \mathrm{Re}_v^{\ 0.12} \frac{\phi_{l,lt} \sqrt{8\,\mathrm{Re}_l}\, k_l}{5\left[1 + \frac{\ln(1 + 5\,\mathrm{Pr}_l)}{\mathrm{Pr}_l} \right] D} \tag{2.52}$$

where $\phi_{l,lt}^2 = 1 + \frac{1}{X_{lt}} + \frac{12}{X_{lt}^{\ 2}}$ (2.52.1)

The fraction of the tube perimeter under the film condensation is a parameter, β,

$$\beta = \mathrm{Re}_v^{0.1} \qquad \text{for} \qquad \frac{\mathrm{Re}_v^{0.6}\,\mathrm{Re}_l^{0.5}}{Ga} < 6.4 \cdot 10^{-5} \tag{2.53.1}$$

$$\beta = \frac{1.74 \cdot 10^{-5} Ga}{\sqrt{\mathrm{Re}_v\,\mathrm{Re}_l}} \qquad \text{if} \qquad \frac{\mathrm{Re}_v^{0.6}\,\mathrm{Re}_l^{0.5}}{Ga} > 6.4 \cdot 10^{-5} \tag{2.53.2}$$

Thus, the averaged Nusselt number is given by,

$$Nu = \beta \cdot Nu_{top} + (1 - \beta) Nu_{bot} \tag{2.54}$$

2.4.2.2 Annular Flow

The annular flow regime is the result of the interfacial shear stresses dominating the gravitational forces forming a nearly symmetric annular film around the tube with a high-speed vapor core.

2.4.2.2.1 Shear stress based approaches

The correlation developed by Carpenter and Colburn [13] featured the wall shear stress term composed of the friction, acceleration and gravity components.

$$\tau_w = \tau_f + \tau_{acc} + \tau_g \tag{2.55}$$

$$h = 0.045\,\Pr_l^{0.5}(\frac{k_l}{\mu_l})(\rho_l \tau_w)^{0.5} \tag{2.56}$$

Later, Soliman et al. [57] modified the Carpenter and Colburn correlation in Eq. (2.56) as,

$$h = 0.036\,\Pr_l^{0.65}(\frac{k_l}{\mu_l})(\rho_l \tau_w)^{0.5} \tag{2.57}$$

By applying the phase-change shear stresses into Eq (2.57), the Soliman correlation is

$$h = 0.036\,\Pr_l^{0.65}(\frac{k_l}{D})\,\mathrm{Re}_{lo}(\frac{\rho_l}{\rho_v})^{0.5}\sqrt{\frac{2(0.046)x^2}{\mathrm{Re}_v^{0.2}}\phi_v^2 + Bo\sum_{n=1}^{5} a_n(\frac{\rho_v}{\rho_l})^{n/3}} \tag{2.58}$$

$$a_1 = x(2-\beta) - 1$$
$$a_2 = 2(1-x)$$
where $a_3 = 2(\beta - 1)(x-1)$ and β=1.25.
$$a_4 = \frac{1}{x} - 3 + 2x$$
$$a_5 = \beta(2 - \frac{1}{x} - x)$$

This model was further modified by Chen et al. [16] as follows:

$$h = 0.018\,\mathrm{Pr}_l^{0.65} (\frac{k_l}{D})(\frac{\rho_l}{\rho_v})^{0.39} (\frac{\mu_v}{\mu_l})^{0.078}\, \mathrm{Re}_l^{0.2} (\mathrm{Re}_{lo} - \mathrm{Re}_l)^{0.7}\, \mathrm{Pr}_l^{0.65} \qquad (2.59)$$

2.4.2.2.2 Two-phase multiplier approach

Based on modifications of the Dittus and Boelter single-phase heat transfer correlation and the two-phase multipliers, F_{tp}, numerous condensation correlations were derived in the following general form,

$$Nu = C\,\mathrm{Re}^m\, \mathrm{Pr}^n\, F_{TP} \qquad (2.60)$$

Akers and Rosson [2] defined an equivalent Reynolds number, Re_{eq}, as

$$\mathrm{Re}_{eq} = \mathrm{Re}_l[(1-\bar{x}) + \bar{x}\sqrt{\frac{\rho_l}{\rho_v}}] \qquad (2.61)$$

and a stepwise correlation yields

$$Nu = \frac{\bar{h} D_h}{k_l} = 0.0265\,\mathrm{Re}_{eq}^{0.8}\, \mathrm{Pr}^{1/3} \qquad \text{for} \qquad \mathrm{Re}_{eq} > 50000 \qquad (2.62.1)$$

$$Nu = \frac{\bar{h} D_h}{k_l} = 5.03\,\mathrm{Re}_{eq}^{1/3}\, \mathrm{Pr}^{1/3} \qquad \text{for} \qquad \mathrm{Re}_{eq} \le 50000 \qquad (2.62.2)$$

Boyko and Kruzhilin [8] developed another correlation,

$$Nu = \frac{\bar{h} D_h}{k_l} = 0.024\,\mathrm{Re}_l^{0.8}\,\mathrm{Pr}^{0.43}\,\frac{\sqrt{\rho/\rho_m}\Big|_{in} + \sqrt{\rho/\rho_m}\Big|_{out}}{2} \tag{2.63}$$

where $$\rho/\rho_m = 1 + \left(\frac{\rho_l - \rho_v}{\rho_v}\right)x \tag{2.63.1}$$

Another correlation was developed by Cavallini and Zecchin [14],

$$Nu = \frac{\bar{h} D_h}{k_l} = 0.05\,\mathrm{Re}_q^{0.8}\,\mathrm{Pr}^{1/3} \tag{2.64}$$

where $$\mathrm{Re}_q = \mathrm{Re}_v\left(\frac{\mu_v}{\mu_l}\right)\left(\frac{\rho_l}{\rho_v}\right)^{0.5} + \mathrm{Re}_l \tag{2.64.1}$$

Shah [53] introduced the reduced pressure, P_{re}, and obtained a correlation,

$$h = 0.023\,\mathrm{Re}_l^{0.8}\,\mathrm{Pr}^{0.4}\left\{1 + \frac{3.8}{\left[\left(\frac{1-x}{x}\right)^{0.8}(P_{re})^{0.4}\right]^{0.95}}\right\} \tag{2.65}$$

where $$P_{re} = \frac{P_{sat}}{P_{cr}} \tag{2.65.1}$$

Carey [12] recommended another correlation based on the Lockhart and Martinelli pressure-drop, two-phase multiplier, ϕ_l^2,

$$Nu = \frac{h D_h}{k_l} = 0.28\,\mathrm{Re}_l^{0.9}\,\mathrm{Pr}^{0.5}\,\phi_l \tag{2.66}$$

where $\phi_l = 1 + \frac{20}{X_{tt}} + \frac{1}{X_{tt}^2}$ (2.66.1)

Lately, Dobson [24] fitted a form of Carey's,

$$h = 0.023 \mathrm{Re}_l^{0.8} \mathrm{Pr}^{0.4} (1 + \frac{2.22}{X_{tt}^{0.889}}) \tag{2.67}$$

2.4.2.2.3 Boundary-layer approach

These analyses represent the solutions to simplified forms of the continuity, momentum, and energy equations.

Azer [5] developed a correlation for R-12 as,

$$Nu = \frac{hD_h}{k_l} = 0.039 \mathrm{Re}_v^{0.9} \mathrm{Pr}_l^{0.337} \frac{\mu_v}{\mu_l} (\frac{\rho_l}{\rho_v})^{0.5} (1 + 1.10986 X_{tt}^{0.039}) \frac{x^{0.9}}{4.67 - x} \tag{2.68}$$

Travis et al. [65] derived a piece-wise correlation using a similar approach,

$$Nu = \frac{hD_h}{k_l} = \frac{\sqrt{0.023} \mathrm{Re}_l^{0.9} \mathrm{Pr}_l^{0.5} \phi_l}{F_2} \tag{2.69.1}$$

or $$Nu = \frac{hD_h}{k_l} = \frac{\mathrm{Re}_l^{0.9} \mathrm{Pr}_l^{0.5}}{F_2} [0.15(\frac{1}{X_{tt}} + \frac{2.85}{X_{tt}^{0.476}})] \tag{2.69.2}$$

where $F_2 = 0.707 \mathrm{Re}_l^{0.5} \mathrm{Pr}_l$ for $\mathrm{Re}_l<50$ (2.69.3)

or $F_2 = 5 \mathrm{Pr}_l + 5 \ln[1 + \mathrm{Pr}_l (0.09636 \mathrm{Re}_l^{0.585} - 1)]$ for $50<\mathrm{Re}_l<1125$ (2.69.4) else

$$F_2 = 5[\mathrm{Pr}_l + \ln(1+5\,\mathrm{Pr}_l)] + 2.5\ln(0.00313\,\mathrm{Re}_l^{0.812}) + 2.5\ln\left[\frac{M(30-\frac{2.5}{\mathrm{Pr}_l}) - 0.095\,\mathrm{Re}_l^{0.812}}{M(0.095\,\mathrm{Re}_l^{0.812} - \frac{2.5}{\mathrm{Pr}_l}) - 0.095\,\mathrm{Re}_l^{0.812}}\right] \quad (2.69.5)$$

2.5 Performance of the Microchannel Tube

Because of the innovative development of microchannel technology, few studies have been published. There are some SAE papers presenting the in-system performance of full condensers written by Govdremote et al. [30], Struss et al. [61], Struss and Gabbey [60], Sugihara and Lukas [62], and Tait et al. [63]. The major improvements include reduced system charges, size miniaturization, and better heat transfer performance.

Webb and Yang [66], [67], utilized a HFC 134a-to-H_2O counterflow facility to examine the plain and microfinned extruded aluminum rectangular, 4-port tubes with hydraulic diameters 2.637mm and 1.564 mm, respectively.

There is a 17% increase in the friction factors of the single-phase liquid in the plain tubes compared to the Blasius correlation for the smooth, round tube. The Petukhov [47] correlation provided good predictions for the single-phase heat transfer coefficients in the range of the Reynolds number between 3000 and 24000.

For the condensation heat transfer, they pointed out the Akers and Rosson [2] correlation representing their results well, especially at lower mass flux. Some heat transfer coefficient enhancement factors on the order of 2 were found in the two-phase flows with 400 Kg/m^{2}s mass flux and quality larger than 0.5.

QUANITY	INTERPRETATION	DEFINATION
Reynolds number, Re	Ratio of inertial effects to viscous forces	$\mathrm{Re} = \dfrac{GD_h}{\mu}$
Superficial Reynolds number	Flow rate of single phase occupies entire tube	$\mathrm{Re}_l = \dfrac{GD_h(1-x)}{\mu_l}$ $\mathrm{Re}_v = \dfrac{GD_h x}{\mu_v}$
Single phase only Reynolds number	All flow rate consists of the single phase	$\mathrm{Re}_{lo} = \dfrac{GD_h}{\mu_l}$ $\mathrm{Re}_{vo} = \dfrac{GD_h}{\mu_v}$
Nusselt number, Nu	Dimensionless heat transfer coefficient	$Nu = \dfrac{hD_h}{k_l}$
Prandtl number, Pr	Ratio of momentum diffusivity to heat diffusivity	$\mathrm{Pr} = \dfrac{\mu Cp}{k}$
Galileo number, Ga	Ratio of gravitational to viscous forces	$Ga = \dfrac{\rho_l(\rho_l - \rho_v)gD_h^3}{\mu_l^2}$
Jakob number, Ja	Ratio of sensible to latent energy transfer	$Ja_l = \dfrac{Cp_l(T_{sat} - T_{wall})}{i_{fg}}$
Froude number, Fr	Ratio of inertial to gravitational forces	$Fr_l = \dfrac{(G/\rho_l)^2}{gD_h}$
Weber number, We	Ratio of inertial to surface tension forces	$We = \dfrac{G^2 D_h}{\rho_v \sigma}$
Bond number, Bo	Ratio of gravitational to surface tension forces	$Bo = \dfrac{g(\rho_l - \rho_v)D_h^2}{\sigma}$
Lockhart-Martinelli parameter, X_{tt}	Dimensionless liquid inventory	$X_{tt} = \left(\dfrac{\rho_v}{\rho_l}\right)^{0.5}\left(\dfrac{\mu_l}{\mu_v}\right)^{0.1}\left(\dfrac{1-x}{x}\right)^{0.9}$
Heat transfer Lockhart-Martinelli parameter, $X_{tt,q}$	Ratio of liquid to vapor heat transfer	$X_{tt,q} = \left(\dfrac{k_l}{k_v}\right)^{0.3}\left(\dfrac{\mu_v}{\mu_l}\right)^{0.2}\left(\dfrac{1-x}{x}\right)^{0.4}\left(\dfrac{Cp_l}{Cp_v}\right)^{0.2}$

Table 2.1 Dimensionless groups

Geometry	D_h	D_h^*	D_{le}^*	D_{lc}^*
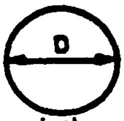 circle	D	1.0	1.0	1.0
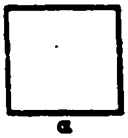 square	α	1.0	1.125	1.207
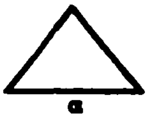 equilateral triangle	$\frac{\sqrt{3}}{3}\alpha$	1.0	1.200	1.500
 rectangle: $\beta/\alpha = 1/2$	$\frac{2}{3}\alpha$	1.0	1.029	1.126
 rectangle: $\beta/\alpha = 1/4$	$\frac{2}{5}\alpha$	1.0	0.878	1.090

Table 2.2 Length scales for constant-area ducts

Liquid-gas	C
Turbulent-turbulent (tt)	20
Viscous-turbulent (vt)	12
Turbulent-viscous (tv)	10
Viscous-viscous (vv)	5

Table 2.3 Values of constant C

Cross-sectional shape	b/a	Nu* q'' = constant	Nu T_w = constant
	–	4.364	3.66
	1.0	3.63	2.98
	1.4	3.78	
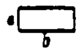	2.0	4.11	3.39
	3.0	4.77	
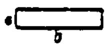	4.0	5.35	4.44
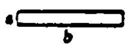	8.0	6.60	5.95
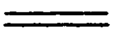	∞	8.235	7.54
 (insulated)	∞	5.385	4.86
	–	3.00	2.35

Source: From Kays

*The constant-heat-rate solutions are based on constant *axial* heat rate but with constant *temperature* around the tube periphery. Nusselt numbers are averages with respect to tube periphery.

Table 2.4 Nusselt number for laminar fully developed velocity and temperature profiles in tubes of various cross sections

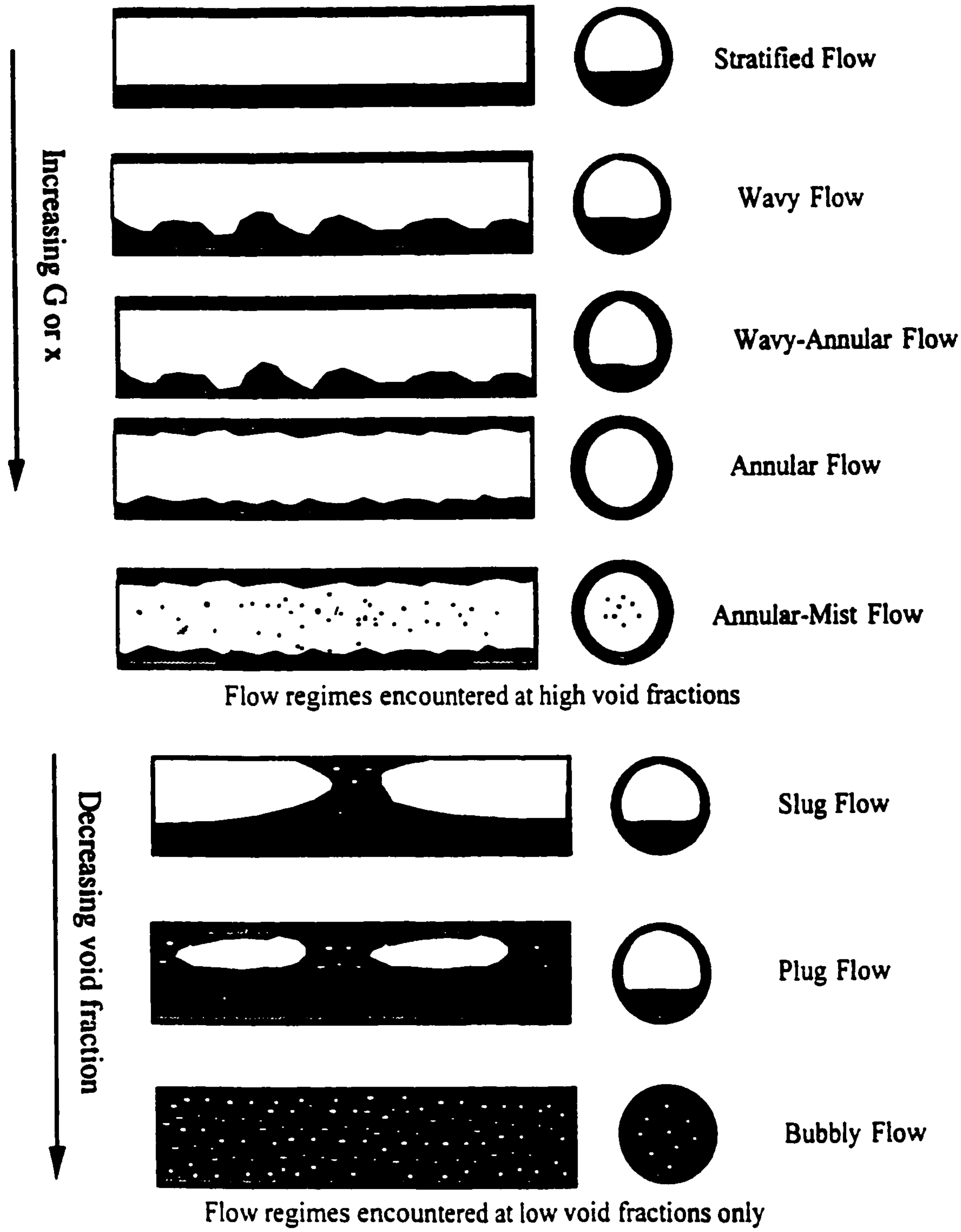

Figure 2.1 Flow regimes typically encountered in condensation processes.

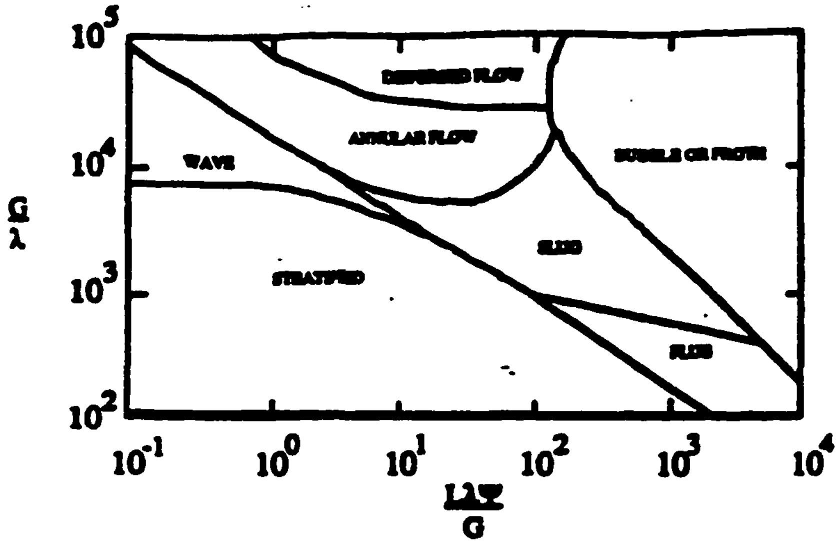

Figure 2.2 Flow regime map developed by Baker [1954].

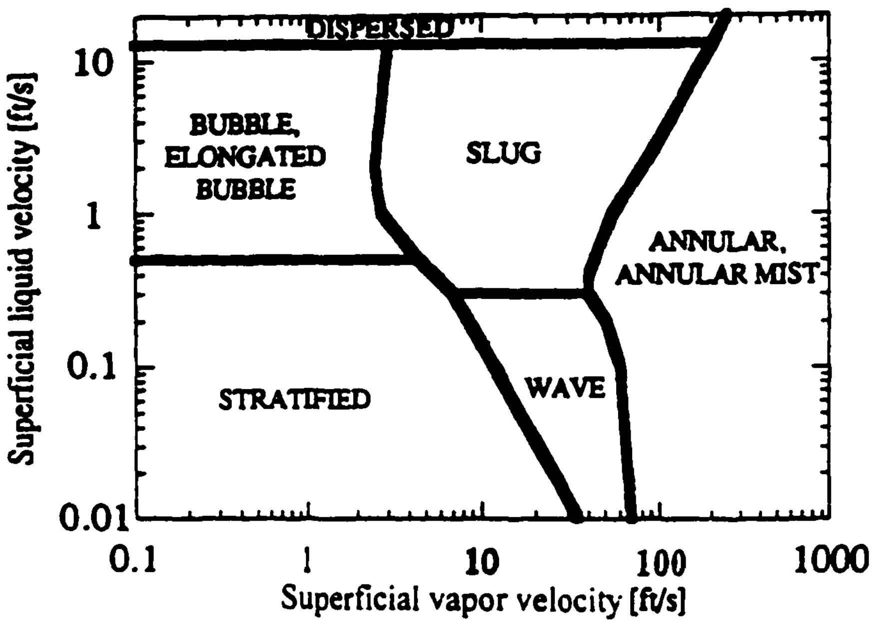

Figure 2.3 The flow regime map of Mandhane et al. [1974].

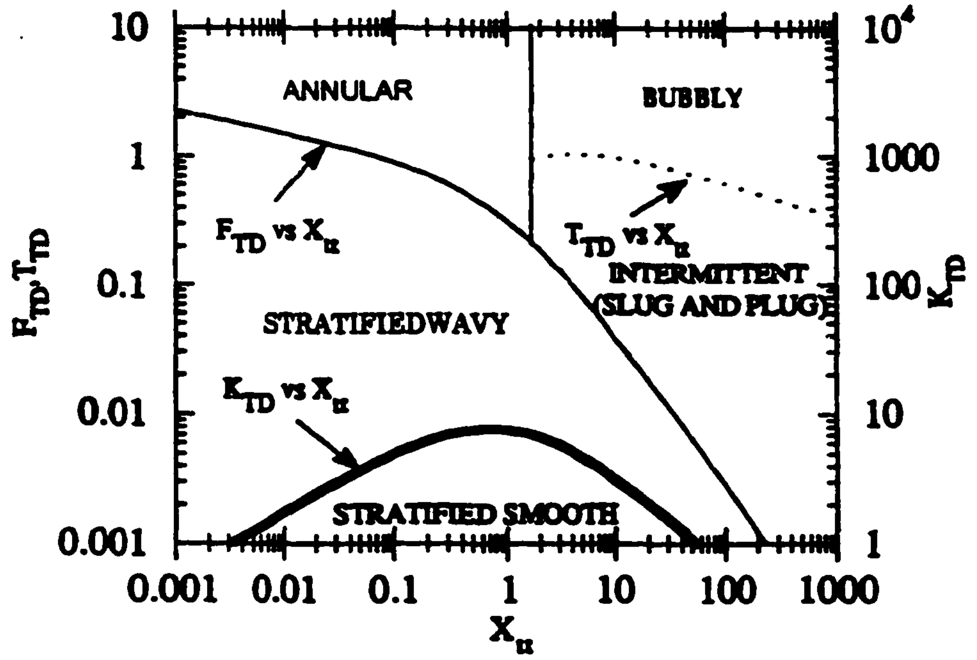

Figure 2.4 Flow regime map proposed by Taitel-Dukler for horizontal flow with both phases flowing turbulently.

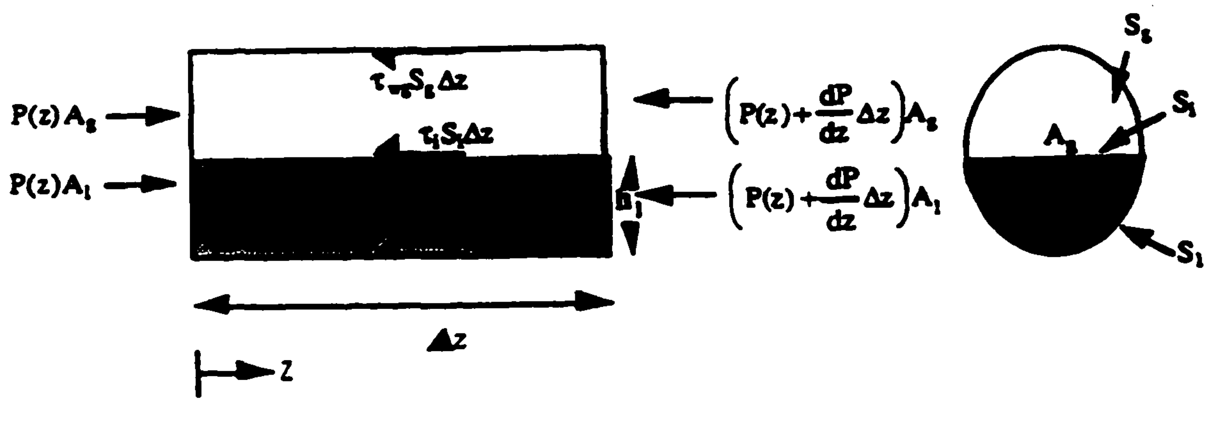

Figure 2.5 Stratified flow schematic from Taitel and Dukler

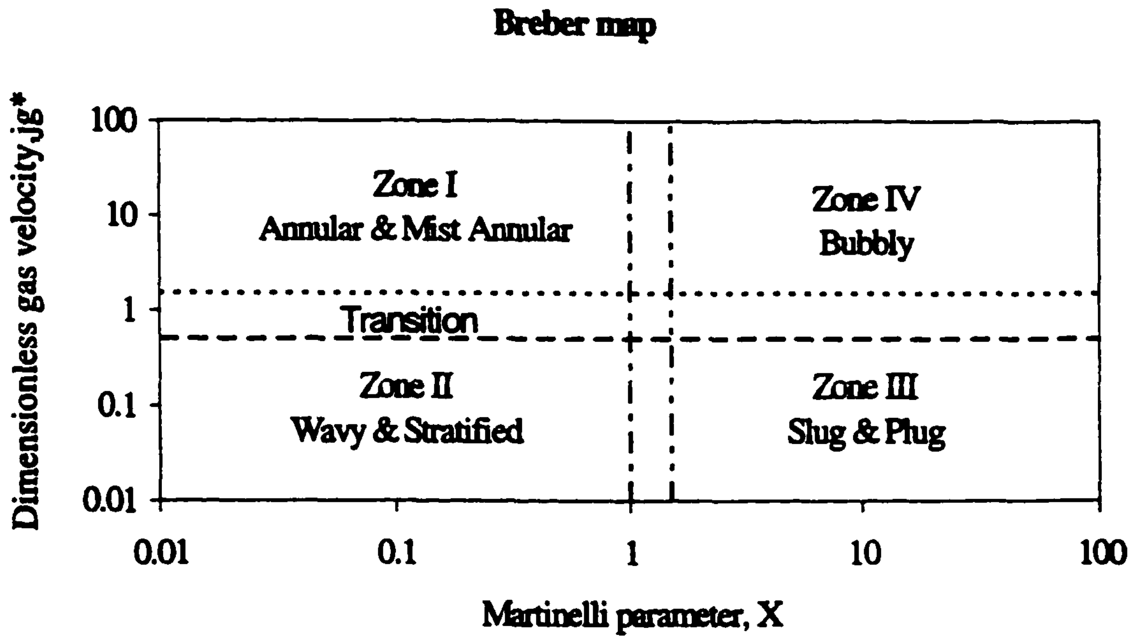

Figure 2.6 Breber map

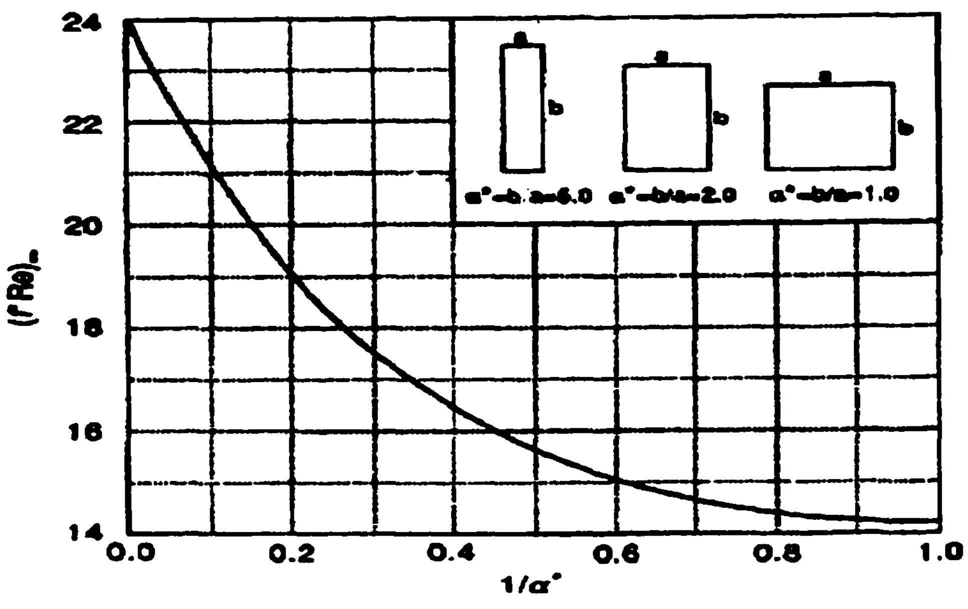

Figure 2.7 Product of laminar friction factor and Reynolds number for fully developed flow with rectangular geometry.

CHAPTER 3

EXPERIMENTAL FACILITY AND DATA ANALYSIS

3.1 Experimental Facility

In order to simulate the real operating conditions, air was chosen to be the heat-sink fluid in the crossflow geometry as shown in Figure 3.1. However, the airside thermal resistance is so dominating that some experimental resolution on the refrigerant-side heat transfer has been sacrificed to compensate for the unfavorable thermal resistance imbalance.

3.1.1 Refrigerant Loop

The schematic of the refrigerant loop is depicted in Figure 3.2. A variable speed gear pump powered by a three-phase motor which was controlled by an AC inverter drives the fluid. Either the adjustment on the AC inverter or the position of the needle valve can control the flow rate.

The operating pressure in the loop was stabilized by the pressurized accumulator with two attached strip heaters. By adjusting the variable voltage transformer connected to the heater strips, a desired operating pressure could be reached and held steady during the test.

The refrigerant flow rate was measured by an ABB K-flow K-5 mass flow meter in the range of 0 to 2.5 lb/min. A 2000-watt serpentine heater was the source for heating the subcooled refrigerant. The preferred state at the inlet of the test condenser could be controlled. An after-heater provided the ability to superheat the condensate. At the end, a coiled shell-and-tube water-cooled after condenser returned the refrigerant to a liquid, 50 to 70 F subcooled.

3.1.2 Air Loop

A detail schematic of the air loop is shown in Figure 3.3, which was an open-type air passage. Air was drawn by a vacuum which was connected to a variable voltage transformer. There were two laminar flow elements measuring the air flow rates. One was in the inlet open end, and the other was between the outlet of the air channel and the vacuum. Each element was connected to a differential pressure manometer.

The center piece of the loop was an air duct constructed of Plexiglas and insulated by foam boards and fiberglass. Both upstream and downstream air temperatures were measured by thermocouples. In order to reduce the stratification obscuring the downstream reading, a pair of mixing blade flow conditioners were installed.

3.1.3 Test Section

3.1.3.1 Refrigerant side

The test section as shown in Figure 3.1 was connected to the refrigerant loop with a pair of end blocks providing the transitions from the 1/2 inch stainless steel tube to the microchannel tube. To observe the status of the refrigerant, a pair of sight glasses were installed fore and aft of the test section. In addition to the bulk temperature and pressure measurements made at the inlet and outlet conditions, 7 pairs of thermocouples were attached to the tube walls by percussion welding to obtain the local heat transfer information.

The geometry of the testing tube is displayed in Figure 3.4. The length of the tubing is 24 inches.

3.1.3.2 Air side

To cope with the local measurements on the refrigerant side, 7 pairs of thermocouples were installed in each sub-section to measure the air temperature changes.

3.1.4 Instrumentation

The instrumentation used in this study included thermocouples, resistance temperature devices (RTD), absolute pressure transducers, differential pressure transducers, multimeters, mass flow meter, and laminar flow elements.

3.1.4.1 Temperature measurements

Type-T, copper-Constantine, thermocouples were used to measure the air temperatures and the wall temperatures of the testing tube, with an uncertainty of +/- 0.5F.

For the refrigerant temperature measurements, platinum RTD probes were submerged into the refrigerant fluid with an uncertainty of +/- 0.4F.

All the thermocouples and RTDs were calibrated in both isothermal ice and boiling water baths using NIST-traceable thermometers with a uncertainty of +/- 0.1F. Separate calibration curves were developed for each probe, which were able to predict measured temperature within +/- 0.25F.

3.1.4.2 Absolute pressure

Two strain-gage type pressure transducers were used to indicate the high end and low end system pressures, which were separated by the needle valve, in order to verify the saturation temperature measurement during condensation tests. Both a 300-psi and a 500-psi transducer were installed and calibrated on a dead weight tester over their range of applicability with a uncertainty of +/- 1.5psi.

3.1.4.3 Differential pressure

The pressure drops across the testing tube were obtained by a strain-gage type differential pressure transducer with a range from 0 to 10 psi corresponding to 0-20 ma output. The uncertainty of this transducer was estimated as +/- 0.1psi.

3.1.4.4 Power

The power inputs into the heaters were measured by two multimeters; one was used for the voltage, and the other was responsible for the current measurement.

3.1.4.5 Mass flow rate

An ABB K-5 mass flow meter was installed to measure the HFC-134a flow rate. A 4 ~ 20 mA output with an uncertainty of +/- 0.2% was estimated for the full scale reading of the flow meter from 0 ~ 5 lb/min.

3.1.4.6 Air flow rate

Two laminar flow elements were used to monitor the air volume flow rate. The one with a 0 to 20 CFM range was used for lower flow rates and the other with a 0 to 408 CFM range was for higher flow rates. Both elements had full range readings of 8 inches water differential pressure, and linear curve fitting calibration charts were available with an uncertainty of +/- 0.25% of the reading.

3.1.5 Data acquisition

All electrical signal were collected by an Omega high-speed temperature and process signal measurement system, OMB-Tempscan-1000. Via a built-in RS232 interface and Windows-based software, real-time data were displayed on the monitor. When steady state had been reached, the data were stored over a period of time as Excel files. There were 10 RTD channels, 32 thermocouple channels and 5 voltage channels used during the course of an experiment.

3.2 System Operation

3.2.1 Preparation

After installing all the instrumentation, the system was ready for leak testing. The refrigerant loop was filled with a compressed gas, and leak-free conditions were verified by a leak detector and soapy water solution.

Once the system was deemed leak-free over several hours, evacuation took place for at least 20 hours using a vacuum pump. Then, the refrigerant loop was charged with liquid HFC-134a by connecting a heated inverted refrigerant tank. The amount of charging was monitored by the level in the sightglass of the pressurized accumulator.

3.2.2 Data collection

Before operating the system, the mass flow meter needed zeroing showing no sign of fluctuation. Once the zero state was completed, the refrigerant pump and the air vacuum were turned on and adjusted to the desired rates.

After reaching the target saturation pressure by heating up the pressurized accumuiator, normally for 2 hours, all the instrumentation was monitored closely to verify a steady-state condition. When all the system parameters remained constant within their target ranges for 3 to 5 minutes, data collection began.

Once the collected data were deemed consistent, the operating conditions were altered and the process repeated.

3.3 Data Analysis

Two Microsoft Excel spreadsheet files were written for each data point. One file contained command macros that averaged and calibrated the raw data. The other file dealt with thermophysical properties, and heat transfer coefficients. The thermodynamic and transport properties came from 3 sources; 1) REFPROP [Gallagher, 28], 2) Dupont [Transport Properties of SUVA Refrigerants, 26], and 3) ASHRAE Handbook of Fundamental [4].

3.3.1 Energy Balance

Because of the straight forward availability of the thermophysical properties based merely on temperature and pressure measurements single-phase liquid tests were used to verify the instrumentation function and examine the energy balance across the test section and the refrigerant heater,

The power of heater input was, $\dot{Q}_h$,

$$\dot{Q}_h = I \cdot V \tag{3.1}$$

Which should be equal to the enthalpy increase of the refrigerant and heat loss, $\dot{Q}_{h,l}$,

$$\dot{Q}_h = \dot{m}_r (i_{h,o} - i_{h,i}) + \dot{Q}_{h,l} \tag{3.2}$$

Define the heater efficiency, η_h, as

$$\eta_h = \frac{\dot{Q}_h - \dot{Q}_{h,l}}{\dot{Q}_h} = \frac{\dot{m}_r (i_{h,o} - i_{h,i})}{\dot{Q}_h} \tag{3.3}$$

Therefore, empirical expressions for the heater efficiency were used to decide the inlet refrigerant enthalpy, $i_{r,i}$, and the inlet quality, $x_{r,i}$, for two-phase test runs.

$$\eta_h i_{r,i} = i_{h,i} + \frac{\dot{Q}_h \cdot \eta_h}{\dot{m}_r} \tag{3.4}$$

$$x_{r,i} = \frac{i_{r,i} - i_l(P_{sat,i})}{i_{fg}(P_{sat,i})} \tag{3.5}$$

For the energy balance of the test section,

$$\dot{m}_r (i_{r,i} - i_{r,o}) = \rho_a \cdot Q_a \cdot Cp_a \cdot (T_{a,o} - T_{a,i}) + \dot{Q}_{loss} \tag{3.6}$$

where the heat loss to the environment, $\dot{Q}_{loss}$, was determined.

3.3.2 Heat Transfer

3.3.2.1 Overall

Using the Wilson plot analysis [52], the overall heat transfer coefficients on both sides of the heat exchanger were determined based on the bulk property measurements.

The overall heat transfer of the condenser can be expressed as,

$$\frac{1}{UA} = \frac{1}{[hA]_r} + \frac{1}{[\eta hA]_a} + R_w = R_{tot} \tag{3.7}$$

where

$$\frac{1}{UA}=\frac{F\cdot LMTD}{Q_{tot}} \quad , \quad LMTD=\frac{\delta T_1-\delta T_2}{\ln({\delta T_1}/{\delta T_2})}$$

$$\delta T_1 = T_{r,o}-T_{a,i} \quad , \quad \delta T_2 = T_{r,i}-T_{a,o}$$

The Nusselt number for each side, based on the correlation of Sieder and Tate [47], was assumed as follows,

$$Nu_a = \left.\frac{h\cdot D_h}{k}\right|_a = C_a \cdot \mathrm{Re}^a \cdot \mathrm{Pr}^{\frac{1}{3}} \tag{3.8}$$

$$Nu_r = \left.\frac{h\cdot D_h}{k}\right|_r = C_r \cdot \mathrm{Re}^b \cdot \mathrm{Pr}^{\frac{1}{3}} \tag{3.9}$$

Substituting Equation (3.8) and (3.9) into (3.6),

$$\frac{1}{UA}=\frac{F\cdot LMTD}{Q_{tot}}=\frac{1}{C_a \mathrm{Re}^a \mathrm{Pr}^{\frac{1}{3}}(A\frac{k}{D_h})\Big|_a}+\frac{1}{C_r \mathrm{Re}^b \mathrm{Pr}^{\frac{1}{3}}(A\frac{k}{D_h})\Big|_r}+R_w \tag{3.10}$$

There are four unknowns in equation (3.10), C_a, C_r, a, and b, which can be solved by applying three modified Wilson plots.

Rewrite Equation (3.10) as,

$$(\frac{1}{UA}-R_w)\cdot(\mathrm{Re}^b \mathrm{Pr}^{\frac{1}{3}}(A\frac{k}{D_h})\Big|_r)=\frac{1}{C_a}\frac{\mathrm{Re}^b \mathrm{Pr}^{\frac{1}{3}}(A\frac{k}{D_h})\Big|_r}{\mathrm{Re}^a \mathrm{Pr}^{\frac{1}{3}}(A\frac{k}{D_h})\Big|_a}+\frac{1}{C_r} \tag{3.11}$$

Plot the data based on Eq (3.11), by choosing

$$X = \frac{\left.\mathrm{Re}^b\, \mathrm{Pr}^{\frac{1}{3}}(A\frac{k}{D_h})\right|_r}{\left.\mathrm{Re}^a\, \mathrm{Pr}^{\frac{1}{3}}(A\frac{k}{D_h})\right|_a} \tag{3.12}$$

$$Y = (\frac{1}{UA} - R_w)\cdot(\left.\mathrm{Re}^b\, \mathrm{Pr}^{\frac{1}{3}}(A\frac{k}{D_h})\right|_r) \tag{3.13}$$

and assuming values of a and b. A linear regression curve can be obtained, with the slope of 1/Ca and the intersection of 1/Cr.

Using the new value of C_a, computing h_a from Eq. (3.8), and determining h_r from Eq (3.7), Eq (3.9) can be written as

$$\left.\frac{h\cdot D_h}{k}\cdot \mathrm{Pr}^{-1/3}\right|_r = C_r \cdot \mathrm{Re}^b \tag{3.14}$$

or take the natural logarithm on both sides,

$$\ln(\left.\frac{h\cdot D_h}{k}\cdot \mathrm{Pr}^{-1/3}\right|_r) = \ln C_r + b\cdot \ln \mathrm{Re}_r \tag{3.15}$$

Plot the data according to Eq (3.15) by choosing

$$X_r = \ln \mathrm{Re}_r \tag{3.16}$$

$$Y_r = \ln(\left.\frac{h\cdot D_h}{k}\cdot \mathrm{Pr}^{-1/3}\right|_r \tag{3.17}$$

Another linear curve can be obtained with the slope of b and the intersection of $\ln(C_r)$.

Using new values of b and C_r, computing h_r from Eq (3.9), a value of h_a can be obtained from Eq (3.7). Rewrite Eq (3.8) and take the natural logarithm of both sides.

$$\ln(\frac{h \cdot D_h}{k} \cdot \Pr^{-1/3})\Big|_a = \ln C_a + a \cdot \ln \mathrm{Re}_a \tag{3.18}$$

Plot Eq (3.18), by choosing

$$X_a = \ln \mathrm{Re}_a \tag{3.19}$$

$$Y_a = \ln(\frac{h \cdot D_h}{k} \cdot \Pr^{-1/3}\Big|_a) \tag{3.20}$$

A linear regression curve is obtained with the slope of a and the intersection of $\ln(C_a)$.

Iterations of the three modified Wilson plots were continued until a, and b converge within the desired accuracy, 0.1%. Figure 3.5 shows the iterative scheme.

3.3.2.2 Local heat transfer

The local heat transfer coefficients of both the refrigerant and the air sides can be obtained from the wall temperature measurements. Figure 3.6 shows the schematic of each subsection.

The energy balance of the refrigerant and the air can be written as,

$$\dot{Q} = \rho_a \cdot Q_a \cdot Cp_a \cdot (T_{a,a} - T_{a,f}) + \dot{Q}_l = \dot{m}_r (i_{r,i} - i_{r,o}) + \dot{Q}_l \tag{3.21}$$

The refrigerant outlet enthalpy, i_{ro}, can be derived from Eq (3.21), as well as the outlet temperature of the subcooled liquid, $T_{r,o}$.

The overall resistance between the refrigerant and the wall surface is as follows:

$$R_{tot,rw} = \frac{1}{UA_{rw}} = \frac{1}{[hA]_r} + R_w \tag{3.22}$$

where, $\frac{1}{UA_{rw}} = \frac{F \cdot LMTD_{rw}}{\dot{Q}}$, $\quad LMTD_{rw} = \frac{\left(T_{ro-} - T_{a,f}\right) - \left(T_{ri} - T_{a,a}\right)}{\ln\left(\frac{T_{ro-} - T_{a,f}}{T_{ri} - T_{a,a}}\right)}$

Therefore, the local heat transfer coefficient of the refrigerant inside the microchannel tube is,

$$h_r = \frac{1}{A_r}\left(\frac{LMTD_{rw}}{\dot{Q}} - R_w\right)^{-1} \tag{3.23}$$

3.3.3 Pressure Drop and Friction Factor

To convert the measured pressure drop into the dimensionless friction factor, the entrance effect and the minor losses of the fittings and elbows have to be taken into account.

$$\frac{\Delta P}{\frac{1}{2}\rho V^2} = f \cdot \frac{D_h}{L} + \sum_i K_i \tag{3.24}$$

where f is the fully developed Darcy friction factor and ΣK_i is the sum of the minor losses. Rewriting Eq (3.24), the friction factor, f, is as follows:

$$f = \left(\frac{\Delta P}{\frac{1}{2}\rho V^2} - \sum_i K_i\right) \cdot \frac{D_h}{L} \tag{3.25}$$

3.3.4 Uncertainty

According to the uncertainty analysis method proposed by Moffat [44], the uncertainty of a dependent variable R with n independent variables, x_i, can be expressed as follows,

$$\delta R = \sqrt{\sum_{i=1}^{n}\left(\frac{\partial R}{\partial x_i}\delta x_i\right)^2} \tag{3.26}$$

The uncertainty of the heat transfer coefficient can be evaluated by applying Eq. (3.26) to Eq. (3.23). The resulting fractional uncertainty was able to be expressed as,

$$\frac{\delta h}{h} = \left[\begin{array}{l} \dfrac{(\rho_a Cp_a Q_a)^2(\delta T_{a,a}^2 + \delta T_{a,f}^2) + (\rho_a Cp_a (T_{a,a} - T_{a,f}))^2 \delta Q_a^2 + \delta \dot{Q}_l^2}{(\rho_a Cp_a Q_a (T_{a,a} - T_{a,f}) + \dot{Q}_l)^2} + \\ \dfrac{(\delta T_{ro} + \delta T_{a,f})^2 (\ln\dfrac{T_{ro} - T_{a,f}}{T_{ri} - T_{a,a}} - \dfrac{T_{ri} - T_{a,a}}{T_{ro} - T_{a,f}}(T_{ro} - T_{a,f} - T_{ri} + T_{a,a}))^2}{((T_{ro} - T_{a,f} - T_{ri} + T_{a,a})\ln\dfrac{T_{ro} - T_{a,f}}{T_{ri} - T_{a,a}})^2} + \\ \dfrac{(\delta T_{ri} + \delta T_{a,a})^2 (-\ln\dfrac{T_{ro} - T_{a,f}}{T_{ri} - T_{a,a}} + \dfrac{(T_{ro} - T_{a,f} - T_{ri} + T_{a,a})}{(T_{ro} - T_{a,f})(T_{ri} - T_{a,a})})^2}{((T_{ro} - T_{a,f} - T_{ri} + T_{a,a})\ln\dfrac{T_{ro} - T_{a,f}}{T_{ri} - T_{a,a}})^2} + \left(\dfrac{\delta A}{A_r}\right)^2 \end{array}\right]^{0.5}$$

(3.27)

Uncertainties of temperature measurements and air flow rate contributed predominately to the uncertainty in the heat transfer coefficient derivation. As for the heat loss concern, even a 50% uncertainty of heat loss resulted in only 1% of the overall uncertainty. Based on estimated uncertainties of various instrumentation listed previously, the overall uncertainty of the heat transfer coefficient was estimated less than 8%.

The uncertainty of the inlet enthalpy of the refrigerant was derived from Eq. (3.2) and (3.4) as follows:

$$\delta i_{r,i} = \left[\delta i_{h,i}^2 + \frac{\delta Q_h^2 + \delta Q_{h,l}^2}{\dot{m}_r^2} + \left(\frac{Q_h - Q_{h,l}}{\dot{m}_r} \right)^2 \left(\frac{\delta \dot{m}_r}{\dot{m}_r} \right)^2 \right]^{0.5} \tag{3.28}$$

3.4 Flow Visualization

Flow visualization gave the spatial and temporal resolution of the phase distribution inside the tube and also providing verification of the measured local heat transfer coefficient.

3.4.1 Experiment

The test section was constructed from an actual tube specimen without the top surface. A clear window was bonded on to seal the tube while providing a view of the working fluid. The refrigerant loop of the heat transfer experiment provided the working fluid at subcooled, saturated, or superheated conditions with flow rates of up to 2 lb/min. The loop was instrumented to measure the temperature, pressure, and quality at the inlet and outlet of the test section as well as the loop mass flow rate. These data allowed unambiguous determination of the energy balance and pressure drop across the section.

The test section was mounted in a machined block of aluminum, which was cooled by municipal water. Control of the water flow rate and temperature were maintained. A diagram of the test section is shown in Figure 3.7.

The secondary coolant channels are also shown in the figure. Water from the municipal supply was directed across the test section in a direction perpendicular to the refrigerant flow to minimize axial temperature gradient in the test section. The rate of heat removal was controlled by varying the mass flow rate and by using a heater to control the water temperature. An energy balance on the secondary side was made possible by measuring inlet and outlet temperatures and mass flow rate.

The actual heat transfer boundary condition for the test section was determined by attaching thermocouples to the outside wall of the test section at the junction with the cooled aluminum block. These measurements allowed accurate determination of the local heat transfer coefficient as well as the inside wall temperature at axial locations where two-phase flow exists.

Flow visualization was accomplished by directing light through the window to illuminate the fluid while the scattered light from the fluid was recorded with either a video or still camera through the window at a different angle. A broad region of light should be useful in identifying periodic or unsteady flow regimes like slug/plug flow. Annular flow was better characterized by using an angled light sheet to illuminate a cross-section of the fluid at a desired axial location. Polarizing of the light streams and/or directing the illumination at the Brewster angle of either the vapor/window or liquid/window interface allowed good resolution of the fluid and vapor regions. An antireflection coating was applied to the window to reduce unwanted scatter.

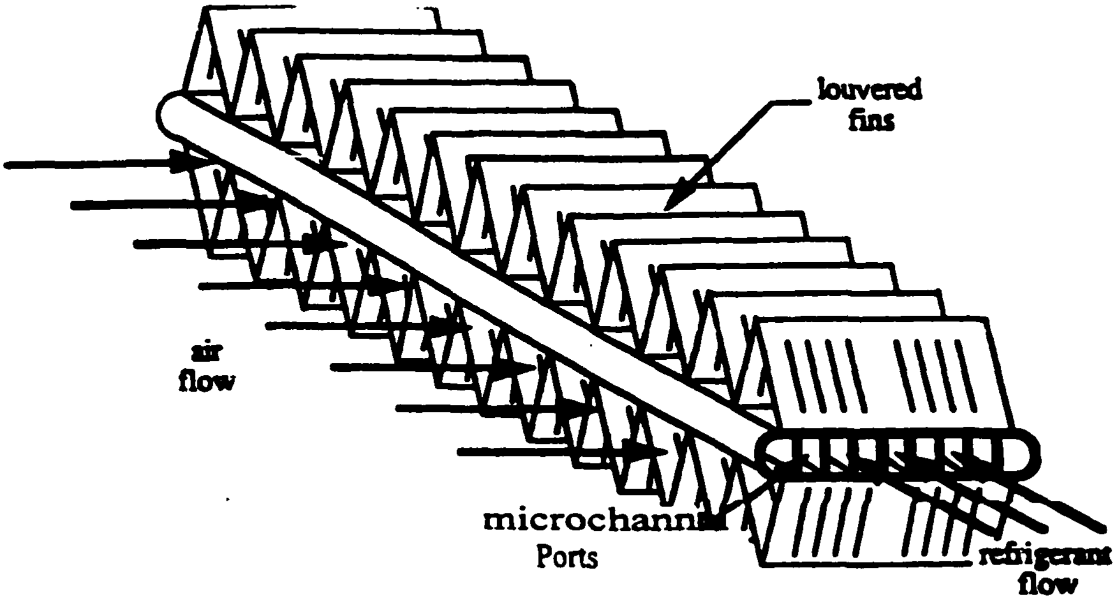

Figure 3.1 Single-tube Test Facility crossflow test section.

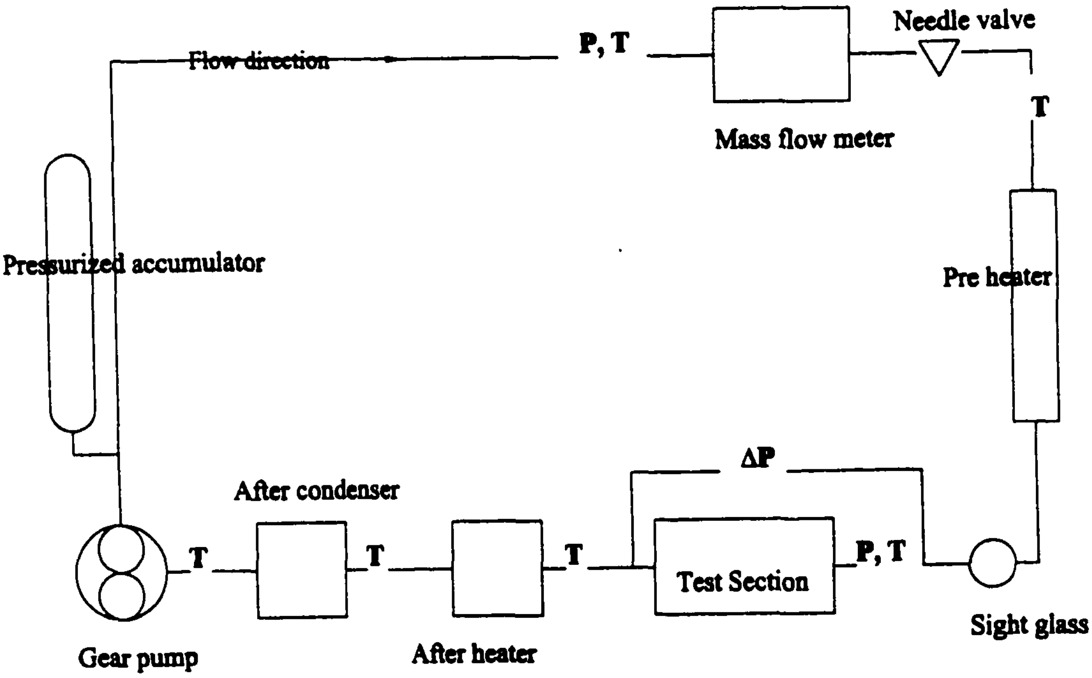

Figure 3.2 HFC-134a Loop

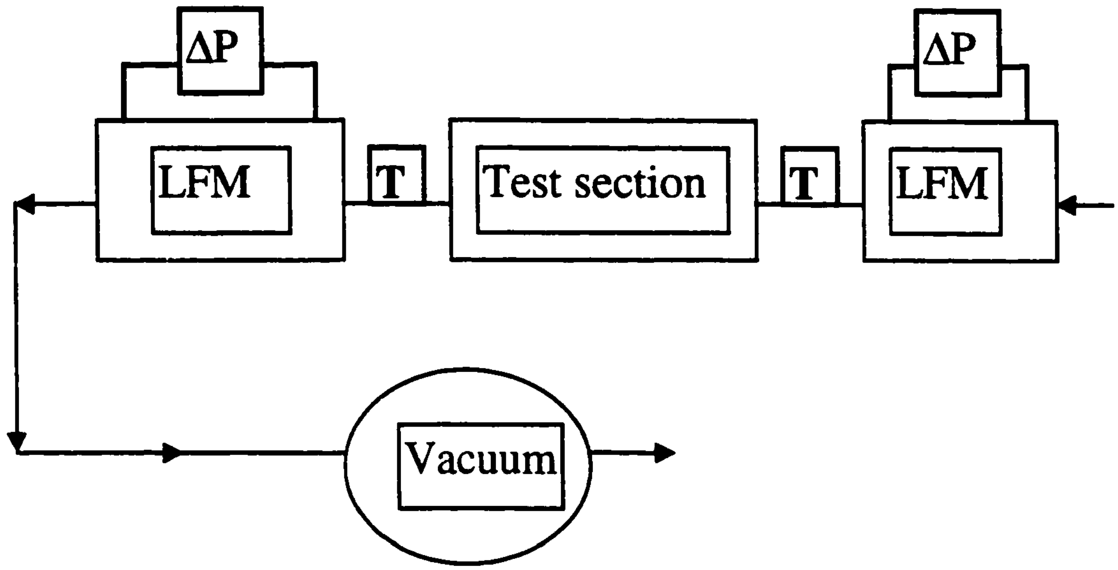

Figure 3.3 Air Loop

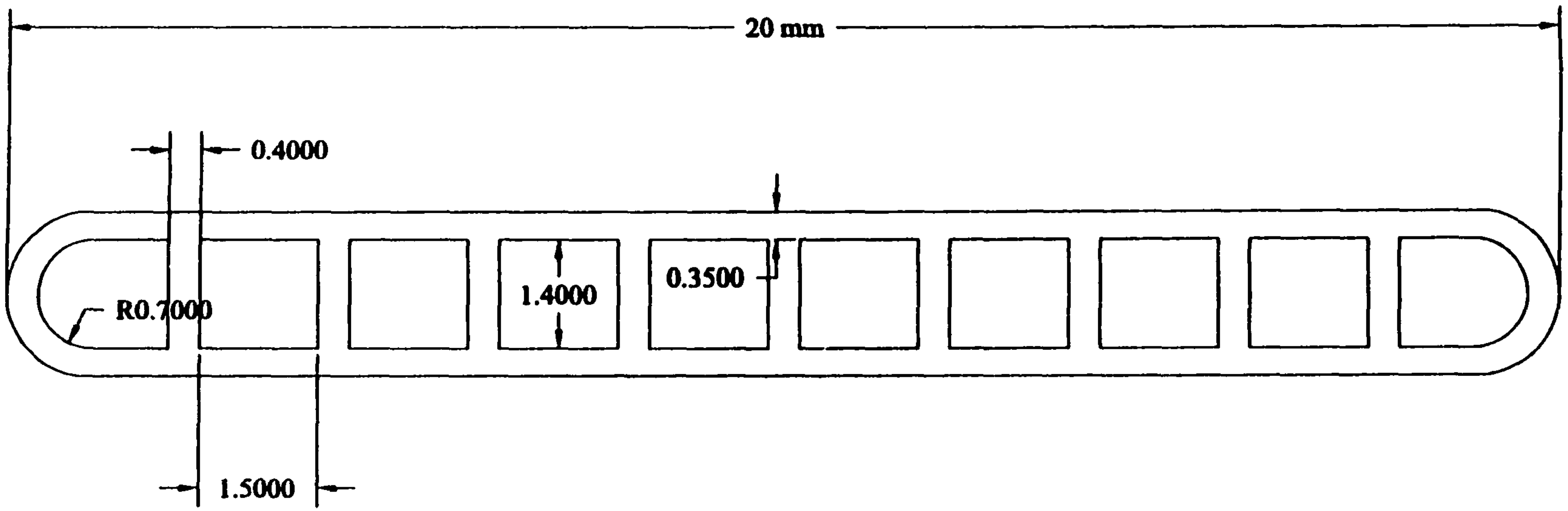

Figure 3.4 The geometry of the testing tube crosssection

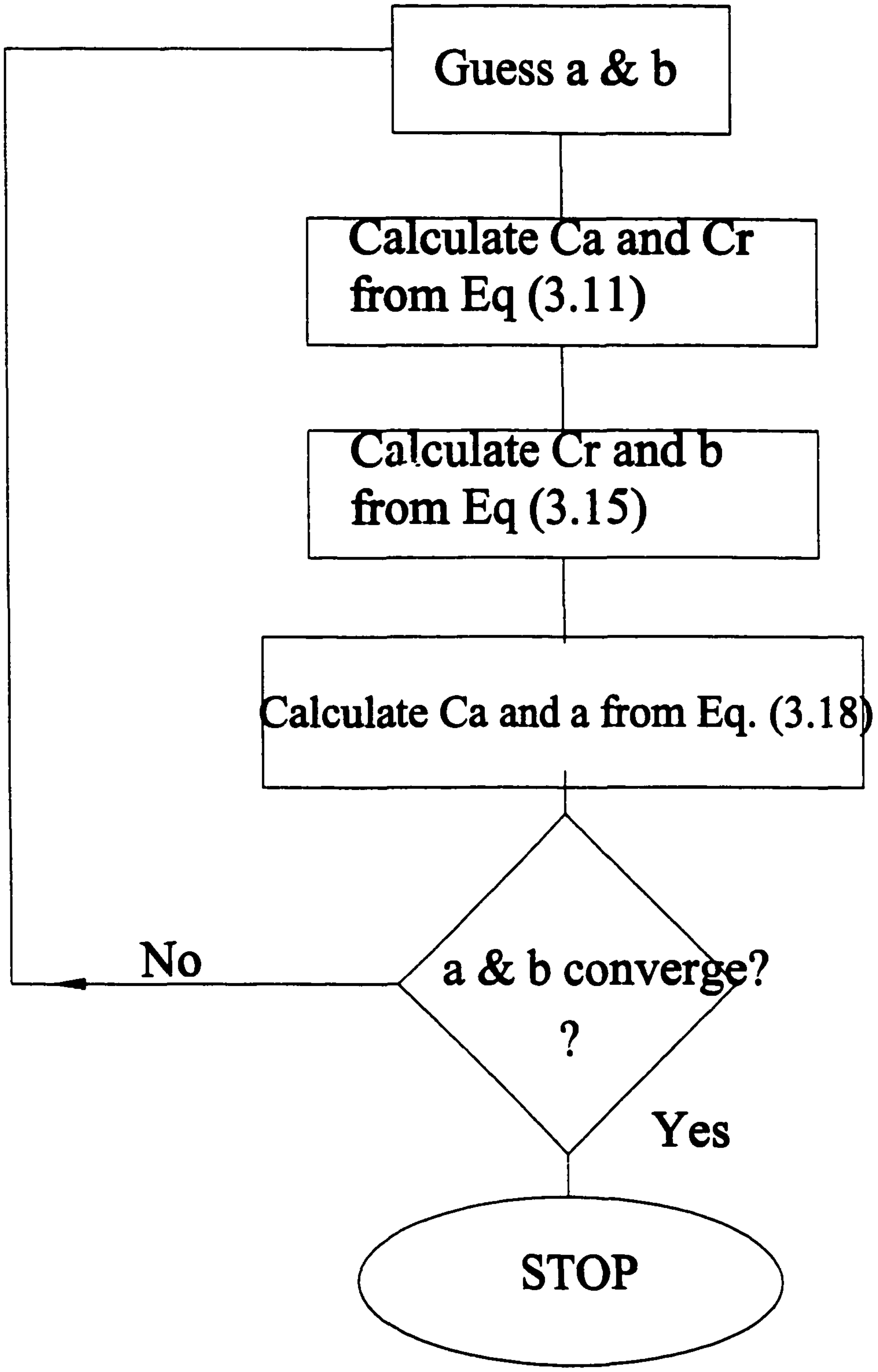

Figure 3.5 Iterative scheme of the Wilson plot

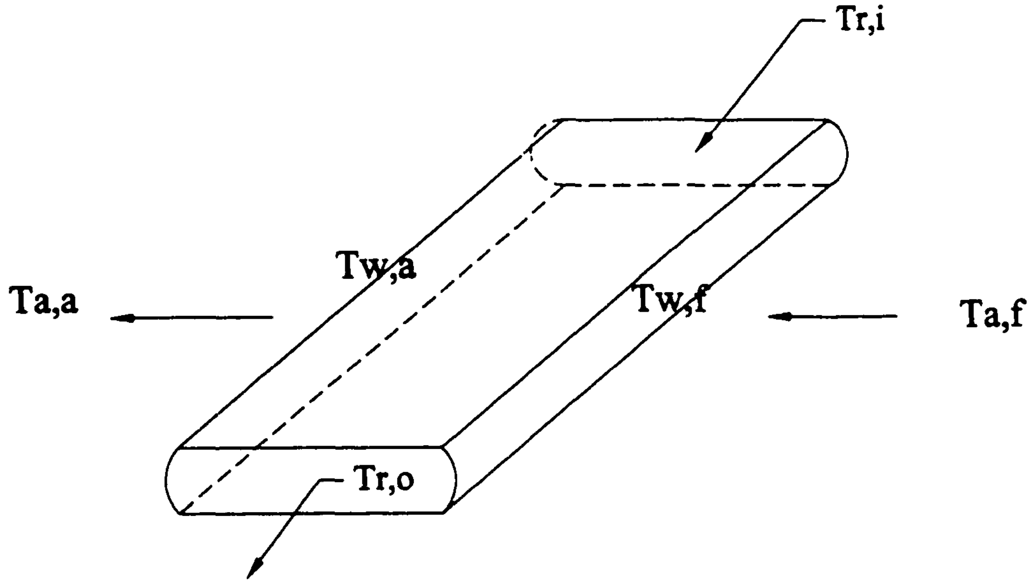

Figure 3.6 Subsection measurements

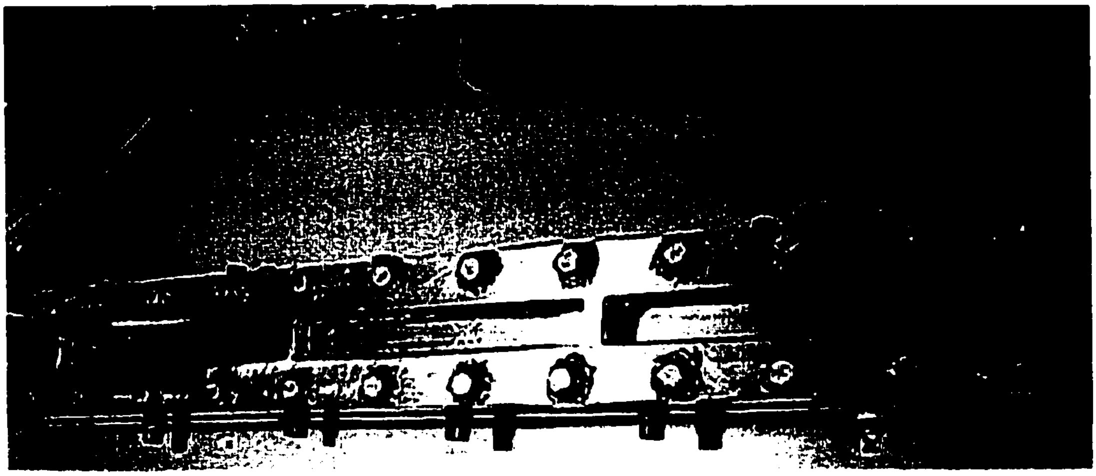

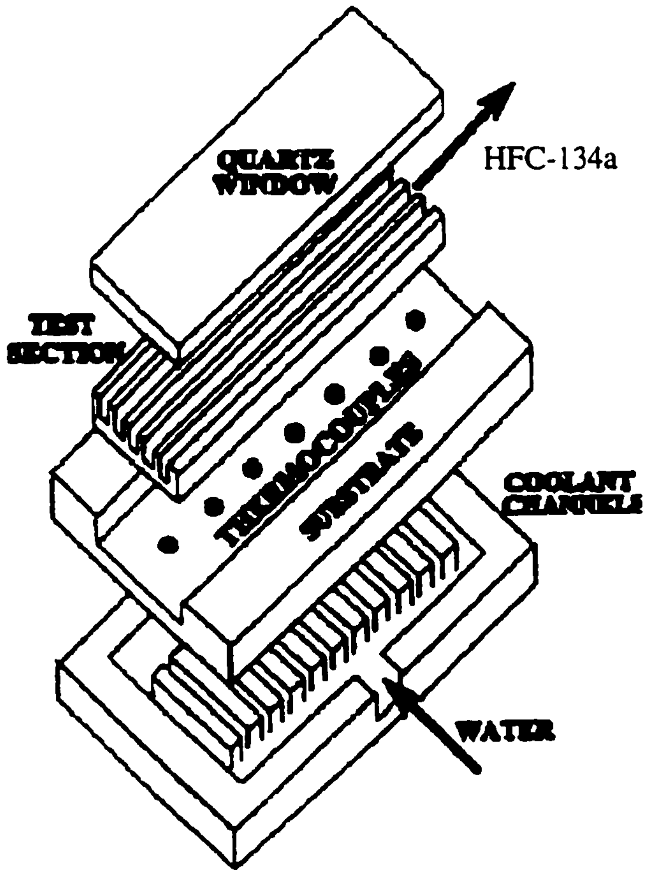

Figure 3.7 The test section and water channel of the flow visualization

CHAPTER 4

RESULTS

All the data collected are analyzed and presented in this chapter.

4.1 Single Phase

The range of parameters covered by the test conditions are given below:

1) R134a inlet saturation pressure: 260 ~ 285 psia.
2) R134a mass flow rate: 0.22 ~ 2.22 lb/min
3) R134a mass flux: 55 ~ 550 klb/ft^{2}hr.
4) R134a inlet temperature: 115 ~ 145 F.
5) R134a inlet subcooling degree: 5 ~ 35 F.
6) Room temperature: 67 ~ 76 F.
7) Air inlet temperature: 68 ~ 75 F.
8) Air flow rate: 8 ~ 36 CFM.

4.1.1 Energy balance

The single-phase heat transfer test provided a verification of the experimental apparatus and instrumentation. Because the thermal-physical properties of the single-phase liquid condition are well known and characterized, the energy balance between the refrigerant and air across the test section could be verified.

Define the energy balance index, e, as follows,

$$e = \frac{\rho_a \cdot Q_a \cdot Cp_a \cdot (T_{a,o} - T_{a,i})}{\dot{m}_r (i_{r,i} - i_{r,o})} \qquad (4.1)$$

The resulting index, e, plotted against mass flux, G, is shown in Figure 4.1. Data were scattered between 89% and 96%, which meant heat losses across the test section were less than 10% for the worst case.

4.1.1 Single-phase friction factor

Differential pressure drop measurements across the test section provided data for calculating the single-phase friction factors. At first, the measured hydraulic diameter was used to predict friction factors as shown in Figure 4.2. It appeared that in the laminar regime, the trend of friction factors was further away from the line for the round tubing, where f/4*Re=16, but was closer to the line for the rectangular tubing, f/4*Re = 14.23. The averaged number of f/4*Re for the experimental data was 14.45. Compared with the result for round tubing, there is a 16 /14.23 increase in the hydraulic diameter. Then, using this factor and defining a laminar equivalent Reynolds number as Eq. (2.20), Re_{le} = (16/14.23)*Re, a chart was plotted against the Churchill [19] correlation, Eq. (2.19), shown in Figure 4.3. It shows good agreement between test data and the well-known correlation. There is apparently a transition for Reynolds numbers between 1200 and 2300. The data for Reynolds numbers less than 1300 are right on the line predicted by the analytical solution of fully developed laminar flow.

4.1.3 Single-Phase Heat Transfer

Single-phase heat transfer coefficients have been calculated and plotted in Figure 4.4. As shown in Figure 4.4, there is a transition around a Reynolds number of 1350, which separates the flow regime of laminar and turbulent. To validate the data, two widely accepted correlations, Dittus-Bolter [20] Eq. (2.41) and Gnielinski [24] Eq. (2.45), are plotted against Nusselt numbers in Figure 4.5. For the turbulent flow regime, Re > 2000, experimental data are just between those two correlations. To further illustrate, a comparison ratio chart based on the Gnielinski correlation is shown in Figure 4.6. For Reynolds numbers greater than 3000, ratios are within 7%.

On the other hand, the Gnielinski correlation seems independent of the Reynolds number as the coefficients show a flat trend for those data in the laminar regime, Reynolds number < 1350. As shown on Figure 4.5, Nusselt numbers are around 7 for Reynolds number < 1350, which is the analytical solution for a rectangular channel with aspect ratio of 10 under the constant heat flux boundary condition. The aspect ratio of the whole tested microchannel tube was also 10. On the other hand, the aspect ratio for each individual microchannel was 1.

4.1.4 Summary

Results of the single-phase friction factor and heat transfer are now summarized,

1) By choosing the effective Reynolds number, a laminar equivalent Reynolds number,

Re_{le}, the Churchill correlation can predict friction factors of the microchannel tube.

2) The characteristic of single-phase friction inside the microchannel tubing can be described with the analytical solution of a simplified square channel.
3) There is good agreement between the Gnielinski correlation prediction and single-phase microchannel heat transfer data in the turbulent flow regime for Reynolds numbers greater than 3000.
4) The microchannel heat transfer in the laminar flow regime for Reynolds numbers smaller than 1350 can be described with the analytical solution of the rectangular channel, based on the aspect ratio of the entire tube.

4.2 Condensation

The range of parameters covered by the test conditions are given below:

1) R134a inlet saturation pressure: 260 ~ 285 psia.
2) R134a mass flow rate: 0.22 ~ 2.12 lb/min
3) R134a mass flux: 55 ~ 550 klb/ft^{2}hr.
4) R134a inlet temperature: 143 ~ 151 F.
5) R134a inlet quality: 0.03 ~ 0.94.
6) Room temperature: 67 ~ 76 F.
7) Air inlet temperature: 68 ~ 75 F.
8) Air flow rate: 8 ~ 36 CFM.

4.2.1 Experimental data

Overall, 180 sets of data are presented here. Extensive ranges of mass flux and quality have been covered. Figure 4.7 shows the mass flux, G, plotted against the quality, x, for all the collected data. Basically, the inlet quality for each mass flux was set at five different values ranging from 0.1, 0.3, 0.5, 0.7, to 0.9. As condensation took place along the tube, the quality decreased from the inlet value. To illustrate the quality change at each segment along the tube, Figure 4.8 is platted at various mass fluxes. As can be seen, multiple quality data points were taken at each mass flux.

The condensation heat transfer coefficients plotted against mass flux is presented in Figure 4.9. The heat transfer coefficient of the microchannel tube is greater for higher mass flux. For the Nusselt number at different mass fluxes, the result is illustrated in Figure 4.10, again demonstrating that at a given Reynolds number, high mass fluxes result in higher heat transfer coefficients.

4.2.2 Trends of data

Effects of parameters are described for mass flux, quality, and temperature difference.

4.2.2.1 Effect of mass flux

Figure 4.11 presents the variation of Nusselt number with average quality. General effects of mass flux and quality are illustrated. At lower mass fluxes, the Nusselt number increased modestly as the quality increased. As mass fluxes became larger, a much more pronounced effect of quality is seen. For the higher mass flux, a transition appeared in the low quality region. This is evident when looking at mass flux of 350 klb/ft^2hr, which is plotted in figure 4.11. Straight-line segments at the two extremes indicate a definite change in slope at a reference.

4.2.2.2 Effect of quality

Figure 4.12 presents the variation of Nusselt number with mass flux at different qualities. At low mass fluxes, there were not large differences in the qualities. As mass fluxes increase, trends of Nusselt number versus mass flux exhibited distinct changes in slope. As qualities decrease, the offset point would retreat toward the higher mass flux. On the other hand, the trend of heat transfer against mass flux became steeper at higher quality.

The changing behaviors of Figure 4.11 and Figure 4.12 can be attributed to the mechanism of two-phase flow regime. At lower mass fluxes, a wavy or wavy-annular flow pattern prevailed over much of the quality range. The mechanism of heat transfer in the wavy regime is primary conduction across the condensate film at the top of the tube. Therefore, the key factor of condensation heat transfer in this region is the film thickness of the condensate. However, the film thickness in the wavy flow regime is not very dependent on mass flux, and neither is the heat transfer.

For higher mass fluxes, the annular flow pattern dominated for most qualities. In the annular flow regime, forced convection at the two-phase interface is the major mechanism of condensation heat transfer. Furthermore, velocity and the mass flux are the driving fources behind the forced convection. As a result, the condensation heat transfer in the high mass flux annular flow regime is highly quality-dependent.

4.2.2.3 Effect of temperature difference

Based on the review of literature in Chapter two, the temperature difference between the refrigerant and the wall has a profound impact on the condensation heat transfer in the wavy flow regime. However, there is no significant effect on temperature difference or the heat flux in the annular flow. By examining the effect of temperature difference on the heat transfer coefficients, assessment of the flow pattern in film-wise or forced convection condensation can be made without the aid of flow visualization.

Nusselt number versus quality at various mass fluxes for different temperature differences are presented in Figure 4.13 through 4.20. As the mass flux increases, the dependence of heat transfer on temperature difference diminished. In other words, the film condensation mechanism was replaced by convective condensation as mass flux increased. As pointed out by Nusselt theory, the Nusselt number of film condensation was lower for the higher temperature difference, which can be seen on Figures 4.13 through 4.15 for mass flux, G, from 60 to 185 klb/ft^{2}hr. To validate the temperature difference effect on Nusselt theory, the quantity $Nu/(GaPr/Ja)^{0.25}$ was plotted against quality for four different mass fluxes in Figures 4.21 through 4.24. For film condensation, the effect of temperature difference is eliminated and the data merge into one single trend, which is displayed in Figure 4.21 for G=60 klb/ft^{2}hr. As mass flux increases, data began to depart from one single trend, as shown in Figures 4.22 through 4.24, which indicates that the mechanism of condensation has changed from film-wise to convection-wise. At G=230 klb/ft^2hr of Figure 4.24, there apparently are different trends at each temperature difference.

4.3 Correlation Comparison

In order to assess experiment data, some well-known condensation heat transfer correlations were referred to and compared. Because of the different condensation mechanisms involved, two categories of correlations were selected. For the high mass flux data, the annular flow type correlation of Akers et al. [2], Azer [5], Cavallini et al. [13], Shah [47], Chen [15], Dobson et al. [21], and Traviss et al. [58] were compared with the data. The film condensation correlation of Chato [14], and Jaster et al. [31] were campared with data in the low mass flux, wavy flow. Only the best predictors (Akers and Jaster et al.) are shown in the following section; however, the predictions of the rest correlations are compiled in the appendix.

4.3.1 Annular Flow Correlation (700 points out of 800 data points)

As pointed out in the chapter two, three types of approaches were encompassed in those correlations. Akers, Cavallini, Shah, and Dobson's were two-phase multiplier type. Azers used boundary layer analysis to develop a correlation. A shear-based correlation was proposed by Chen.

The predictions of the Akers correlation are shown in Figures 4.25 and 4.26. An equivalent Reynolds number with the same wall shear stress as the two-phase flow is introduced in Figure 4.26. The correlation provides good agreement with the experimental data, with a mean deviation of 15.2%. Most of the data (83.7%) were predicted within +/-25%. The correlation tended to over-predict data at high mass fluxes with lower quality. On the other hand, it seemed to underestimate data with low mass flux, where wavy flow pattern prevailed. In general, the Akers correlation covered extended ranges of flow conditions with fairly satisfactory predictions.

4.3.2 Gravity-dominated correlation (250 points out of 800 data points)

Figure 4.27 displays the prediction of the Jaster correlation. By taking the void fraction into consideration, Jaster and Kosky accounted for the liquid pool depth and quality variation. The prediction was much improved over the Chato correlation and agreed well with the experimental data. The mean deviation between the experimental data and predicted values is 16.3%, and most are within +/-25%.

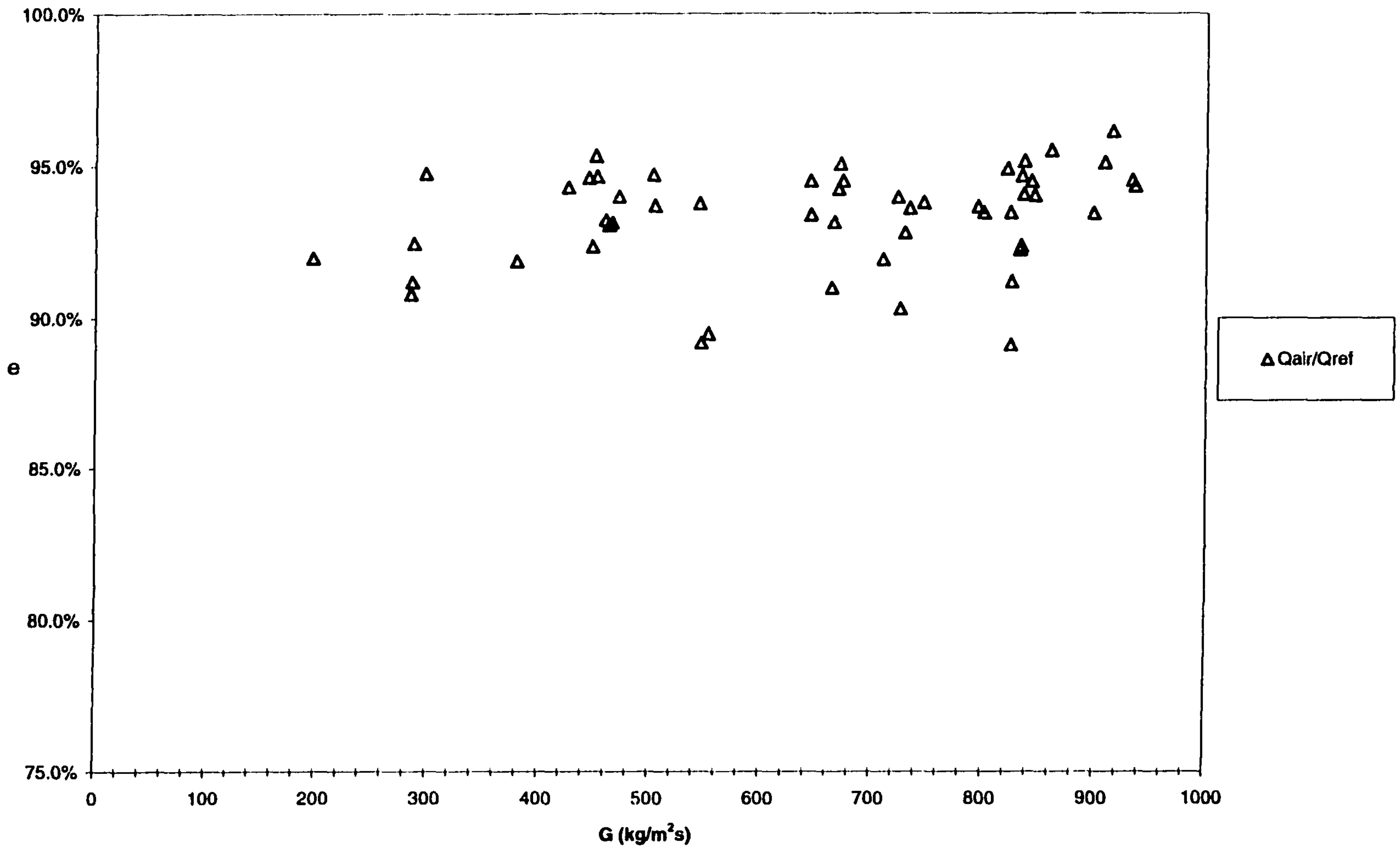

Fig 4.1 The Subcooled Liquid Energy Balance

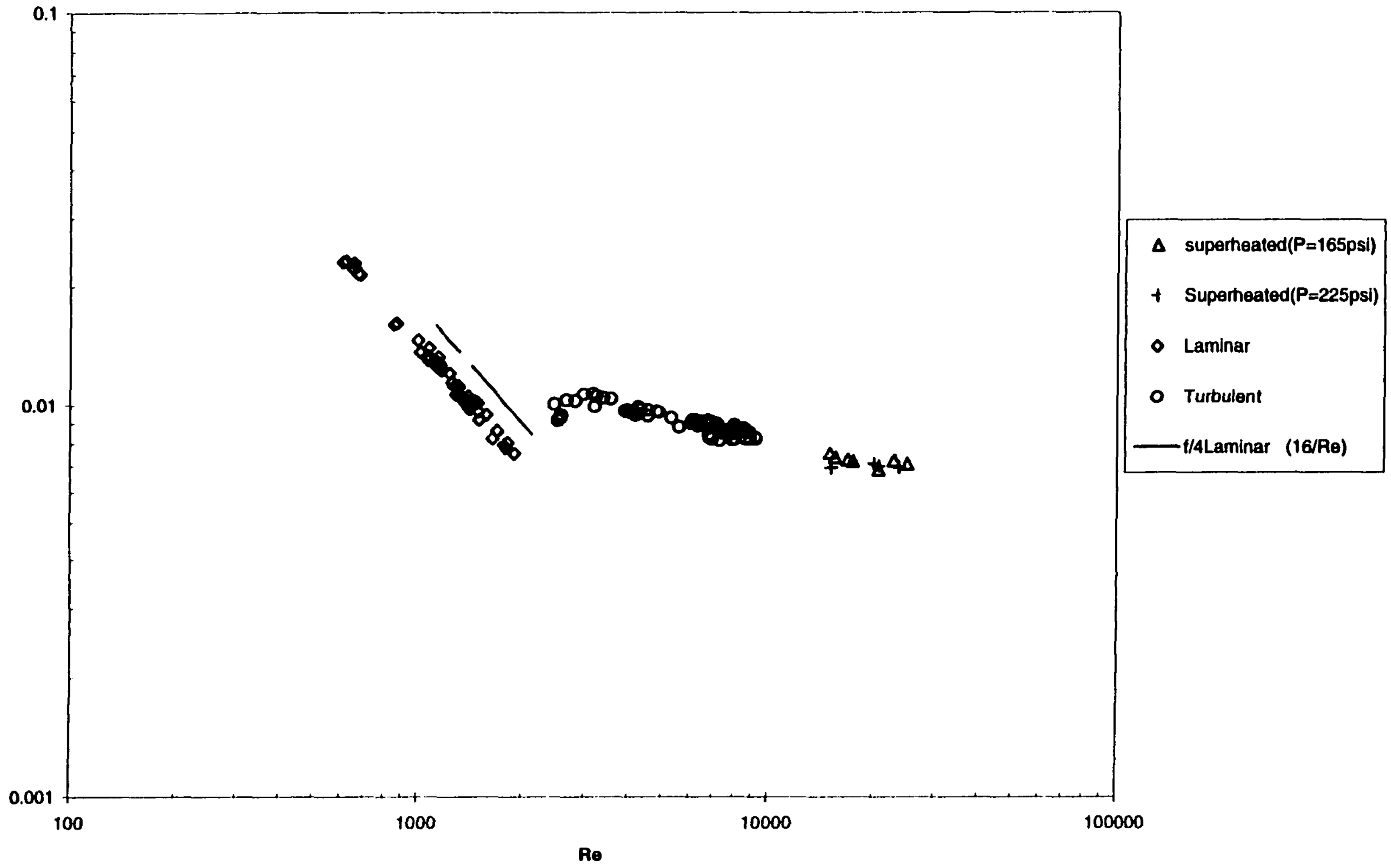

Figure 4.2 Friction Factor of Single-Phased R134a Based on the Measured Reynolds Number

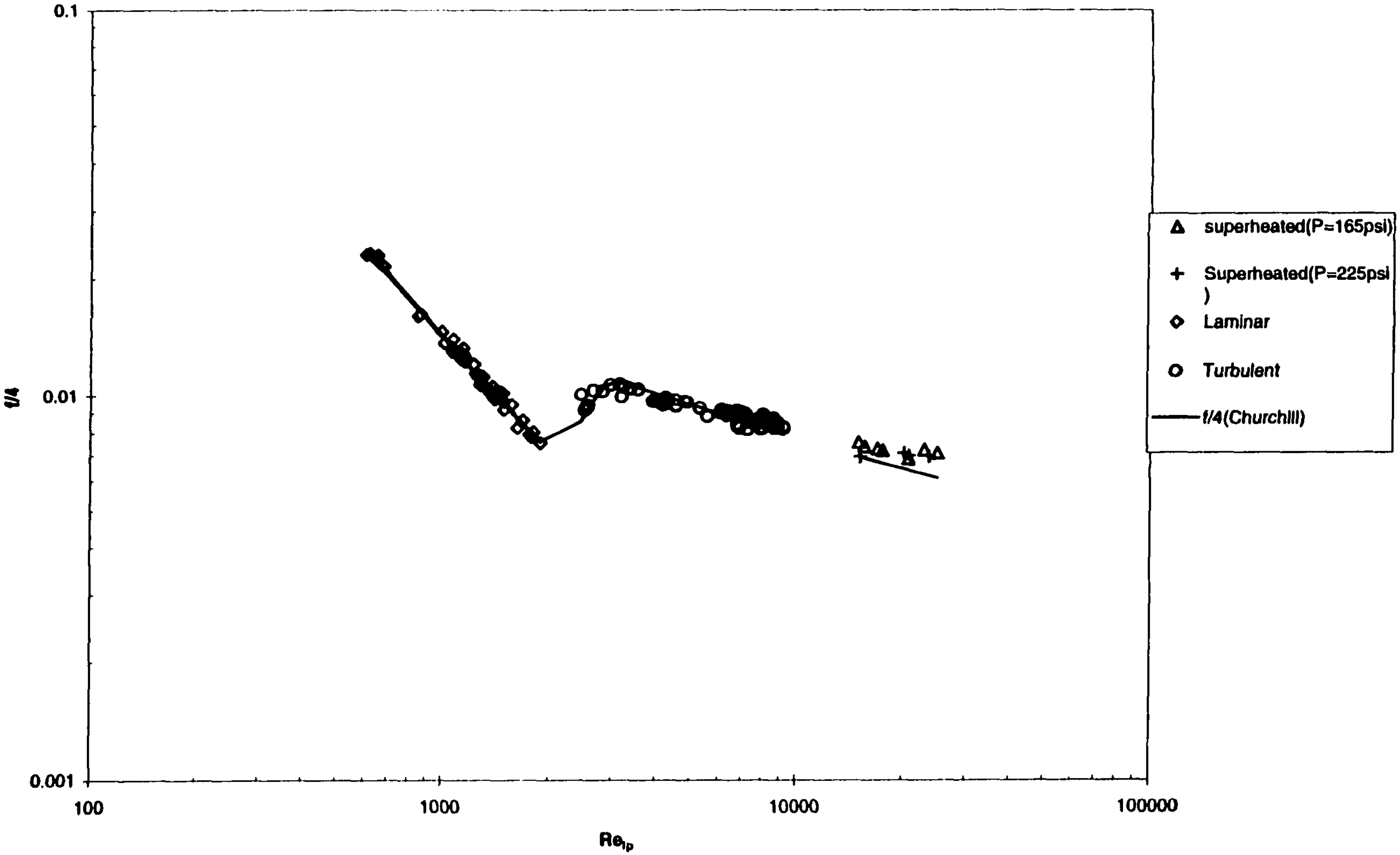

Figure 4.3 Friction Factor of Single-Phased R134a Based on the Modified Reynolds Number

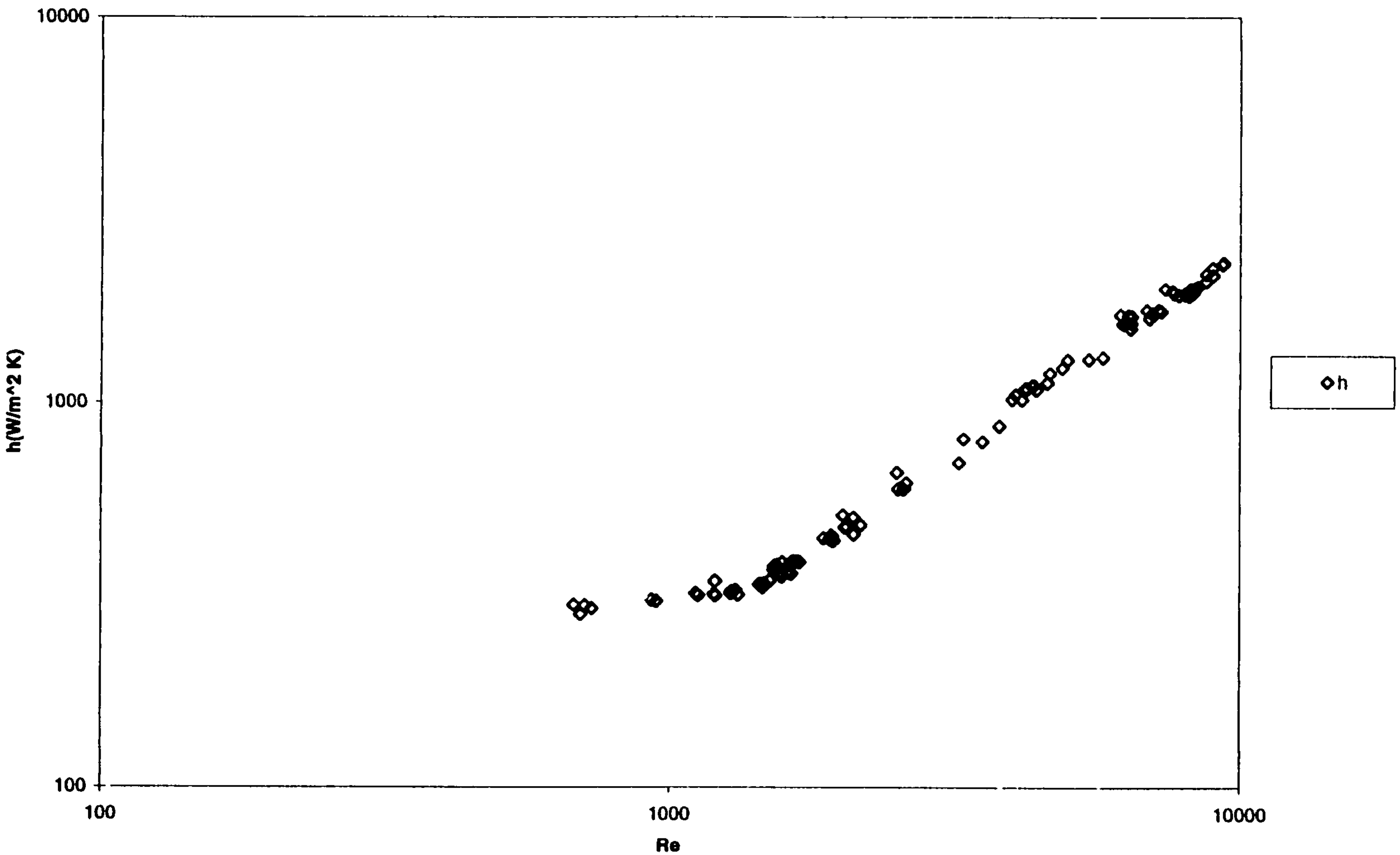

Figure 4.4 The Subcooled Liquid Heat transfer Coefficient vs. Reynolds Number

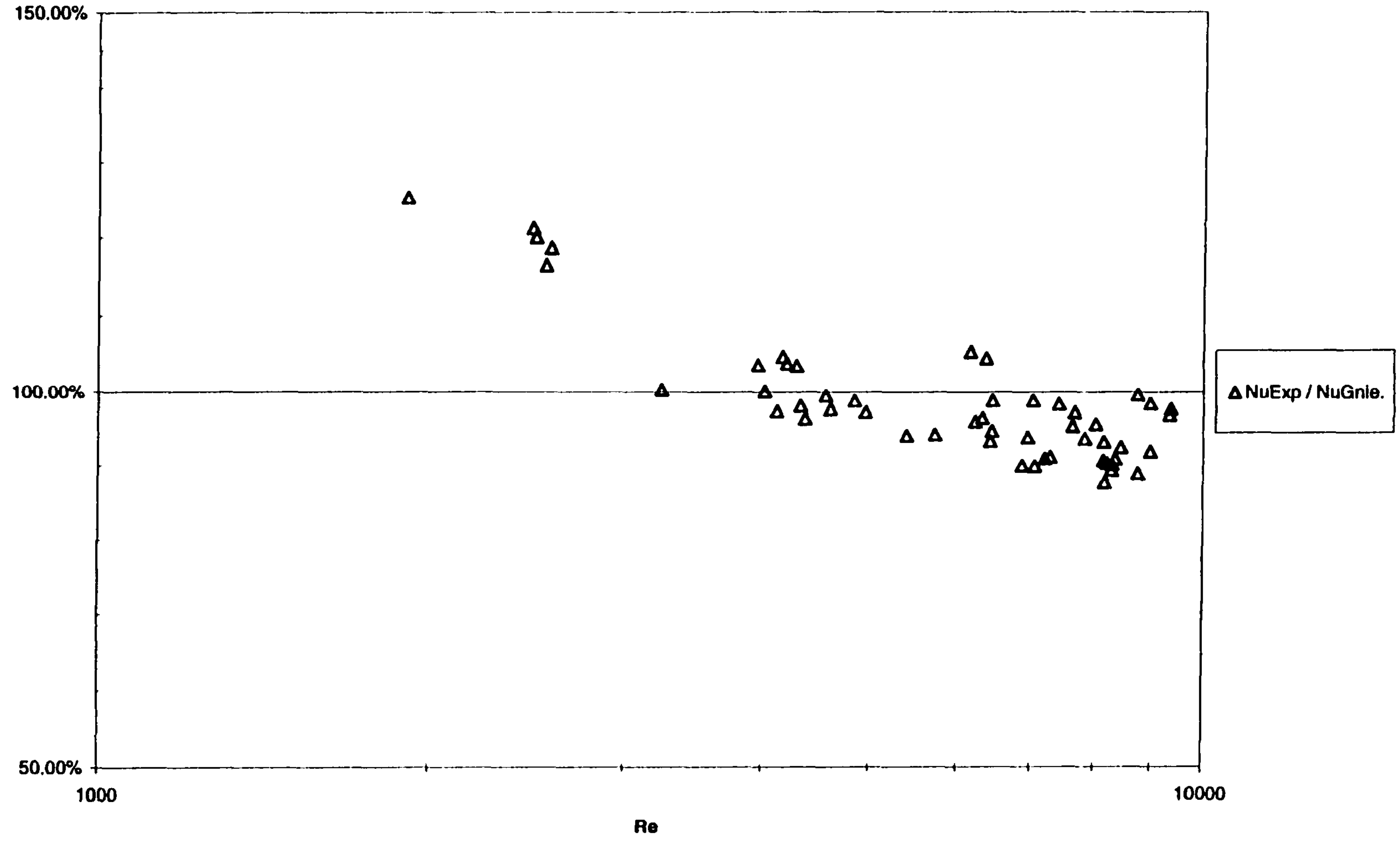

Figure 4.6 The Comparison of Experimental Data with Predictions of Gnielinski Correlation for the Subcooled Liquid

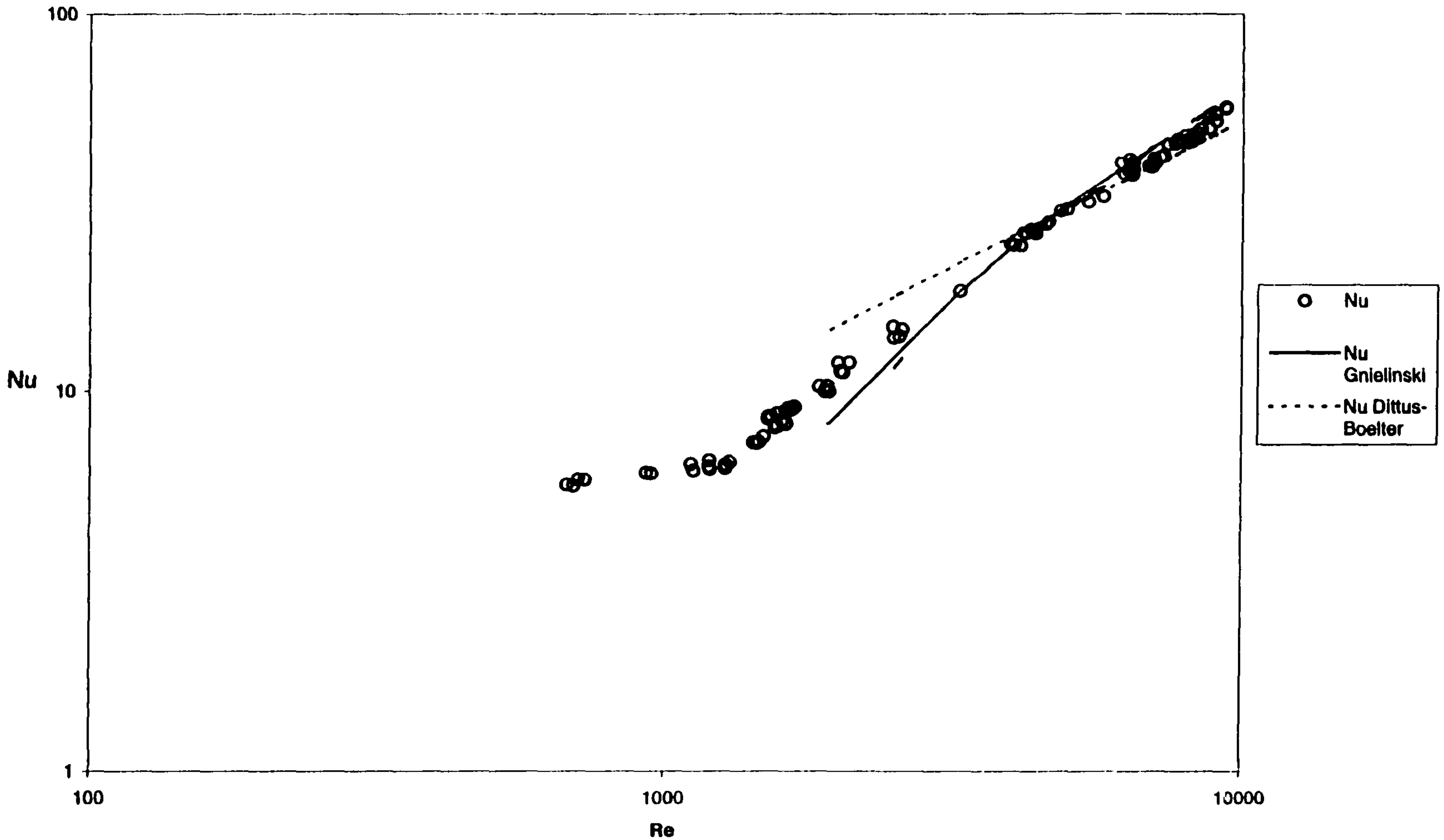

Figure 4.5 The Nusselt Number of the Subcooled Liquid vs. Reynolds Number

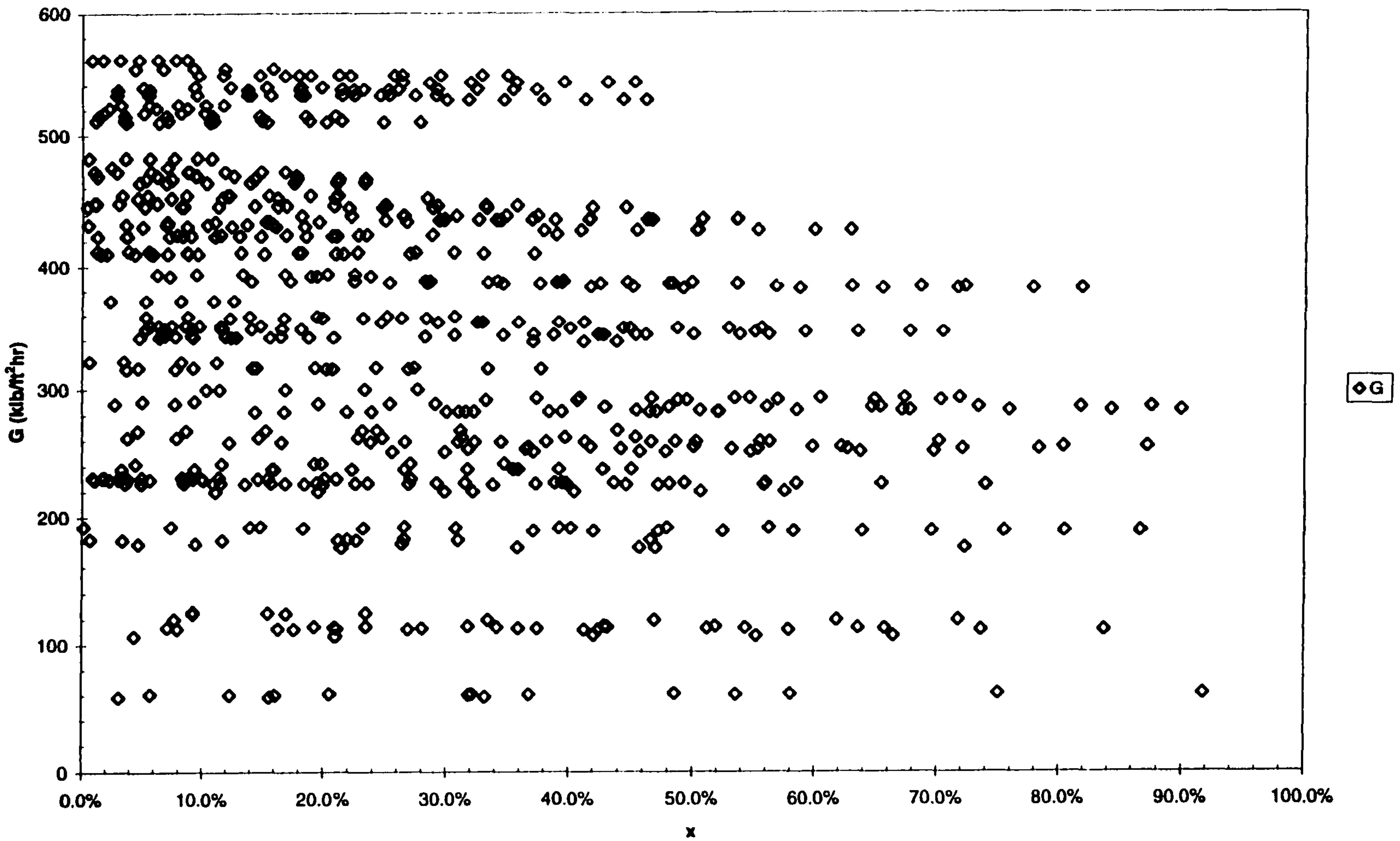

Figure 4.7 Mass Flux vs. Quality

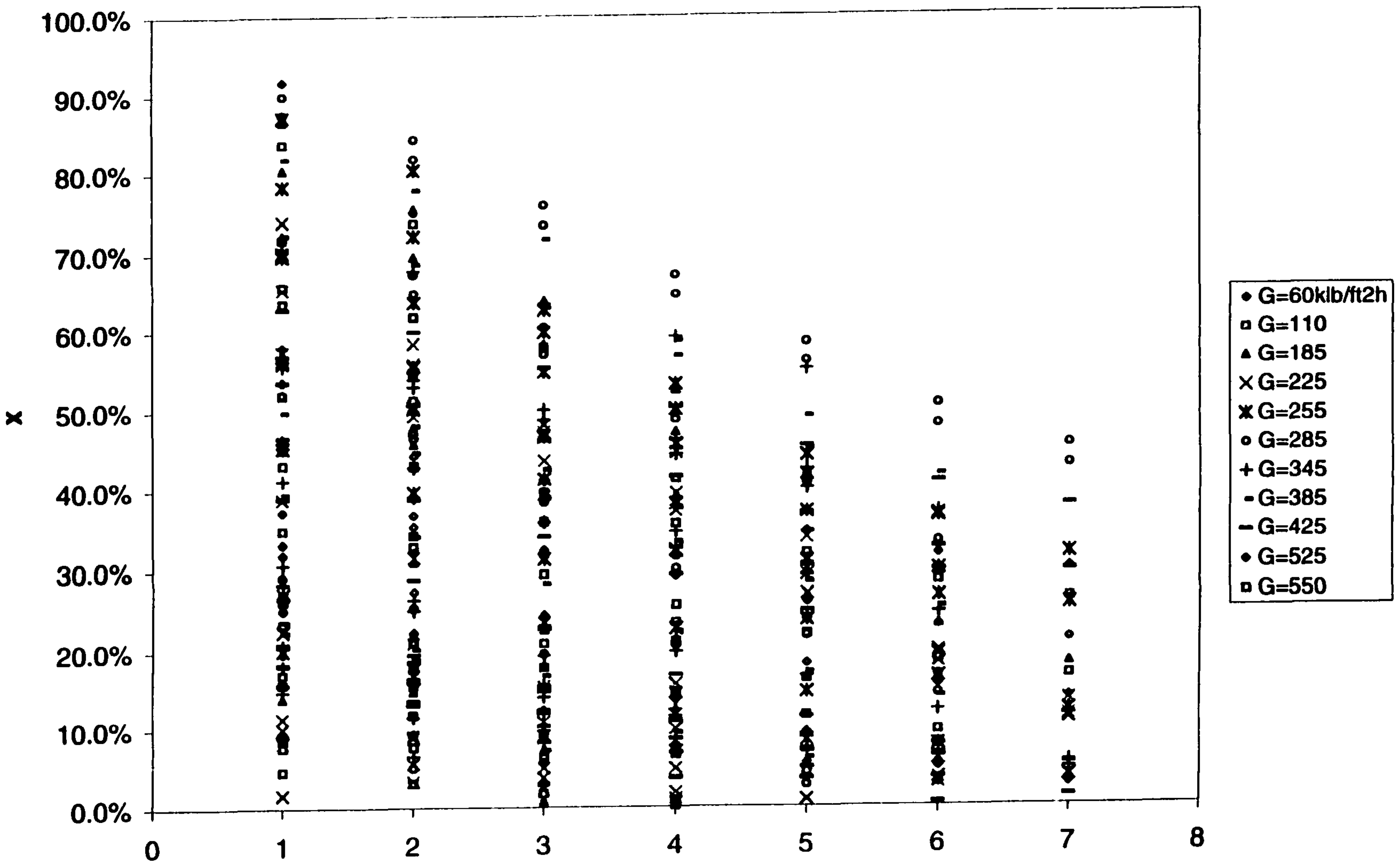

Figure 4.8 Qulaity Change along Tube Segment at Various Mass Fluxes

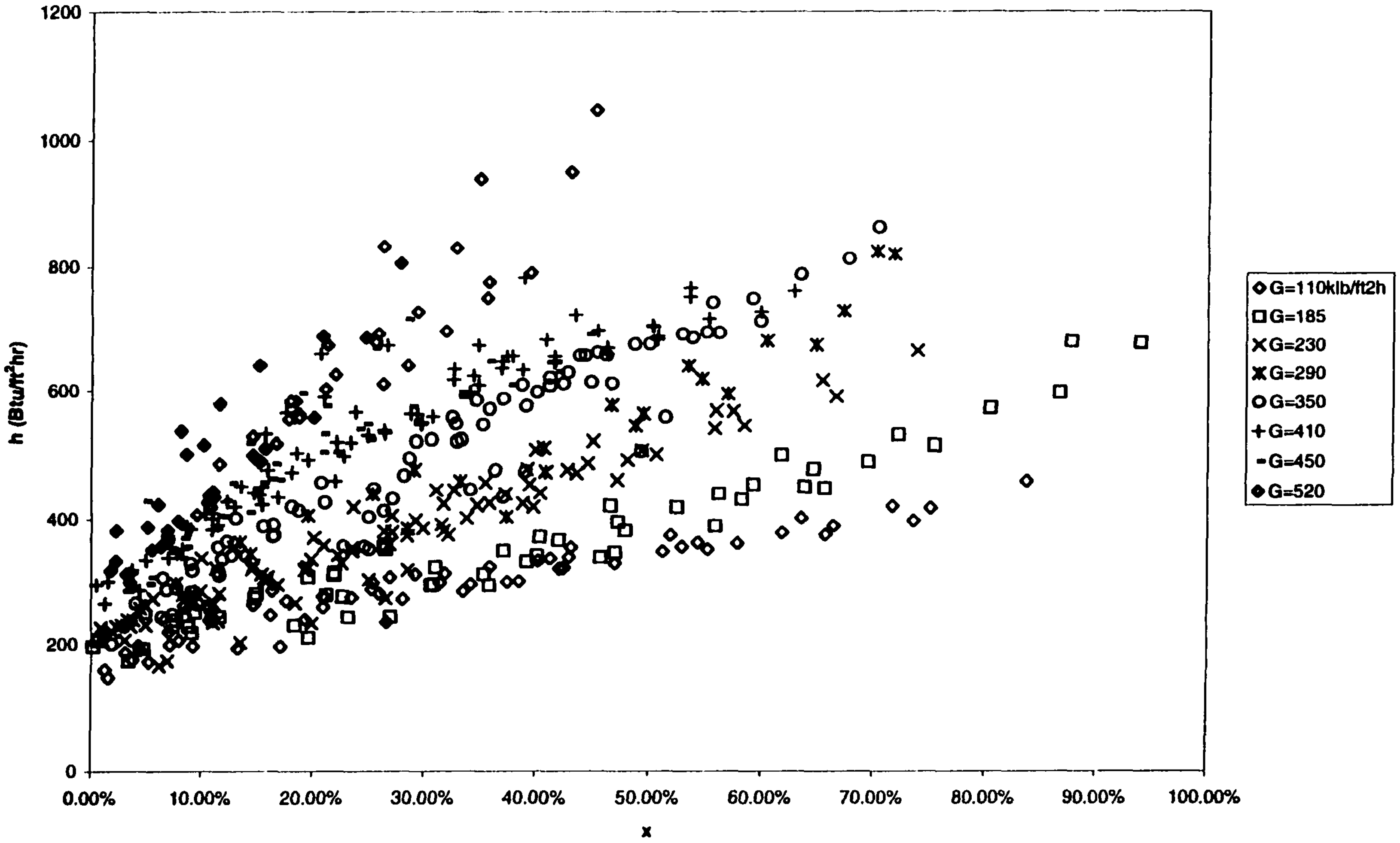

Figure 4.9 Heat Transfer Coefficient vs. Quality

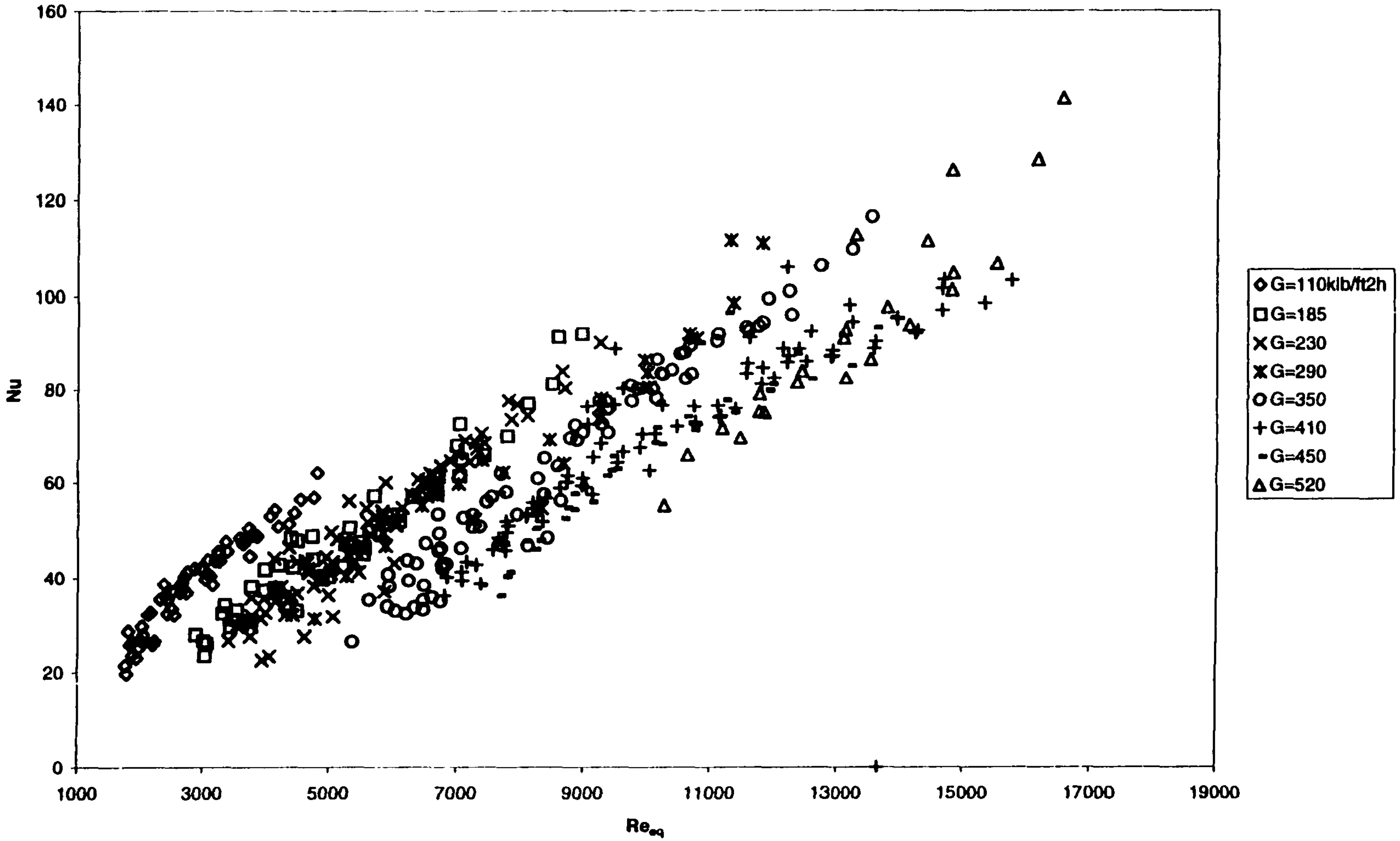

Figure 4.10 Nusselt Number vs. Equivalent Reynolds Number

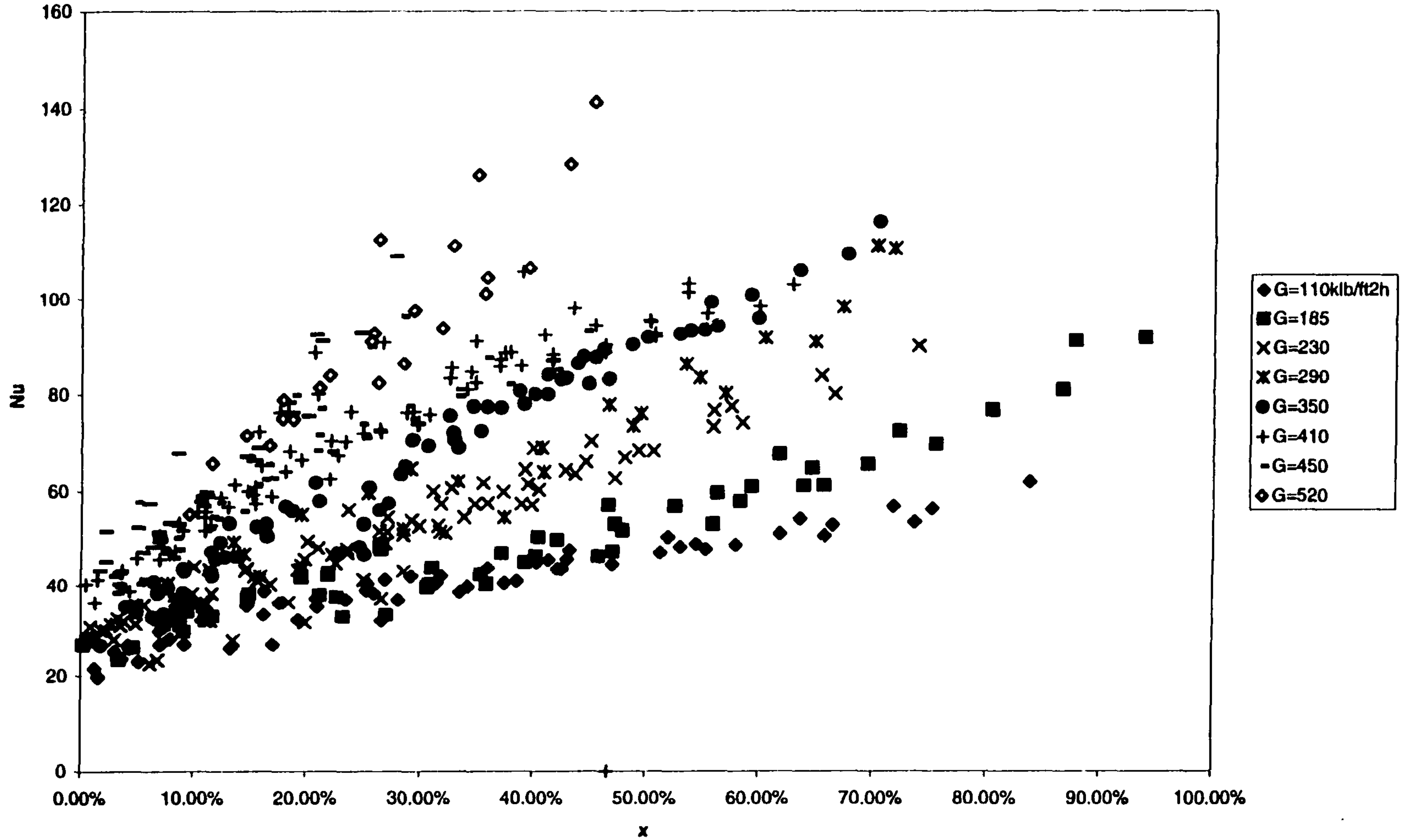

Figure 4.11 Nusselt Number vs. Quality

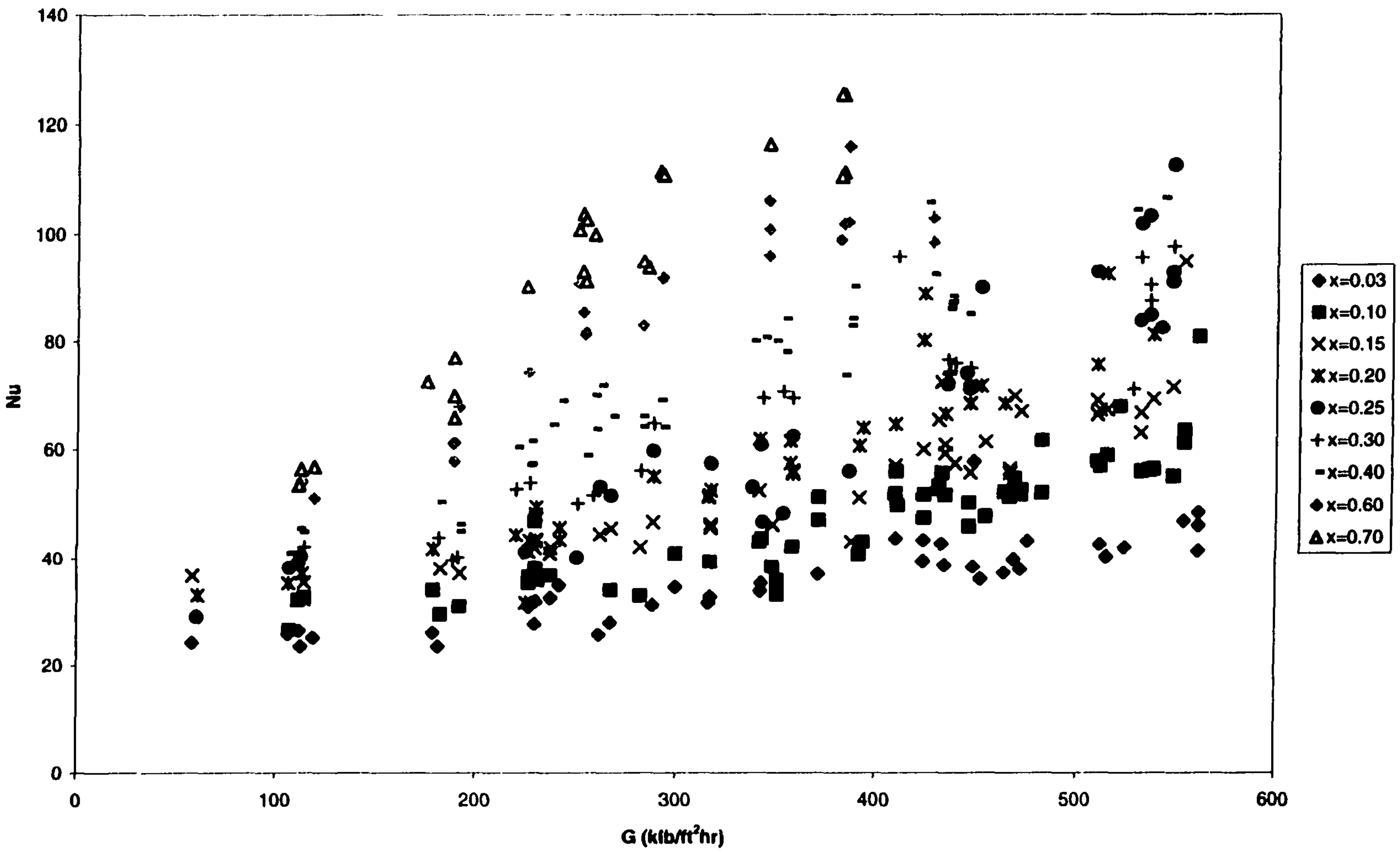

Figure 4.12 Nusselt Number vs. Mass Flux

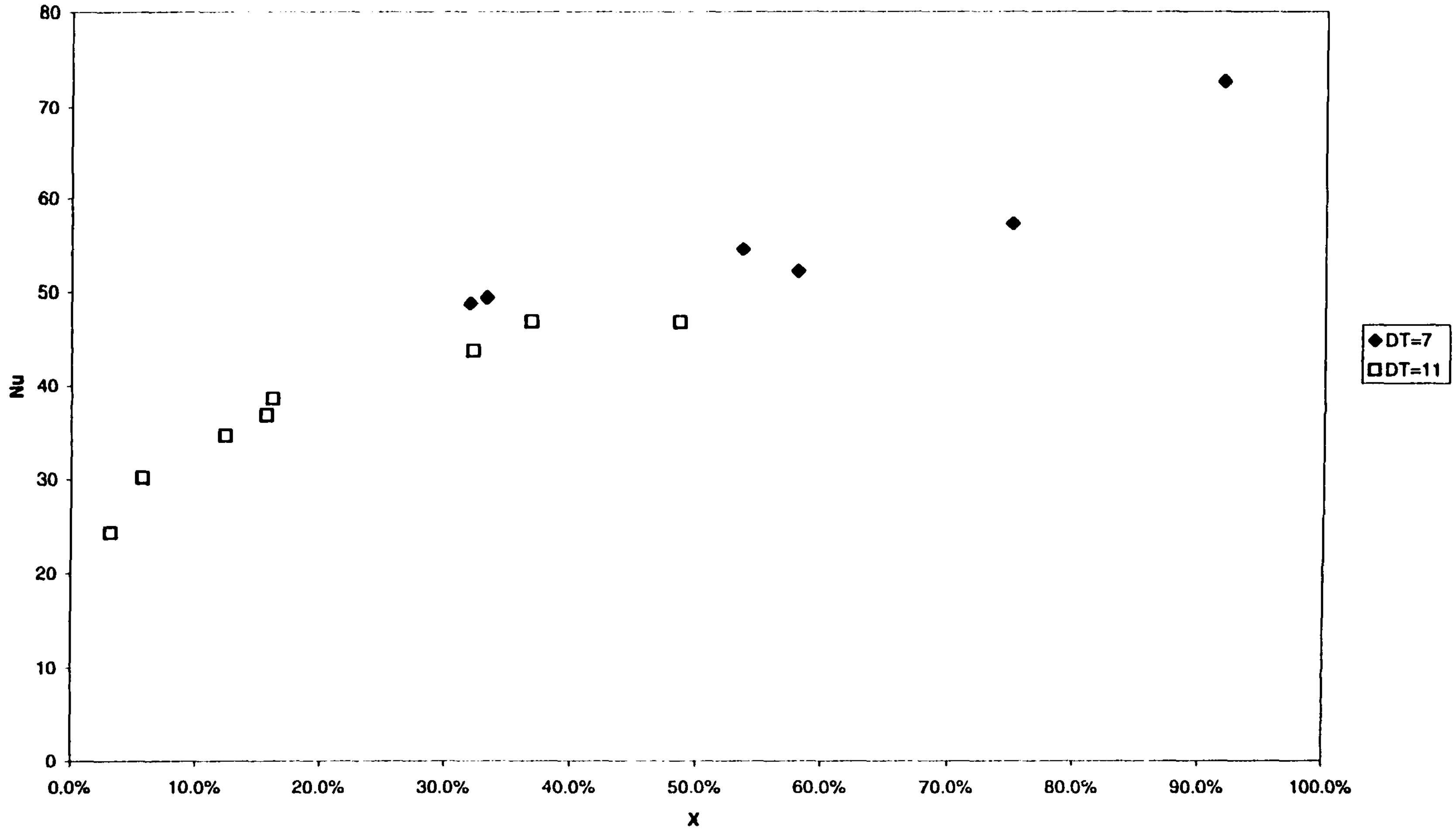

Figure 4.13 The Temperature Difference Effect for G=60klb/ft^{2}hr

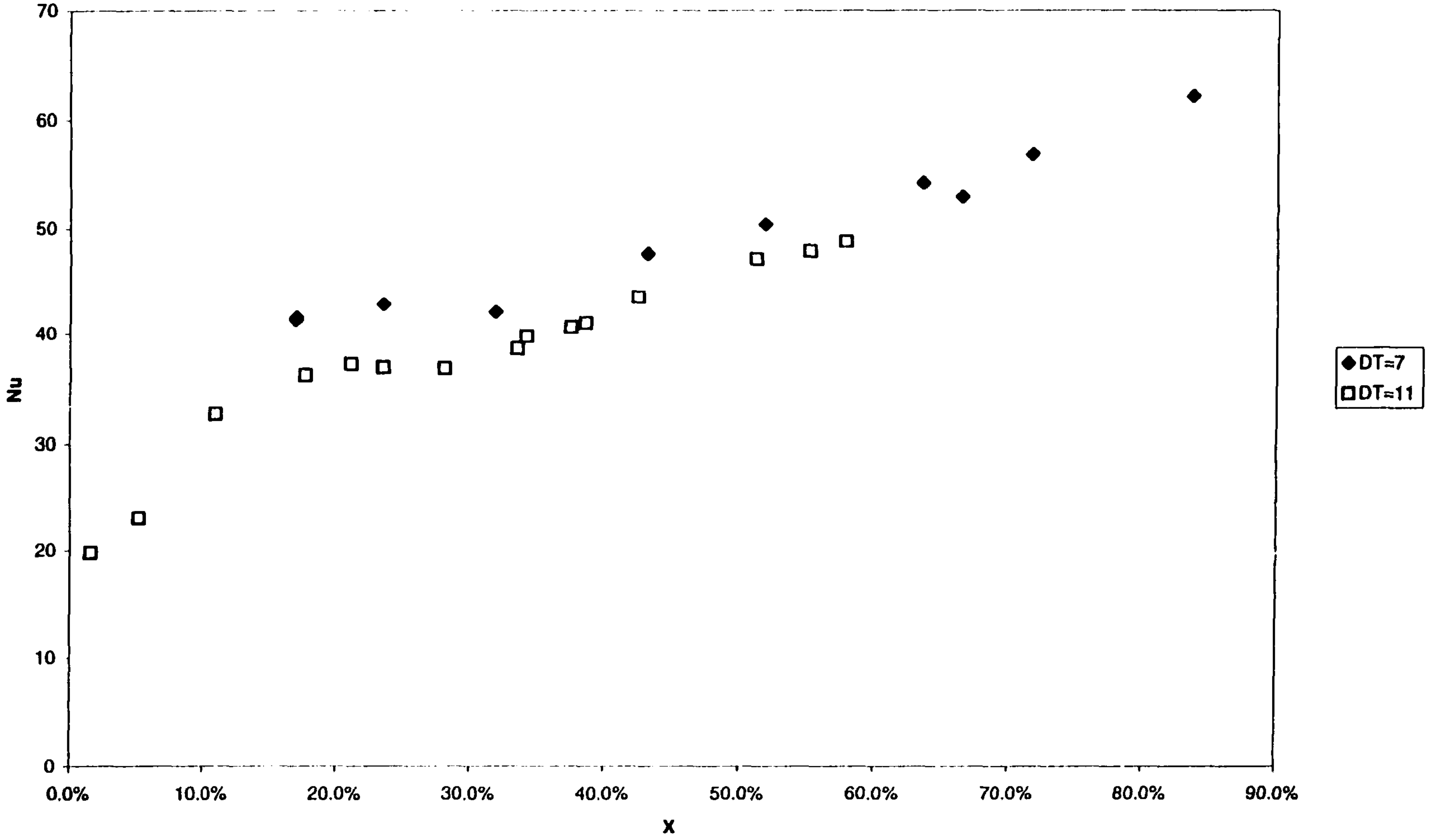

Figure 4.14 The Temperature Difference Effect for G=115 klb/ft^{2}hr

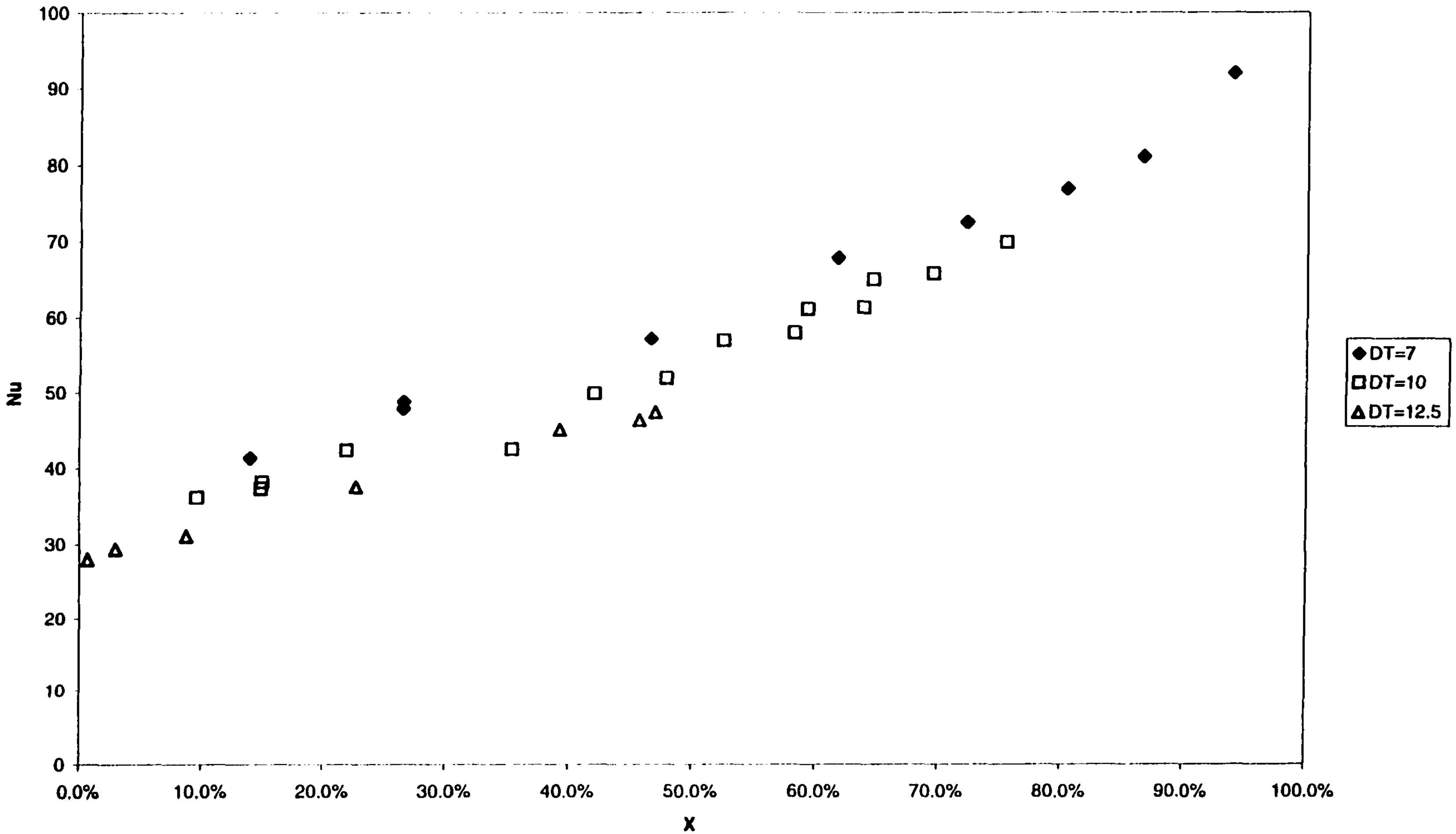

Figure 4.15 The Temperature Difference Effect for G=185 klb/ft2hr

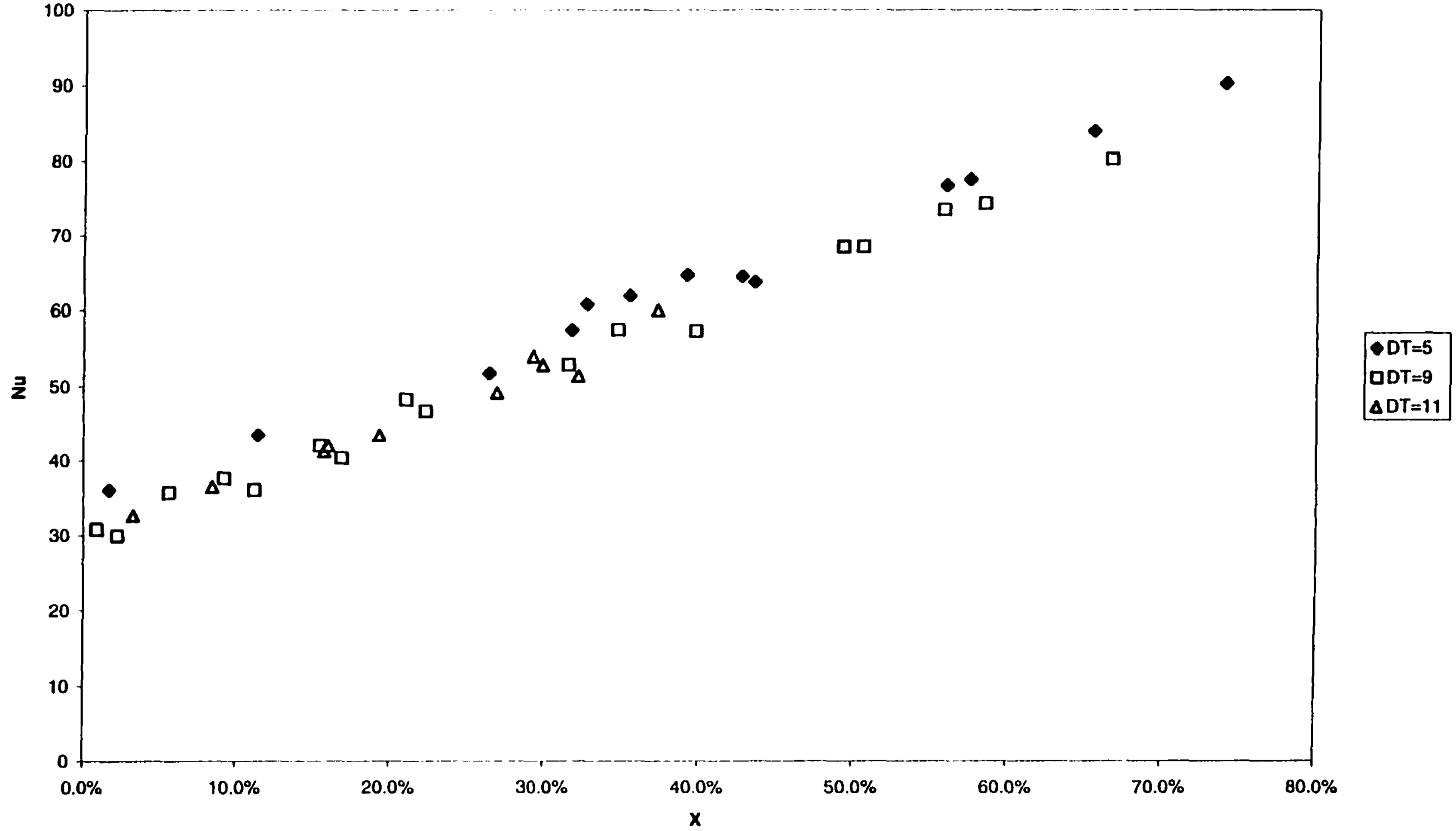

Figure 4.16 The Temperature Difference Effect for G=230 klb/ft^{2}hr

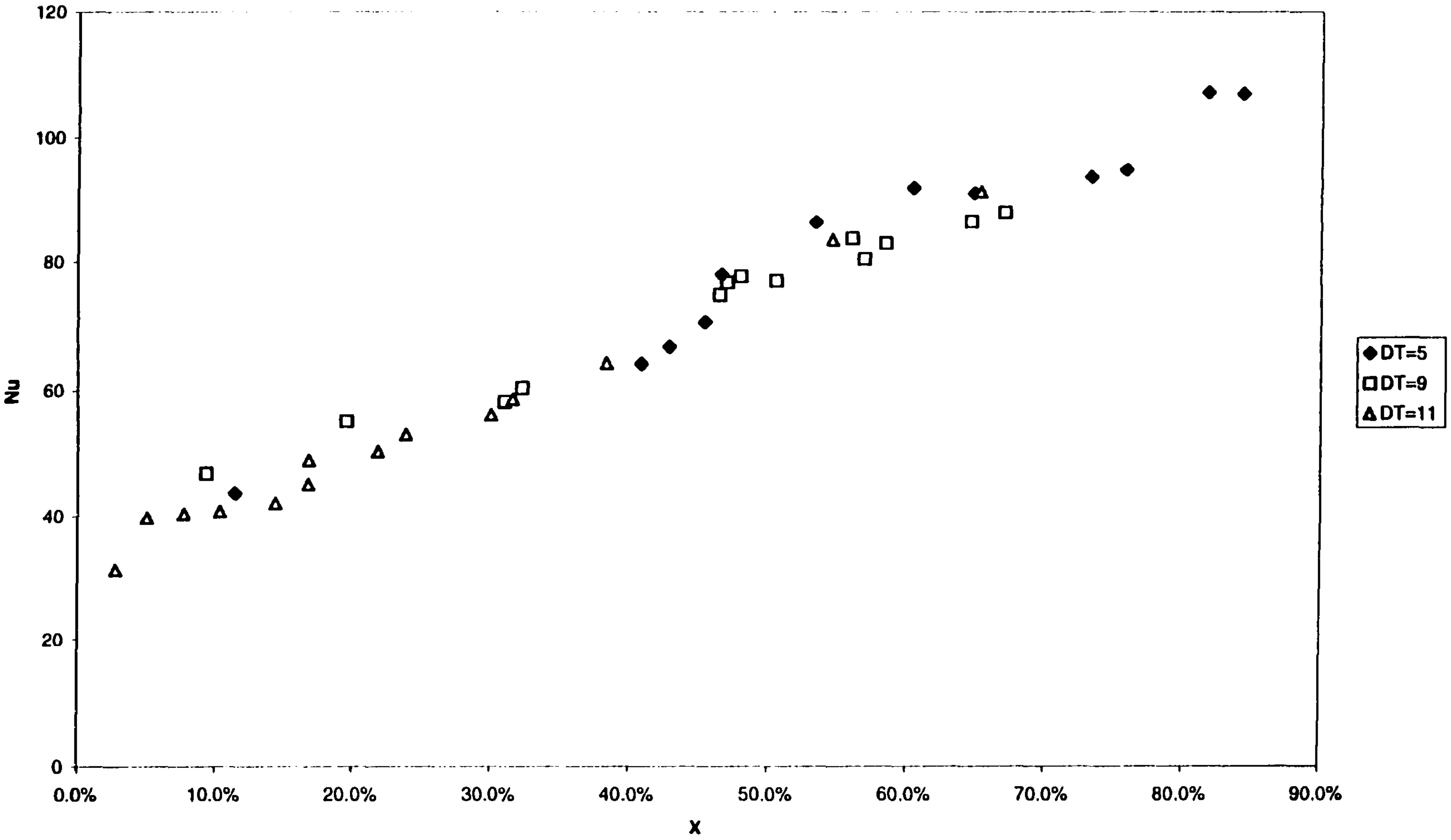

Figure 4.17 The Temperature Difference Effect for G=290 klb/ft^{2}hr

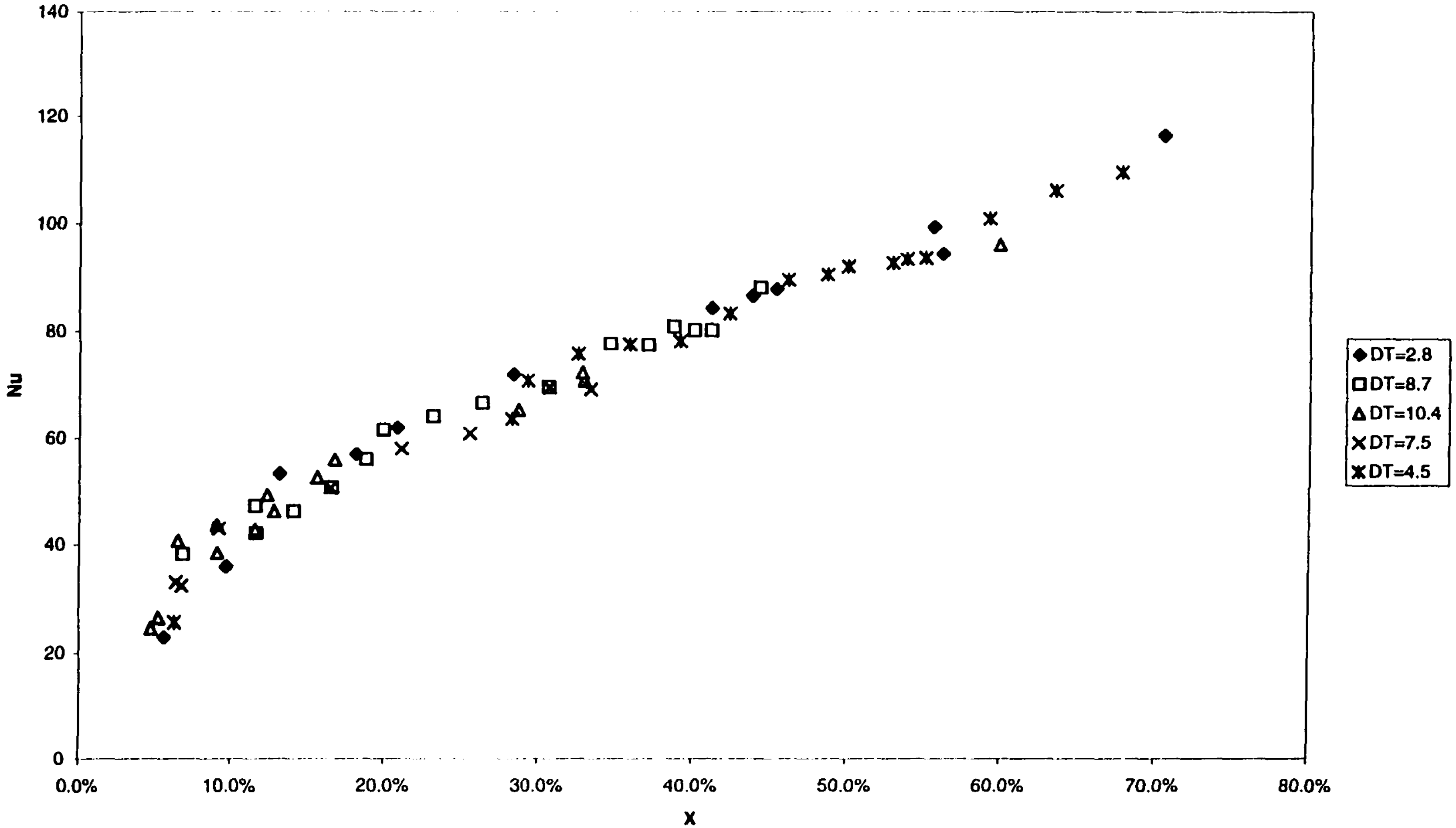

Figure 4.18 The Temperature Difference Effect for G=350 klb/ft^{2}hr

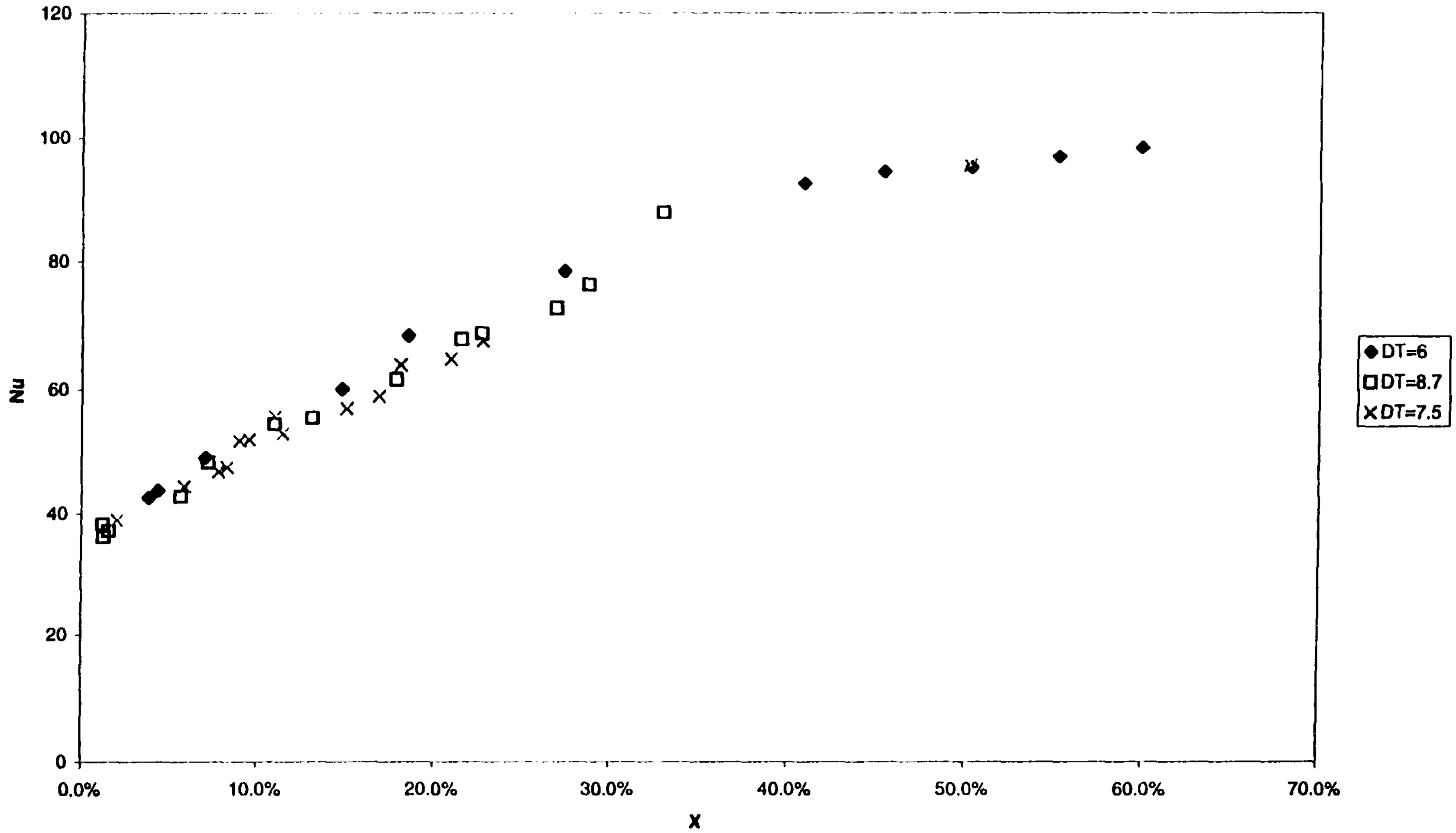

Figure 4.19 The Temperature Difference Effect for G=415 klb/ft^{2}hr

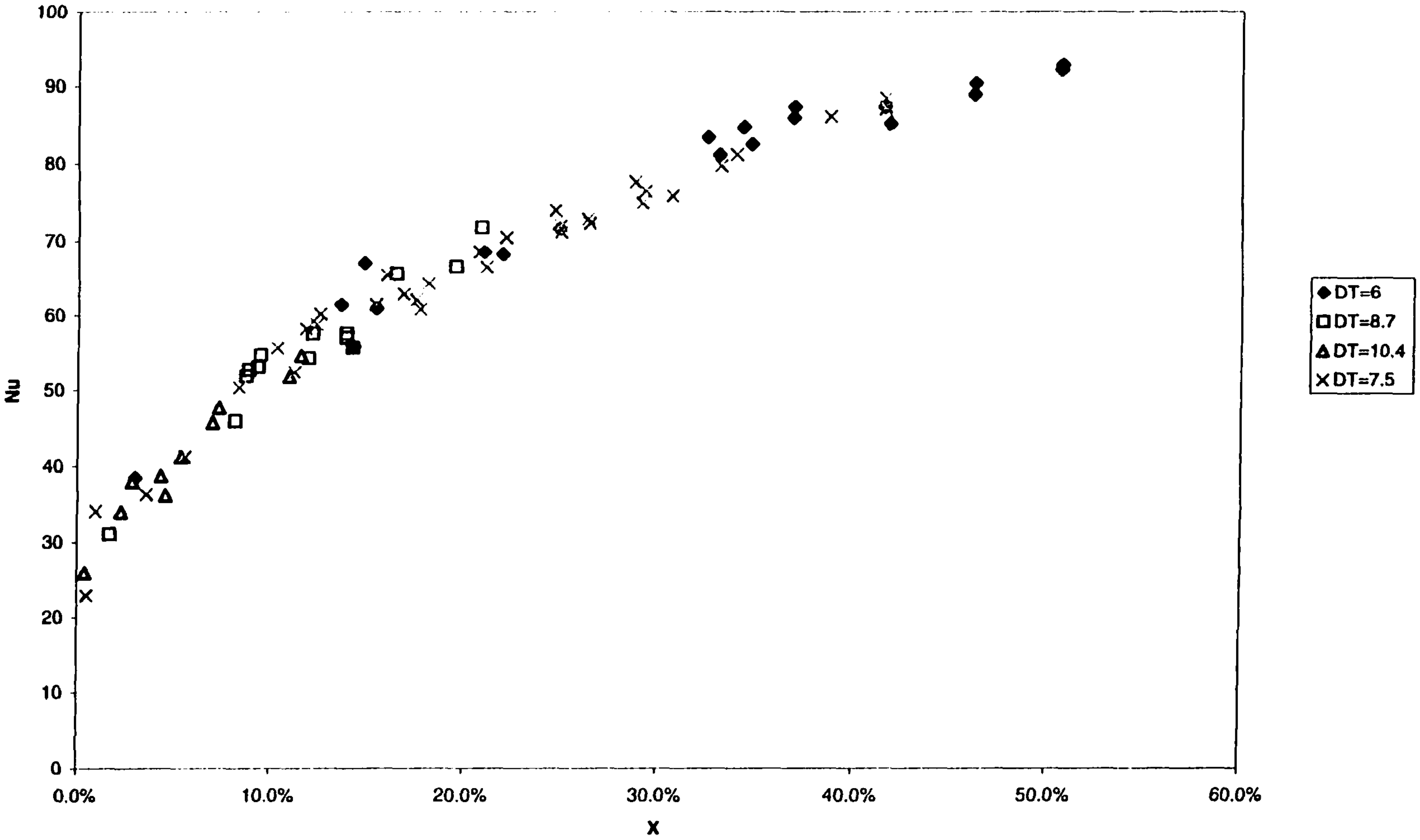

Figure 4.20 The Temperature Difference Effect for G=460 klb/ft^{2}hr

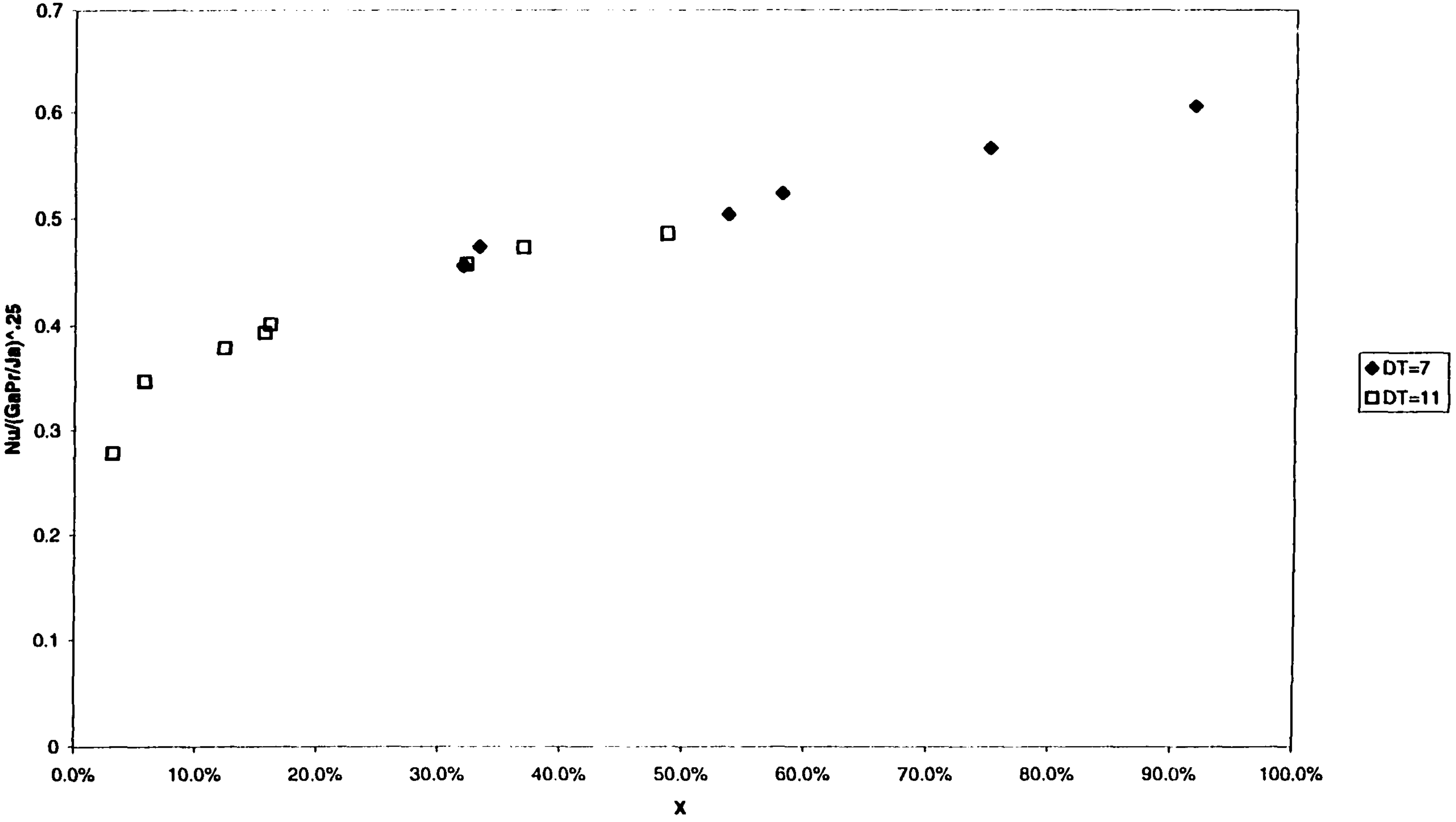

Figure 4.21 The Temperature Difference Effect on $Nu/(GaPr/Ja)^{0.25}$ for $G=60\ klb/ft^2hr$

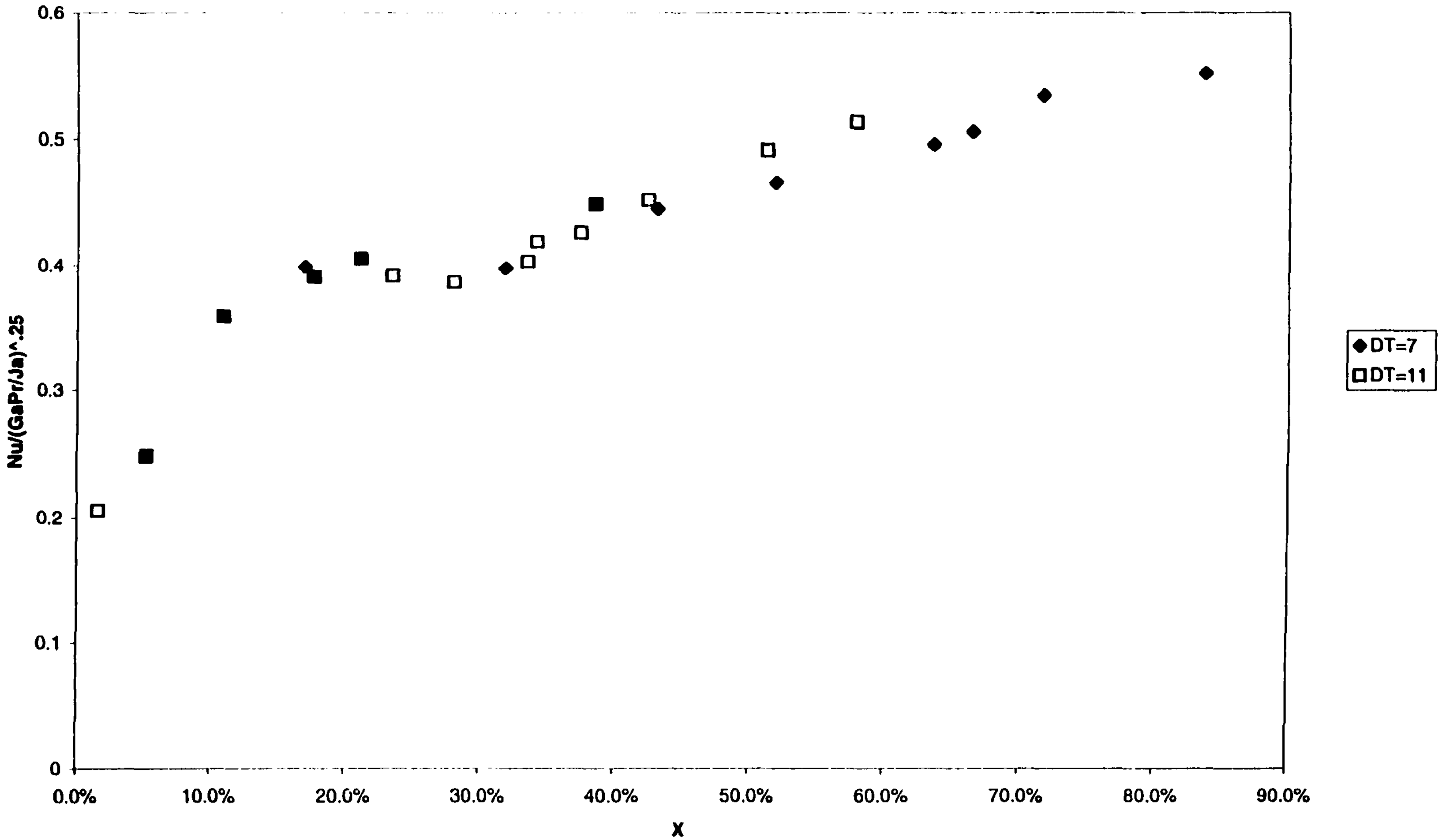

Figure 4.22 The Temperature Difference Effect on $Nu/(GaPr/Ja)^{0.25}$ for G=110 klb/ft2hr

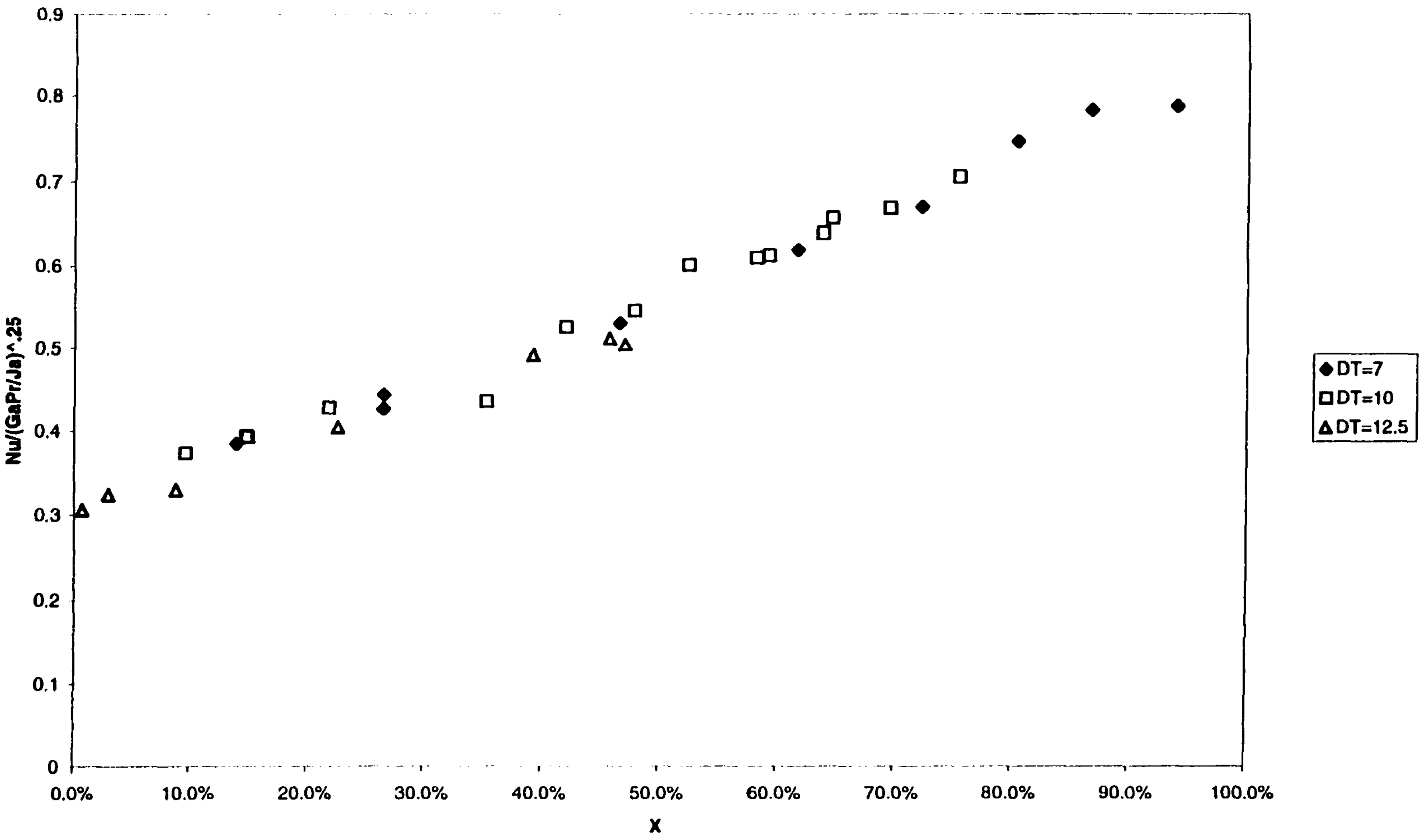

Figure 4.23 The Temperature Difference Effect on Nu/(GaPr/Ja)$^{0.25}$ for G=185 klb/ft^{2}hr

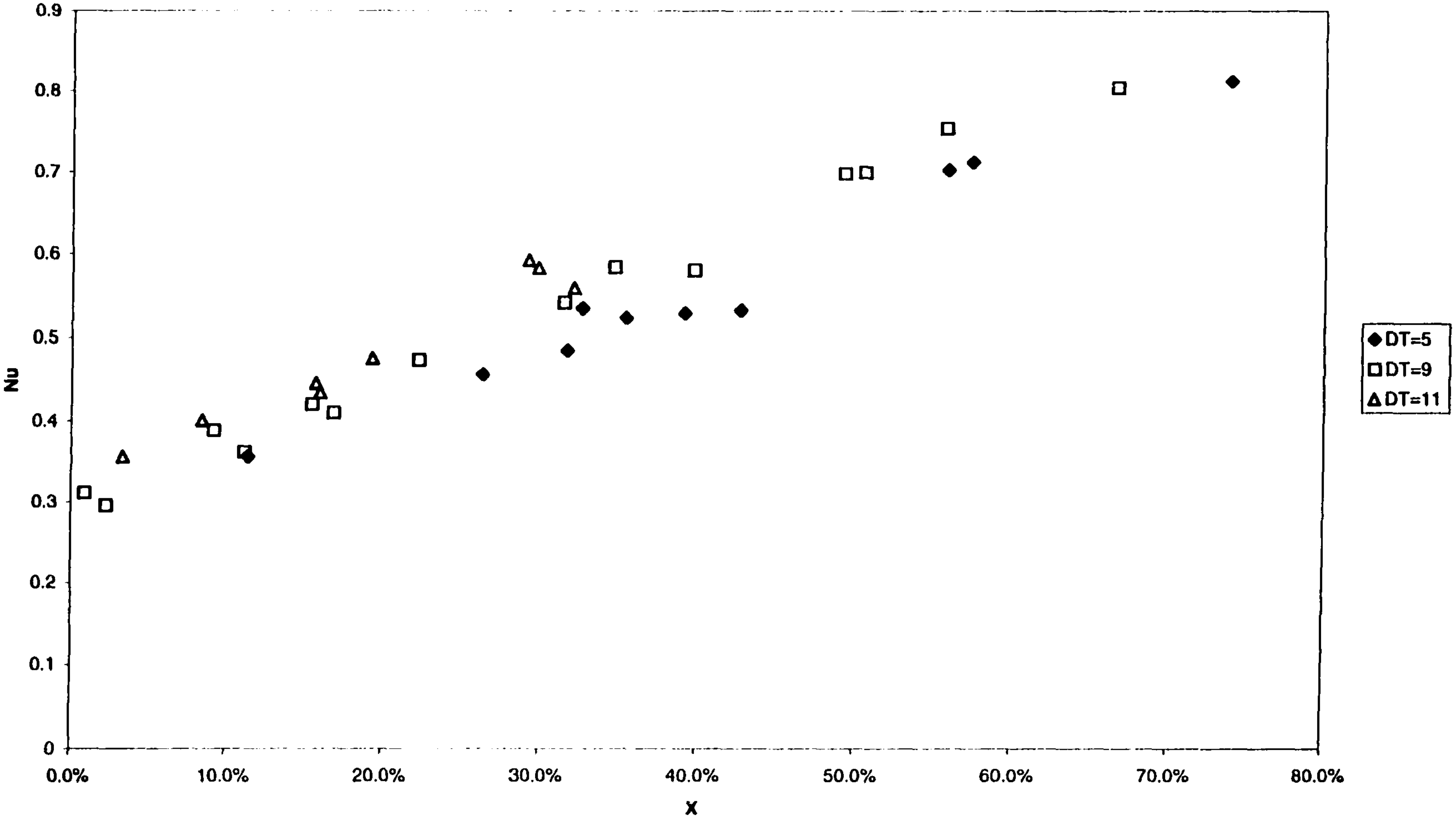

Figure 4.24 The Temperature Difference Effect on Nu/(GaPr/Ja)0.25 for G=230 klb/ft^{2}hr

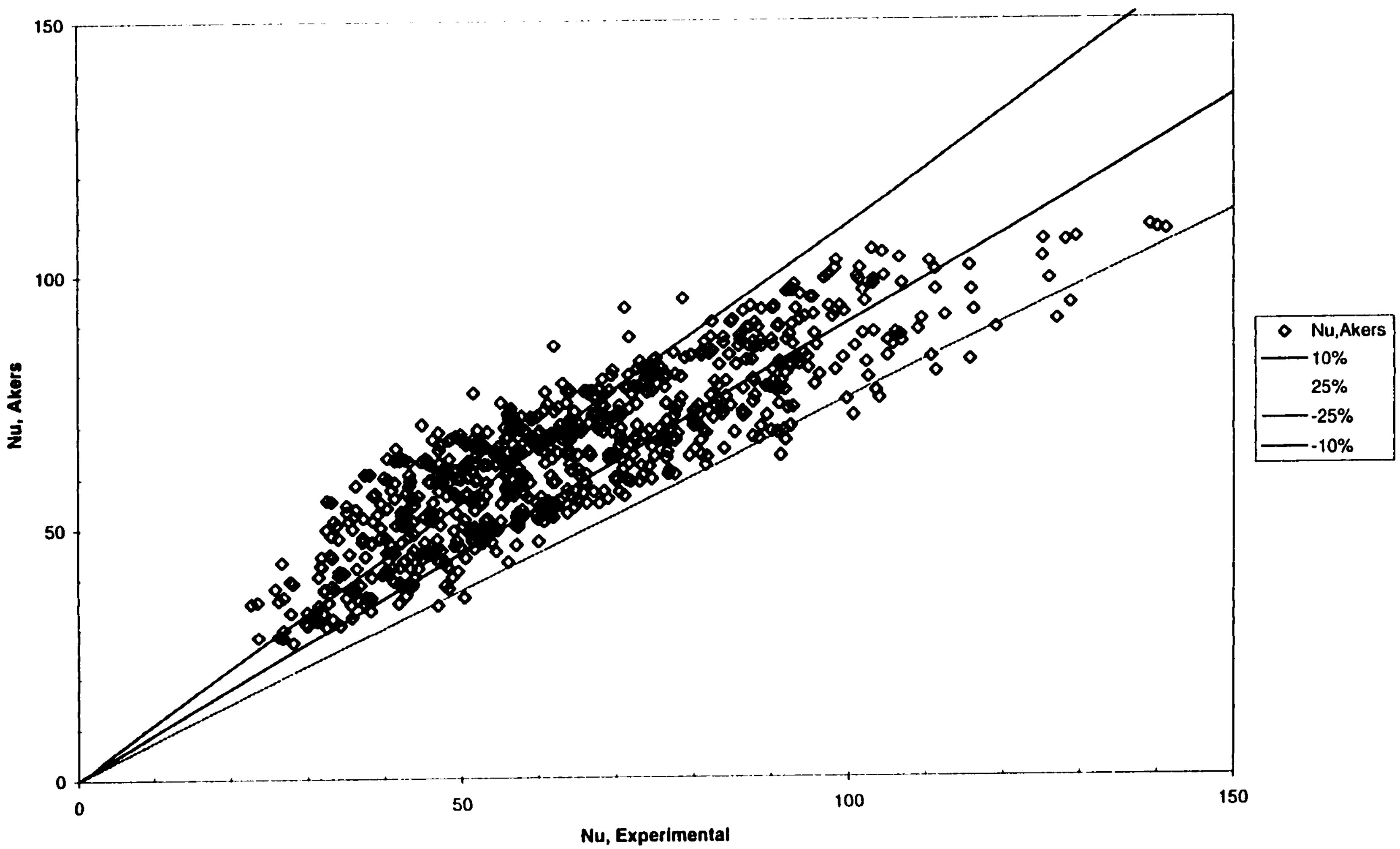

Figure 4.25 Comparision of experimental data with prediction of Akers correlation

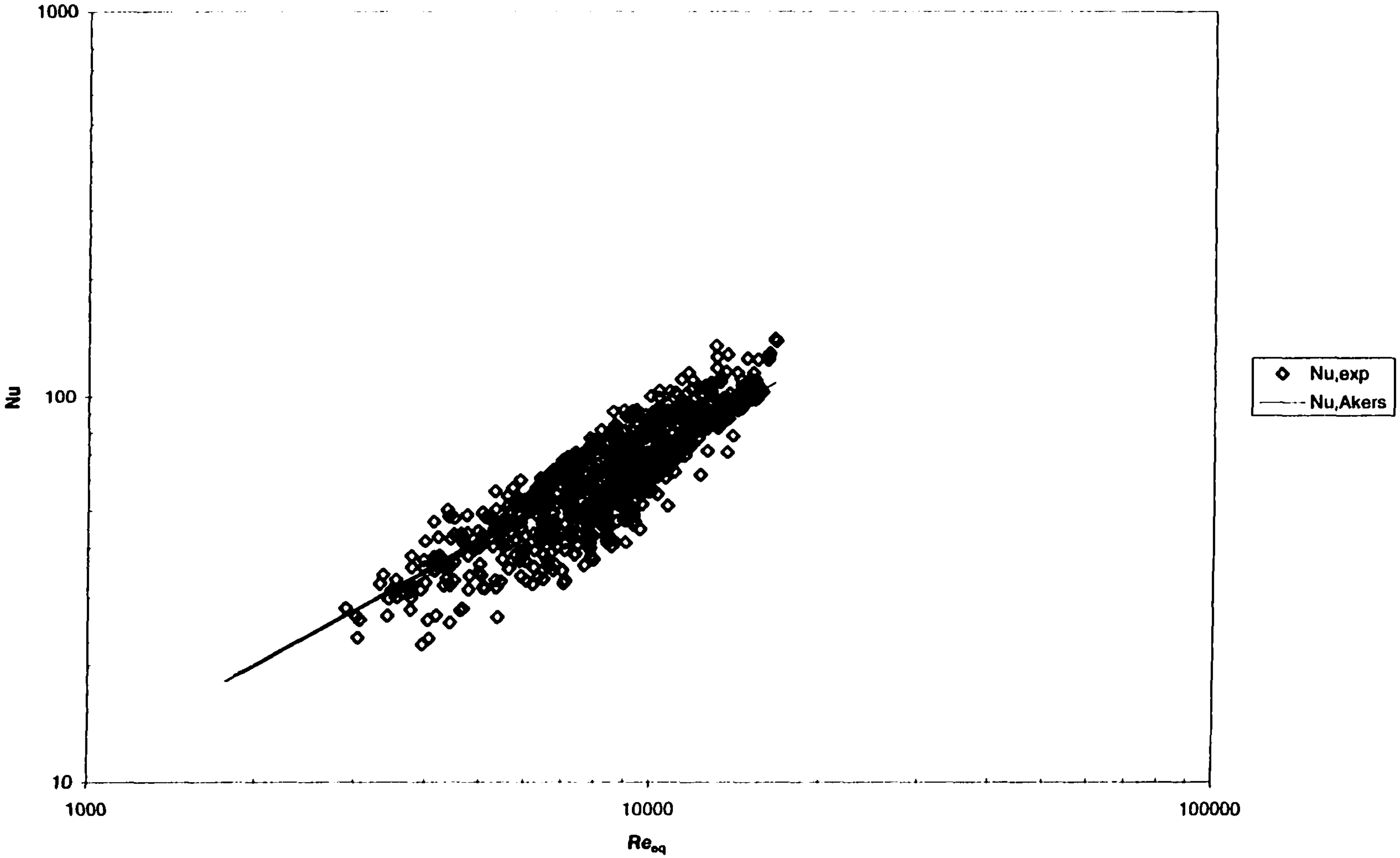

Figure 4.26 Comparision of experimental data with prediction of Akers correlation Based on the Equivalent Reynolds Number

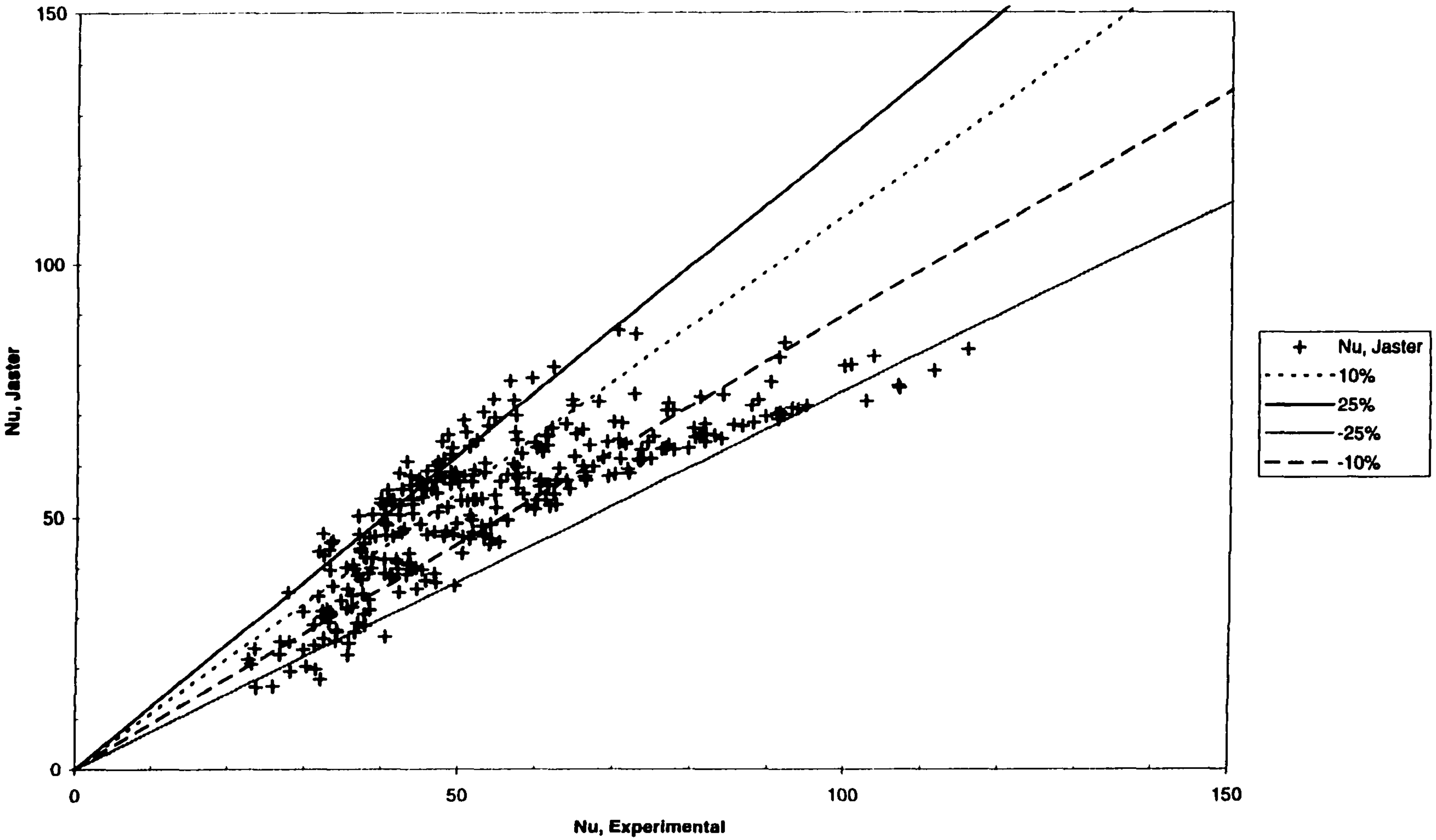

Figure 4.27 Comparison of experimental data with prediction of Jaster correlation

CHAPTER 5

FLOW REGIME VISUALIZATION

5.1 Visualization

5.1.1 Flow regime map

Various flow patterns were observed during the flow visualization. Included were slug flow, wavy flow, wavy-annular, followed by annular flow. The observation results of various mass fluxes are shown in Figure 5.1 by plotting j_v^* against X_{tt}. Categorized by the flow pattern observations, a flow map is generated as Figure 5.2 by choosing j_v^* and X_{tt} as coordinates.

The quality and mass flux are major factors affecting flow pattern distributions. At a specific mass flux, as the quality increased from zero, slug flow was initially seen, then some wavy pulses were observed. As the frequency of the pulse increased, the wavy-annular pattern was visualized. When the pulse was fast enough, a continuous liquid film was annularly formed. According to the flow visualization presented in the Figure 5.2, a flow regime map for the microchannel condensation is developed by including wavy/slug and wavy/annular flow patterns in the transitions as shown in figure 5.3. Four flow regimes including annular, dispersed bubble, stratified wavy and slug are separated by the transition zones.

5.1.2 Transitions

As mass flux increased, the flow pattern change occurred at lower quality. As a result, the annular regime would occur over most of the quality range at higher mass fluxes.

For the mass flux of 55 klb/ft^2h, plug / slug flow was observed for a quality less than 0.27, followed sequentially by the wavy flow. The wavy-annular flow began to appear where the quality became greater than 0.45. However, the pure annular regime was observed at 0.88 quality.

At a mass flux of 75 klb/ft^2h, plug/slug flow was observed for a quality less than 0.17, followed sequentially by wavy flow until the quality reached 0.38; then, wavy-annular flow began to appear. Not until the quality reached 0.7, did the annular regime prevail.

As the mass flux increased to 110 klb/ft^2h, the slug/wavy flow was observed to show signs of annular flow at qualities greater than 0.21. The annular regime was visualized when the quality reached 0.42.

When the mass flux reached 185 klb/ft^2h, the transition between slug/wavy and wavy/annular occurred at a quality of 0.14. The flow pattern changed to annular when the quality reached 0.3.

At a mass flux of 220 klb/ft^2h, the change from slug/wavy to wavy/annular occurred at a quality of 0.12. When the quality reached 0.22, the flow pattern became annular flow. Even at a quality of 0.98, annular mist flow was not observed. Both transitions occur at lower qualities, 0.1 and 0.17 respectably, at 250 klb/ft^2h.

For mass fluxes higher than 330 klb/ft^{2}h, annular flow occurred at a quality less than 0.1 and remained for most of the condensation process.

The transitions of flow regimes are summarized as Table 5.1 for various mass fluxes. By plotting the mass flux against the quality, three flow regimes are separated by two transitions shown in Figure 5.4. As the mass flux increases, the transitions occur at lower quality.

MASS FLUX G (klb/ft^{2}h)	SLUG/WAVY TO WAVY/ANNULAR	WAVY/ANNULAR TO ANNULAR
55	X=0.45	X=0.88
75	X=0.38	X=0.7
110	X=0.21	X=0.42
185	X=0.14	X=0.3
220	X=0.12	X=0.22
250	X=0.1	X=0.17

Table 5.1 Transitions of flow regimes

5.2 Verification

Condensation heat transfer is closely related to flow patterns while different condensation mechanisms take place. Predicting flow patterns correctly is the key to a satisfactory heat transfer correlation. Verifying various predicting flow maps from literature for the innovative microchannel tubing provided precious information for future applications without the expense of repeated flow visualization testing. Various maps including works from Mandhane [43], Taitel and Dukler [64], Breber [9] and Soliman [56], [57], [58] were evaluated. Only the Breber's map and Soliman's transitions are discussed below; however, the others' efforts are compiled in the appendix.

5.2.1 Breber map

Based on the dimension-less vapor velocity and Martinelli parameter, the prediction of the Breber map is shown in Figure 5.5. Modifying the Taitel and Dukler map, accounting for transitions between flow patterns and broadening the wavy region produced predictions on the Breber map that more clearly defined the flow pattern categories. Furthermore, the uncertainty of terminology as discussed in the previous section was reduced.

Compared to the flow visualization results shown in Figure 5.5, the Breber's map predicted well for the wavy and slug flows. The annular flow occurs at 0.8 ft/s superficial vapor velocity, j_v^*, instead of 1.5 ft/s predicted by the Breber map. As expected, the annular flow occurs at lower superficial vapor velocity in the microchannel tube. Due to the reduced passage and rectangular geometry, the surface tension may draw the condensate liquid around the perimeter of the microchannel forming an annular liquid film at lower vapor velocity compared with larger diameter round tubes, which were the references of the Breber's map.

5.2.2 Soliman transitions

There were two transitions proposed by Soliman [54], [56], defining boundaries between wavy/slug flow and annular flow, and between annular and mist flow. As shown in Figure 5.6, based on the mass flux and quality, there was some agreement between the Soliman transitions and the observed transitions. The transition between wavy and annular flow at a quality higher than 30% was well predicted. For a quality less than 30%, the Soliman transition extended to higher mass flux regions where slug flow was identified on the Taitel-Dukler map, because both wavy and slug flow patterns were included in the same regime by Soliman. Unlike the Taitel-Dukler map, the Soliman transition between slug and annular flow is not fixed at a specified quality, which is closed to the observation. As the mass flux decreases, the boundary of the transition extends to higher quality, where wavy/slug-annular flow may persist. Compared with the transition map in Figure 5.4, the Soliman's prediction is just between those two transitions based on the observation.

There is also a transition between the mist and annular flow predicted on the Soliman map. The mist or spray flow is a regime where entrained droplets form a core flow with an unstable film along the wall. Based on the Soliman transition, no mist flow occurred at a mass flux less than 300 klb/ft^{2}hr. Neither should mist flow be seen at 550 klb/ft^2hr for a quality less than 45%. Because of the requirement of high mass flux and high quality, mist flow was not easily obtained or observed. The minute diameter of the microchannel tube is the reason attributed to the delay of mist flow. The liquid film on the wall was stabilized by the micro channel and sustained to higher quality and mass flux.

5.3 Conclusion of Flow Regime Observation

There were various flow patterns observed in the condensation of R-134a inside the microchannel tube. As the quality increased, the flow pattern changed from plug/slug to slug/wavy, then became wavy/annular, and finally annular. Both a transition prediction map and a flow regime map are developed from the observation of the microchannel tube.

To verify the flow regime visualization, two flow maps were cited. Because of the definition of flow pattern, terminology, and the subjectivity of visualized determination, both agreements and discrepancies were shown.

By including transition zones, the Breber map provided more detailed predictions. The transition between the wavy and annular flow accounted for data with intermediate mass flux and high quality. Compared to the flow visualization results shown in Figure 5.5, the Breber map predicted well for the wavy and slug flows. The annular flow occurs at 0.8 ft/s superficial vapor velocity, j_v^*, instead of 1.5 ft/s predicted by the Breber map, which is attributed to the surface tension effect in the smaller microchannel tube.

The Soliman map included two transitions and was divided into three flow regimes: wavy/slug, annular, and mist flow pattern. Combined with slug, stratified and wavy flow, a broadening regime was predicted over the low mass flux or high mass flux with low quality. The prediction is right on between the observed transitions. The surface tension over the micro-channel stabilized the annular-mist flow; therefore, the onset of the mist was extended to the high flux with high quality regions.

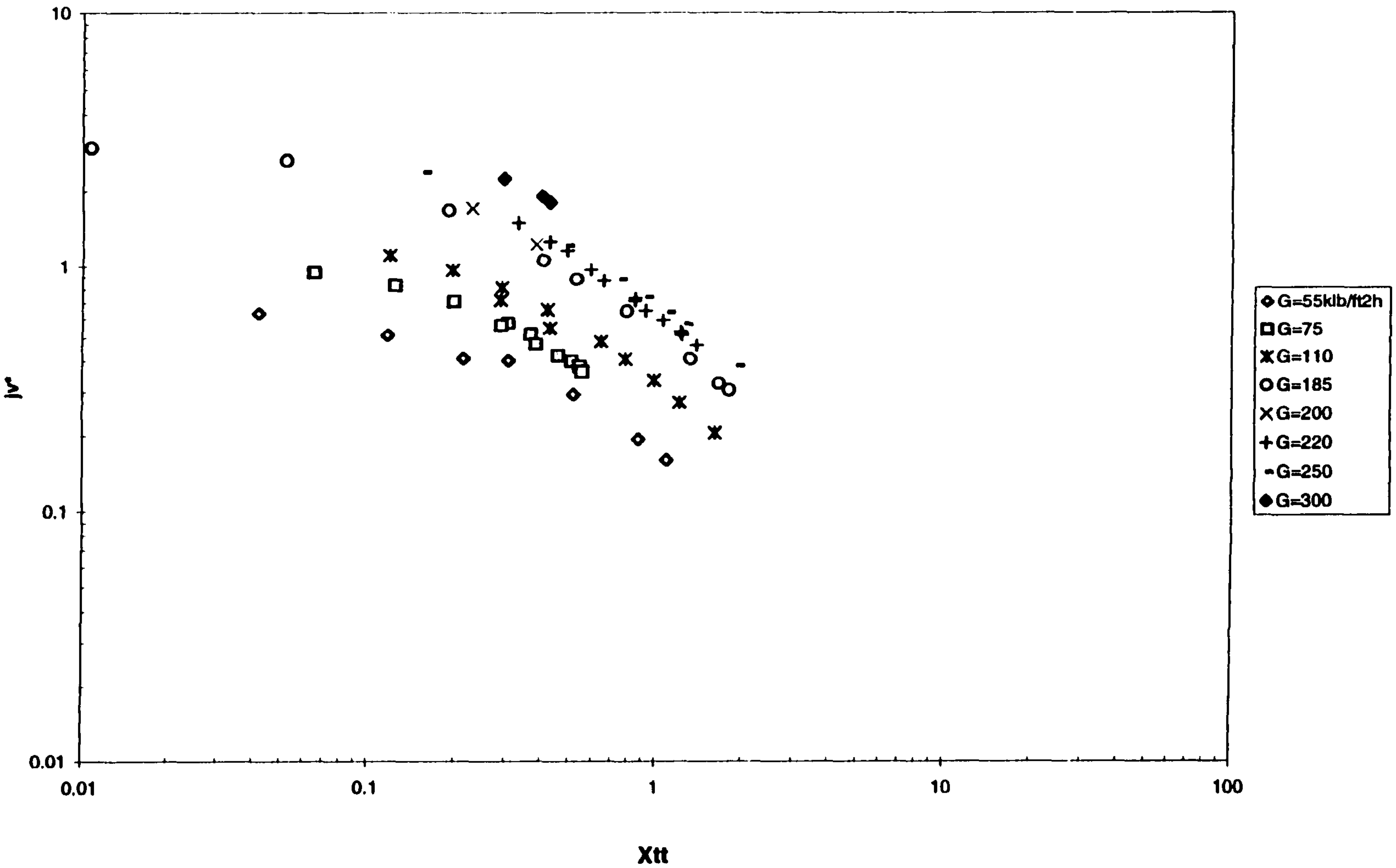

Figure 5.1 Flow visualization data at various mass fluxes for HFC-134a at 95F

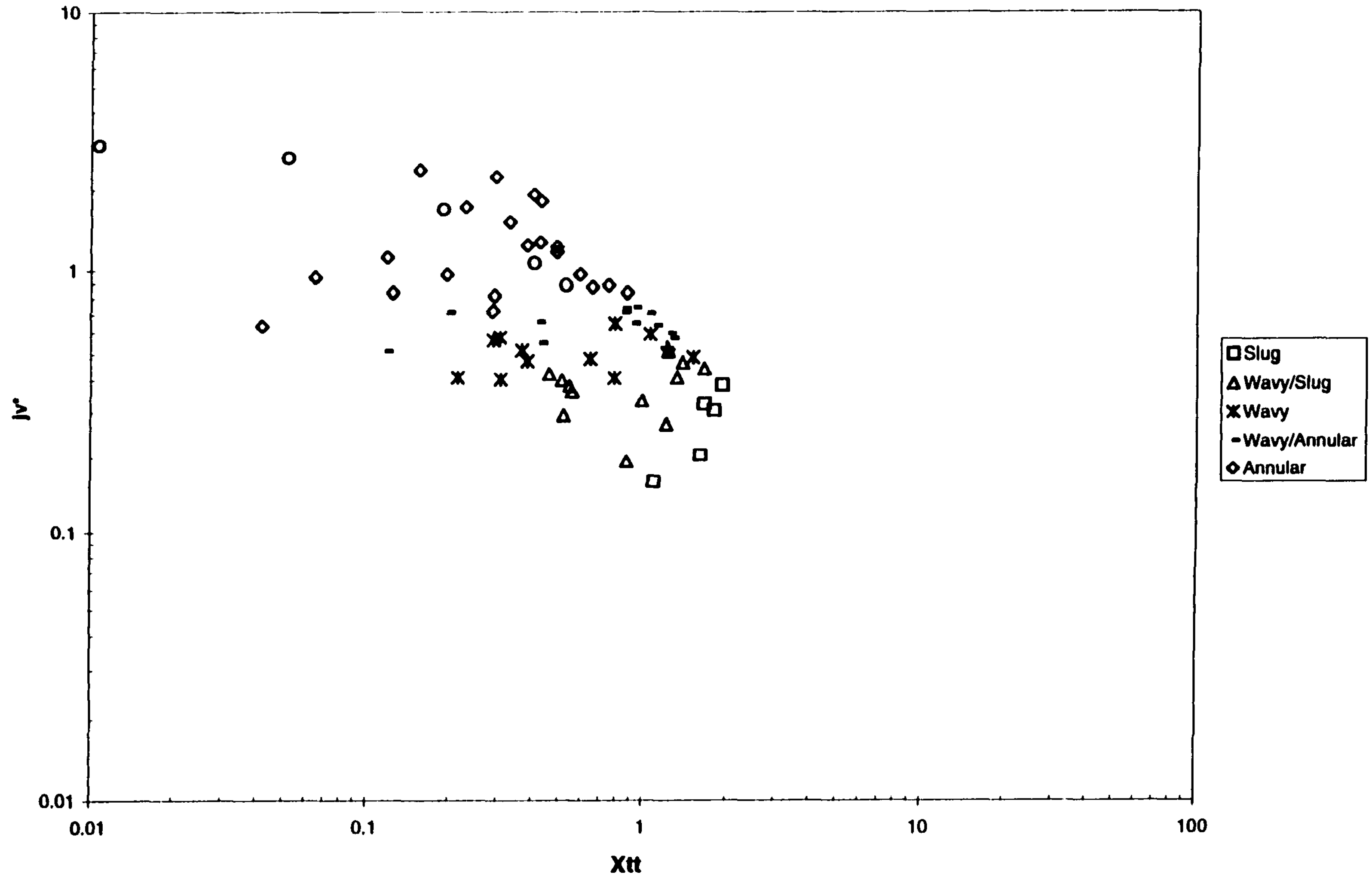

Figure 5.2 Flow regime map

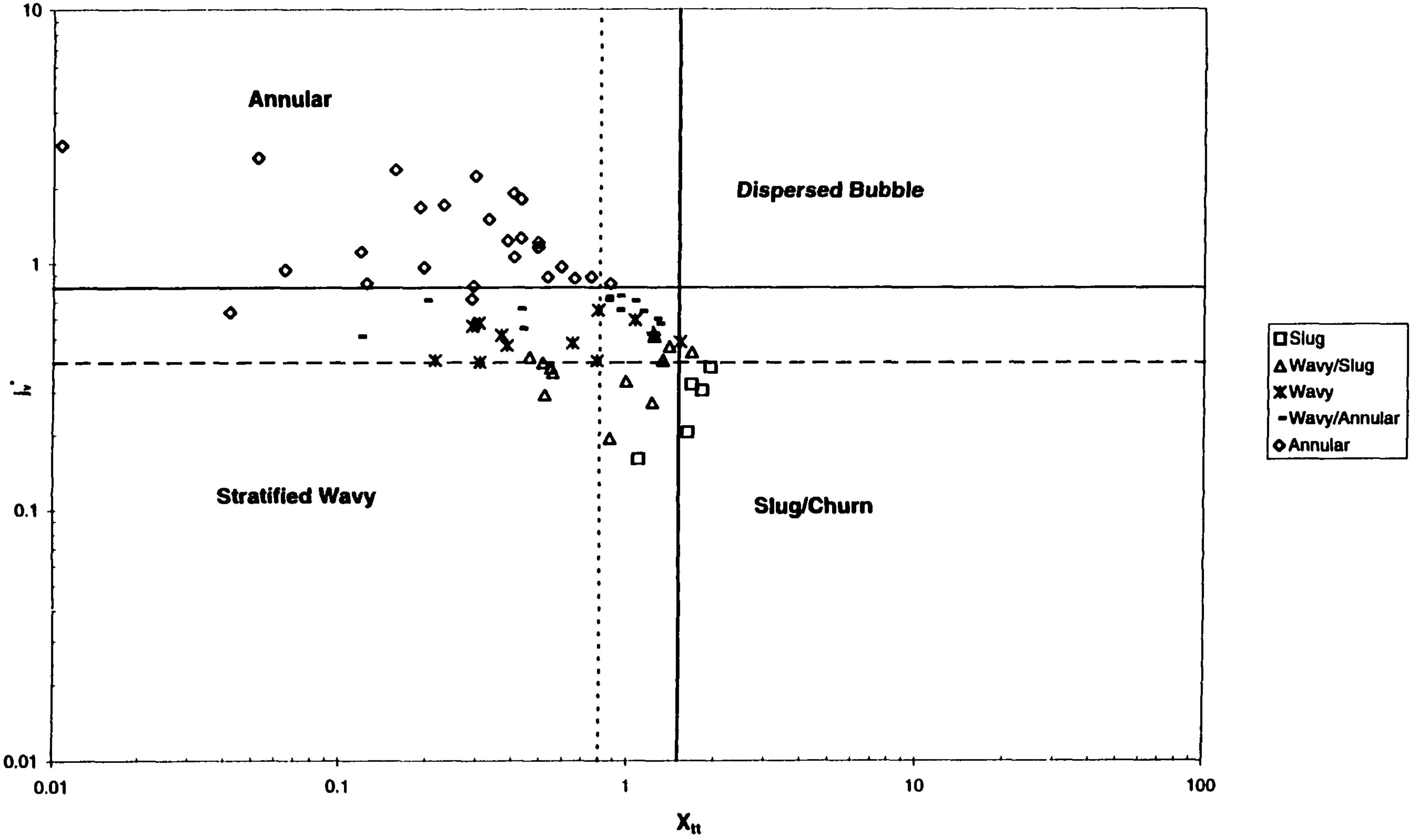

Figure 5.3 Flow regime map for HFC-134a in Microchannel Tube

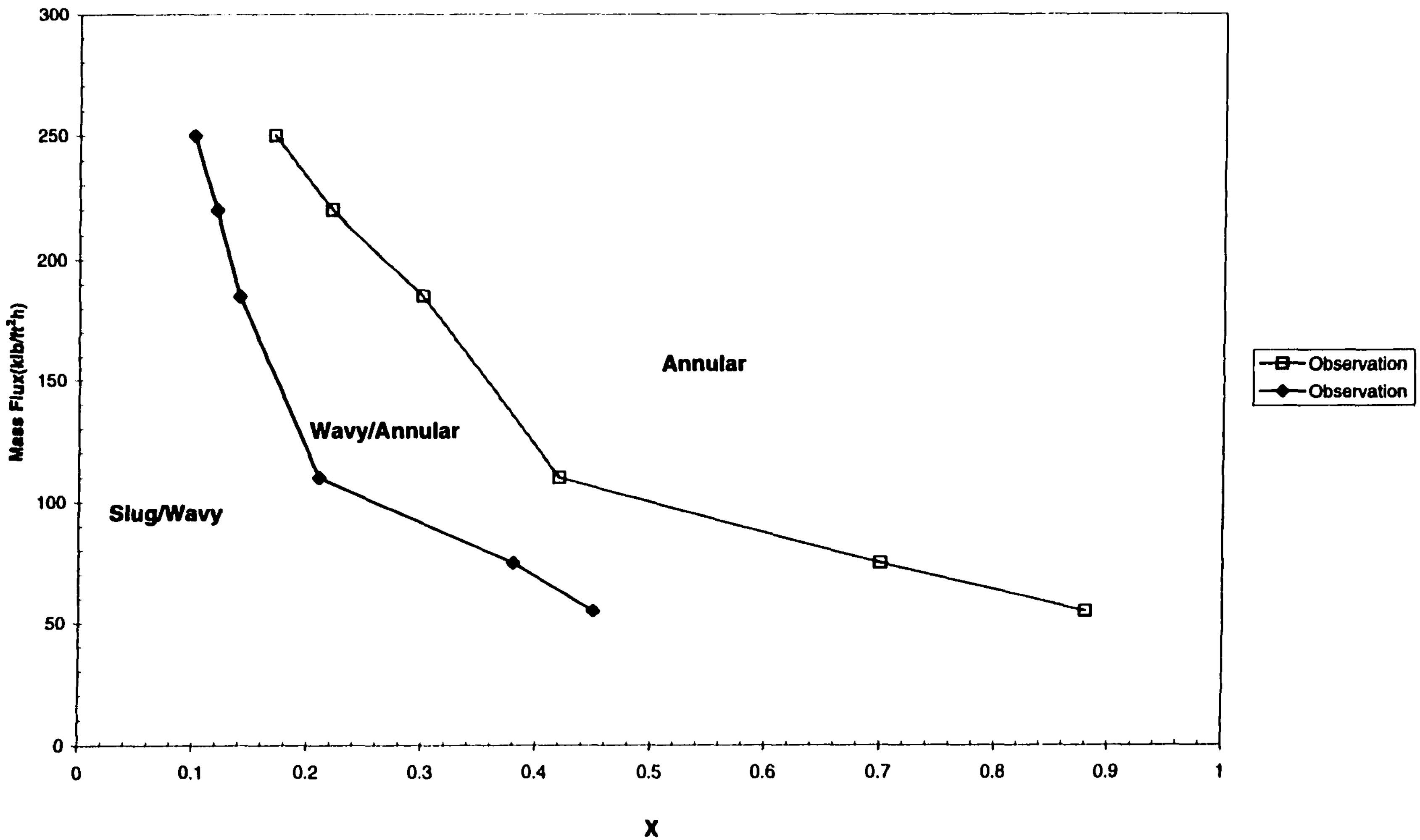

Figure 5.4 Flow transition map for mass flux vs. quality

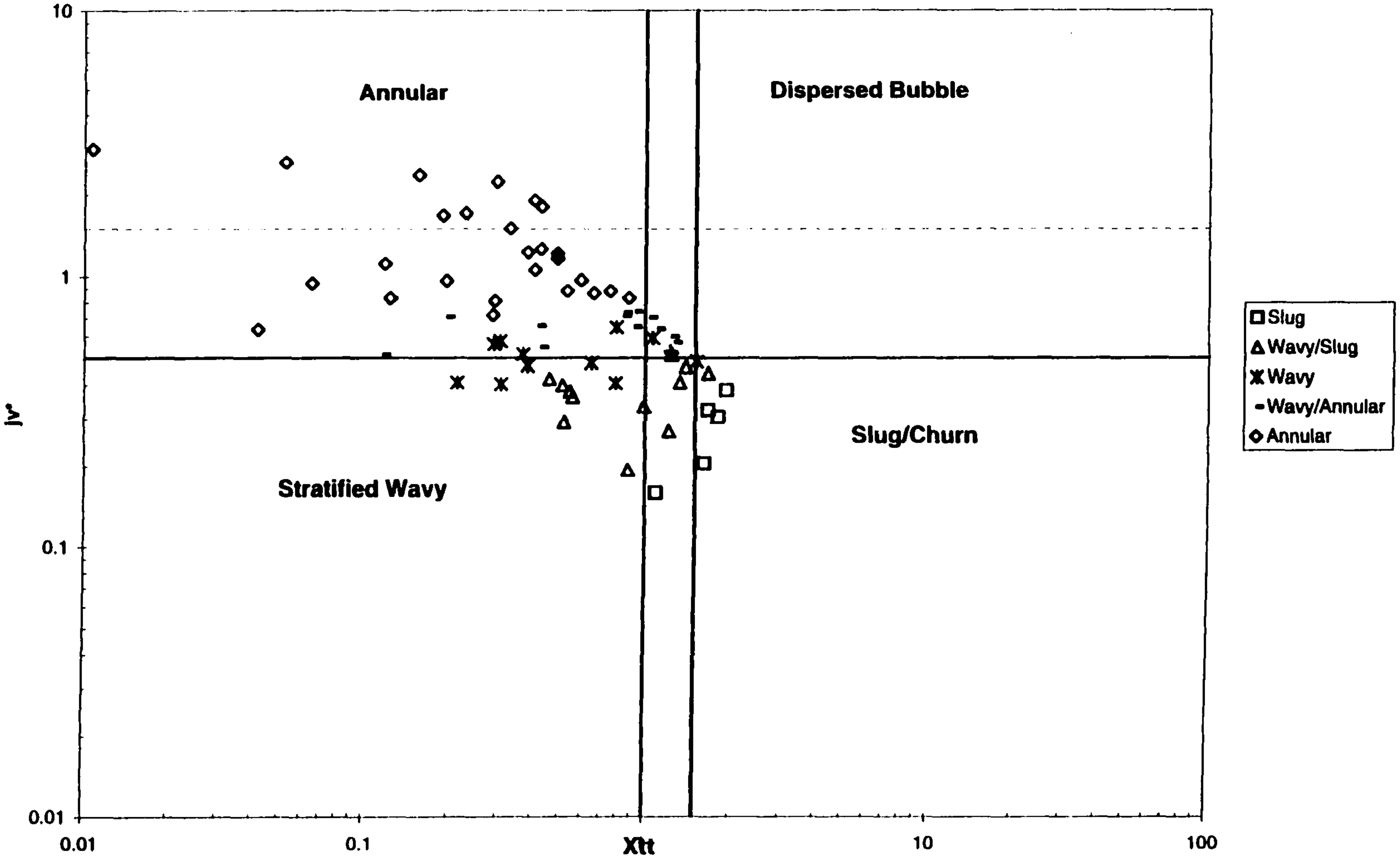

Figure 5.5 Flow regime visualization plotted in the Breber map

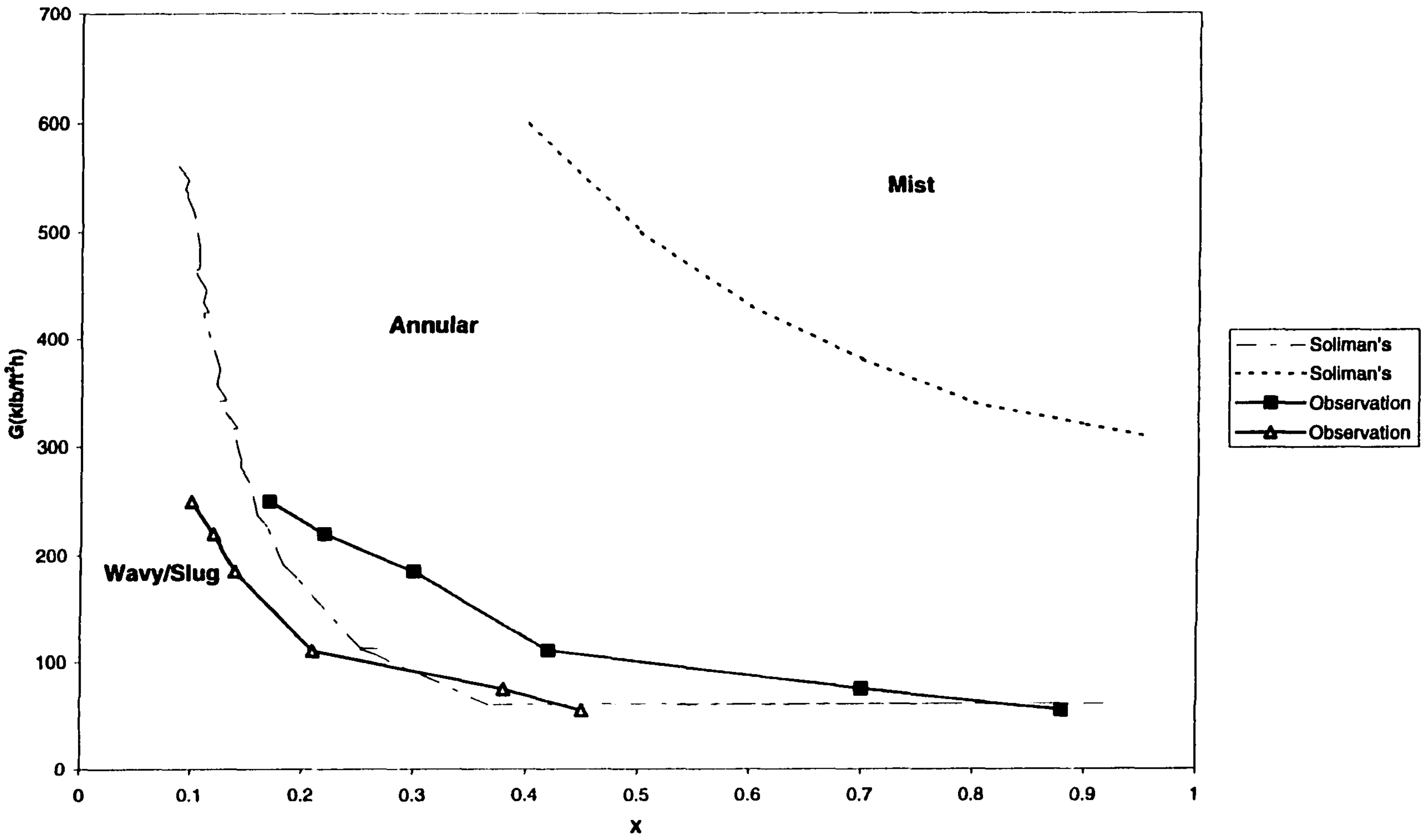

Figure 5.6 Flow map based on the Soliman transitions

CHAPTER 6

CONDENSATION HEAT TRANSFER CORRELATION

The condensation heat transfer correlation was developed, presented and compared to experimental data in this chapter. Based on the flow visualization, two different correlations were developed for the two dominant flow regimes. First is the annular flow heat transfer correlation, based on boundary layer analysis. The other one is the wavy/slug flow heat transfer correlation, based on the superposition of film-wise condensation and single-phase forced convection. For purposes of simplicity, an alternative correlation for the annular flow is also developed using the two-phase multiplier approach. Finally, an asymptotic correlation is presented to cover all the experimental data.

6.1 Annular flow correlation

6.1.1 Boundary layer approach

The boundary layer approach uses the continuity, momentum, and energy equations of the turbulent boundary layer in simpler forms for the annular flow based on some assumptions. 1) The liquid film is annular and axisymmetric. 2) There is no entrainment of liquid in the vapor core. 3) Both the liquid and vapor are turbulent. 4) The universal velocity profile is valid. 5) The liquid film thickness is much smaller than the hydraulic diameter of the tube.

The heat flux of the turbulent flow can be defined including the eddy heat flux as follows,

$$\dot{q} = \rho_l \cdot Cp_l \cdot (\alpha_l + \varepsilon_h) \cdot \frac{\partial T}{\partial y} \tag{6.1}$$

Also, from the energy equation for turbulent flow,

$$\frac{\partial}{\partial y}\left(\rho_l \cdot Cp_l \cdot (\alpha_l + \varepsilon_h) \cdot \frac{\partial T}{\partial y} \right) = 0 \tag{6.2}$$

It implies that the heat flux is constant in the y direction and equal to the wall heat flux. Eq. (6.1) can be rearranged and integrated from the wall to the interface in the following form,

$$\int_{T_w}^{T_\delta} \frac{dT}{\dot{q}} = \int_0^{\delta} \frac{dy}{\rho_l \cdot Cp_l \cdot (\alpha_l + \varepsilon_h)} \tag{6.3}$$

By defining wall coordinates as follows,

$$y^+ = y \cdot \frac{u_\tau}{\nu_l} \tag{6.4.1}$$

$$\delta^+ = \delta \cdot \frac{u_\tau}{\nu_l} \tag{6.4.2}$$

$$u^+ = \frac{\bar{u}}{u_\tau} \tag{6.4.3}$$

$$\text{where } u_\tau = \left(\frac{g \cdot \tau_w}{\rho_l} \right)^{\frac{1}{2}} \tag{6.4.4}$$

Then, Eq. (6.3) can be written as,

$$\frac{1}{h}=\int_{T_w}^{T_s}\frac{dT}{\dot{q}}=\int_0^{\delta^+}\frac{\nu_l}{\rho_l\cdot Cp_l\cdot(\alpha_l+\varepsilon_h)\cdot u_\tau}\cdot dy^+ \tag{6.5}$$

Therefore, the heat transfer coefficient, h, can be derived by solving for the unknowns of δ^+, u_τ, τ_w, and ε_h as functions of y^+. u_τ, τ_w, the wall shear stress can be obtained from the frictional pressure gradient correlation. The dimensionless film thickness, δ^+, can be found from the continuity of the liquid film. In order to obtain ε_h, the Reynolds analogy is introduced to relate ε_h with ε_m, by assuming the turbulent Prandtl number, $\varepsilon_m/\varepsilon_h$, equal to one.

The frictional pressure gradient is defined as follows,

$$\left(\frac{dP}{dz}\right)_f=\tau_w\cdot\frac{4}{D_h} \tag{6.6}$$

Which can be related to the pressure gradient for vapor only flow by the method of Lockhart and Martinelli [42] as,

$$\left(\frac{dP}{dz}\right)_f=\phi_v^2\left(\frac{dP}{dz}\right)_v \tag{6.7}$$

where $$\left(\frac{dP}{dz}\right)_v=\frac{2\cdot\left(\frac{4}{\pi}\right)^{2-0.2}0.046\cdot\mu_v^{0.2}\cdot\left(\dot{m}_v\right)^{2-0.2}}{D_h^{4.8}\cdot\rho_v\cdot g}=0.1421\cdot\frac{\mu_v^{0.2}\cdot\mu_v^{0.2}\cdot\left(\dot{m}_v\right)^{1.8}}{D_h^{4.8}\cdot\rho_v\cdot g}$$

(6.7.1)

Therefore, $$u_\tau=\left(\frac{g\cdot\tau_w}{\rho_l}\right)^{\frac{1}{2}}=0.152\cdot\left(\mathrm{Re}_v^{0.9}\cdot x^{0.9}\cdot\frac{\mu_v}{D_h}\left(\frac{\rho_v}{\rho_l}\right)^{\frac{1}{2}}\right)\cdot\phi_v \tag{6.8}$$

Substituting Eq. (6.8) into Eq. (6.5) and rearranging, the Nusselt number can be written as follows,

$$Nu = \frac{h \cdot D_h}{k_l} = \frac{\rho_l C p_l D_h}{k_l} \cdot u_\tau \cdot T_\delta^{-1}$$

$$= \frac{\rho_l C p_l D_h}{k_l} \cdot 0.152 \cdot \left(\mathrm{Re}_v^{0.9} \cdot x^{0.9} \cdot \frac{\mu_v}{D_h} \left(\frac{\rho_v}{\rho_l} \right)^{\frac{1}{2}} \right) \cdot \phi_v \cdot T_\delta^{-1} \tag{6.9}$$

$$= 0.152 \cdot \mathrm{Pr}_l \cdot \mathrm{Re}_l^{0.9} \cdot \frac{1}{X_{tt}} \cdot \phi_v \cdot T_\delta^{-1}$$

With the modification and the suggestion of deSouza [25], the vapor only pressure drop multiplier can be approximated as follows,

$$\phi_v = \sqrt{1.376 + 8 \cdot X_{tt}^{1.655}} \tag{6.10}$$

Finally, the dimensionless temperature drop across the liquid film, T_δ, can be obtained by plotting T_δ against Re_l/x as shown at Figure 6.1. According to the regression result, T_δ can be expressed as follows,

$$T_\delta = 5.4895 \cdot \left(\frac{\mathrm{Re}_l}{x} \right)^{0.2197} \tag{6.11}$$

Therefore, combining Eq. (6.9), (6.10), (6.11), the final form of the correlation is,

$$Nu_{anul} = 0.0277 \cdot \mathrm{Pr}_l \cdot \mathrm{Re}_v^{0.9} \cdot \left(\frac{1.376 + 8 X_{tt}^{1.655}}{X^2_{tt}} \right)^{0.5} \cdot \left(\frac{\mathrm{Re}_l}{x} \right)^{-0.2197} \tag{6.12}$$

The prediction of Equation (6.12) compared to the experimental data is shown in Figure 6.2. This is better agreement with data than the predictions of chapter 4, with an average deviation of 8.46%. Nearly 2/3 of data (65.9%) was predicted within +/-10%, and 95.7% of points were predicted to within +/-25%. This is a dramatic improvement over the accuracy of existing correlation.

6.1.2 Two-phase multiplier approach

Before imposing the two-phase pressure correlation into the boundary layer approach in the previous section, the heat transfer correlation can be described as follows,

$$Nu = a \cdot \Delta \cdot \mathrm{Re}_l^m \cdot \mathrm{Pr}_l^n \tag{6.13}$$

By substituting the Lockhart and Martinelli two-phase multiplier, Δ in Eq. (6.13) can be evaluated, and the Nusselt number can be written as follows,

$$Nu = \mathrm{Re}_l^m \cdot \mathrm{Pr}_l^n \cdot f(X_{tt}) \tag{6.14}$$

Once the Dittus-Boelter correlation for single-phase heat transfer is substituted, the Eq. (6.14) can be rearranged in the form,

$$Nu = 0.023 \cdot \mathrm{Re}_l^{0.8} \cdot \mathrm{Pr}_l^{0.4} \cdot f(X_{tt}) \tag{6.15}$$

where $$f(X_{tt}) = \sum_{n=0,1,2,3} \frac{c_n}{X_{tt}^n} \tag{6.15-1}$$

Values of c and n in Eq. (6.15-1) can be obtained by curve fitting the experimental data plotted in Figure 6.3. The best regression result is c_0=0.92473, c_1=1.23078, c_2=0.01057, c_3=-0.00037, and the final correlation is as follows,

$$Nu = 0.023 \cdot \mathrm{Re}_l^{0.8} \cdot \mathrm{Pr}_l^{0.4} \cdot \left[0.92473 + \frac{1.23078}{X_{tt}} + \frac{0.01057}{X_{tt}^2} - \frac{0.00037}{X_{tt}^3} \right] \tag{6.16}$$

The prediction of Equation (6.16) is plotted in Figure 6.4. The agreement was excellent with a mean deviation of 8.33%. 2/3 of the data was predicted within +/-10%, and almost all were described within +/-25%. The improvement of prediction based on Eq. (6.16) is summarized in Table 6.1.

Correlation	Mean Deviation	Percentage of data within +/- 10%	Percentage of data within +/- 25%	Percentage of data within +/- 50%
Eq. (6.16)	8.33%	65.3%	98.6%	100%
Eq. (6.12)	8.46%	65.9%	95.7%	100%
Akers	15.2%	41.2%	83.7%	100%

Table 6.1 Comparison of Eq. (6.12) and Eq. (6.16) with Akers' correlation

6.2 Wavy/Slug flow correlation

The heat transfer of wavy/slug flow is the combination of the film-wise condensation in the top portion of the tube and the heat transfer in the bottom liquid pool. For flow with a low mass flux, the heat transfer in the bottom pool is small compared to the condensation in the top portion of the tube and can be neglected. In addition, the negligible vapor flow effect on the liquid film on the top makes the Nusselt theorem a reasonable approach as pointed out by Chato [15] and Jaster, Kosky [36].

As the mass flux increases, neglecting the heat transfer in the bottom liquid pool is no longer reasonable. As shown in the result of Chapter 4, the departure from the

$Nu/(GaPr/Ja)^{0.25}$ curve at various ΔT's verified the effect of bottom pool heat transfer. In order to account for the additional heat transfer, some researchers such as Rosson and Myers [48] developed a superposition correlation.

A superposition correlation is proposed here based on the experimental observations and flow regime visualization. The Nusselt number of the wavy/slug flow is given as,

$$Nu_{wysg} = \alpha \cdot Nu_{film} + (1-\alpha) \cdot Nu_{convection} \tag{6.17}$$

where α is the void fraction, since there is vapor in the α fraction of the tube volume where film-wise condensation takes place, and the rest of the volume is the liquid pool where forced convection dominates. The void fraction, α, was derived from Zivi [68] correlation.

$$\alpha = \left(1 + \frac{1-x}{x}\left(\frac{\rho_v}{\rho_l}\right)^{\frac{2}{3}}\right)^{-1} \tag{6.18}$$

The first term of Eq. (6.17) was derived from the Chato [15] correlation for falling film condensation on a horizontal cylinder and is defined as,

$$Nu_{film} = 0.555 \cdot \left(\frac{\rho_l(\rho_l - \rho_v) g h_{fg} D_h^3}{k_l \mu_l (T_{sat} - T_w)}\right)^{\frac{1}{4}} \tag{6.19}$$

For the second term of Eq. (6.17), a Dittus-Boelter [22] type correlation was introduced to account for the convection heat transfer in the liquid pool in the form

$$Nu_{convection} = 0.023 \cdot \mathrm{Re}_l^{0.8} \cdot \mathrm{Pr}_l^{0.4} \tag{6.20}$$

The prediction of Equation (6.17) is illustrated in Figure 6.5. There is much improvement over previous results from literature, with a mean deviation of

9.34%. Nearly half the data were predicted within +/-10%, and only 5% of data points were not predicted within +/-25%. The comparison of the results from various correlations and Eq. (6.17) is listed in Table 6.2.

Correlation	Mean Deviation	Percentage of data within +/- 10%	Percentage of data within +/- 25%	Percentage of data within +/- 50%
Equation (6.17)	9.34%	44.9%	95.2%	100.0%
Jaster	16.0%	34.5%	80.4%	100.0%

Table 6.2 Comparison of Eq. (6.17) with Jaster and Kosky's correlation

6.3 Overall flow correlation

The correlations developed in the previous sections were specified for particular flow conditions; therefore, there were limitations for each correlation. To examine the validity of the correlations, each correlation was plotted for the entire set of data. The deviation of each correlation was plotted against the Froude number, Fr_{so}. For the correlation derived for the wavy/slug flow as shown on Figure 6.6, the deviation was almost within +/-20% for Fr_{so} less than 18 and spread to -40% as Fr_{so} increased. On the other hand, the deviation of the annular correlation as displayed in Figure 6.7 showed the opposite trend.

Two additional figures were generated for each correlation versus the quality. As shown at Figure 6.8, the wavy/slug flow correlation changed from over-prediction at low quality to under-prediction for higher qualities. For the annular correlation in Figure 6.9, under-prediction was observed for both ends of the quality.

Based on Figures 6.6 to 6.9 and the method of Churchill and Usagi [18], an asymptotic correlation is proposed to account for the entire set of data regardless of flow regime. A combination of the Nusselt numbers, Nu_{anul} from Eq. (6.12), and Nu_{wysg} of Eq. (6.17), yielded following expression:

$$Nu_{all} = \left[(Nu_{anul})^n + (Nu_{wysg})^n \right]^{\frac{1}{n}} \tag{6.21}$$

where the exponent n is 8.

The prediction of Eq. (6.21) was plotted for the complete set of data as Figure 6.10. The agreement between this prediction and the experimental data was the best of all, with the mean deviation of 7.63%. Over 70% of data were predicted within +/-10%, and merely 2.2% of data were not predicted within +/-25%. The comparison with other correlations is summarized in Table 6.3.

Correlation	Mean Deviation	Percentage of data within +/- 10%	Percentage of data within +/- 25%	Percentage of data within +/- 50%
Eq. (6.21), Nu_{all}	7.63%	70.7%	97.8%	100%
Eq. (6.16), Nu	8.33%	65.3%	98.6%	100%
Eq.(6.12), Nu_{anul}	8.46%	65.9%	95.7%	100%
Eq(6.17),Nu_{wysg}	9.34%	44.9%	95.2%	100%

Table 6.3 Comparison of Eq. (6.21) with correlation from present literature

6.4 Summary

Correlations of condensation heat transfer inside the microchannel tube were derived and compared to the experimental data and flow visualization. For the wavy/slug flow regime, a superposition correlation accounting for both the film-wise condensation in the top of the tube and the convection heat transfer in the bottom liquid pool was developed. Both a boundary-layer and a two-phase multiplier approach were introduced to generate correlations for condensation in the annular flow regime. Finally, an asymptotic correlation was developed for the extended range of flow conditions regardless of the flow regime.

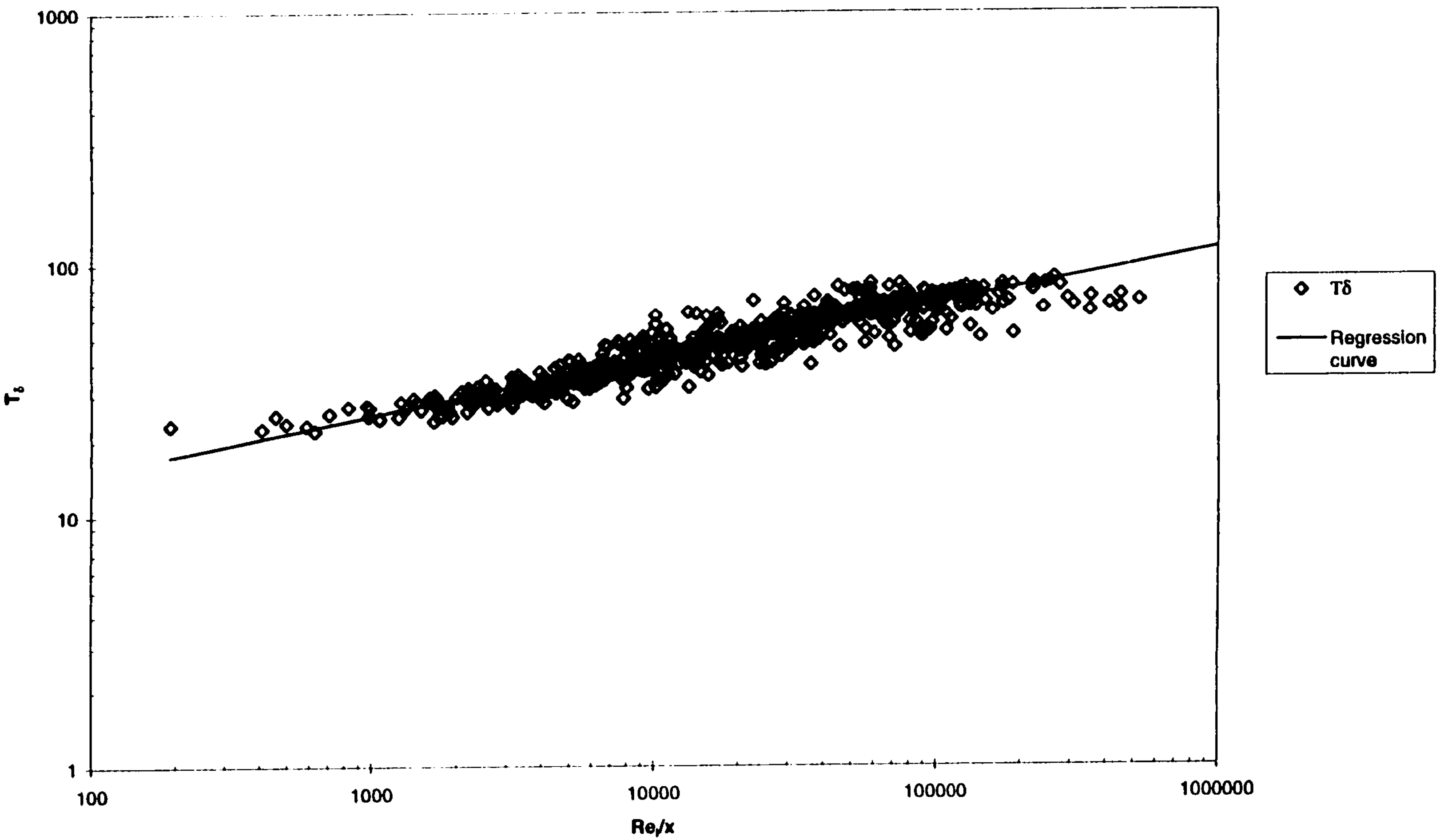

Figure 6.1 Distribution of T_δ against Re_l/x

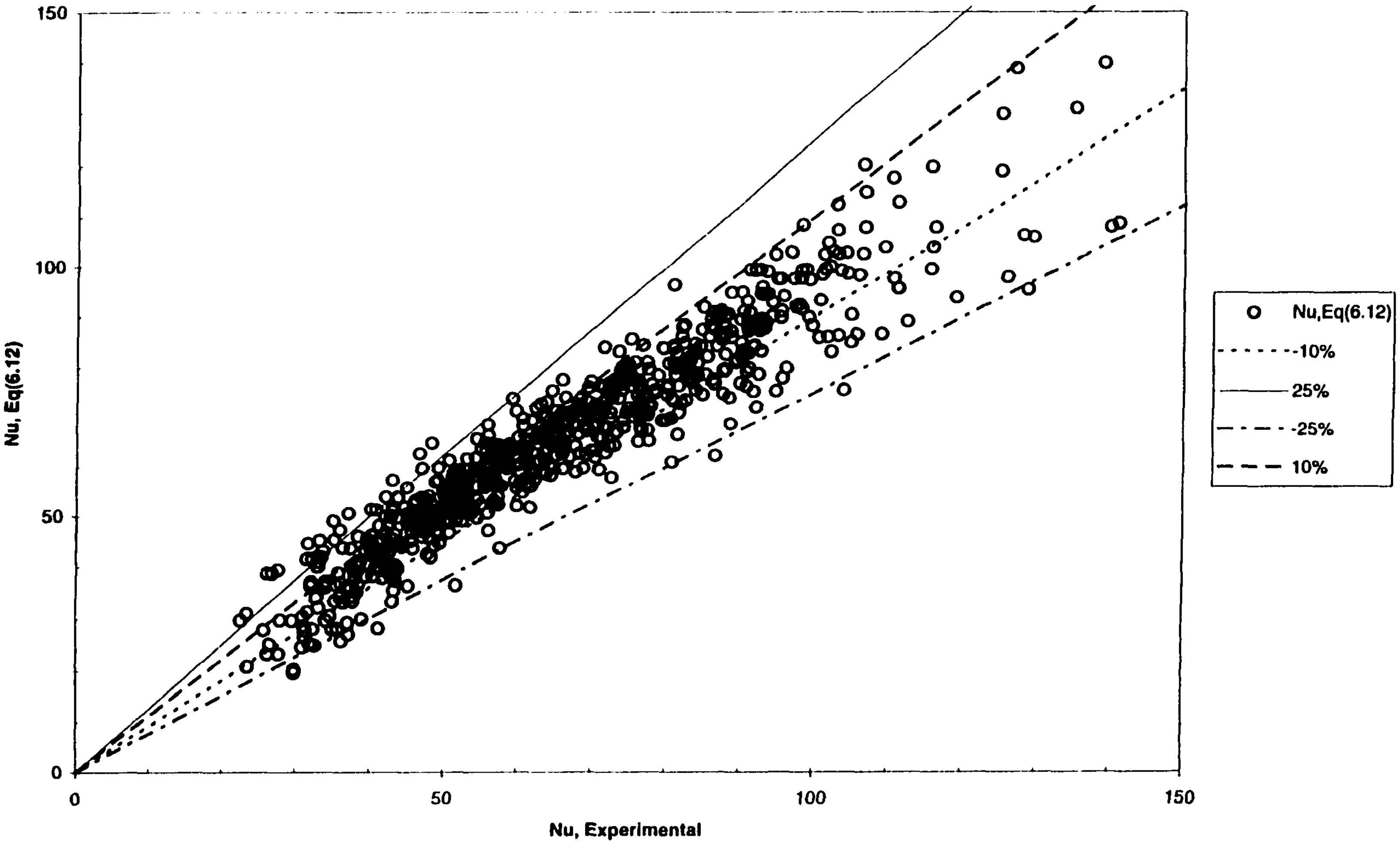

Figure 6.2 Comparison of experimental data with prediction of Eq. (6.12)

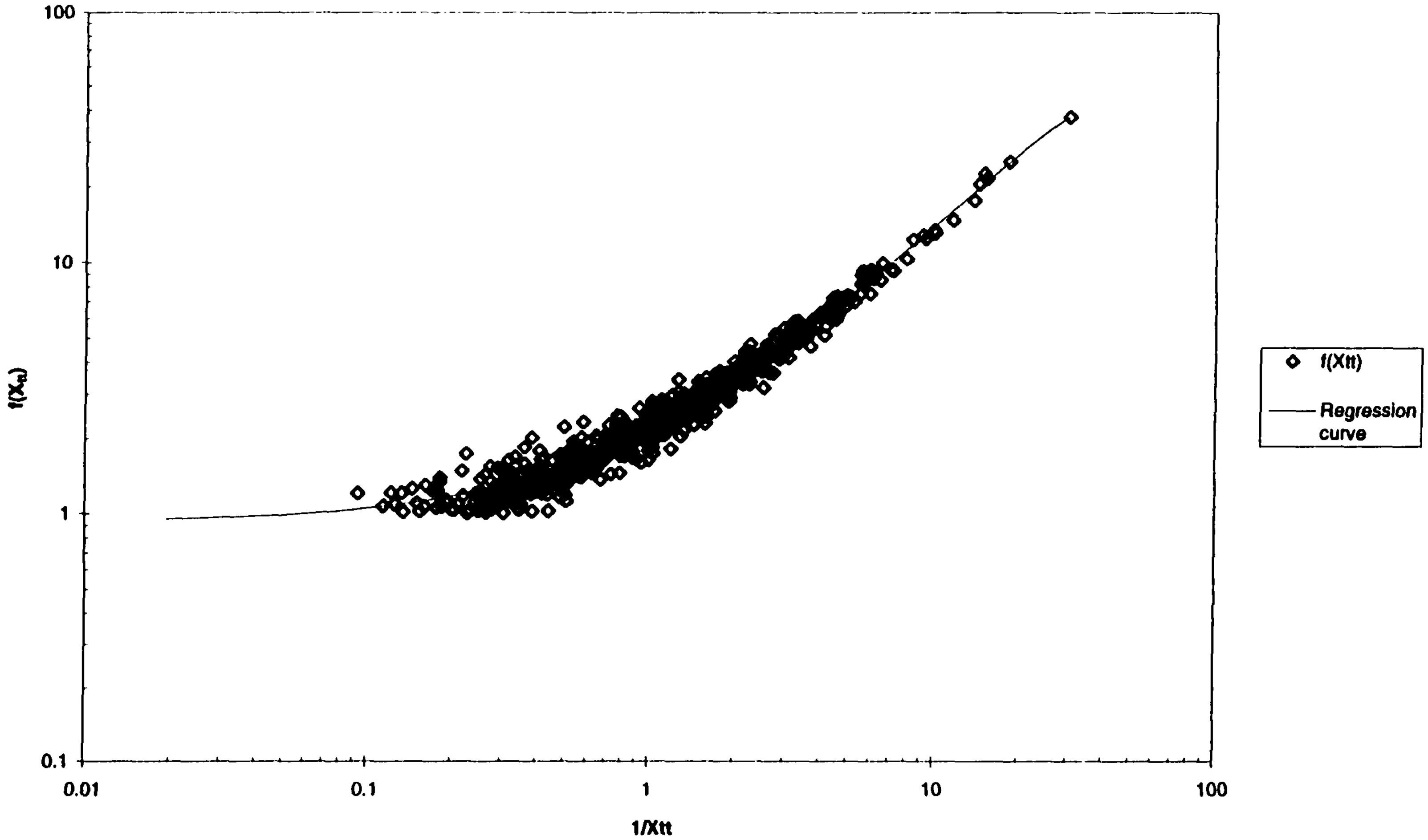

Figure 6.3 Distribution of $f(X_{tt})$ against $1/X_{tt}$

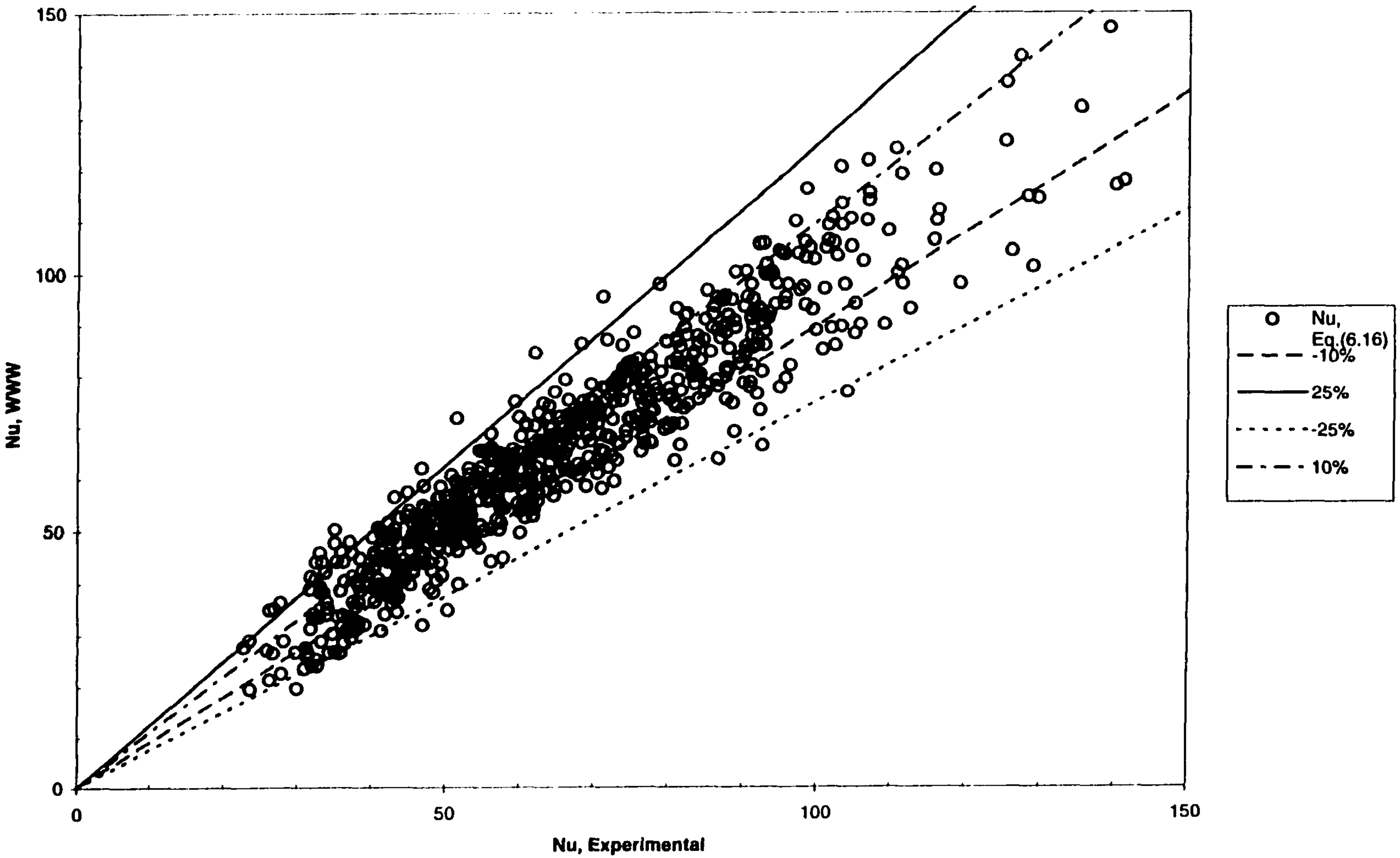

Figure 6.4 Comparison of experimental data with prediction of Eq.(6.16)

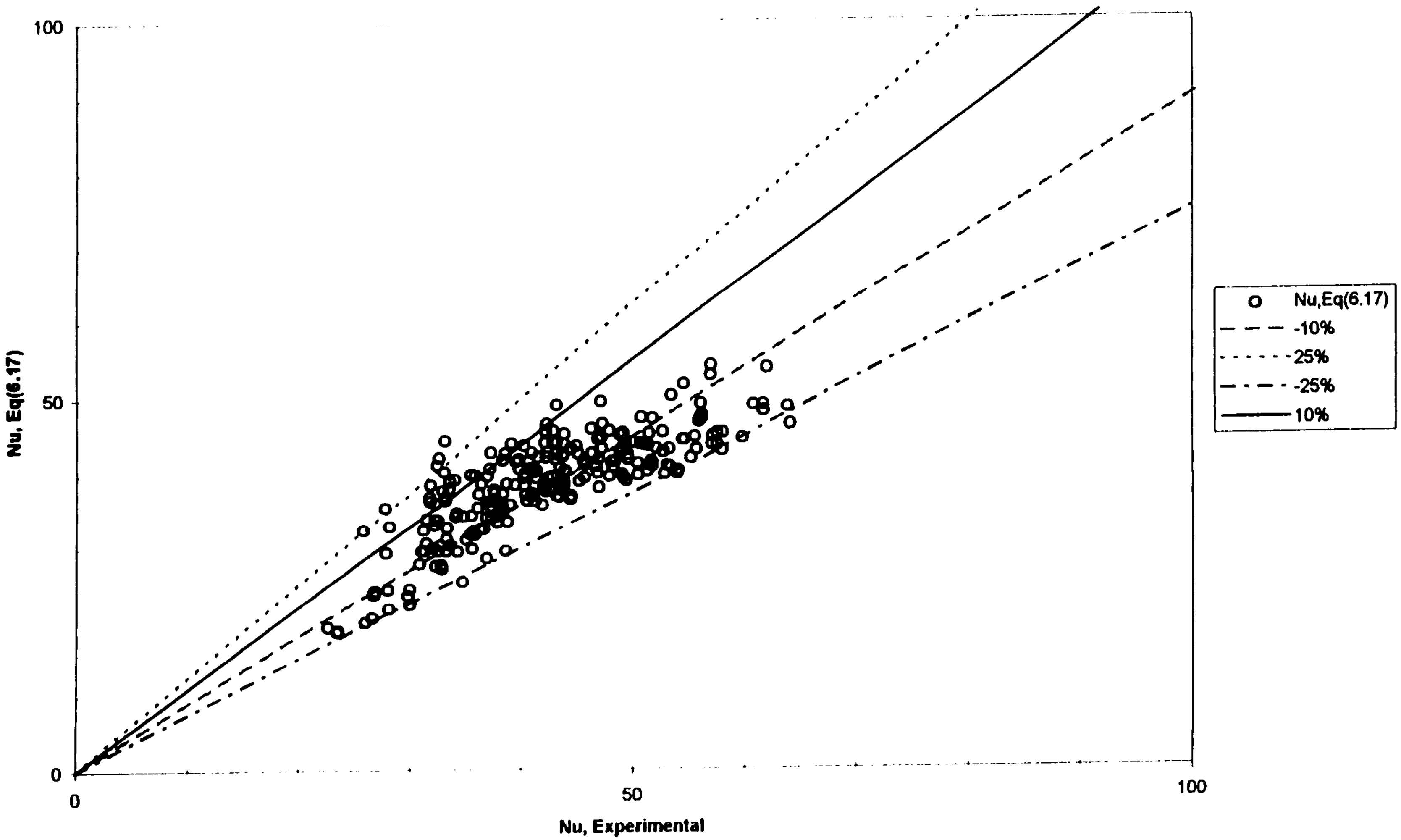

Figure 6.5 Comparision of experimental data with prediction of Eq.(6-17)

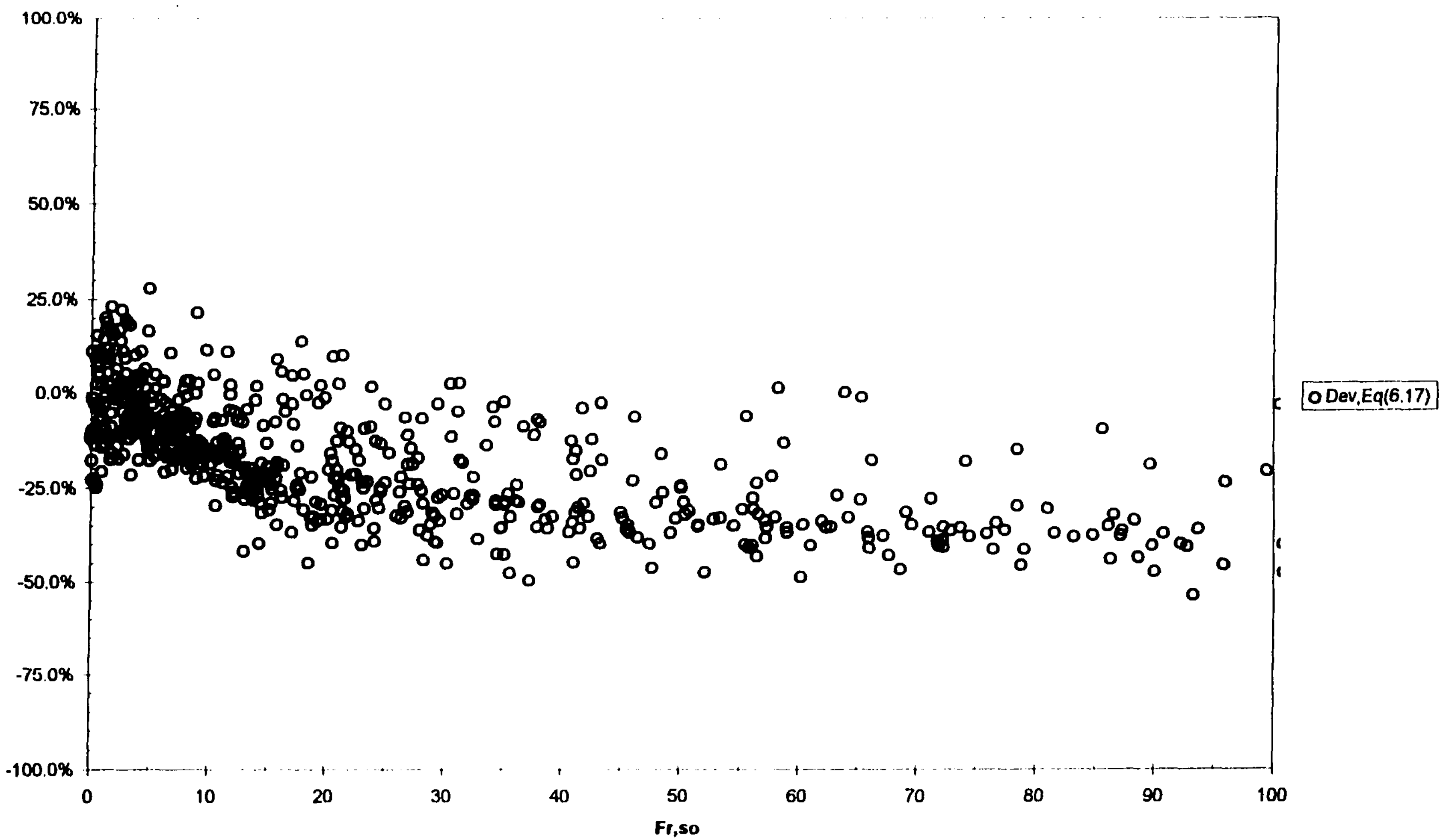

Fig 6.6 Deviation of Eq.(6.17) vs. Froude Number

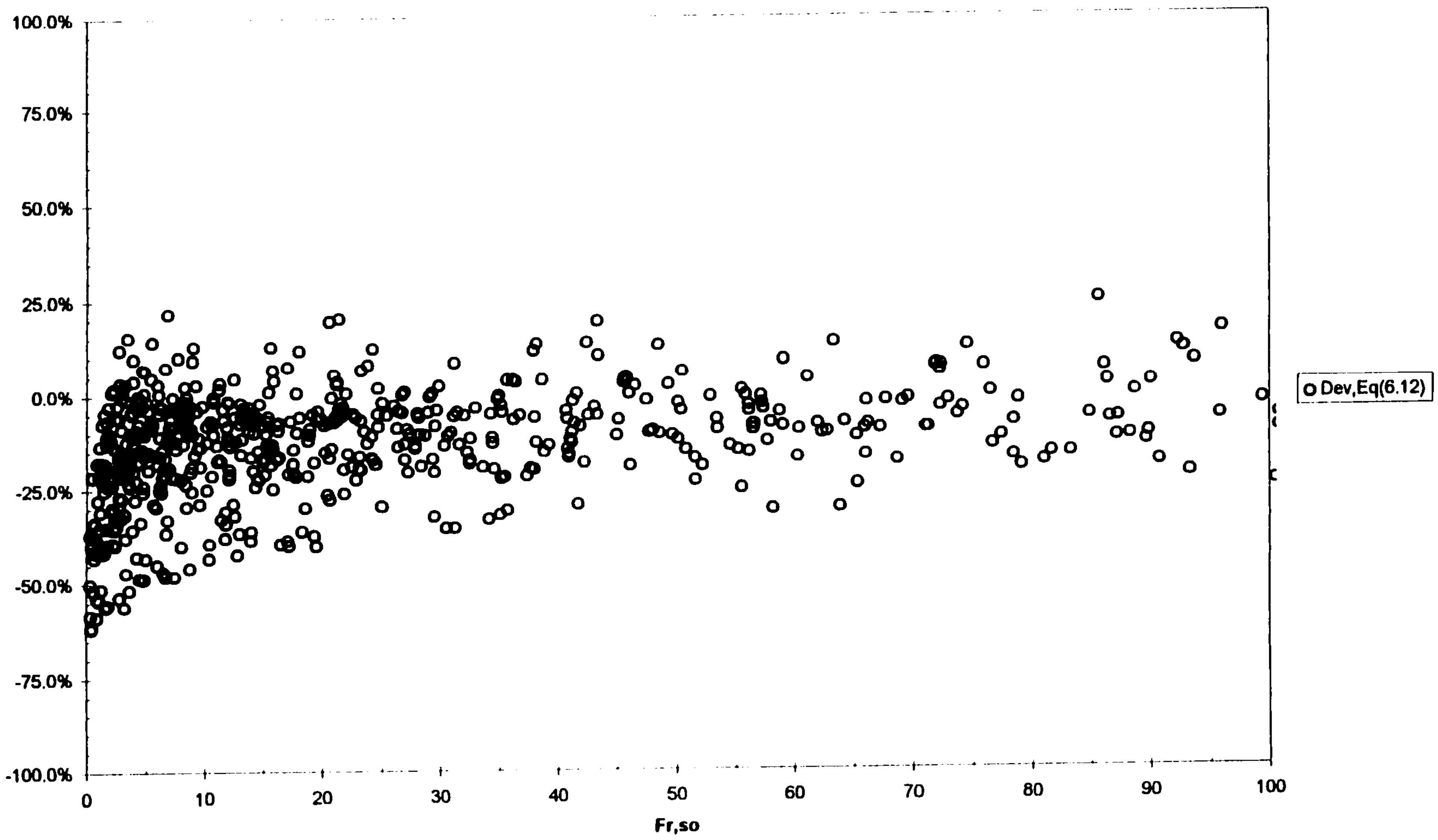

Fig 6.7 Deviation of Eq.(6.12) vs. Froude Number

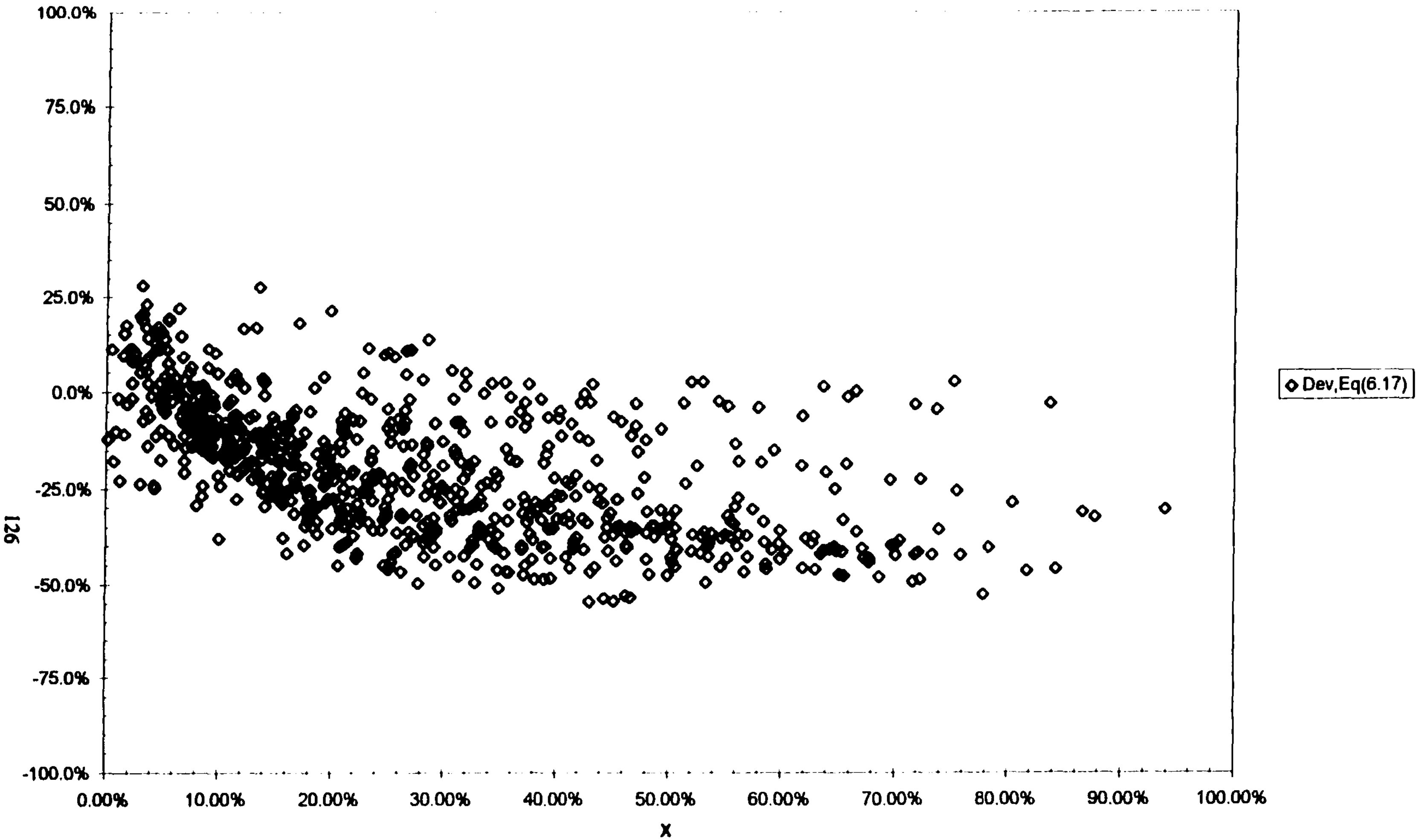

Fig 6.8 Deviation of Eq.(6.17) vs. Quality

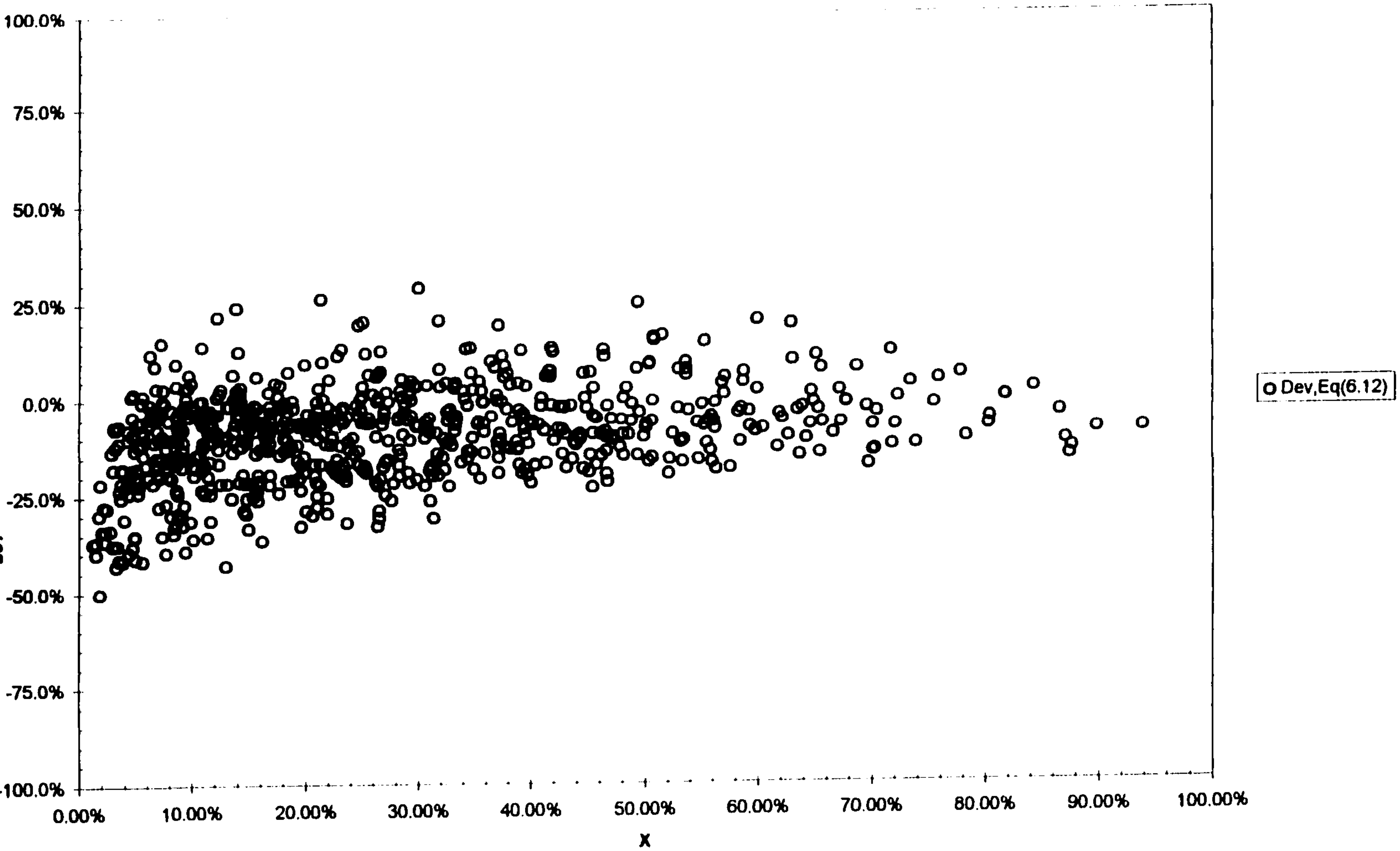

Fig 6.9 Deviation of Eq.(6.12) vs. Quality

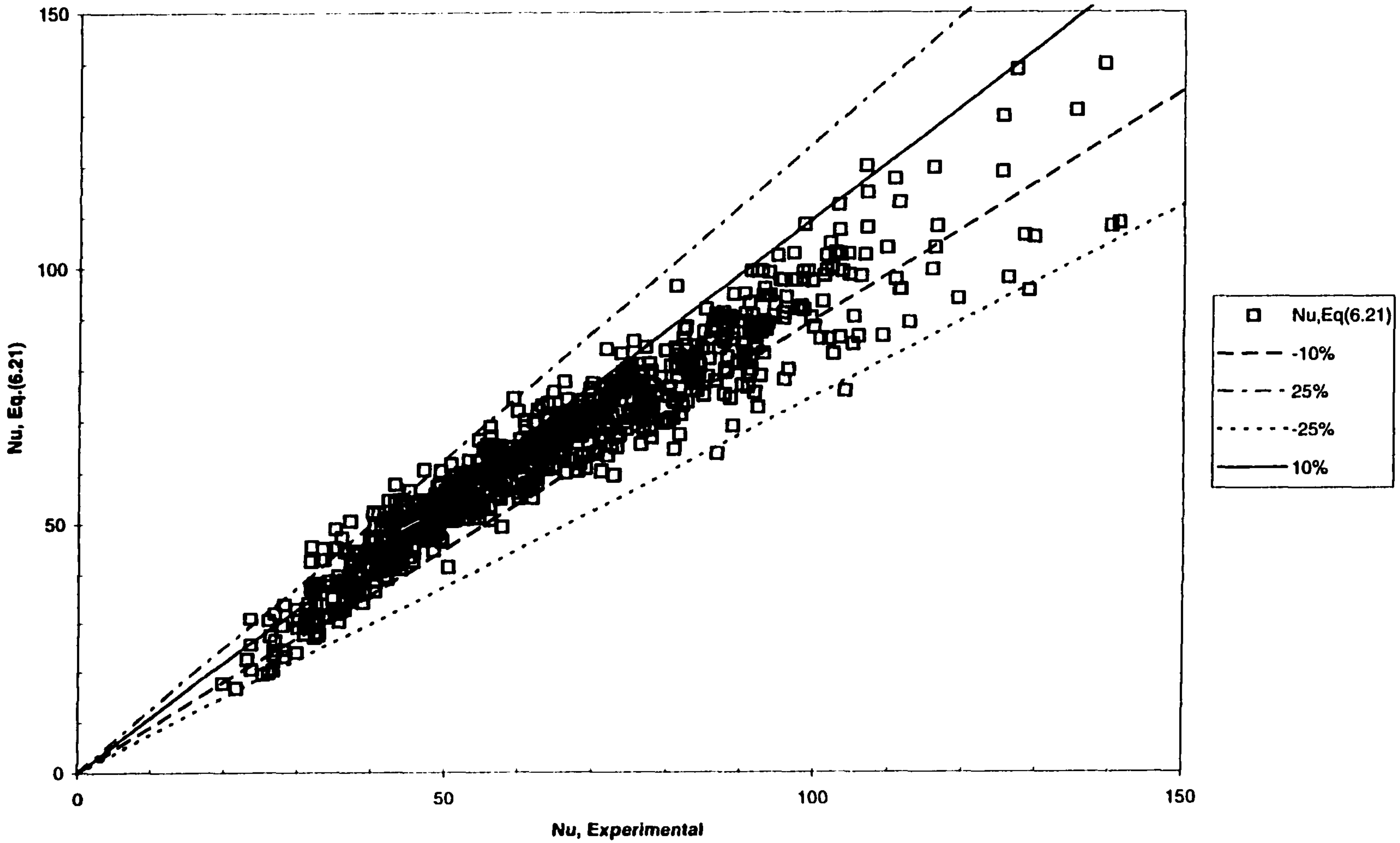

Figure 6.10 Comparison of experimental data with prediction of Eq. (6.21)

CHAPTER 7

CONCLUSIONS

This dissertation explored the results of an experimental study of the heat transfer and fluid dynamics inside microchannel tubes with the compliment of flow visualizations. Following are the conclusions drawn from this study and recommendations proposed for future work.

7.1 Conclusions

7.1.1 Heat transfer

The single-phase heat transfer inside the microchannel tube was described using the Gnielinski correlation for turbulent flow, and by the analytical solution of the governing equations for a rectangular channel with the same aspect ratio for laminar flow.

The condensation heat transfer inside the microchannel tube was affected by the flow regime. At low mass fluxes or low qualities, flow regimes were dominated by gravity; therefore, the film-wise condensation mechanism was dominant. The heat transfer dependence on temperature difference and the insensitivity to quality characterized such a flow pattern. As mass fluxes or qualities increased, the forced convection mechanism prevailed. The significant influence of quality and mass flux was observed; therefore, a different flow pattern was expected.

The validity of correlations from the literature was assessed by comparing with the experimental data. The Akers' correlation provided reasonable predictions; however, other correlations from the literature over-predicted the annular flow data. The correlation by Jaster and Kosky apparently did a good job at low mass fluxes. On the other hand, the correlation of Chato failed to account for the increasing influence from the bottom pool.

7.1.2 Flow regimes

Various flow regimes were observed in the flow visualization, including slug, wavy, wavy/annular, annular, and annular/mist. As the mass flux increased, the shear-dominated mechanism took over and the annular flow pattern prevailed. On the other hand, as the mass flux decreased at lower qualities, the gravity-dominated film condensation mechanism brought out the slug and wavy flow patterns. Both a transition prediction map and a flow regime map are developed from the observation of the microchannel tube.

Two flow mapping methods were cited to evaluate the flow regime visualization. Because of the definition of flow pattern, terminology, and the subjectivity of visualized determination, both agreements and discrepancies were shown.

By including transition zones, the Breber map provided more detailed predictions. The transition between the wavy and annular flow accounted for data with intermediate mass fluxes and high qualities. The Breber's map predicted well for the wavy and slug flows. The annular flow occurs at 0.8 ft/s superficial vapor velocity, j_v^*, instead of 1.5 ft/s predicted by the Breber map. Due to the reduced passage and rectangular geometry, the surface tension may draw the condensate liquid around the perimeter of the microchannel forming an annular liquid film at lower vapor velocity.

The Soliman map included two transitions and was divided into three flow regimes: the wavy/slug, annular, and mist flow patterns. Combined with slug, stratified and wavy flow, a broad regime was predicted for the low mass fluxes or high mass fluxes with low qualities. The surface tension over the micro-channel stabilized the annular-mist flow; therefore, the onset of the mist was extended to high flux with high quality regions

7.1.3 Correlation

Two correlations were developed for the annular flow condensation heat transfer. Both the theoretical boundary-layer and the simpler two-phase multiplier approaches were utilized. Both correlations predicted the data with average deviations less than 9%, and less than 5% of data did not fall within +/-25% of predictions, as compared with Akers' with 16% of data not within +/-25%.

Another correlation specified for the wavy/slug flow heat transfer was also derived. By weighting the contribution from either the film-wise condensation in the top potion of the tube and the forced convection in the bottom liquid pool via void fraction, a superposition correlation was proposed with an average deviation from the data of less than 9.5%.

To account for various flow conditions regardless of flow regimes, an asymptotic correlation was proposed by smoothing the transition between each correlation for a specified flow pattern. As a result, even without knowing the flow regime, the asymptotic correlation provided the better prediction with an average deviation of 7.63%.

7.2 Recommendations

Extensive work has been done regarding the single-phase and condensation heat transfer inside the smooth microchannel tube. However, there are some areas recommended for future work.

The enhancement for improving the heat transfer coefficient inside the microchannel tube is an area that has drawn a lot of attention. There are two basic ways to enhance the heat transfer: increasing the surface area by adding micro fins, or inducing the mixing and turbulence of the working fluids by opening channels with offset fins. Some efforts have been focused on the enhancement techniques. Because of the confidentiality of the innovative design, information from the research effort is not available to the public.

As a result of the diminished flow passage due to the enhancement treatment, the increase in the friction factor and pressure drop is the tradeoff to improve the heat transfer performance. To understand more details of the fluid mechanics inside the microchannel tube, an adiabatic pressure drop investigation is necessary.

To simulate the real world operation, an air cooling channel was utilized in the experiment. The thermal resistance of the air side is as much as 100 times larger than the refrigerant side. Improvements to the experimental uncertainty and the overall heat transfer can be achieved by reducing the airside thermal resistance.

As a practical case study, the presence of the lubricant in the refrigerant should be taken into consideration. The variation of the heat transfer performance under different concentrations of the lubricant would be a valuable extension of this work.

In addition to the HFC-134a tested in this study, other working fluids of zeotropic mixtures can be assessed to extend the findings of the present work to various refrigerants with different properties.

With the improved understanding of the physics in microchannel tubes from the present study, optimized designs for microchannel condensers will be achieved.

REFERENCES

1. Adams, T. M., S. I. Abdel-Khalik, S. M. Jeter, and Z. H. Qureshi, "An experimental investigation of single-phase forced convection in microchannels" ***Int. J. Heat Mass Transfer, 41***, 851-857, 1998.

2. Akers, W.W., and H.F. Rosson. "Condensation inside a Horizontal Tube." ***Chemical Engineering Progress Symposium Serb 30(56):*** 145-149, 1960.

3. Ahmed, S., and Brundrett, E., " Characteristic Lengths for Non-Circular Ducts," ***Int. J. Heat Mass Transfer*, 14**, 157-159,1971.

4. ***ASHRAE Fundamentals,*** American Society of Heating, Refrigerating, and Air Conditioning Engineers, 1997.

5. Azer, N.Z., L.V. Abis, and H.M. Soliman, "Local heat transfer coefficients during annular flow condensation", ***ASHRAE Transactions, 1(78),*** 135-143, 1972.

6. Baker, O., "Simultaneous flow of oil and gas", ***Oil and Gas Journal, 53,*** 185-195, 1954.

7. Barnea, D., Y. Luninski, and Y. Taitel,"Flow Pattern in Horizontal and Vertical Two Phase Flow in Small Diamete Pipes", ***The Canadian Journal of Chemical Engineering, 61***, 617-620, 1983.

8. Boyko, L.D. and G.N. Kruzhilin. "Heat Transfer and Hydraulic Resistance During Condensation of Steam in a Horizontal Tube and in a Bundle of Tubes." ***International Journal of Heat and Mass Transfer 10:*** 361-373, 1967.

9. Breber, G., Palen, J. W. And Taborek, J., "Prediction of horizontal tubeside condensation of pure components using flow regime criteria", ***Journal of Heat Transfer, 102***, 471-476, 1980.

10. Butterworth, D., "A visual study of mechanisms in horizontal, air-water flow", ***AERE Report M2556***, Hanvell, England' 1972.

11. Buyukalaca, O., J. D. Jackson, "The correlation to take account of variable property effects on turbulent forced convection to water in a pipe" ***Int. J. Heat Mass Transfer, 41***, 665-669, 1998.

12. Carey, V.P., ***Liquid-vapor phase change phenomena:*** An introduction to the themophysics of vaporization and condensation processes in heat transfer equipment, Hemisphere, New York, 1992.

13. Carpenter, E.F. and A.P. Colburn, "The effect of vapor velocity on condensation inside tubes", ***Proceedings of General Discussion on Heat Transfer***, 20-26,1951.

14. Cavallini, A., and R. Zecchin, "A dimensionless correlation for heat transfer in forced convective condensation", ***Proceedings of the Fifth International Heat Transfer Conference,*** Japan Society of Mechanical Engineers, ***3***, 309-313, 1974.

15. Chato, J.C., "Laminar condensation inside horizontal and inclined tubes", ***ASHRAE Journal, 4,*** 52-60, 1962.

16. Chen, S.L., F.M. Gemer, and C.L. Tien, "General film condensation correlations", ***Experimental Heat Transfer,*** 1, 93-107,1987.

17. Chisholm, D., "The influence of mass velocity on friction pressure gradients during steam-water flow", ***Proceedings of the Institute of Mechanical Engineers, 182(3),*** 336-341, 1968.

18. Churchill, S. W., and R. Usagi, " A General Expression for the Correlation inside a Vertical Tube." ***Proc. 5th Int. Heat Transfer Conf., 3,*** 1121-1128, 1972.

19. Churchill, S. W., " Friction-Factor Equation Spans All Fluid-flow Regimes," ***Chemical Engineering, 84***, 91-92, 1977.

20. Churchill, S. W. " Comprehensive Correlating Equations for Heat, Mass, and Momentum Transfer in Fully Developed Flow in Smooth Tubes," ***Ind. Eng. Chem. Fundamentals 16(1):*** 109-116, 1977.

21. Colburn, A. P., ***Trans. AIChE, 29***, 174, 1933.

22. Dittus, F.W., and L.M.K. Boelter, ***University of California Publications on Engineering, 2***, 443, 1930.

23. Dobson, M.K., J.C. Chato, D.K. Hinde, and S.P. Wang, "Experimental determination of internal condensation of refrigerants 134a and R- 12 in horizontal tubes", ***ASHRAE Transactions,*** 1994.

24. Dobson, M.K., J.C. Chato, "Condensation in Smooth Horizontal Tubes", ***Journal of Heat Transfer, 120,*** 193-213,1998.

25. deSouza, A.M., J.C. Chato, and J. P. Wattelet, "Pressure Drop during Tow-Phase Flow of Refrigerants in Horizontal Smooth Tubes", ***ACRC TR-25***, University of Illinois, 1992.

26. DuPont, Thermodynamic Properties of HFC-134a (1, 1, 1, 2 Tetrafluoroethane), T-134a-ENG, ***Document H-4775l-1, E.I. du Pont de Nemours and Co***., Wilmington, DE, 1993.

27. Galbiati, L. and P. Andreini. 1992. "The Transition between Stratified and Annular Regimes for Horizontal Two-Phase Flow in Small Diameter Tubes." ***International Communications in Heat and Mass Trader 19: 185490.***

28. Gallagher, J., M. McLinden, G. Morrison, and M. Huber, ***REFPROP.*** National Institute of Standards and Technology. Gaithersburg, MD, 1994.

29. Gnielinski, V., "New equations for heat and mass transfer in turbulent pipe and channel flow", ***International Chemical Engineering, 16,*** 359-368,1976.

30. Goodremote, C.E., L.A. Guntly, and N.F. Costello. "Compact Air Cooled Air Conditioning Condenser.'* ***SAE Technical Paper Series,*** paper number 880445, 1988

31. Guntly, L. "Use of HCFC-22 in a Vehicular Air Conditioning System." ***SAE Technical Paper Series,*** paper number 900599, 1990.

32. Hanratty, T.J., L. R. Williams, L.A. Dykhno, "Droplet Flux Distributions and Entrainment in Horizontal Gas-Liquid Flows". ***International Journal of Multiphase Flow, 22 [1],*** 1-18, 1996.

33. Hausen, H., "Darstellung des Warmeiiberganges in ***Rohren durch verallgemeinerte Potenzbeziehungen,"VDI 2, Suppl. Verfahrenstecchnik,***". ***4***, 91-98, 1943.

34. Hewitt, G. F. and D. N. Roberts, "Studies of two-phase flow patterns by simultaneous X-ray and flash photograph" ***AERE-M2159***, 1969.

35. Hubbard, M.G., and A.E. Dukler, ' The characterization of flow regimes for horizontal two-phase flow: statistical analysis of wall pressure fluctuations", ***Proceedings of the 1966 Heat Transfer and Fluid Mechanics Institute***, 100- 121,1966.

36. Jaster, H., and P.G. Kosky, "Condensation in a mixed flow regime", ***International Journal of Heat and Mass Transfer***, 19, 95-99, 1976.

37. Jeffreys, H., "On the formation of water waves by wind", ***Proceedings of the Royal Society***, A107, 189, 1925.

38. Jeffreys, H., "On the formation of water waves by wind", ***Proceedings of the Royal Society***, A110, 241, 1926.

39. Jones, O.C., "An improvement in the calculation of turbulent friction in rectangular ducts", ASME ***Journal of Fulids Engineering, 98***, 173-181, 1976.

40. Kays, W. N., *Trans. ASME, 77,* 1265, 1955.

41. Lin, P.Y. and T.J. Hanratty, "Detection of slug flow from pressure measurements", ***International Journal of Multiphase Flow, 15(2)***, 209-226,1989.

42. Lockhart, R.W. and R.C. Martinelli, "Proposed correlation of data for isothermal, two-phase, two-component flow in pipes", ***Chemical Engineering Progress, 45(l)***, 39-48, 1947.

43. Mandhane, J.M., G.A. Gregory, and K. Aziz, "A flow pattern map for gas-liquid flow in horizontal and inclined pipes", ***International Journal of Multiphase Flow***, 1, 537-553, 1974.

44. Moffat, R.J., "Describing the Uncertainties in Experimental Results", ***Experimental Thermal and Fluid Science 1***, 3-17, 1988.

45. Nicholson, M. K., K. Aziz, and G. A. Gregory, "Intermittent Two Phase Flow: Predictive Models", *27th Canadian Chemical Engineering Conference, Calgary, Alberta,* 1987.

46. Obot, N. T., " Determination of Incompressible Flow Friction in Smooth Circular and Noncircular Passages: A Generalized Approach Including Validation of the Nearly Century-Old Hydraulic Diameter Concept," *J. Fluids Eng., 110,* 431-440, 1988.

47. Petukhov, B. S., in T.F. Irvrine and J.P. Hartnett, Eds., ***Advances in Heat Transfer, 6, Academic Press, NY***, 1970.

48. Rosson, H-F., and J.A. Meyers, "Point values of condensing film coefficients inside a horizontal tube", ***Chemical Engineering Progress Symposium Series,*** 61(59), 190-199, 1965.

49. Rowland, F.S., and M.R. Molina, "Stratospheric sink for chloroflouromethanes: Chlorine atom catalyzed destruction of ozone", ***Nature,*** 249, 810-812, 1974.

50. Shah, R. K., and London, A. L., *Laminar Flow Forced Convection in Ducts,* Advances in ***Heat Transfer, suppl. 1, Academic Press, New York***, 1978.

51. Shah, R. K., and Bhatti, M. S., Laminar Convective Heat Transfer in Ducts, Ch. 3 in ***Handbook of Single-Phase Convective Heat Transfer*** (eds. Kakac, S., Shah; R. K., and Aung, W.), Wiley-Interscience, New York, 1987.

52. Shah, R. K., "Assessment of Modified Wilson plot techniques for obtaining heat exchanger design data" ***Heat Transfer, 2, 51-56, McGraw-Hill, NY***, 1990.

53. Shah, M.M., "A general correlation for heat transfer during film condensation inside pipes", ***International Journal of Heat and Mass Transfer, 22,*** 547-556, 1979.

54. Sieder, E. N. and G. E. Tate, ***Ind. Eng. Chem., 28***, 1429, 1936.

55. Soliman, M., J.R. Schuster, and P.J. Berenson, "A general heat transfer correlation for annular flow condensation", ***Journal of Heat Transfer, 90,*** 267-276, 1968.

56. Soliman, H.M., "On the annular-to-wavy flow pattern transition during condensation inside horizontal tubes", ***The Canadian Journal of Chemical Engineering, 60,***475- 481, 1982.

57. Soliman, H.M., "Correlation of mist-to-annular transition during condensation", ***The Canadian Journal of Chemical Engineering, 61,*** 178~182, 1983.

58. Soliman, H.M., "The mist-annular transition during condensation and its influence on the heat transfer mechanism", ***International Journal of Multiphase Flow, 12(2),*** 277-288, 1986.

59. Souza, A.M., J.C. Chato, and J.P. Wattelet, "Pressure drop during two-phase flow of refrigerant in horizontal smooth tubes", ***ACRC Technical Report 25,*** 1992.

60. Struss, RA. and L.W. Gabbey. "Performance Comparison of HFC-134a and CFC-12 in a Heavy Truck Air Conditioning System." ***SAE Technical Paper Series, paper number*** - 902261, 1990.

61. Struss, R.A., J.P. Henkes, and L.W. Gabbey "Performance Comparison of HFC-134a and CFC-12 with Various Heat Exchangers in Automotive Air Conditioning Systems." *SAE Technical Paper Series, paper number 900598*, 1990,

62. Sugihara, A. and H.G. Lukas, "Performance of Parallel Flow Condensers in Vehicular Applications." SAE ***Technical Paper Series,*** paper number 900597, 1990.

63. Tait, R.D., C.J. Rogers, A.J. Cottonc, J.P. He&s, and Z.P. Saperstein, "Corrosion Resistance of the As Brazed PF Heat Exchanger as Achieved by Alloy Selection." ***SAE Technical Paper Series,*** paper number 910594, 1991.

64. Taitel, Y., and A.E. Dukler, "A model for predicting flow regime transitions in horizontal and hear horizontal gas-liquid flow", ***American Institute of Chemical Engineering Journal, 22(l),*** 47-55, 1976.

65. Traviss, D.P., W.M. Rohsenow, and A.B. Baron, "Forced convective condensation in tubes: A heat transfer correlation for condenser design", ***ASHRAE Transactions, 79(l***), 157-165, 1973.

66. Yang, C. Y., R. L. Webb, "Condensation of R-12 in small hydraulic diameter extruded aluminum tubes with and without micro-fins" ***Int. J. Heat Mass Transfer,*** ***39***, 791-800, 1996.

67. Yang, C. Y., R. L. Webb, "Friction pressure drop of R-12 in small hydraulic diameter extruded aluminum tubes with and without micro-fins" ***Int. J. Heat Mass Transfer,*** ***39***, 801-809, 1996.

68. Zivi, S.M., "Estimation of steady-state steam void-fraction by means of the principle of minimum entropy production, ***Journal of Heat Transfer, 86,*** 247-252, 1964.

APPENDIX A
THERMOPHYSICAL PROPERTIES
OF HFC-134A

T	P	Density	Enthalpy	Cp	Viscosity	Therm Cond	Phase
deg F	psia	lb/ft3	Btu/lb	Btu/lb.F	lb/ft.h	Btu/h.ft.F	
50	60.12	1.262	110.06	0.2222	2.76E-02	7.38E-03	V
50	60.12	78.67	27.94	0.3267	0.6121	5.13E-02	L
52	62.38	1.308	110.32	0.2235	2.78E-02	7.44E-03	V
52	62.38	78.43	28.6	0.3276	0.604	5.10E-02	L
54	64.71	1.356	110.59	0.2248	2.79E-02	7.49E-03	V
54	64.71	78.19	29.26	0.3285	0.596	5.07E-02	L
56	67.1	1.405	110.85	0.2262	2.80E-02	7.55E-03	V
56	67.1	77.95	29.91	0.3295	0.5882	5.04E-02	L
58	69.56	1.456	111.11	0.2276	2.82E-02	7.61E-03	V
58	69.56	77.71	30.58	0.3304	0.5805	5.00E-02	L
60	72.09	1.508	111.37	0.229	2.83E-02	7.67E-03	V
60	72.09	77.46	31.24	0.3314	0.5729	4.97E-02	L
62	74.68	1.562	111.63	0.2304	2.84E-02	7.72E-03	V
62	74.68	77.22	31.9	0.3324	0.5654	4.94E-02	L
64	77.35	1.617	111.89	0.2318	2.86E-02	7.78E-03	V
64	77.35	76.97	32.57	0.3334	0.5581	4.90E-02	L
66	80.09	1.674	112.15	0.2333	2.87E-02	7.84E-03	V
66	80.09	76.72	33.24	0.3345	0.5508	4.87E-02	L
68	82.9	1.733	112.4	0.2348	2.89E-02	7.90E-03	V
68	82.9	76.47	33.91	0.3355	0.5437	4.84E-02	L

70	85.79	1.793	112.65	0.2363	2.90E-02	7.96E-03	V
70	85.79	76.21	34.58	0.3366	0.5366	4.81E-02	L
72	88.75	1.855	112.9	0.2379	2.91E-02	8.02E-03	V
72	88.75	75.96	35.26	0.3377	0.5296	4.77E-02	L
74	91.79	1.919	113.15	0.2394	2.93E-02	8.07E-03	V
74	91.79	75.7	35.93	0.3388	0.5228	4.74E-02	L
76	94.9	1.984	113.39	0.2411	2.94E-02	8.13E-03	V
76	94.9	75.44	36.61	0.3399	0.516	4.71E-02	L
78	98.1	2.051	113.64	0.2427	2.96E-02	8.19E-03	V
78	98.1	75.18	37.29	0.3411	0.5093	4.68E-02	L
80	101.4	2.121	113.88	0.2444	2.97E-02	8.25E-03	V
80	101.4	74.91	37.98	0.3422	0.5027	4.64E-02	L
82	104.7	2.192	114.12	0.2461	2.99E-02	8.31E-03	V
82	104.7	74.65	38.66	0.3434	0.4962	4.61E-02	L
84	108.2	2.265	114.36	0.2478	3.00E-02	8.37E-03	V
84	108.2	74.38	39.35	0.3447	0.4898	4.58E-02	L
86	111.7	2.341	114.59	0.2496	3.02E-02	8.43E-03	V
86	111.7	74.11	40.04	0.3459	0.4834	4.55E-02	L
88	115.3	2.418	114.82	0.2514	3.04E-02	8.49E-03	V
88	115.3	73.84	40.73	0.3472	0.4772	4.51E-02	L
90	119	2.498	115.05	0.2533	3.05E-02	8.55E-03	V
90	119	73.57	41.43	0.3485	0.471	4.48E-02	L
92	122.8	2.58	115.28	0.2552	3.07E-02	8.61E-03	V
92	122.8	73.29	42.13	0.3498	0.4648	4.45E-02	L
94	126.7	2.664	115.51	0.2572	3.08E-02	8.67E-03	V
94	126.7	73.01	42.83	0.3512	0.4588	4.42E-02	L

96	130.6	2.751	115.73	0.2592	3.10E-02	8.73E-03	V
96	130.6	72.73	43.53	0.3526	0.4528	4.38E-02	L
98	134.7	2.84	115.95	0.2612	3.12E-02	8.79E-03	V
98	134.7	72.44	44.23	0.3541	0.4469	4.35E-02	L
100	138.8	2.931	116.16	0.2633	3.13E-02	8.86E-03	V
100	138.8	72.16	44.94	0.3555	0.441	4.32E-02	L
102	143.1	3.025	116.38	0.2655	3.15E-02	8.92E-03	V
102	143.1	71.87	45.65	0.3571	0.4352	4.29E-02	L
104	147.4	3.122	116.59	0.2677	3.17E-02	8.98E-03	V
104	147.4	71.57	46.37	0.3586	0.4295	4.26E-02	L
106	151.9	3.222	116.8	0.27	3.19E-02	9.05E-03	V
106	151.9	71.28	47.08	0.3602	0.4238	4.22E-02	L
108	156.4	3.325	117	0.2724	3.21E-02	9.11E-03	V
108	156.4	70.98	47.8	0.3619	0.4182	4.19E-02	L
110	161.1	3.43	117.2	0.2748	3.22E-02	9.18E-03	V
110	161.1	70.68	48.52	0.3636	0.4126	4.16E-02	L
112	165.8	3.539	117.4	0.2773	3.24E-02	9.24E-03	V
112	165.8	70.37	49.25	0.3653	0.4071	4.13E-02	L
114	170.6	3.65	117.59	0.2799	3.26E-02	9.31E-03	V
114	170.6	70.06	49.98	0.3671	0.4016	4.10E-02	L
116	175.6	3.765	117.78	0.2825	3.28E-02	9.38E-03	V
116	175.6	69.75	50.71	0.369	0.3962	4.07E-02	L
118	180.7	3.883	117.97	0.2853	3.30E-02	9.44E-03	V
118	180.7	69.44	51.44	0.3709	0.3908	4.03E-02	L
120	185.8	4.005	118.15	0.2881	3.32E-02	9.51E-03	V
120	185.8	69.12	52.18	0.3729	0.3855	4.00E-02	L
122	191.1	4.13	118.33	0.2911	3.34E-02	9.58E-03	V
122	191.1	68.8	52.92	0.3749	0.3802	3.97E-02	L

124	196.5	4.26	118.5	0.2941	3.37E-02	9.66E-03	V
124	196.5	68.47	53.67	0.377	0.375	3.94E-02	L
126	202	4.393	118.67	0.2973	3.39E-02	9.73E-03	V
126	202	68.14	54.41	0.3792	0.3698	3.91E-02	L
128	207.6	4.529	118.84	0.3006	3.41E-02	9.80E-03	V
128	207.6	67.8	55.17	0.3815	0.3646	3.88E-02	L
130	213.4	4.671	119	0.3041	3.43E-02	9.88E-03	V
130	213.4	67.47	55.92	0.3839	0.3595	3.84E-02	L
132	219.2	4.816	119.15	0.3076	3.46E-02	9.95E-03	V
132	219.2	67.12	56.68	0.3864	0.3544	3.81E-02	L
134	225.2	4.966	119.3	0.3114	3.48E-02	1.00E-02	V
134	225.2	66.77	57.45	0.3889	0.3493	3.78E-02	L
136	231.3	5.121	119.45	0.3153	3.51E-02	1.01E-02	V
136	231.3	66.42	58.21	0.3916	0.3443	3.75E-02	L
138	237.5	5.281	119.59	0.3193	3.53E-02	1.02E-02	V
138	237.5	66.06	58.99	0.3944	0.3392	3.72E-02	L
140	243.9	5.445	119.72	0.3236	3.56E-02	1.03E-02	V
140	243.9	65.7	59.76	0.3974	0.3343	3.69E-02	L
142	250.4	5.615	119.85	0.3281	3.58E-02	1.04E-02	V
142	250.4	65.33	60.54	0.4004	0.3293	3.66E-02	L
144	257	5.791	119.97	0.3328	3.61E-02	1.05E-02	V
144	257	64.96	61.33	0.4037	0.3244	3.62E-02	L
146	263.7	5.973	120.08	0.3378	3.64E-02	1.05E-02	V
146	263.7	64.58	62.12	0.407	0.3195	3.59E-02	L
148	270.6	6.161	120.19	0.343	3.67E-02	1.06E-02	V
148	270.6	64.19	62.92	0.4106	0.3146	3.56E-02	L

150	277.6	6.355	120.28	0.3486	3.70E-02	1.07E-02	V
150	277.6	63.8	63.72	0.4144	0.3097	3.53E-02	L
152	284.7	6.556	120.37	0.3545	3.73E-02	1.08E-02	V
152	284.7	63.4	64.53	0.4183	0.3048	3.50E-02	L
154	292	6.764	120.46	0.3607	3.76E-02	1.09E-02	V
154	292	62.99	65.34	0.4225	0.3	3.47E-02	L
156	299.4	6.98	120.53	0.3674	3.80E-02	1.10E-02	V
156	299.4	62.58	66.16	0.427	0.2951	3.44E-02	L
158	307	7.203	120.59	0.3745	3.83E-02	1.12E-02	V
158	307	62.15	66.99	0.4318	0.2903	3.41E-02	L
160	314.7	7.435	120.65	0.3821	3.87E-02	1.13E-02	V
160	314.7	61.72	67.82	0.4368	0.2854	3.37E-02	L
162	322.5	7.676	120.69	0.3902	3.91E-02	1.14E-02	V
162	322.5	61.28	68.66	0.4422	0.2806	3.34E-02	L
164	330.6	7.927	120.73	0.399	3.95E-02	1.15E-02	V
164	330.6	60.83	69.51	0.448	0.2758	3.31E-02	L
166	338.7	8.188	120.75	0.4085	3.99E-02	1.17E-02	V
166	338.7	60.37	70.37	0.4543	0.2709	3.28E-02	L
168	347	8.459	120.76	0.4187	4.03E-02	1.18E-02	V
168	347	59.9	71.23	0.461	0.2661	3.25E-02	L
170	355.5	8.742	120.75	0.4299	4.07E-02	1.19E-02	V
170	355.5	59.42	72.11	0.4683	0.2612	3.22E-02	L
172	364.1	9.038	120.73	0.4421	4.12E-02	1.21E-02	V
172	364.1	58.93	72.99	0.4763	0.2563	3.19E-02	L
174	372.9	9.347	120.7	0.4555	4.17E-02	1.23E-02	V
174	372.9	58.42	73.88	0.485	0.2514	3.16E-02	L
176	381.9	9.671	120.65	0.4702	4.22E-02	1.24E-02	V
176	381.9	57.89	74.79	0.4945	0.2465	3.13E-02	L

178	391	10.01	120.58	0.4866	4.28E-02	1.26E-02	V
178	391	57.36	75.71	0.5051	0.2415	3.10E-02	L
180	400.3	10.37	120.49	0.5048	4.34E-02	1.28E-02	V
180	400.3	56.8	76.64	0.5168	0.2365	3.07E-02	L
182	409.8	10.74	120.38	0.5253	4.40E-02	1.30E-02	V
182	409.8	56.23	77.58	0.5299	0.2315	3.04E-02	L
184	419.5	11.14	120.25	0.5484	4.46E-02	1.33E-02	V
184	419.5	55.63	78.54	0.5446	0.2264	3.01E-02	L
186	429.3	11.56	120.09	0.5748	4.53E-02	1.35E-02	V
186	429.3	55.01	79.52	0.5614	0.2212	2.98E-02	L
188	439.3	12	119.9	0.6052	4.61E-02	1.38E-02	V
188	439.3	54.37	80.51	0.5807	0.2159	2.95E-02	L
190	449.6	12.48	119.68	0.6406	4.69E-02	1.41E-02	V
190	449.6	53.7	81.53	0.6031	0.2106	2.92E-02	L

APPENDIX B
HEAT TRANSFER DATA

G klb/ft^2hr	x	h Btu/ft^2hF	Nu	T, sat(F)	T,wall(F)	Fr,so	Nu,Eq. (6.12)	Dev,Eq. (6.12)	Nu, Eq.(6.16)	Dev,Eq. (6.16)	Nu,Eq. (6.17)	Dev,Eq. (6.17)	Nu,Eq. (6.21)	Dev,Eq. (6.21)
58.47595	0.33206	366.2849	49.41614	148.1422	140.6639	0.703037	21.07931	-57.34%	42.54169	-13.91%	45.62421	-7.7%	45.62623	-7.67%
58.47595	0.17911	246.2155	33.21737	146.1571	138.1804	0.509573	17.06818	-48.62%	32.71128	-1.52%	32.71128	-1.52%	32.71617	-1.51%
58.47595	0.156105	272.8601	36.81204	148.1422	136.6611	0.468339	16.30406	-55.71%	28.45452	-22.70%	28.45452	-22.70%	28.46536	-22.67%
60.0493	0.318926	361.2557	48.77876	148.3227	141.522	0.689938	21.16411	-56.61%	42.90287	-12.05%	42.90287	-12.05%	42.90653	-12.04%
60.0493	0.160517	285.5822	38.5609	148.3227	137.9781	0.476058	16.77054	-56.51%	29.5211	-23.44%	29.5211	-23.44%	29.53141	-23.42%
60.31152	0.535963	403.8246	54.48069	148.1422	141.7251	0.846159	26.67947	-51.03%	51.56043	-5.36%	51.56043	-5.36%	51.56752	-5.35%
60.31152	0.367853	347.2495	46.84804	148.1422	138.9093	0.734827	22.3773	-52.23%	41.96092	-10.43%	41.96092	-10.43%	41.96872	-10.42%
60.31152	0.123145	256.8297	34.64935	148.0628	135.5009	0.400762	15.37646	-55.62%	25.27663	-27.05%	25.27663	-27.05%	25.29411	-27.00%
60.83597	0.32139	322.6257	43.77197	149.4055	138.8104	0.689403	21.49693	-50.89%	38.60672	-11.80%	38.60672	-11.80%	44.2568	1.11%
61.09819	0.485883	344.4492	46.81222	149.7575	139.5607	0.815211	25.60926	-45.29%	44.57254	-4.78%	44.57254	-4.78%	44.58998	-4.75%
61.09819	0.20526	244.098	33.17404	149.7575	133.5004	0.546609	18.53584	-44.13%	29.51786	-11.02%	29.51786	-11.02%	29.54588	-10.94%
61.09819	0.3485	245.9849	33.43048	149.4488	136.7965	0.714039	22.23907	-33.48%	38.04603	13.81%	38.04603	13.81%	38.06371	13.86%
106.7252	0.266	236.748	32.20248	149.3622	136.7746	6.732621	29.56042	-8.20%	25.44272	-20.99%	35.67486	10.78%	36.18505	12.37%
106.7252	0.664717	389.5528	52.98701	149.9469	142.7303	63.76353	45.90869	-13.36%	41.83181	-21.05%	53.09339	0.20%	54.21997	2.33%
106.7252	0.552236	352.0192	47.88168	149.9469	139.2747	34.02428	40.14737	-16.15%	36.40737	-23.96%	46.07715	-3.77%	47.12511	-1.58%
106.7252	0.385265	301.3949	40.99577	149.9469	137.3606	13.89412	33.78902	-17.58%	29.86527	-27.15%	40.23435	-1.86%	40.88671	-0.27%
106.7252	0.209727	259.9938	35.36438	149.9469	134.0845	4.459043	27.3024	-22.80%	23.22596	-34.32%	31.82458	-10.01%	32.45299	-8.23%
106.7252	0.043485	190.9048	25.96689	147.7917	130.2132	0.432799	15.92337	-38.68%	13.86065	-46.62%	19.5484	-24.72%	19.78633	-23.80%
107.2496	0.171	197.4115	26.78364	148.865	137.4569	3.222453	25.54091	-4.64%	21.6162	-19.29%	31.64583	18.15%	31.99871	19.47%
107.2496	0.529529	356.4283	48.35812	149.4055	141.7857	30.40157	39.27887	-18.78%	35.51348	-26.56%	49.58499	2.54%	50.04751	3.49%
107.2496	0.420896	321.5201	43.62197	149.4055	138.0681	17.04557	35.10746	-19.52%	31.24778	-28.37%	42.37099	-2.87%	42.97671	-1.48%
107.2496	0.259423	281.6953	38.21877	149.4055	136.2735	6.491399	29.34586	-23.22%	25.2391	-33.96%	35.52684	-7.04%	36.0202	-5.75%
107.2496	0.092303	197.1913	26.75377	149.4055	129.3911	1.264948	20.74861	-22.45%	17.57542	-34.31%	23.73912	-11.27%	24.29446	-9.19%
111.4452	0.837311	460.2134	62.0882	148.1082	142.6465	238.8702	63.01454	1.49%	56.83901	-8.45%	60.18535	-3.06%	66.17659	6.58%
111.4452	0.736443	397.3856	53.61199	148.1082	138.781	106.425	52.41209	-2.24%	47.53707	-11.33%	51.21151	-4.48%	55.56398	3.64%
111.4452	0.578858	361.6291	48.78802	148.1082	137.3766	41.61923	42.50783	-12.87%	38.62596	-20.83%	46.78598	-4.10%	48.32893	-0.94%
111.4452	0.412928	337.6334	45.55072	148.1082	136.1202	17.15327	35.61473	-21.81%	31.75026	-30.30%	41.78874	-8.26%	42.56529	-6.55%
111.4452	0.252789	288.7044	38.94962	148.1082	135.5312	6.514824	29.70253	-23.74%	25.62962	-34.20%	35.84205	-7.98%	36.35521	-6.66%
111.4452	0.107482	239.1352	32.26215	148.1082	133.8782	1.662369	22.29618	-30.89%	18.94469	-41.28%	26.60793	-17.53%	27.03056	-16.22%
111.4452	0.42455	322.4945	43.5083	147.6676	137.41	18.27181	36.04368	-17.16%	32.19698	-26.00%	43.25506	-0.58%	43.90716	0.92%
111.9696	0.269127	307.8718	41.30341	146.8414	138.7115	7.406938	30.21498	-26.85%	26.33202	-36.25%	40.5273	-1.88%	40.73736	-1.37%
111.9696	0.176418	270.0559	36.23011	146.8414	134.8299	3.618189	26.20268	-27.68%	22.47208	-37.97%	32.47688	-10.36%	32.83785	-9.36%

111.9696	0.042655	198.0544	26.57055	145.1725	129.2971	0.453942	16.04633	-39.61%	14.19439	-46.58%	20.16829	-24.10%	20.36447	-23.36%
111.9696	0.0155	147.4143	19.77678	148.655	138.2512	0.114822	11.10455	-43.85%	10.46956	-47.06%	17.66646	-10.67%	17.6834	-10.59%
112.4941	0.751485	417.8562	56.45302	148.4692	142.6893	119.006	54.01842	-4.31%	49.07822	-13.06%	57.92193	2.60%	60.30956	6.83%
112.4941	0.163302	286.53	38.71064	149.2125	140.3876	3.17042	25.86784	-33.18%	22.01225	-43.14%	34.03691	-12.07%	34.24962	-11.52%
112.4941	0.657504	375.46	50.72523	148.4692	139.2978	65.22608	47.11868	-7.11%	42.96881	-15.29%	50.10006	-1.23%	52.31556	3.14%
112.4941	0.512343	348.7435	47.11579	148.4692	138.1073	29.3775	39.76661	-15.60%	36.02089	-23.55%	45.76983	-2.86%	46.78436	-0.70%
112.4941	0.358986	324.3163	43.81563	148.4692	136.8014	12.78055	33.91002	-22.61%	29.9646	-31.61%	40.44746	-7.69%	41.09292	-6.21%
112.4941	0.210668	275.5221	37.22347	148.4692	136.1443	4.795611	28.15472	-24.36%	24.12303	-35.19%	34.00079	-8.66%	34.48404	-7.36%
112.4941	0.070331	220.3218	29.76582	149.2125	134.8486	0.905623	19.41473	-34.78%	16.68139	-43.96%	23.61487	-20.66%	23.92859	-19.61%
112.4941	0.079392	207.0046	27.96664	148.4692	133.8657	1.076831	20.25118	-27.59%	17.33315	-38.02%	24.21745	-13.41%	24.59476	-12.06%
112.4941	0.3745	300.5985	40.61132	148.0249	137.3639	13.96138	34.4713	-15.12%	30.55608	-24.76%	41.40652	1.96%	42.02535	3.48%
112.7563	0.036847	175.0589	23.60423	149.3233	136.1674	0.370966	15.44947	-34.55%	13.68992	-42.00%	20.35824	-13.75%	20.48367	-13.22%
113.0185	0.635913	402.4463	54.26424	147.9653	141.8633	58.0567	45.97461	-15.28%	41.87452	-22.83%	55.00407	1.36%	55.8574	2.94%
113.0185	0.5435	363.1003	48.95898	147.9653	138.658	34.96453	41.23911	-15.77%	37.43287	-23.54%	47.72904	-2.51%	48.73484	-0.46%
113.0185	0.402316	333.6476	44.9877	147.9653	137.3463	16.4427	35.55456	-20.97%	31.68029	-29.58%	42.74553	-4.98%	43.3791	-3.58%
113.0185	0.253412	299.3108	40.35787	147.9653	135.5771	6.647688	29.99814	-25.67%	25.92911	-35.75%	36.05857	-10.65%	36.59397	-9.33%
113.0185	0.109861	243.0363	32.77003	147.9653	134.3042	1.744638	22.66463	-30.84%	19.2857	-41.15%	27.08769	-17.34%	27.51204	-16.05%
113.0185	0.2806	273.1228	36.82678	147.3227	136.7019	7.989444	31.06639	-15.64%	27.00547	-26.67%	37.99009	3.16%	38.4699	4.46%
113.543	0.431476	355.4438	47.63234	147.4221	140.6942	19.44603	36.5696	-23.23%	32.80976	-31.12%	48.60589	2.04%	48.88125	2.62%
113.543	0.34163	296.8313	39.77779	147.4221	136.5506	11.7599	33.25998	-16.39%	29.35553	-26.20%	40.63067	2.14%	41.14885	3.45%
113.543	0.209016	277.3282	37.16422	147.4221	135.7647	4.817165	28.03594	-24.56%	24.09569	-35.16%	34.42338	-7.37%	34.84179	-6.25%
113.543	0.071319	199.2303	26.69847	147.4188	129.5159	0.940243	19.46658	-27.09%	16.78475	-37.13%	22.89981	-14.23%	23.31541	-12.67%
113.543	0.133	193.7089	25.95856	147.1247	137.1219	2.346894	24.1036	-7.15%	20.55114	-20.83%	30.36834	16.99%	30.657	18.10%
114.3297	0.519077	374.6208	50.41327	147.5365	141.1263	31.17966	40.4392	-19.78%	36.6431	-27.31%	51.71034	2.57%	52.13659	3.42%
114.3297	0.318296	313.9008	42.06524	146.602	139.5696	10.36514	32.57722	-22.56%	28.56775	-32.09%	44.14936	4.95%	44.35621	5.45%
114.3297	0.052	171.8125	23.02426	146.9324	134.8947	0.610778	17.49153	-24.03%	15.26707	-33.69%	22.30265	-3.13%	22.49164	-2.31%
114.3297	0.429104	339.2526	45.65372	147.5365	137.7794	19.31802	36.79554	-19.40%	32.96184	-27.80%	44.44382	-2.65%	45.07443	-1.27%
114.3297	0.234621	275.3909	36.9046	146.602	135.5116	5.941297	29.28758	-20.64%	25.25848	-31.56%	36.24202	-1.80%	36.65106	-0.69%
114.3297	0.291833	312.5485	42.06011	147.5365	136.4116	8.723936	31.68949	-24.66%	27.64671	-34.27%	38.62849	-8.16%	39.1313	-6.96%
114.3297	0.193	240.7426	32.39708	147.541	136.003	4.248024	27.54178	-14.99%	23.57763	-27.22%	33.67478	3.94%	34.1007	5.26%
114.3297	0.109508	244.2593	32.73271	146.602	133.8916	1.775687	22.66817	-30.75%	19.33501	-40.93%	27.55313	-15.82%	27.92155	-14.70%
114.3297	0.147532	263.9433	35.51923	147.5365	133.6688	2.769723	25.17988	-29.11%	21.44858	-39.61%	29.77839	-16.16%	30.29293	-14.71%
119.0497	0.717596	420.6363	56.89265	148.6836	142.0745	100.505	52.96323	-6.91%	48.73727	-14.33%	55.02724	-3.28%	57.96525	1.89%
119.0497	0.618316	378.5347	51.19825	148.6836	138.724	55.39456	46.39242	-9.39%	42.72271	-16.55%	48.03514	-6.18%	50.67107	-1.03%
119.0497	0.469745	329.7259	44.59668	148.6836	137.0835	24.92545	39.4105	-11.63%	35.80657	-19.71%	43.27227	-2.97%	44.72953	0.30%
119.0497	0.313784	299.3527	40.48858	148.6836	135.0767	10.39249	33.48394	-17.30%	29.50724	-27.12%	37.40149	-7.62%	38.48557	-4.95%
119.0497	0.162433	247.8792	33.5266	148.6836	134.101	3.342563	26.82512	-19.99%	22.958	-31.52%	30.30726	-9.60%	31.10116	-7.23%
119.0497	0.030385	186.6878	25.25023	146.5555	130.0153	0.300409	14.96294	-40.74%	13.46859	-46.66%	19.30536	-23.54%	19.45133	-22.97%
119.0497	0.3347	285.5025	38.61529	148.2967	135.6432	11.79148	34.27251	-11.25%	30.34322	-21.42%	38.45352	-0.42%	39.52497	2.36%
175.4279	0.722779	530.9857	72.5123	150.8492	144.5107	152.5198	69.87141	-3.64%	67.7189	-6.61%	56.11522	-22.61%	70.61482	-2.62%
175.4279	0.656808	449.0393	61.32156	150.8492	141.4854	101.3034	63.78343	4.01%	61.86165	0.88%	49.93674	-18.57%	64.31491	4.88%
175.4279	0.558663	389.4216	53.18007	150.8492	139.5946	58.62433	56.80043	6.81%	54.81452	3.07%	46.13379	-13.25%	57.47306	8.07%
175.4279	0.457068	339.2075	46.32276	150.8492	137.9019	34.17511	51.09824	10.31%	48.648	5.02%	42.74223	-7.73%	51.89658	12.03%

175.4279	0.358229	295.287	40.32489	150.8492	136.7983	19.8445	46.22119	14.62%	43.13706	6.97%	39.78178	-1.35%	47.16133	16.95%
175.4279	0.269823	245.0198	33.46032	150.8492	136.4686	11.50043	41.81401	24.97%	38.23307	14.26%	37.16478	11.07%	42.95086	28.36%
175.4279	0.47	346.874	47.3697	149.3201	138.1141	36.6092	51.76937	9.29%	49.39391	4.27%	43.1668	-8.87%	52.55463	10.95%
178.8368	0.263977	356.1696	48.32302	149.4055	141.0631	11.3998	41.7919	-13.52%	38.25556	-20.83%	41.65458	-13.80%	44.71841	-7.46%
178.8368	0.195664	308.0765	41.79803	149.4055	137.1245	6.822262	37.81076	-9.54%	34.14786	-18.30%	35.81837	-14.31%	39.58543	-5.29%
178.8368	0.094218	251.9574	34.18411	149.4055	133.8132	2.218672	29.58169	-13.46%	26.63229	-22.09%	29.42519	-13.92%	31.62201	-7.50%
178.8368	0.047	193.1748	26.20883	149.2459	137.1515	0.827345	23.19107	-11.51%	21.40812	-18.32%	26.79112	2.22%	27.3653	4.41%
181.459	0.465948	421.5304	57.15849	149.2661	142.7704	37.55042	52.55303	-8.06%	50.17343	-12.22%	50.71887	-11.27%	55.42021	-3.04%
181.459	0.2265	276.705	37.52052	149.2619	137.4572	8.860455	40.07667	6.81%	36.45385	-2.84%	37.4532	-0.18%	41.75759	11.29%
181.459	0.403614	372.3157	50.4851	149.2661	139.673	26.83354	49.31443	-2.32%	46.5797	-7.74%	44.79368	-11.27%	50.93718	0.90%
181.459	0.309884	323.4277	43.85601	149.2661	137.7179	15.59601	44.60798	1.71%	41.31123	-5.80%	40.45755	-7.75%	46.05672	5.02%
181.459	0.211905	279.3814	37.88343	149.2661	135.6533	7.915279	39.19764	3.47%	35.5553	-6.15%	35.87194	-5.31%	40.57373	7.10%
181.459	0.116643	244.7796	33.19151	149.2661	134.805	3.091006	32.11678	-3.24%	28.87625	-13.00%	31.18189	-6.05%	33.9541	2.30%
181.459	0.033777	173.8089	23.56806	149.0321	132.4355	0.533572	20.79581	-11.76%	19.57331	-16.95%	25.24673	7.12%	25.58819	8.57%
182.5079	0.265363	352.6439	47.84467	149.4055	143.8878	11.75349	42.44919	-11.28%	38.96365	-18.56%	45.65756	-4.57%	47.49134	-0.74%
182.5079	0.219204	314.838	42.71539	149.4055	140.8145	8.421905	39.81063	-6.80%	36.19376	-15.27%	39.61811	-7.25%	42.56594	-0.35%
182.5079	0.149425	281.2407	38.1571	149.4055	139.5901	4.530889	35.0535	-8.13%	31.55457	-17.30%	35.14406	-7.90%	37.61822	-1.41%
182.5079	0.091	218.8019	29.68577	148.4529	140.1216	2.154183	29.63774	-0.16%	26.76713	-9.83%	31.58308	6.39%	32.95421	11.01%
182.5079	0.077042	239.0136	32.42797	149.4055	137.4185	1.694103	27.98096	-13.71%	25.38089	-21.73%	29.51831	-8.97%	30.91114	-4.68%
188.8013	0.877471	679.752	91.32164	147.1863	142.0103	644.6194	99.39753	8.84%	95.08375	4.12%	61.70352	-32.43%	99.48169	8.94%
188.8013	0.593	454.751	61.09376	148.4871	139.662	78.34352	61.78438	1.13%	59.67191	-2.33%	51.89475	-15.06%	62.78758	2.77%
188.8013	0.6465	478.445	64.96771	148.387	139.2554	103.9417	66.12144	1.78%	64.40013	-0.87%	48.72845	-25.00%	66.42742	2.25%
188.8013	0.866507	597.0508	81.0731	149.5877	142.0139	555.8335	96.37907	18.88%	93.29326	15.07%	55.86311	-31.10%	96.42024	18.93%
188.8013	0.80434	572.4425	76.90509	147.1863	139.4386	309.1624	84.39528	9.74%	80.83047	5.10%	54.83589	-28.70%	84.50779	9.89%
188.8013	0.754637	514.676	69.88749	149.5877	140.5507	206.8006	77.20696	10.47%	74.97884	7.29%	51.97365	-25.63%	77.35325	10.68%
188.8013	0.695572	489.7567	65.79663	147.1863	137.8338	142.0936	70.5732	7.26%	68.06771	3.45%	50.83824	-22.73%	70.83436	7.66%
188.8013	0.353161	312.5871	42.44598	149.5877	139.9376	20.99895	48.12018	13.37%	45.21433	6.52%	43.49973	2.48%	49.63886	16.95%
188.8013	0.306024	295.2816	39.66976	147.1863	137.1396	16.11892	45.26125	14.10%	42.06312	6.03%	41.92242	5.68%	47.02212	18.53%
188.8013	0.638843	451.3009	61.28183	149.5877	139.2501	99.45493	65.48445	6.86%	63.77487	4.07%	48.60424	-20.69%	65.80938	7.39%
188.8013	0.582635	431.488	57.96848	147.1863	136.4896	74.03173	61.0352	5.29%	58.92962	1.66%	47.47369	-18.10%	61.51269	6.11%
188.8013	0.420233	367.0459	49.84091	149.5877	138.7587	30.54813	51.57698	3.48%	49.12275	-1.44%	44.03474	-11.65%	52.55119	5.44%
188.8013	0.524806	419.1732	56.91923	149.5877	138.7551	53.32659	57.44433	0.92%	55.56413	-2.38%	46.15154	-18.92%	58.05764	2.00%
188.8013	0.472178	395.7347	53.16519	147.1863	136.0551	41.08807	54.06653	1.70%	51.73532	-2.69%	45.03795	-15.29%	54.87913	3.22%
188.8013	0.371259	349.7861	46.99219	147.1863	136.0168	23.71644	48.65848	3.55%	45.8142	-2.51%	42.75535	-9.02%	49.85259	6.09%
191.1613	0.617727	500.414	67.83576	149.225	143.1607	89.63276	64.3175	-5.19%	62.6326	-7.67%	55.01481	-18.90%	65.55341	-3.36%
191.1613	0.4015	341.902	46.34798	149.225	137.8583	28.01075	50.97031	9.97%	48.42715	4.49%	43.18587	-6.82%	51.86756	11.91%
191.1613	0.562168	440.4627	59.7088	149.225	140.2896	66.11889	60.29718	0.99%	58.55728	-1.93%	49.07996	-17.80%	61.02602	2.21%
191.1613	0.478743	382.3207	51.82712	149.225	138.503	42.44319	55.15823	6.43%	53.08924	2.44%	45.43392	-12.34%	55.90421	7.87%
191.1613	0.392144	332.4114	45.06144	149.225	136.8273	26.59918	50.48236	12.03%	47.87644	6.25%	42.12976	-6.51%	51.25426	13.74%
191.1613	0.307675	296.6113	40.20841	149.225	136.0436	16.24675	46.08696	14.62%	42.93016	6.77%	39.48465	-1.80%	46.98577	16.86%
191.1613	0.2319	243.9525	33.07002	149.225	135.5365	9.743337	41.83742	26.51%	38.33863	15.93%	36.88465	11.54%	42.89534	29.71%
192.2102	0.265513	359.1615	48.77028	149.5859	143.6018	12.40017	44.02381	-9.73%	40.65351	-16.64%	45.13543	-7.45%	47.81259	-1.96%
192.2102	0.088	229.0455	31.10193	149.7958	138.7867	2.162545	30.38325	-2.31%	27.62258	-11.19%	31.32709	0.72%	33.10444	6.44%

192.2102	0.218881	311.5559	42.30596	149.5859	140.4509	8.854077	41.26116	-2.47%	37.7341	-10.81%	39.4449	-6.76%	43.34711	2.46%
192.2102	0.148269	274.564	37.28285	149.5859	138.715	4.718041	36.25664	-2.75%	32.82791	-11.95%	34.92027	-6.34%	38.20294	2.47%
192.2102	0.073759	229.759	31.19881	149.5859	136.0921	1.677721	28.58169	-8.39%	26.11335	-16.30%	29.52415	-5.37%	31.17486	-0.08%
220.0059	0.575054	567.8514	77.59088	151.0315	144.8529	80.93126	67.48248	-13.03%	67.03848	-13.60%	53.96281	-30.45%	68.17144	-12.14%
220.0059	0.3215	375.6705	51.3314	150.9098	138.6892	20.19321	51.86072	1.03%	49.3149	-3.93%	40.94083	-20.24%	52.3288	1.94%
220.0059	0.50623	500.9761	68.45309	151.0315	141.5558	56.055	62.68642	-8.42%	61.80901	-9.71%	47.46888	-30.65%	63.0646	-7.87%
220.0059	0.404111	441.7662	60.36267	151.0315	140.2468	32.44615	56.54334	-6.33%	54.76907	-9.27%	44.07191	-26.99%	56.99471	-5.58%
220.0059	0.298446	386.2509	52.77709	151.0315	138.0699	17.50939	50.52352	-4.27%	47.78344	-9.46%	39.95794	-24.29%	50.98758	-3.39%
220.0059	0.195506	324.5309	44.34372	151.0315	137.1262	8.349921	43.85117	-1.11%	40.56288	-8.53%	36.49209	-17.71%	44.50412	0.36%
220.0059	0.110536	235.0591	32.11833	151.0315	136.654	3.440128	36.26037	12.90%	33.33566	3.79%	33.03462	2.85%	37.48478	16.71%
225.2504	0.739432	664.0857	90.17572	149.5716	143.8335	223.4153	84.95945	-5.78%	84.33757	-6.47%	58.01084	-35.67%	85.14476	-5.58%
225.2504	0.666569	590.9481	80.24442	149.5716	140.7752	140.5306	76.51673	-4.65%	76.12149	-5.14%	51.15602	-36.25%	76.65216	-4.48%
225.2504	0.472	462.45	62.79576	149.757	139.5099	48.44902	61.29424	-2.39%	60.15032	-4.21%	46.33922	-26.21%	61.65822	-1.81%
225.2504	0.558211	540.8025	73.43518	149.5716	139.8993	76.57864	67.15539	-8.55%	66.55904	-9.36%	48.30862	-34.22%	67.4005	-8.22%
225.2504	0.198932	233.8424	31.75329	149.5716	138.7142	8.902548	44.51901	40.20%	41.35023	30.22%	38.54146	21.38%	45.47417	43.21%
225.2504	0.445792	487.8254	66.24146	149.5716	138.237	42.13377	59.67747	-9.91%	58.32077	-11.96%	44.58795	-32.69%	59.99334	-9.43%
225.2504	0.33796	402.3764	54.6384	149.5716	137.6511	23.08875	53.37018	-2.32%	51.05552	-6.56%	41.84938	-23.41%	53.82163	-1.49%
225.2504	0.250086	303.796	41.25224	149.5716	137.5058	13.1476	48.04777	16.47%	45.07569	9.27%	39.44923	-4.37%	48.67807	18.00%
226.0371	0.654578	616.6836	84.00034	150.3132	144.41	130.6709	75.54174	-10.07%	75.38057	-10.26%	56.15141	-33.15%	75.92199	-9.62%
226.0371	0.584816	545.4307	74.29476	150.3132	141.1834	88.24728	69.4333	-6.54%	69.11372	-6.97%	49.37924	-33.54%	69.65974	-6.24%
226.0371	0.480769	492.9139	67.1413	150.3132	140.1256	50.65589	62.10539	-7.50%	61.12983	-8.95%	46.32382	-31.01%	62.42875	-7.02%
226.0371	0.37272	440.2422	59.96673	150.3132	138.2757	28.16903	55.64974	-7.20%	53.68893	-10.47%	42.49862	-29.13%	56.01428	-6.59%
226.0371	0.268869	360.3699	49.08708	150.3132	137.4836	14.93338	49.51013	0.86%	46.6569	-4.95%	39.47951	-19.57%	50.00213	1.86%
226.0371	0.184331	266.7294	36.33202	150.3132	137.2153	7.843564	43.6619	20.17%	40.46177	11.37%	36.75884	1.17%	44.38641	22.17%
226.0371	0.398	419.7765	57.17903	149.1477	139.9407	32.44169	57.11249	-0.12%	55.39245	-3.12%	44.48562	-22.20%	57.56545	0.68%
226.5615	0.263676	380.7152	51.65323	149.4037	144.0883	14.55026	49.07167	-5.00%	46.20653	-10.54%	47.19865	-8.62%	51.67735	0.05%
226.5615	0.225393	330.6936	44.86658	149.4037	141.0426	11.05745	46.55084	3.75%	43.48387	-3.08%	41.58383	-7.32%	47.87428	6.70%
226.5615	0.1115	265.9769	36.0862	148.6264	139.8525	3.636731	36.80199	1.98%	33.99871	-5.78%	35.363	-2.00%	38.74103	7.36%
226.5615	0.168369	296.6836	40.2523	149.4037	140.0508	6.844572	42.25517	4.98%	39.10547	-2.85%	38.37318	-4.67%	43.64299	8.42%
226.5615	0.108768	260.8808	35.39479	149.4037	138.0712	3.505136	36.49331	3.10%	33.72252	-4.72%	34.37796	-2.87%	38.12916	7.73%
226.5615	0.049164	231.3217	31.38439	149.4037	137.4105	1.126412	27.6808	-11.80%	26.22975	-16.42%	30.58136	-2.56%	31.55748	0.55%
226.8238	0.436253	472.6182	63.69016	147.8867	142.3453	40.83227	59.11327	-7.19%	57.58812	-9.58%	52.56586	-17.47%	60.72736	-4.65%
226.8238	0.559402	568.5762	76.77232	148.3173	142.1609	78.35662	67.44433	-12.15%	66.67994	-13.15%	53.97788	-29.69%	68.13848	-11.25%
226.8238	0.388681	425.7182	57.36991	147.8867	139.6739	31.48644	56.27268	-1.91%	54.37087	-5.23%	46.86894	-18.30%	57.1173	-0.44%
226.8238	0.493216	507.1209	68.47429	148.3173	138.855	55.11905	62.78417	-8.31%	61.68936	-9.91%	47.51699	-30.61%	63.16094	-7.76%
226.8238	0.31522	391.7672	52.79467	147.8867	138.2196	20.53956	51.96171	-1.58%	49.46828	-6.30%	43.33849	-17.91%	52.75181	-0.08%
226.8238	0.394443	455.4529	61.49779	148.3173	137.6707	32.40434	56.69297	-7.81%	54.8513	-10.81%	44.29725	-27.97%	57.15639	-7.06%
226.8238	0.235494	355.0341	47.8445	147.8867	136.6143	12.07391	46.97269	-1.82%	43.98254	-8.07%	39.65392	-17.12%	47.77209	-0.15%
226.8238	0.035435	229.6723	30.9507	147.8867	136.0685	0.726067	24.45106	-21.00%	23.60872	-23.72%	29.48139	-4.75%	29.90668	-3.37%
226.8238	0.156853	305.5848	41.1807	147.8867	135.8404	6.197781	41.01444	-0.40%	37.94901	-7.85%	36.31112	-11.82%	42.0912	2.21%
226.8238	0.29215	399.3455	53.92185	148.3173	135.594	17.72092	50.66603	-6.04%	47.99612	-10.99%	40.2752	-25.31%	51.15468	-5.13%
226.8238	0.084243	270.9934	36.51915	147.8867	135.1275	2.442838	33.21297	-9.05%	30.88278	-15.43%	32.50375	-11.00%	35.23514	-3.52%
226.8238	0.068773	173.7471	23.46031	148.3173	135.0705	1.821323	31.02007	32.22%	29.0104	23.66%			31.02007	32.22%

226.8238	0.194346	320.7907	43.31494	148.3173	134.5857	8.710209	44.14072	1.91%	41.0169	-5.31%	36.86875	-14.88%	44.82105	3.48%
226.8238	0.114814	238.1505	32.1564	148.3173	134.2881	3.834706	37.00931	15.09%	34.20738	6.38%	33.6593	4.67%	38.24063	18.92%
226.8238	0.317	381.754	51.54655	141.892	134.2251	20.69697	52.15631	1.18%	49.67302	-3.63%	40.00687	-22.39%	52.51291	1.87%
226.8238	0.23535	349.32	47.07447	142.8449	135.1774	12.06117	46.96304	-0.24%	43.97227	-6.59%	38.73235	-17.72%	47.60578	1.13%
229.9704	0.310691	446.43	59.99267	147.2416	142.4033	20.36427	52.05941	-13.22%	49.58069	-17.36%	50.34778	-16.08%	54.94735	-8.41%
229.9704	0.270901	405.7622	54.52759	147.2416	139.7648	15.77295	49.60594	-9.03%	46.85619	-14.07%	44.47796	-18.43%	51.06327	-6.35%
229.9704	0.1542	312.096	41.94044	146.5701	137.7342	6.151956	41.04559	-2.13%	38.04487	-9.29%	37.81309	-9.84%	42.57082	1.50%
229.9704	0.210054	358.4327	48.16731	147.2416	138.5048	10.13366	45.50838	-5.52%	42.48704	-11.79%	40.86083	-15.17%	46.86182	-2.71%
229.9704	0.146042	320.9067	43.12445	147.2416	137.149	5.653138	40.30509	-6.54%	37.3396	-13.41%	37.05059	-14.08%	41.77535	-3.13%
229.9704	0.083722	280.9539	37.75546	147.2416	136.6887	2.468187	33.35065	-11.67%	31.0826	-17.67%	33.39214	-11.56%	35.76664	-5.27%
229.9704	0.030024	206.8077	27.79146	147.2416	135.5205	0.590279	23.17343	-16.62%	22.64495	-18.52%	29.24168	5.22%	29.51553	6.20%
230.2327	0.236409	420.3998	56.1021	145.6299	140.908	12.55766	47.09555	-16.05%	44.17899	-21.25%	47.55339	-15.24%	50.72645	-9.58%
230.2327	0.20087	370.9837	49.50754	145.6299	138.3078	9.532772	44.57514	-9.96%	41.56566	-16.04%	41.96049	-15.24%	46.56116	-5.95%
230.2327	0.147329	326.6274	43.58822	145.6299	137.1574	5.807067	40.17403	-7.83%	37.24805	-14.55%	38.25602	-12.23%	42.14169	-3.32%
230.2327	0.09183	281.9956	37.63214	145.6299	135.6314	2.859673	34.2074	-9.10%	31.84351	-15.38%	34.11097	-9.36%	36.61123	-2.71%
230.2327	0.038125	239.7144	31.98974	145.6299	134.8602	0.829324	25.09014	-21.57%	24.21132	-24.32%	29.93175	-6.43%	30.40873	-4.94%
230.2327	0.099	286.2	38.19322	145.6299	137.373	3.191771	35.10317	-8.09%	32.62732	-14.57%	35.48549	-7.09%	37.83252	-0.94%
231.0193	0.113717	321.7779	43.43603	148.2208	144.2648	3.855574	37.33662	-14.04%	34.59192	-20.36%	40.80044	-6.07%	42.23209	-2.77%
231.0193	0.088353	266.5671	35.98325	148.2208	141.0203	2.660673	34.24946	-4.82%	31.86548	-11.44%	35.45097	-1.48%	37.40125	3.94%
237.3127	0.450408	521.8165	70.45857	148.3209	146.1325	46.0215	61.93154	-12.10%	60.82397	-13.67%	65.98118	-6.35%	68.85119	-2.28%
237.3127	0.392062	478.4608	64.60444	148.3209	144.3797	33.51886	58.31925	-9.73%	56.70549	-12.23%	55.65952	-13.85%	61.22813	-5.23%
237.3127	0.427662	477.0695	64.41658	148.3209	144.2264	40.72761	60.50061	-6.08%	59.20206	-8.09%	56.26523	-12.65%	62.93638	-2.30%
237.3127	0.317374	424.9235	57.37554	148.3209	143.8584	21.74279	53.80805	-6.22%	51.52829	-10.19%	51.54941	-10.15%	56.5756	-1.39%
237.3127	0.354674	458.2266	61.87231	148.3209	143.8214	27.12865	56.06595	-9.38%	54.11358	-12.54%	52.78673	-14.68%	58.56764	-5.34%
237.3127	0.285087	319.0567	43.08082	148.3209	143.2979	17.74775	51.80383	20.25%	49.26524	14.36%	49.01647	13.78%	54.21192	25.84%
237.3127	0.3585	426.236	57.55276	149.7846	141.1498	27.73365	56.2961	-2.18%	54.37823	-5.52%	47.67265	-17.17%	57.28219	-0.47%
237.3127	0.265704	274.6209	37.08084	148.3209	144.5606	15.60757	50.56064	36.35%	47.88444	29.14%			50.56064	36.35%
237.5749	0.326819	446.3948	60.71866	149.9487	144.7032	22.76868	54.75554	-9.82%	52.58575	-13.39%	49.93333	-17.76%	56.6202	-6.75%
237.5749	0.28485	374.4574	50.93373	149.9487	141.5282	17.52463	52.1695	2.43%	49.62703	-2.57%	43.84219	-13.92%	53.02078	4.10%
237.5749	0.1595	308.4645	41.95737	149.7782	139.7034	6.57404	42.98666	2.45%	39.94896	-4.79%	37.84773	-9.79%	44.06082	5.01%
237.5749	0.222515	342.8739	46.63774	149.9487	140.7049	11.31872	48.00149	2.92%	45.05222	-3.40%	41.00254	-12.08%	48.91234	4.88%
237.5749	0.157939	301.0297	40.94609	149.9487	138.8737	6.473174	42.84635	4.64%	39.81251	-2.77%	37.3022	-8.90%	43.81372	7.00%
237.5749	0.093328	270.4448	36.78592	149.9487	138.2098	2.928154	35.87842	-2.47%	33.40219	-9.20%	34.04895	-7.44%	37.58736	2.18%
242.0328	0.399671	508.1241	68.9783	149.5395	143.4699	35.35839	59.79014	-13.32%	58.43675	-15.28%	50.58836	-26.66%	60.82919	-11.81%
242.0328	0.347211	422.5207	57.35756	149.5395	140.1987	26.27418	56.60216	-1.32%	54.7218	-4.60%	44.68571	-22.09%	57.11322	-0.43%
242.0328	0.270575	379.6658	51.53998	149.5395	139.108	16.31242	51.8143	0.53%	49.2455	-4.45%	41.68486	-19.12%	52.37471	1.62%
242.0328	0.192639	319.6514	43.39296	149.5395	136.9262	9.101057	46.24873	6.58%	43.28097	-0.26%	37.90738	-12.64%	46.84574	7.96%
242.0328	0.116157	281.9357	38.27302	149.5395	136.0409	4.13646	39.06042	2.06%	36.35087	-5.02%	34.71952	-9.28%	40.123	4.83%
242.0328	0.198475	336.5015	45.68038	144.5009	136.4743	9.558698	46.70845	2.25%	43.75336	-4.22%	37.85514	-17.13%	47.25033	3.44%
250.9746	0.697152	754.2303	100.7356	143.9914	139.2435	195.0222	85.91012	-14.72%	85.20001	-15.42%	60.57421	-39.87%	86.16753	-14.46%
250.9746	0.637058	680.8542	90.9354	143.9914	136.6023	136.2209	79.15245	-12.96%	78.70168	-13.45%	53.42497	-41.25%	79.30643	-12.79%
250.9746	0.547292	612.3209	81.78205	143.9914	135.8395	83.16912	71.05712	-13.11%	70.56705	-13.71%	50.72943	-37.97%	71.29784	-12.82%
250.9746	0.255452	300.6238	40.15155	143.9914	135.7335	15.71776	51.32557	27.83%	48.81574	21.58%	43.78761	9.06%	52.28844	30.23%

250.9746	0.478	534.5775	71.39858	147.0485	139.0742	57.58937	65.8727	-7.74%	65.0583	-8.88%	55.73295	-21.94%	67.0171	-6.14%
250.9746	0.456853	546.9383	73.04949	143.9914	134.7845	51.46677	64.41306	-11.82%	63.46097	-13.13%	47.69361	-34.71%	64.7252	-11.40%
250.9746	0.298579	375.21	50.11333	143.9914	134.3799	20.90596	54.20964	8.17%	51.99541	3.76%	43.70486	-12.79%	54.80797	9.37%
250.9746	0.371011	467.6105	62.45442	143.9914	134.3701	32.18479	58.8252	-5.81%	57.20238	-8.41%	45.46651	-27.20%	59.25813	-5.12%
253.2297	0.783188	776.0704	103.6525	149.2322	144.5793	357.3654	99.26044	-4.24%	97.90424	-5.55%	61.78896	-40.39%	99.34682	-4.15%
253.2297	0.720664	695.9661	92.95375	149.2322	141.8267	228.8967	89.50715	-3.71%	88.72208	-4.55%	54.21782	-41.67%	89.56649	-3.64%
253.2297	0.317806	337.2851	45.04806	149.2322	141.2841	23.77512	55.78832	23.84%	53.7693	19.36%	45.79026	1.65%	56.51802	25.46%
253.2297	0.626767	639.0537	85.35249	149.2322	141.2261	129.6752	78.59634	-7.92%	78.24738	-8.32%	51.85063	-39.25%	78.7182	-7.77%
253.2297	0.531912	572.9504	76.52368	149.2322	140.1787	77.34356	70.26928	-8.17%	69.79787	-8.79%	48.87209	-36.13%	70.45319	-7.93%
253.2297	0.364572	413.3905	55.21275	149.2322	139.9644	31.31704	58.77415	6.45%	57.14823	3.51%	45.42263	-17.73%	59.20629	7.23%
253.2297	0.441646	493.1329	65.86321	149.2322	139.82	47.89085	63.77659	-3.17%	62.77754	-4.68%	46.84968	-28.87%	64.06257	-2.73%
253.2297	0.553	561.4875	74.9927	149.5759	141.3757	86.54765	71.95504	-4.05%	71.55509	-4.58%	50.91252	-32.11%	72.17821	-3.75%
254.6719	0.871896	854.1188	115.8819	149.5859	144.8484	808.8679	119.7624	3.35%	120.0975	3.64%	62.89591		119.7815	3.37%
254.6719	0.6215	598.874	81.25174	149.5258	140.6976	123.1769	78.54577	-3.33%	79.22308	-2.50%	50.46721	-37.89%	78.63945	-3.22%
254.6719	0.803278	756.6525	102.6582	149.5859	142.0807	411.2832	103.0702	0.40%	103.4216	0.74%	55.19781		103.0901	0.42%
254.6719	0.367036	363.4727	49.31385	149.5859	141.5086	31.07887	59.81664	21.30%	58.42349	18.47%	46.83916	-5.02%	60.3159	22.31%
254.6719	0.700969	672.028	91.17684	149.5859	141.2805	197.2996	87.19988	-4.36%	87.9201	-3.57%	52.46208	-42.46%	87.25391	-4.30%
254.6719	0.598217	601.8477	81.65519	149.5859	140.2352	108.2137	76.38996	-6.45%	76.9865	-5.72%	49.50791	-39.37%	76.48925	-6.33%
254.6719	0.417499	433.9495	58.87574	149.5859	140.0552	41.13443	63.00983	7.02%	62.16054	5.58%	46.21207	-21.51%	63.28796	7.49%
254.6719	0.500666	521.4761	70.75084	149.5859	139.9091	64.1339	68.61383	-3.02%	68.57622	-3.07%	47.56377	-32.77%	68.78765	-2.77%
258.5791	0.502542	586.5891	79.51758	148.8641	140.3128	65.91388	69.43925	-12.67%	69.51276	-12.58%	49.10095	-38.25%	69.65325	-12.41%
258.5791	0.412893	516.53	70.02043	148.8641	139.2666	40.82103	63.3334	-9.55%	62.52326	-10.71%	46.1632	-34.07%	63.5965	-9.17%
258.5791	0.121925	233.3765	31.63635	148.8641	138.0236	4.776523	41.46922	31.08%	38.89509	22.94%	36.90275	16.65%	42.60883	34.68%
258.5791	0.322904	454.7433	61.64467	148.8641	137.889	24.41945	57.58769	-6.58%	55.80622	-9.47%	42.97486	-30.29%	57.88894	-6.09%
258.5791	0.237614	377.6623	51.19562	148.8641	137.0728	13.91295	51.80304	1.19%	49.27578	-3.75%	40.29153	-21.30%	52.20818	1.98%
258.5791	0.165399	296.9914	40.25994	148.8641	136.8019	7.64506	45.9249	14.07%	43.16161	7.21%	37.9602	-5.71%	46.56668	15.67%
258.5791	0.562679	653.0294	88.52418	148.8641	143.3968	90.77368	74.09616	-16.30%	74.61042	-15.72%	55.79437	-36.97%	74.51937	-15.82%
258.5791	0.3445	445.7745	60.42886	148.5496	140.26	27.76797	58.96941	-2.42%	57.4153	-4.99%	45.78888	-24.23%	59.42322	-1.66%
258.8151	0.701337	736.5952	99.85231	148.5496	143.8165	201.4312	88.21339	-11.66%	89.03608	-10.83%	60.35992	-39.55%	88.40987	-11.46%
258.8151	0.642728	660.7126	89.56572	148.5496	141.0711	141.5761	81.52864	-8.97%	82.35843	-8.05%	53.06513	-40.75%	81.63921	-8.85%
258.8151	0.265899	311.2277	42.1898	148.5496	140.3618	16.98808	53.84184	27.62%	51.52832	22.13%	44.14023	4.62%	54.53823	29.27%
258.8151	0.554914	597.5221	80.99966	148.5496	140.3538	87.15117	73.50511	-9.25%	73.97998	-8.67%	50.51656	-37.63%	73.67609	-9.04%
258.8151	0.466169	540.4848	73.26773	148.5496	139.3424	54.40944	66.91357	-8.67%	66.66032	-9.02%	47.63115	-34.99%	67.13379	-8.37%
258.8151	0.38144	470.1815	63.73746	148.5496	139.018	34.33935	61.35521	-3.74%	60.20857	-5.54%	45.61139	-28.44%	61.66438	-3.25%
258.8151	0.309323	381.3568	51.69645	148.5496	139.0091	22.49342	56.74412	9.76%	54.82965	6.06%	43.95353	-14.98%	57.17062	10.59%
258.8151	0.4855	528.5745	71.65317	149.0746	138.297	60.28535	68.2597	-4.74%	68.18947	-4.83%	46.78875	-34.70%	68.41441	-4.52%
262.0404	0.453586	601.6177	81.62399	149.0445	143.3273	51.45889	66.64715	-18.35%	66.38735	-18.67%	52.93286	-35.15%	67.28461	-17.57%
262.0404	0.2475	392.6905	53.27796	149.225	137.7945	15.12284	53.03779	-0.45%	50.63421	-4.96%	41.01385	-23.02%	53.43002	0.29%
262.0404	0.396795	529.8875	71.89206	149.0445	140.041	37.82689	62.89948	-12.51%	62.01876	-13.73%	46.53916	-35.27%	63.20213	-12.09%
262.0404	0.312499	459.9927	62.40913	149.0445	138.8006	23.19881	57.47383	-7.91%	55.66149	-10.81%	43.42479	-30.42%	57.81312	-7.36%
262.0404	0.227551	396.9885	53.86108	149.0445	137.018	13.07195	51.56585	-4.26%	49.02764	-8.97%	39.97044	-25.79%	51.95606	-3.54%
262.0404	0.146509	327.4736	44.42971	149.0445	135.9776	6.400188	44.5485	0.27%	41.86156	-5.78%	36.99953	-16.72%	45.19972	1.73%
262.0404	0.078322	250.4794	33.98359	149.0445	135.5927	2.526333	36.00035	5.93%	34.07768	0.28%	34.23848	0.75%	37.7456	11.07%

267.5996	0.43894	530.8455	70.90013	151.2102	145.7636	49.98866	66.02867	-6.87%	65.40112	-7.76%	53.1239	-25.07%	66.74327	-5.86%
267.5996	0.243	386.515	51.62324	150.9449	139.8101	15.38616	52.7044	2.09%	50.3949	-2.38%	40.79836	-20.97%	53.0981	2.86%
267.5996	0.388861	494.7889	66.08437	151.2102	142.4737	38.03253	62.6332	-5.22%	61.56415	-6.84%	46.64492	-29.42%	62.95439	-4.74%
267.5996	0.311505	457.3206	61.08009	151.2102	141.4551	24.22523	57.50057	-5.86%	55.71833	-8.78%	43.84182	-28.22%	57.87142	-5.25%
267.5996	0.230885	404.2765	53.99548	151.2102	139.7465	14.08114	51.79549	-4.07%	49.41633	-8.48%	40.43144	-25.12%	52.21495	-3.30%
267.5996	0.045993	210.2081	28.07556	151.2102	139.2773	1.254801	29.7542	5.98%	28.93863	3.07%	32.87443	17.09%	33.92308	20.83%
267.5996	0.152437	341.2094	45.57219	151.2102	138.8291	7.152059	45.05552	-1.13%	42.53767	-6.66%	37.51512	-17.68%	45.72989	0.35%
267.5996	0.086101	255.2299	34.0887	151.2102	138.2829	3.042101	37.09429	8.82%	35.20561	3.28%	34.69763	1.79%	38.66202	13.42%
282.4152	0.3225	450.79	60.35896	148.0276	140.0651	27.27267	60.51253	0.25%	59.17598	-1.96%	48.97068	-18.87%	61.20482	1.40%
282.4152	0.31	427.9725	58.21286	148.1753	139.5849	24.59829	60.43884	3.82%	59.03218	1.41%	43.65592	-25.01%	60.66853	4.22%
282.4152	0.521402	655.0421	87.7075	146.4036	140.9098	81.54795	74.84911	-14.66%	75.39722	-14.04%	55.29718	-36.95%	75.20397	-14.26%
282.4152	0.520545	675.2298	91.84482	149.9469	144.0054	79.03531	75.26516	-18.05%	76.42028	-16.79%	53.96678	-41.24%	75.53123	-17.76%
282.4152	0.47039	572.2667	76.6242	146.4036	138.2348	62.23886	70.86616	-7.51%	71.02364	-7.31%	49.45727	-35.45%	71.05805	-7.26%
282.4152	0.465047	549.0844	74.68651	149.9469	141.0809	58.89973	71.06381	-4.85%	71.60865	-4.12%	48.18864	-35.48%	71.20856	-4.66%
282.4152	0.394261	493.8414	66.12336	146.4036	136.6914	41.25374	65.43074	-1.05%	64.84883	-1.93%	46.17345	-30.17%	65.62843	-0.75%
282.4152	0.383754	471.954	64.19523	149.9469	139.3513	37.88349	65.42801	1.92%	64.94925	1.17%	44.88954	-30.07%	65.57767	2.15%
282.4152	0.315837	438.1967	58.67278	146.4036	135.3819	26.1886	60.05173	2.35%	58.64741	-0.04%	43.39254	-26.04%	60.28079	2.74%
282.4152	0.122612	279.7996	37.46404	146.4036	135.3726	5.393021	43.53426	16.20%	41.34332	10.35%	37.9158	1.21%	44.52062	18.84%
282.4152	0.238562	395.9718	53.01902	146.4036	134.5929	15.68456	54.44133	2.68%	52.35949	-1.24%	41.0611	-22.55%	54.75725	3.28%
282.4152	0.167862	337.0515	45.12984	146.4036	134.3229	8.762234	48.3839	7.21%	46.03085	2.00%	38.96144	-13.67%	48.91188	8.38%
282.4152	0.300228	412.8596	56.1572	149.9469	137.8168	23.14343	59.76195	6.42%	58.24138	3.71%	42.07587	-25.07%	59.93844	6.73%
282.4152	0.218302	370.2258	50.35814	149.9469	136.8963	13.11617	53.65116	6.54%	51.36541	2.00%	39.76372	-21.04%	53.91363	7.06%
282.4152	0.143755	309.7235	42.12862	149.9469	136.4945	6.692448	46.70713	10.87%	44.25992	5.06%	37.66141	-10.60%	47.22333	12.09%
283.2019	0.899209	937.3053	127.1681	149.3983	145.1042	1292.571	138.936	9.25%	141.5195	11.29%	64.89687		138.9429	9.26%
283.2019	0.842907	787.0575	106.7834	149.3983	142.7998	659.3435	120.1524	12.52%	121.9573	14.21%	57.5737	-46.08%	120.16	12.53%
283.2019	0.454376	519.4263	70.47274	149.3983	142.5245	56.02327	70.31961	-0.22%	70.70866	0.33%	50.93799	-27.72%	70.59445	0.17%
283.2019	0.758778	698.9051	94.82338	149.3983	141.8454	325.1744	102.413	8.00%	104.3154	10.01%	54.58654	-42.43%	102.4319	8.02%
283.2019	0.505835	567.0669	76.93633	149.3983	141.1415	73.60857	74.15383	-3.62%	75.10919	-2.37%	49.73434	-35.36%	74.28928	-3.44%
283.2019	0.671436	648.1072	87.93142	149.3983	141.0827	183.7451	89.98448	2.33%	91.94809	4.57%	52.14748	-40.70%	90.02285	2.38%
283.2019	0.585225	611.2647	82.93283	149.3983	140.8929	112.547	80.88253	-2.47%	82.50346	-0.52%	50.63458	-38.95%	80.957	-2.38%
283.2019	0.6775	673.7045	91.4043	147.6419	140.1917	190.5851	90.72259	-0.75%	92.69412	1.41%	50.9483	-44.26%	90.75086	-0.71%
285.8242	0.875217	1005.593	135.3621	147.6419	143.2543	962.0489	130.9619	-3.25%	131.9341	-2.53%	64.31182		130.9726	-3.24%
285.8242	0.817655	794.6044	106.961	147.6419	140.9749	532.1043	114.8447	7.37%	115.7474	8.21%	57.20117	-46.52%	114.8555	7.38%
285.8242	0.428891	495.3991	66.68527	147.6419	140.6264	50.00818	68.62303	2.91%	68.61943	2.90%	50.35966	-24.48%	68.92775	3.36%
285.8242	0.733555	696.2178	93.7173	147.6419	139.9474	278.989	99.04259	5.68%	100.3519	7.08%	54.12207	-42.25%	99.06608	5.71%
285.8242	0.480286	576.8706	77.65208	147.6419	139.2631	65.8034	72.3839	-6.78%	72.91411	-6.10%	49.2875	-36.53%	72.53752	-6.59%
285.8242	0.646821	642.6409	86.50536	147.6419	139.1909	162.6664	87.60532	1.27%	89.06905	2.96%	51.73524	-40.19%	87.65041	1.32%
285.8242	0.560627	622.3219	83.77024	147.6419	139.0403	100.8363	78.96625	-5.73%	80.13178	-4.34%	50.27398	-39.99%	79.05222	-5.63%
285.8242	0.6535	678.385	91.31684	147.6419	140.1917	169.1116	88.36976	-3.23%	89.83759	-1.62%	53.44335	-41.47%	88.42743	-3.16%
288.6037	0.290888	478.0134	64.79914	149.2268	144.4448	22.43021	59.80415	-7.71%	58.30557	-10.02%	50.88139	-21.48%	60.89809	-6.02%
288.6037	0.253588	440.4221	59.7033	149.2268	141.1459	17.481	57.05845	-4.43%	55.17703	-7.58%	44.65273	-25.21%	57.53196	-3.64%
288.6037	0.195581	406.3937	55.09043	149.2268	140.2736	11.23076	52.31925	-5.03%	50.03154	-9.18%	42.08447	-23.61%	52.88427	-4.00%
288.6037	0.1445	344.9425	46.76015	149.2268	139.9662	6.937861	47.31019	1.18%	44.97351	-3.82%	40.09066	-14.26%	48.14414	2.96%

288.6037	0.135235	363.8883	49.32843	149.2268	138.777	6.266013	46.27213	-6.20%	43.97118	-10.86%	39.04605	-20.84%	47.05653	-4.61%
288.6037	0.076975	298.2872	40.43559	149.2268	137.8899	2.728977	38.17629	-5.59%	36.58253	-9.53%	36.38278	-10.02%	40.05833	-0.93%
288.6037	0.027356	231.2558	31.34886	149.2268	137.2661	0.648856	26.40979	-15.76%	26.61719	-15.09%	33.85279	7.99%	34.12538	8.86%
291.3309	0.702977	824.7465	111.4559	148.5031	143.5109	231.733	95.67564	-14.16%	98.09251	-11.99%	59.79443		95.76226	-14.08%
291.3309	0.495	563.5805	76.16203	148.4914	139.8868	72.17853	74.47128	-2.22%	75.79167	-0.49%	49.29118	-35.28%	74.59059	-2.06%
291.3309	0.648873	673.8984	91.07035	148.5031	141.0809	167.0259	88.87591	-2.41%	91.24211	0.19%	53.48017	-41.28%	88.93108	-2.35%
291.3309	0.284707	385.316	52.07144	148.5031	140.0659	21.91079	59.45796	14.19%	58.22394	11.82%	45.2925	-13.02%	59.83801	14.92%
291.3309	0.569558	594.7845	80.37892	148.5031	139.9153	107.3544	80.76345	0.48%	82.74636	2.95%	50.49007	-37.18%	80.83679	0.57%
291.3309	0.487768	544.7452	73.61663	148.5031	139.026	69.46741	73.90917	0.40%	75.15266	2.09%	48.09622	-34.67%	74.00921	0.53%
291.3309	0.33223	460.0361	62.16908	148.5031	138.7819	29.4321	62.8225	1.05%	62.1517	-0.03%	45.05004	-27.54%	63.04483	1.41%
291.3309	0.40687	511.8256	69.1679	148.5031	138.6607	45.01348	67.99452	-1.70%	68.27596	-1.29%	46.34475	-33.00%	68.14025	-1.49%
292.6944	0.718237	820.5667	110.8287	148.362	144.6604	258.2018	97.66832	-11.87%	100.014	-9.76%	63.93381	-42.31%	97.80851	-11.75%
292.6944	0.373573	403.9279	54.55594	148.362	142.5262	37.77714	65.7739	20.56%	65.38408	19.85%	50.77674	-6.93%	66.25242	21.44%
292.6944	0.673228	728.633	98.41175	148.362	142.2812	194.8003	91.65424	-6.87%	93.97371	-4.51%	55.90955	-43.19%	91.71942	-6.80%
292.6944	0.604738	680.4876	91.90907	148.362	141.8945	131.393	84.0768	-8.52%	86.13766	-6.28%	54.02436	-41.22%	84.17714	-8.41%
292.6944	0.534356	639.7085	86.4013	148.362	141.2105	89.8058	77.6626	-10.11%	79.18581	-8.35%	51.60946	-40.27%	77.79205	-9.96%
292.6944	0.466561	577.2687	77.96796	148.362	141.203	62.69711	72.3413	-7.22%	73.13665	-6.20%	50.40894	-35.35%	72.53422	-6.97%
292.6944	0.408614	474.3874	64.07244	148.362	141.1664	45.89944	68.19306	6.43%	68.26209	6.54%	49.22657	-23.17%	68.45066	6.83%
292.6944	0.5465	618.631	83.5545	147.2369	136.0508	95.80786	78.69304	-5.82%	80.32683	-3.86%	45.55841	-45.47%	78.72626	-5.78%
299.722	0.276367	532.1693	71.07693	146.3375	140.2709	21.78364	59.5162	-16.27%	58.05658	-18.32%	48.43039	-31.86%	60.23364	-15.26%
299.722	0.233064	433.4644	57.89384	146.3375	136.7653	16.10149	56.12671	-3.05%	54.30145	-6.21%	43.069	-25.61%	56.5119	-2.39%
299.722	0.168625	366.7671	48.98569	146.3375	134.6659	9.433296	50.34284	2.77%	48.24307	-1.52%	39.83774	-18.67%	50.80777	3.72%
299.722	0.103048	306.0272	40.87323	146.3375	132.5866	4.449136	42.62303	4.28%	40.85142	-0.05%	36.93796	-9.63%	43.54611	6.54%
299.722	0.03976	259.539	34.66423	146.3375	131.0116	1.154628	30.50688	-11.99%	30.30606		34.29995	-1.05%	35.23815	1.66%
299.722	0.11415	327.3095	43.7157	149.9317	139.0175	5.178186	44.13758	0.97%	42.24663	-3.36%	40.56983	-7.20%	45.74635	4.65%
316.2421	0.376927	556.3767	75.67841	149.9415	144.2451	41.03418	70.14144	-7.32%	70.48176	-6.87%	51.81756	-31.53%	70.47388	-6.88%
316.2421	0.2066	379.6265	51.63683	149.8829	138.334	13.45763	56.88177	10.16%	55.07636	6.66%	41.41149	-19.80%	57.11534	10.61%
316.2421	0.333555	478.4346	65.07671	149.9415	140.8314	31.9347	66.99036	2.94%	66.67944	2.46%	45.98029	-29.34%	67.14422	3.18%
316.2421	0.268314	429.0587	58.3606	149.9415	139.5901	21.16386	62.07566	6.37%	60.87899	4.32%	43.56226	-25.36%	62.25317	6.67%
316.2421	0.20184	377.17	51.3027	149.9415	138.0592	12.9463	56.44446	10.02%	54.60633	6.44%	41.14747	-19.79%	56.67926	10.48%
316.2421	0.137089	321.0969	43.67562	149.9415	136.7912	7.001685	49.64013	13.66%	47.66227	9.13%	39.10688	-10.46%	50.07935	14.66%
316.2421	0.036548	233.1439	31.71225	149.9415	136.7529	1.054403	31.32551	-1.22%	31.34599	-1.15%	36.27801	14.40%	37.03815	16.79%
316.2421	0.076835	281.3134	38.26428	149.9415	136.0685	2.978781	40.74985	6.50%	39.44836	3.09%	37.37503	-2.32%	42.20788	10.31%
317.291	0.27318	481.8028	65.31284	149.2375	144.6533	22.11957	62.33149	-4.56%	61.2127	-6.28%	51.18832	-21.63%	63.15091	-3.31%
317.291	0.241701	423.6955	57.43585	149.2375	141.4596	17.78705	59.80446	4.12%	58.33063	1.56%	45.26197	-21.20%	60.16336	4.75%
317.291	0.192522	388.1888	52.62259	149.2375	140.3627	12.11604	55.44841	5.37%	53.58021	1.82%	42.89495	-18.49%	55.86004	6.15%
317.291	0.144365	336.996	45.68293	149.2375	140.0948	7.669822	50.3927	10.31%	48.42442	6.00%	41.272	-9.66%	51.03846	11.72%
317.291	0.141376	341.3786	46.27704	149.2375	138.9864	7.426226	50.04163	8.13%	48.07979	3.90%	40.5053	-12.47%	50.61525	9.37%
317.291	0.091708	290.3442	39.35885	149.2375	138.0316	3.890204	43.21747	9.80%	41.66962	5.87%	38.53873	-2.08%	44.42728	12.88%
317.291	0.046303	242.3003	32.84605	149.2375	137.0754	1.477941	34.01605	3.56%	33.63409	2.40%	36.70802	11.76%	38.1418	16.12%
338.269	0.438267	656.8644	86.50413	142.5423	139.4547	65.15959	76.85276	-11.16%	77.85272	-10.00%	62.18818	-28.11%	77.73118	-10.14%
338.269	0.227659	357.2089	47.04174	142.5423	137.325	17.98134	59.71511	26.94%	58.55798	24.48%	49.44954	5.12%	60.56413	28.75%
338.269	0.411855	608.2281	80.09909	142.5423	137.3187	56.47674	74.68829	-6.76%	75.42879	-5.83%	54.51324	-31.94%	75.0027	-6.36%

338.269	0.370514	587.279	77.34025	142.5423	137.0656	44.88203	71.39188	-7.69%	71.69087	-7.30%	53.01575	-31.45%	71.74788	-7.23%
338.269	0.327919	548.3663	72.21574	142.5423	136.5225	35.01872	68.037	-5.79%	67.86176	-6.03%	50.93266	-29.47%	68.40402	-5.28%
338.269	0.286389	495.2481	65.22047	142.5423	136.3109	27.04405	64.71484	-0.78%	64.09129	-1.73%	49.50993	-24.09%	65.14618	-0.11%
338.269	0.250015	403.8863	53.1888	142.5423	136.1443	21.15902	61.67917	15.96%	60.70461	14.13%	48.23453	-9.31%	62.18753	16.92%
338.269	0.333	524.4575	69.06713	142.5423	137.1631	36.09883	68.43802	-0.91%	68.3193	-1.08%	52.30865	-24.26%	68.89	-0.26%
341.9401	0.207646	458.3946	61.89499	148.5907	145.5542	14.8978	59.64835	-3.63%	58.35615	-5.72%	53.71031	-13.22%	61.46748	-0.69%
341.9401	0.1876	414.0618	55.90893	148.5907	142.831	12.60291	57.6668	3.14%	56.23567	0.58%	47.08593	-15.78%	58.38479	4.43%
341.9401	0.155844	389.3592	52.57345	148.5907	142.5102	9.374523	54.21383	3.12%	52.67123	0.19%	45.50499	-13.44%	55.08854	4.78%
341.9401	0.123498	365.0098	49.28566	148.5907	141.9051	6.55805	50.14291	1.74%	48.667	-1.26%	43.61186	-11.51%	51.26501	4.02%
341.9401	0.091926	318.6937	43.0318	148.5907	141.4525	4.235862	45.3449	5.38%	44.17959	2.67%	41.92812	-2.56%	47.08362	9.42%
341.9401	0.12775	342.2285	46.2096	149.1927	141.176	6.902472	50.71872	9.76%	49.22141	6.52%	43.15945	-6.60%	51.64805	11.77%
342.7268	0.282039	468.5954	63.5763	149.4055	145.3055	25.29152	66.54396	4.67%	66.10812	3.98%	53.48231	-15.88%	67.25696	5.79%
342.7268	0.254707	448.4134	60.83812	149.4055	142.307	21.03609	64.27011	5.64%	63.46792	4.32%	47.2689	-22.30%	64.56172	6.12%
342.7268	0.16465	373.1602	50.6282	148.1288	140.1888	10.15978	55.58196	9.78%	54.02807	6.72%	42.99238	-15.08%	55.99404	10.60%
342.7268	0.210803	427.1044	57.94703	149.4055	141.5781	15.18558	60.32983	4.11%	59.05283	1.91%	45.34936	-21.74%	60.66861	4.70%
342.7268	0.164525	391.7674	53.15272	149.4055	140.5195	10.14761	55.56798	4.54%	54.01374	1.62%	43.23048	-18.67%	56.0036	5.36%
342.7268	0.119052	336.6119	45.66954	149.4055	139.7781	6.168321	49.86375	9.18%	48.37953	5.93%	41.51556	-9.10%	50.60957	10.82%
342.7268	0.077218	290.8298	39.4581	149.4055	139.1552	3.273218	42.9915	8.95%	42.04892	6.57%	39.98844	1.34%	44.72476	13.35%
343.2512	0.131279	401.9653	53.33075	144.2988	141.5157	7.444768	50.41354	-5.47%	49.0529	-8.02%	50.13191	-6.00%	53.88287	1.04%
343.2512	0.115581	355.8709	47.21518	144.2988	138.9093	6.143827	48.27966	2.25%	47.01165	-0.43%	44.47817	-5.80%	50.07395	6.05%
343.2512	0.090678	329.224	43.6798	144.2988	138.4825	4.297059	44.42492	1.71%	43.43525	-0.56%	42.67928	-2.29%	46.76183	7.06%
343.2512	0.065219	307.0356	40.73596	144.2988	137.8944	2.679931	39.60678	-2.77%	39.12524	-3.95%	40.74971	0.03%	43.10106	5.81%
343.2512	0.040313	266.647	35.3774	144.2988	137.4043	1.370518	33.38321	-5.64%	33.72753	-4.66%	38.93212	10.05%	39.69735	12.21%
343.2512	0.06842	288.1555	38.23104	144.1719	139.0869	2.868106	40.27838	5.36%	39.71738	3.89%	41.79528	9.32%	44.04943	15.22%
343.7757	0.453855	661.6508	87.73605	144.1719	141.2484	71.12872	79.24806	-9.67%	80.81852	-7.88%	63.30317	-27.85%	80.04887	-8.76%
343.7757	0.427931	629.1554	83.42711	144.1719	139.0955	61.8882	77.08566	-7.60%	78.36899	-6.06%	55.1641	-33.88%	77.35298	-7.28%
343.7757	0.387262	609.1492	80.77425	144.1719	138.9824	49.51997	73.80259	-8.63%	74.59817	-7.65%	54.0084	-33.14%	74.12139	-8.24%
343.7757	0.345962	585.169	77.59444	144.1719	138.6237	39.13114	70.53587	-9.10%	70.81246	-8.74%	52.27062	-32.64%	70.88047	-8.65%
343.7757	0.306196	524.134	69.50108	144.1719	138.4967	30.79458	67.37512	-3.06%	67.15738	-3.37%	51.03299	-26.57%	67.78265	-2.47%
343.7757	0.271419	433.1314	57.43398	144.1719	138.2953	24.611	64.52953	12.35%	63.90859	11.27%	49.73535	-13.40%	64.99169	13.16%
343.7757	0.3525	546.94	72.5252	150.1399	145.9797	40.64888	71.05185	-2.03%	71.41101	-1.54%	6.807711		71.05185	-2.03%
344.3001	0.561924	693.2575	94.3504	150.1399	147.7641	120.9253	90.04983	-4.56%	94.08505	-0.28%	68.60968	-27.28%	90.62654	-3.95%
344.3001	0.370719	435.3647	59.25191	150.1399	146.5254	43.19689	73.87669	24.68%	74.92837	26.46%	57.6049	-2.78%	74.46868	25.68%
344.3001	0.500511	675.8001	91.9745	150.1399	145.8928	87.22244	84.32957	-8.31%	87.52717	-4.84%	58.52553	-36.37%	84.54565	-8.08%
344.3001	0.538395	685.834	93.34008	150.1399	145.866	106.6289	87.76878	-5.97%	91.5034	-1.97%	59.18057	-36.60%	87.93781	-5.79%
344.3001	0.461678	657.2265	89.44668	150.1399	145.576	70.99156	81.03941	-9.40%	83.63086	-6.50%	56.77153	-36.53%	81.2672	-9.14%
344.3001	0.423707	611.4646	83.21862	150.1399	145.5417	57.90784	77.98617	-6.29%	79.94656	-3.93%	55.86699	-32.87%	78.25941	-5.96%
344.3001	0.390592	475.0205	64.64895	150.1399	145.1879	48.29318	75.40624	16.64%	76.79965	18.79%	54.22142	-16.13%	75.68035	17.06%
344.3001	0.4665	611.8	83.26427	147.9921	143.9424	72.83608	81.4374	-2.19%	84.10664	1.01%	53.01177	-36.33%	81.54797	-2.06%
346.1357	0.704619	863.1063	116.3778	147.9921	145.5764	280.8492	108.0129	-7.19%	112.3062	-3.50%	71.61152	-38.47%	108.1889	-7.04%
346.1357	0.49272	506.0321	68.23133	147.9921	144.59	85.53139			86.3435		61.70534	-9.56%	61.70534	-9.56%
346.1357	0.635	787.5261	106.1869	147.9921	143.8352	184.9497	98.31824	-7.41%	102.3983	-3.57%	61.5205	-42.06%	98.40833	-7.33%
346.1357	0.677405	812.8031	109.5951	147.9921	143.8174	237.2367	103.9491	-5.15%	108.1932	-1.28%	62.15989	-43.28%	104.0098	-5.10%

346.1357	0.550662	693.8218	93.55214	147.9921	143.4984	116.3332	88.99869	-4.87%	92.42078	-1.21%	58.91083	-37.03%	89.14137	-4.71%
346.1357	0.592111	748.6588	100.9461	147.9921	143.4913	145.5528	93.31627	-7.56%	97.11565	-3.79%	59.62225	-40.94%	93.42153	-7.45%
346.1357	0.514497	558.4413	75.29798	147.9921	143.2676	95.98161	85.55669	13.62%	88.57292	17.63%	57.55406	-23.56%	85.71768	13.84%
346.1357	0.599	711.9765	96.00005	147.9921	144.0109	151.1667	94.07956	-2.00%	97.93175	2.01%	61.53388	-35.90%	94.21349	-1.86%
348.7579	0.181235	420.8661	56.92373	148.6836	146.0906	12.12723	57.89277	1.70%	56.51682	-0.71%	54.08538	-4.99%	60.31432	5.96%
348.7579	0.165406	374.7044	50.68019	148.6836	143.4681	10.47809	56.16024	10.81%	54.71816	7.97%	47.29235	-6.68%	57.0942	12.66%
348.7579	0.140504	341.8217	46.23268	148.6836	143.2088	8.122701	53.18309	15.03%	51.72036	11.87%	45.91831	-0.68%	54.29646	17.44%
348.7579	0.115559	316.2525	42.77435	148.6836	142.6104	6.040103	49.79434	16.41%	48.43842	13.24%	44.19384	3.32%	51.13087	19.54%
348.7579	0.1164	311.316	42.10667	146.5073	141.6978	6.105938	49.91675	18.55%	48.55477	15.31%	43.4261	3.13%	51.03635	21.21%
349.2824	0.555844	741.9686	99.40204	146.5073	143.6811	122.1031	89.89291	-9.57%	93.11775	-6.32%	66.04751	-33.56%	90.29678	-9.16%
349.2824	0.341235	446.7755	59.85482	146.5073	142.2473	38.01159	71.44273	19.36%	71.93543	20.18%	55.14405	-7.87%	71.96168	20.23%
349.2824	0.529212	691.5241	92.64395	146.5073	141.7546	105.9376	87.25778	-5.81%	90.23886	-2.60%	57.86332	-37.54%	87.40021	-5.66%
349.2824	0.487142	675.285	90.46839	146.5073	141.5558	84.77646	83.37933	-7.84%	85.89977	-5.05%	56.5365	-37.51%	83.54907	-7.65%
349.2824	0.443354	656.7623	87.9869	146.5073	141.2221	67.15605	79.6243	-9.50%	81.58545	-7.28%	54.85639	-37.65%	79.81406	-9.29%
349.2824	0.400721	597.7997	80.08763	146.5073	141.1112	53.28434	76.15265	-4.91%	77.51538	-3.21%	53.7377	-32.90%	76.38265	-4.63%
349.2824	0.363726	476.9757	63.90075	146.5073	140.9107	43.30512	73.21822	14.58%	74.04022	15.87%	52.51428	-17.82%	73.47779	14.99%
349.2824	0.4485	614.1345	82.27602	146.5073	141.7833	69.03219	80.05384	-2.70%	82.08415	-0.23%	56.3883	-31.46%	80.29133	-2.41%
354.0024	0.412031	621.1967	84.20897	149.1839	146.6983	56.34437	78.35406	-6.95%	80.29224	-4.65%	64.15549	-23.81%	79.35561	-5.76%
354.0024	0.358428	571.6351	77.49044	149.1839	144.7201	41.75034	74.11433	-4.36%	75.141	-3.03%	54.93853	-29.10%	74.47746	-3.89%
354.0024	0.391224	576.0178	78.08455	149.1839	144.6479	50.24592	76.69836	-1.78%	78.28343	0.25%	55.52716	-28.89%	76.99646	-1.39%
354.0024	0.325098	558.2503	75.67601	149.1839	144.435	34.31614	71.48075	-5.54%	71.95136	-4.92%	53.37947	-29.46%	71.85722	-5.05%
354.0024	0.292512	521.4996	70.6941	149.1839	144.4011	28.03776	68.85093	-2.61%	68.80601	-2.67%	52.43057	-25.83%	69.28964	-1.99%
354.0024	0.263715	413.8937	56.10712	149.1839	144.0179	23.18986	66.43835	18.41%	65.97621	17.59%	50.82637	-9.41%	66.881	19.20%
354.0024	0.329	521.1685	70.64922	148.1404	142.8729	35.13042	71.79103	1.62%	72.3256	2.37%	50.3803	-28.69%	71.99632	1.91%
357.4113	0.283084	532.8807	71.89187	148.1404	145.3358	26.85595	68.22953	-5.09%	68.11926	-5.25%	58.31017	-18.89%	69.53015	-3.29%
357.4113	0.262846	492.8749	66.49462	148.1404	142.9816	23.46643	66.50759	0.02%	66.11614	-0.57%	50.9354	-23.40%	66.95546	0.69%
357.4113	0.231076	474.8169	64.05838	148.1404	142.9085	18.71636	63.66976	-0.61%	62.88923	-1.83%	49.85598	-22.17%	64.20114	0.22%
357.4113	0.198779	456.2646	61.55545	148.1404	142.4705	14.52519	60.5466	-1.64%	59.45886	-3.41%	48.12256	-21.82%	61.12975	-0.69%
357.4113	0.167126	414.0046	55.85408	148.1404	142.2874	10.97153	57.15067	2.32%	55.87971	0.05%	46.80131	-16.21%	57.88222	3.63%
357.4113	0.139234	324.5805	43.78972	148.1404	141.8178	8.250829	53.7676	22.79%	52.46456	19.81%	45.25425	3.34%	54.65751	24.82%
357.4113	0.2025	425.914	57.4608	149.0445	139.0193	14.9778	60.92176	6.02%	59.86392	4.18%	44.44384	-22.65%	61.17701	6.47%
358.7224	0.343071	610.2217	82.6512	149.0445	143.9662	38.75129	73.51766	-11.05%	74.41445	-9.97%	53.16076	-35.68%	73.80006	-10.71%
358.7224	0.306295	513.2357	69.51497	149.0445	140.7761	31.03561	70.5589	1.50%	70.84791	1.92%	47.33	-31.91%	70.68797	1.69%
358.7224	0.250851	461.1906	62.46576	149.0445	139.6658	21.52753	65.86543	5.44%	65.3404	4.60%	45.2095	-27.63%	66.01675	5.68%
358.7224	0.194185	410.5664	55.60898	149.0445	138.3849	13.93357	60.46918	8.74%	59.34456	6.72%	43.20973	-22.30%	60.67587	9.11%
358.7224	0.138792	354.6394	48.03397	149.0445	137.3428	8.185205	54.07341	12.57%	52.75439	9.83%	41.62194	-13.35%	54.45581	13.37%
358.7224	0.087259	311.0926	42.1358	149.0445	136.7841	4.103822	46.18565	9.61%	45.27932	7.46%	40.41813	-4.08%	47.2784	12.20%
358.7224	0.19805	413.954	56.06781	147.7022	141.3648	14.39264	60.86598	8.56%	59.77173	6.61%	45.70758	-18.48%	61.20453	9.16%
371.8336	0.125391	422.9618	56.85484	147.3113	144.3209	7.375562	53.11721	-6.57%	52.10329	-8.36%	50.41426	-11.33%	55.64954	-2.12%
371.8336	0.108768	381.9285	51.33912	147.3113	141.5754	5.961079	50.61577	-1.41%	49.70509	-3.18%	45.26464	-11.83%	52.06879	1.42%
371.8336	0.081337	350.6379	47.13301	147.3113	140.6861	3.900042	45.80578	-2.82%	45.25019	-3.99%	43.35656	-8.01%	47.94128	1.71%
371.8336	0.052153	314.209	42.23621	147.3113	139.677	2.079697	39.19274	-7.21%	39.37087	-6.78%	41.58179	-1.55%	43.45412	2.88%
371.8336	0.02305	275.9074	37.08769	147.3113	138.9209	0.679241	29.20122	-21.26%	30.73099	-17.14%	40.10252	8.13%	40.26749	8.57%

371.8336	0.05265	308.361	41.45012	148.8748	142.6481	2.10737	39.32472	-5.13%	39.48624	-4.74%	43.1949	4.21%	44.64466	7.71%
382.3226	0.818197	1028.432	139.217	148.8748	145.0418	716.8506	139.973	0.54%	146.9597	5.56%	65.6845		139.9802	0.55%
382.3226	0.491616	636.297	86.13437	148.8748	143.3371	93.68134	89.50903	3.92%	93.71303	8.80%	55.3052	-35.79%	89.58135	4.00%
382.3226	0.778142	925.9088	125.3386	148.8748	143.2846	515.3581	129.8598	3.61%	136.6212	9.00%	59.28584	-52.70%	129.8649	3.61%
382.3226	0.716435	817.1057	110.6101	148.8748	142.2349	333.8568	117.5867	6.31%	124.1184	12.21%	56.05126	-49.33%	117.5938	6.31%
382.3226	0.529142	672.2216	90.99742	148.8748	141.9016	114.2823	93.13831	2.35%	97.92438	7.61%	52.96634	-41.79%	93.17121	2.39%
382.3226	0.587317	731.2771	98.99164	148.8748	141.7483	156.2061	99.38291	0.40%	104.9308	6.00%	53.46969	-45.99%	99.40309	0.42%
382.3226	0.650989	762.7709	103.2549	148.8748	141.7229	223.4349	107.4196	4.03%	113.5732	9.99%	54.23431	-47.48%	107.4312	4.04%
382.3226	0.655	790.1535	106.9616	148.8641	142.5619	228.7312	107.9795	0.95%	114.163	6.73%	55.95103	-47.69%	107.9946	0.97%
383.6337	0.722601	925.4178	125.2721	148.8641	145.032	348.8901	118.9693	-5.03%	125.5623	0.23%	64.24351	-48.72%	118.9944	-5.01%
383.6337	0.417335	544.3772	73.69134	148.8641	143.2249	63.20488	83.13311	12.81%	86.05896	16.78%	53.83179	-26.95%	83.24024	12.96%
383.6337	0.68635	822.1611	111.2944	148.8641	143.158	277.0225	112.8999	1.44%	119.3197	7.21%	57.76948	-48.09%	112.9138	1.46%
383.6337	0.629837	753.1418	101.9514	148.8641	142.1867	198.5729	104.8392	2.83%	110.8516	8.73%	54.87114	-46.18%	104.8554	2.85%
383.6337	0.451073	606.6002	82.11436	148.8641	141.8036	75.80238	86.0516	4.79%	89.5888	9.10%	51.71968	-37.02%	86.10439	4.86%
383.6337	0.505967	706.8739	95.68823	148.8641	141.6646	101.4393	91.09007	-4.81%	95.55103	-0.14%	52.26513	-45.38%	91.12524	-4.77%
383.6337	0.567847	735.3872	99.54802	148.8641	141.6356	141.0591	97.43444	-2.12%	102.7783	3.24%	53.04148	-46.72%	97.45669	-2.10%
383.6337	0.5705	726.4665	98.34044	149.4269	143.1987	143.0932	97.72705	-0.62%	103.1042	4.84%	56.23417	-42.82%	97.76587	-0.58%
385.9937	0.619031	855.3949	116.055	149.4269	145.7324	187.2101	103.9156	-10.46%	110.1537	-5.08%	63.05406	-45.67%	103.9857	-10.40%
385.9937	0.586674	753.5344	102.2352	149.4269	143.813	156.542	100.0159	-2.17%	105.8811	3.57%	56.54761	-44.69%	100.0492	-2.14%
385.9937	0.345459	486.8976	66.05944	149.4269	143.7212	42.28912	77.57615	17.43%	79.27002	20.00%	52.34929	-20.75%	77.72673	17.66%
385.9937	0.535864	691.489	93.8172	149.4269	142.8568	119.111	94.51296	0.74%	99.67238	6.24%	53.77396	-42.68%	94.5465	0.78%
385.9937	0.375786	548.8415	74.46363	149.4269	142.3846	50.32937	80.10432	7.58%	82.38152	10.63%	50.58772	-32.06%	80.18478	7.68%
385.9937	0.480144	679.0303	92.12688	149.4269	142.3819	88.65859	89.13115	-3.25%	93.37197	1.35%	52.13847	-43.41%	89.17287	-3.21%
385.9937	0.424862	640.6448	86.91895	149.4269	142.3373	65.97511	84.24118	-3.08%	87.4645	0.63%	51.26662	-41.02%	84.29969	-3.01%
385.9937	0.483	664.378	90.13894	145.7943	138.7817	90.01072	89.39409	-0.83%	93.68505	3.93%	47.50225	-47.30%	89.41012	-0.81%
386.7804	0.533193	892.8631	119.2515	145.7943	141.6583	120.9731	93.86966	-21.28%	98.09704	-17.74%	60.21402	-49.51%	93.9798	-21.19%
386.7804	0.498827	787.4526	105.1728	145.7943	140.0294	100.8303	90.40294	-14.04%	94.2245	-10.41%	55.14632	-47.57%	90.46723	-13.98%
386.7804	0.252572	419.7311	56.05961	145.7943	138.9966	24.15514	68.61594	22.40%	68.69046	22.53%	48.83351	-12.89%	68.84132	22.80%
386.7804	0.446564	656.0508	87.62264	145.7943	138.5181	76.38462	85.51638	-2.40%	88.6126	1.13%	51.50901	-41.21%	85.56998	-2.34%
386.7804	0.389543	620.115	82.82303	145.7943	137.8289	55.99902	80.52912	-2.77%	82.73237	-0.11%	49.65947	-40.04%	80.59293	-2.69%
386.7804	0.283508	488.6612	65.26596	145.7943	137.6645	29.76143	71.42782	9.44%	71.93652	10.22%	47.7686	-26.81%	71.55463	9.64%
386.7804	0.333419	572.9782	76.5274	145.7943	137.6466	40.57719	75.75503	-1.01%	77.04257	0.67%	48.57003	-36.53%	75.84348	-0.89%
386.7804	0.3935	630.9475	84.26983	149.2232	140.5139	57.24321	80.86815	-4.04%	83.13546	-1.35%	54.41087	-35.43%	81.02062	-3.86%
388.0915	0.430679	775.4982	105.126	149.2232	144.41	68.5775	85.01091	-19.13%	88.38575	-15.92%	56.04645	-46.69%	85.14189	-19.01%
388.0915	0.394897	665.8943	90.26814	149.2232	142.43	56.40671	81.95711	-9.21%	84.64767	-6.23%	51.33772	-43.13%	82.03301	-9.12%
388.0915	0.340902	550.5262	74.62893	149.2232	140.5391	41.47272	77.42827	3.75%	79.0807	5.97%	47.95396	-35.74%	77.49232	3.84%
388.0915	0.140136	317.8626	43.08922	149.2232	139.9171	9.004737	57.28065	32.94%	56.40518	30.90%	44.22749	2.64%	57.69807	33.90%
388.0915	0.28199	520.8484	70.60582	149.2232	139.5785	28.81398	72.37085	2.50%	72.95979	3.33%	46.16941	-34.61%	72.45126	2.61%
388.0915	0.223629	465.4271	63.09296	149.2232	139.0572	19.12202	66.91353	6.06%	66.63282	5.61%	44.94337	-28.77%	67.03753	6.25%
388.0915	0.172152	374.4687	50.76271	149.2232	138.7124	12.42851	61.34591	20.85%	60.57411	19.33%	43.987	-13.35%	61.56281	21.28%
388.0915	0.286	521.64	70.71314	149.1375	140.3322	29.57547	72.72512	2.85%	73.38202	3.77%	46.95076	-33.60%	72.81607	2.97%
392.0249	0.313685	768.1018	104.0939	149.1375	144.6452	35.60753	75.61714	-27.36%	76.86244	-26.16%	54.44298	-47.70%	75.89552	-27.09%
392.0249	0.282525	605.3653	82.03971	149.1375	142.5922	29.23743	72.89188	-11.15%	73.58298	-10.31%	49.84186	-39.25%	73.05314	-10.95%

392.0249	0.237016	479.7132	65.01122	149.1375	140.736	21.36653	68.67093	5.63%	68.65059	5.60%	46.77767	-28.05%	68.81724	5.85%
392.0249	0.188906	420.9546	57.04819	149.1375	139.4769	14.59878	63.67629	11.62%	63.10229	10.61%	44.93957	-21.23%	63.86886	11.96%
392.0249	0.141557	378.2394	51.25939	149.1375	138.7792	9.24765	57.84631	12.85%	57.03863	11.27%	43.77873	-14.59%	58.19336	13.53%
392.0249	0.098976	301.2679	40.82813	149.1375	138.151	5.404834	51.25373	25.54%	50.64651	24.05%	42.84841	4.95%	52.05035	27.49%
392.0249	0.194	447.58	60.65649	149.1375	140.7301	15.24806	64.24084	5.91%	63.71278	5.04%	46.03251	-24.11%	64.46651	6.28%
393.5982	0.224175	544.2136	74.31873	150.851	144.6452	19.2498	68.10175	-8.37%	67.91192	-8.62%	49.1553	-33.86%	68.35873	-8.02%
393.5982	0.202216	468.7023	64.00679	150.851	142.5922	16.1879	65.81956	2.83%	65.35816	2.11%	46.41286	-27.49%	66.01694	3.14%
393.5982	0.167773	398.2328	54.38334	150.851	140.736	11.95866	61.88258	13.79%	61.12253	12.39%	44.47211	-18.22%	62.10629	14.20%
393.5982	0.133	360.6055	49.2449	150.851	140.7301	8.333092	57.28006	16.32%	56.42695	14.58%	43.99777	-10.66%	57.67698	17.12%
393.5982	0.13095	358.2833	48.92777	150.851	139.4769	8.138216	56.98269	16.46%	56.13223	14.72%	43.33873	-11.42%	57.3414	17.20%
393.5982	0.094451	315.4899	43.08383	150.851	138.7792	5.00395	51.01187	18.40%	50.40427	16.99%	42.6901	-0.91%	51.81238	20.26%
409.8561	0.371058	754.2176	102.4436	149.6628	144.2665	52.0679	83.09431	-18.89%	86.01038	-16.04%	53.8473	-47.44%	83.20219	-18.78%
409.8561	0.329699	645.8781	87.72814	149.6628	141.2466	40.93505	79.49898	-9.38%	81.55321	-7.04%	48.49702	-44.72%	79.55554	-9.32%
409.8561	0.269243	534.9094	72.65551	149.6628	139.8441	27.93421	74.05214	1.92%	74.94246	3.15%	46.36857	-36.18%	74.12047	2.02%
409.8561	0.209076	476.1105	64.66899	149.6628	138.6121	18.00656	68.03438	5.20%	68.00421	5.16%	44.82465	-30.69%	68.13852	5.37%
409.8561	0.058488	326.4975	44.34741	149.6628	138.2116	2.654231	44.11696	-0.52%	44.51616	0.38%	43.30471	-2.35%	46.86629	5.68%
409.8561	0.150583	419.6565	57.00098	149.6628	137.7607	10.61668	61.015	7.04%	60.50163	6.14%	43.84797	-23.08%	61.23554	7.43%
409.8561	0.095625	382.7714	51.99096	149.6628	137.3873	5.361301	52.34108	0.67%	52.01177	0.04%	43.31788	-16.68%	53.08118	2.10%
409.8561	0.21495	498.7665	67.74631	149.6628	139.6184	18.86369	68.66304	1.35%	68.70751	1.42%	45.58896	-32.71%	68.77651	1.52%
410.1183	0.087525	414.0385	56.00027	148.6854	145.204	4.750601	50.56106	-9.71%	50.37484	-10.05%	49.03174	-12.44%	53.42689	-4.60%
410.1183	0.070692	362.7328	49.06098	148.6854	142.1591	3.496497	46.94978	-4.30%	47.0706	-4.06%	45.33135	-7.60%	49.52035	0.94%
410.1183	0.0436	323.244	43.71997	148.6854	141.0194	1.777158	39.5769	-9.48%	40.52169	-7.32%	43.97027	0.57%	45.30648	3.63%
410.1183	0.015112	274.8906	37.17999	148.6854	139.4426	0.421557	26.92478	-27.58%	29.46603		42.91115	15.41%	42.95156	15.52%
410.1183	0.02015	288.457	39.0149	148.6854	141.9563	0.620687	29.92446	-23.30%	32.10191	-17.72%	43.42219	11.30%	43.52599	11.56%
410.905	0.30549	701.191	95.78307	150.9707	146.6003	35.06007	77.89113	-18.68%	79.52455	-16.97%	54.85953	-42.73%	78.12198	-18.44%
410.905	0.181	466.601	63.73795	150.9707	142.4658	14.10883	65.37015	2.56%	65.01881	2.01%	46.46359	-27.10%	65.58216	2.89%
410.905	0.273758	574.2422	78.4418	150.9707	143.6089	28.58614	75.00628	-4.38%	76.01307	-3.10%	48.99634	-37.54%	75.11172	-4.25%
410.905	0.226426	502.7561	68.67676	150.9707	142.7036	20.45789	70.38816	2.49%	70.59005	2.79%	47.31206	-31.11%	70.51955	2.68%
410.905	0.17855	450.4688	61.53428	150.9707	141.6013	13.80226	65.07664	5.76%	64.70352	5.15%	45.76109	-25.63%	65.2665	6.07%
410.905	0.056478	313.4226	42.8137	150.9707	141.3723	2.509271	43.94448	2.64%	44.36715	3.63%	44.10651	3.02%	47.18607	10.21%
410.905	0.131438	405.9625	55.4547	150.9707	140.974	8.551021	58.77756	5.99%	58.19902	4.95%	44.82541	-19.17%	59.15747	6.68%
410.905	0.086713	364.982	49.85673	150.9707	140.4001	4.617207	51.03367	2.36%	50.77884	1.85%	44.10854	-11.53%	52.11227	4.52%
423.4918	0.209512	590.0678	80.12489	149.5913	145.7003	18.70524	69.60177	-13.13%	69.84175	-12.83%	53.88724	-32.75%	70.1225	-12.48%
423.4918	0.185166	503.3157	68.34487	149.5913	142.7241	15.26165	66.80966	-2.25%	66.76735	-2.31%	48.4727	-29.08%	67.0749	-1.86%
423.4918	0.147919	442.0606	60.02709	149.5913	141.8784	10.6896	62.00618	3.30%	61.70862	2.80%	47.00963	-21.69%	62.38462	3.93%
423.4918	0.109822	401.0215	54.45442	149.5913	140.8015	6.805268	56.09458	3.01%	55.83998	2.54%	45.6758	-16.12%	56.77496	4.26%
423.4918	0.07222	355.4849	48.27104	149.5913	140.1889	3.702186	48.56117	0.60%	48.80094	1.10%	44.88933	-7.01%	50.41874	4.45%
423.4918	0.036584	319.0585	43.32473	149.5913	139.5313	1.433637	38.15541	-11.93%	39.5564	-8.70%	44.30057	2.25%	45.20743	4.35%
423.4918	0.11033	410.0325	55.67802	148.1215	138.308	6.852113	56.18259	0.91%	55.92483	0.44%	44.45043	-20.17%	56.7005	1.84%
423.754	0.206386	659.2037	88.83449	147.8706	142.8346	18.49031	68.76555	-22.59%	69.00518	-22.32%	48.89046	-44.96%	68.98919	-22.34%
423.754	0.17613	566.3269	76.31838	147.8706	140.2976	14.26973	65.22846	-14.53%	65.16035	-14.62%	46.0127	-39.71%	65.42477	-14.27%
423.754	0.130416	420.3792	56.65043	147.8706	137.4738	8.929919	58.98955	4.13%	58.74042	3.69%	43.97393	-22.38%	59.29492	4.67%
423.754	0.082892	352.4149	47.49153	147.8706	135.6947	4.57188	50.53479	6.41%	50.65107	6.65%	43.2148	-9.01%	51.50363	8.45%

423.754	0.037307	292.9633	39.47981	147.8706	134.1375	1.492712	38.11182	-3.47%	39.53457	0.14%	43.08109	9.12%	44.20446	11.97%
423.754	0.09005	384.5173	51.81766	148.8791	139.1049	5.154025	52.00058	0.35%	52.01269	0.38%	44.37303	-14.37%	52.97805	2.24%
424.5407	0.389237	781.9858	105.856	148.8641	143.445	60.17443	86.52769	-18.26%	90.18962	-14.80%	54.36307	-48.64%	86.61025	-18.18%
424.5407	0.348009	673.5897	91.18261	148.8641	140.5035	47.5958	82.84787	-9.14%	85.63069	-6.09%	49.05916	-46.20%	82.89169	-9.09%
424.5407	0.2337	519.685	70.34881	148.9543	139.4218	22.7016	72.08162	2.46%	72.69491	3.33%	46.67188	-33.66%	72.17443	2.60%
424.5407	0.287542	563.5889	76.292	148.8641	139.1045	32.88422	77.35176	1.39%	78.90548	3.43%	46.94166	-38.47%	77.404	1.46%
424.5407	0.227189	498.3852	67.4655	148.8641	137.865	21.62567	71.40312	5.84%	71.91817	6.60%	45.4163	-32.68%	71.48013	5.95%
424.5407	0.078042	345.7105	46.7982	148.8641	137.521	4.169403	49.79568	6.41%	49.96161	6.76%	44.19246	-5.57%	51.13155	9.26%
424.5407	0.168789	435.2483	58.91877	148.8641	136.9819	13.25829	64.68546	9.79%	64.53938	9.54%	44.47476	-24.52%	64.83658	10.04%
424.5407	0.114599	391.1138	52.94436	148.8641	136.6655	7.309365	56.80972	7.30%	56.5714	6.85%	44.05683	-16.79%	57.24166	8.12%
427.6873	0.628698	760.6442	103.1124	149.225	145.8571	221.0116	112.3991	9.01%	120.737	17.09%	64.51652	-37.43%	112.4427	9.05%
427.6873	0.378568	655.5657	88.86801	149.225	144.1765	57.15266	85.93468	-3.30%	89.52427	0.74%	54.76575	-38.37%	86.02918	-3.19%
427.6873	0.59922	726.6729	98.50725	149.225	143.2222	187.4623	108.4905	10.13%	116.4207	18.18%	55.77555	-43.38%	108.5045	10.15%
427.6873	0.552546	715.3763	96.97589	149.225	143.1152	145.55	102.9034	6.11%	110.0849	13.52%	54.94941	-43.34%	102.9227	6.13%
427.6873	0.408819	682.117	92.46728	149.225	143.027	67.58844	88.64376	-4.14%	92.90756	0.48%	52.85335	-42.84%	88.69397	-4.08%
427.6873	0.454047	696.8623	94.46614	149.225	142.8114	86.27426	92.80861	-1.75%	98.06125	3.81%	53.06867	-43.82%	92.84323	-1.72%
427.6873	0.503275	702.163	95.18469	149.225	142.4483	112.026	97.62576	2.56%	103.8927	9.15%	53.03346	-44.28%	97.64759	2.59%
427.6873	0.5025	704.7545	95.536	151.5423	143.1969	111.5676	97.54687	2.10%	103.7986	8.65%	54.46634	-42.99%	97.57556	2.13%
430.834	0.183374	558.9085	76.63062	151.7498	147.7534	15.04977	68.05978	-11.18%	68.07137	-11.17%	53.10784	-30.70%	68.60901	-10.47%
430.834	0.159728	477.2963	65.44096	151.7498	144.6978	12.07416	65.02789	-0.63%	64.83274	-0.93%	48.2358	-26.29%	65.34862	-0.14%
430.834	0.123472	428.4617	58.74537	151.7498	143.9377	8.123928	59.67968	1.59%	59.3898	1.10%	47.07715	-19.86%	60.21436	2.50%
430.834	0.086261	385.2629	52.82248	151.7498	142.7579	4.786127	52.82593	0.01%	52.82706	0.01%	45.97252	-12.97%	54.01441	2.26%
430.834	0.049617	334.5137	45.86438	151.7498	142.0183	2.187432	43.52991	-5.09%	44.42052	-3.15%	45.43896	-0.93%	47.77532	4.17%
430.834	0.014926	300.7156	41.23041	151.6103	141.1771	0.426585	28.15598	-31.71%	30.93035	-24.98%	45.19858	9.62%	45.2382	9.72%
430.834	0.087	388.8725	53.31739	149.5388	141.4316	4.845569	52.98121	-0.63%	52.97159	-0.65%	45.41569	-14.82%	54.01959	1.32%
432.4074	0.157454	532.5954	72.38216	149.7861	145.9756	12.02382	64.27358	-11.20%	64.16737	-11.35%	52.65846	-27.25%	65.09987	-10.06%
432.4074	0.136092	451.9684	61.42459	149.7861	142.9566	9.592645	61.2211	-0.33%	61.03866	-0.63%	47.95216	-21.93%	61.73344	0.50%
432.4074	0.103227	409.5205	55.65571	149.7861	142.2545	6.33573	55.76335	0.19%	55.68502	0.05%	46.80976	-15.89%	56.66379	1.81%
432.4074	0.069336	363.5948	49.41421	149.7861	140.9628	3.564742	48.60715	-1.63%	49.0293	-0.78%	45.62955	-7.66%	50.72364	2.65%
432.4074	0.035868	314.5001	42.74201	149.7861	140.2254	1.423671	38.46427	-10.01%	40.0138	-6.38%	45.05147	5.40%	45.90259	7.39%
432.4074	0.004368	296.0359	40.23263	149.0342	139.4065	0.08452					44.75271	11.23%	44.75271	11.23%
432.4074	0.0697	373.7097	50.78886	148.3227	139.5922	3.59134	48.69606	-4.12%	49.11004	-3.31%	45.12546	-11.15%	50.59826	-0.38%
434.2429	0.266404	672.8652	90.85401	148.3227	144.0963	29.39688	76.33475	-15.98%	77.72828	-14.45%	54.92284	-39.55%	76.61392	-15.67%
434.2429	0.238048	566.7178	76.52139	148.3227	141.0809	24.09228	73.47516	-3.98%	74.38052	-2.80%	49.19668	-35.71%	73.60716	-3.81%
434.2429	0.195277	492.8344	66.54524	148.3227	140.1399	17.24895	68.77085	3.34%	69.07999	3.81%	47.60606	-28.46%	68.94268	3.60%
434.2429	0.151987	438.7583	59.24359	148.3227	138.9677	11.55445	63.26514	6.79%	63.21906	6.71%	46.16674	-22.07%	63.53095	7.24%
434.2429	0.109631	383.3819	51.76636	148.3227	138.216	7.033731	56.67274	9.48%	56.64272	9.42%	45.33351	-12.43%	57.25314	10.60%
434.2429	0.070058	338.2868	45.67736	148.3227	137.6083	3.673933	48.56543	6.32%	49.05875	7.40%	44.80363	-1.91%	50.39185	10.32%
434.2429	0.1544	450.961	60.89127	149.4716	142.865	11.84212	63.59875	4.45%	63.56401	4.39%	49.85381	-18.13%	64.13505	5.33%
435.5541	0.466321	949.5708	128.9415	149.5574	145.67	93.30872	95.45255	-25.97%	101.2655	-21.46%	59.96844	-53.49%	95.5436	-25.90%
435.5541	0.434505	722.1476	98.05991	149.5574	143.3407	78.71347	92.41133	-5.76%	97.52658	-0.54%	53.50057	-45.44%	92.45035	-5.72%
435.5541	0.21995	460.5468	62.53732	149.5574	143.052	20.9029	72.09959	15.29%	72.73445	16.31%	49.88651	-20.23%	72.27889	15.58%
435.5541	0.3435	623.461	84.65932	149.0429	142.5728	47.34856	84.10194	-0.66%	87.15606	2.95%	51.00122	-39.76%	84.15834	-0.59%

435.5541	0.387829	633.3612	86.00367	149.5574	142.4835	60.98131	88.11419	2.45%	92.1732	7.17%	51.4274	-40.20%	88.15452	2.50%
435.5541	0.340007	597.2728	81.10325	149.5574	141.9934	46.38589	83.78487	3.31%	86.76095	6.98%	50.13733	-38.18%	83.83407	3.37%
435.5541	0.293238	563.4265	76.50728	149.5574	141.825	34.83818	79.46985	3.87%	81.43684	6.44%	49.36045	-35.48%	79.5375	3.96%
435.5541	0.249041	530.3393	72.0144	149.5574	141.7483	25.90466	75.15673	4.36%	76.27	5.91%	48.73305	-32.33%	75.2549	4.50%
435.8163	0.535526	751.3154	101.4468	148.3227	144.7682	136.0334	102.4301	0.97%	109.3046	7.75%	62.58132	-38.31%	102.5041	1.04%
435.8163	0.296815	547.0378	73.86409	148.3227	142.8239	36.00331	79.44675	7.56%	81.46124	10.29%	52.82989	-28.48%	79.58005	7.74%
435.8163	0.506882	682.2227	92.1175	148.3227	142.0727	116.8621	99.32456	7.82%	105.6937	14.74%	54.46742	-40.87%	99.34895	7.85%
435.8163	0.462303	658.1614	88.86862	148.3227	141.8624	92.26834	94.80363	6.68%	100.3122	12.88%	53.48665	-39.81%	94.83456	6.71%
435.8163	0.325387	617.5158	83.38042	148.3227	141.6253	42.94999	82.10308	-1.53%	84.70333	1.59%	51.23803	-38.55%	82.17635	-1.44%
435.8163	0.368922	635.7898	85.84788	148.3227	141.4507	55.38854	86.07463	0.26%	89.60527	4.38%	51.5599	-39.94%	86.12569	0.32%
435.8163	0.415679	644.2256	86.98693	148.3227	141.2257	71.81214	90.36427	3.88%	94.90266	9.10%	51.79973	-40.45%	90.39883	3.92%
435.8163	0.4155	645.9665	87.22199	148.0743	141.9621	71.74231	90.34766	3.58%	94.88224	8.78%	53.05235	-39.18%	90.3916	3.63%
436.3407	0.53584	765.8365	103.3203	148.0743	144.574	136.6178	102.5147	-0.78%	109.3754	5.86%	62.8353	-39.18%	102.5911	-0.71%
436.3407	0.29744	550.2237	74.23164	148.0743	142.6038	36.241	79.51461	7.12%	81.55538	9.87%	52.91192	-28.72%	79.64895	7.30%
436.3407	0.507287	687.3831	92.73606	148.0743	141.8775	117.4198	99.41031	7.20%	105.7732	14.06%	54.59591	-41.13%	99.4351	7.22%
436.3407	0.462819	669.629	90.34083	148.0743	141.702	92.76438	94.88811	5.03%	100.401	11.14%	53.67465	-40.59%	94.91988	5.07%
436.3407	0.325977	634.3829	85.5857	148.0743	141.5211	43.21589	82.1696	-3.99%	84.79355	-0.93%	51.48754	-39.84%	82.24595	-3.90%
436.3407	0.369511	646.7992	87.26081	148.0743	141.2805	55.71985	86.1464	-1.28%	89.69658	2.79%	51.7074	-40.74%	86.19854	-1.22%
436.3407	0.416256	647.1684	87.31063	148.0743	141.002	72.2272	90.44354	3.59%	94.99514	8.80%	51.86131	-40.60%	90.47823	3.63%
436.3407	0.416	655.3045	88.40828	149.0415	142.2266	72.1265	90.41966	2.28%	94.96583	7.42%	54.063	-38.85%	90.47232	2.33%
438.963	0.373785	655.2541	88.7506	149.0517	145.3225	57.04587	87.13972	-1.82%	90.94362	2.47%	58.83128	-33.71%	87.30967	-1.62%
438.963	0.2635	537.8435	72.84797	148.9905	141.928	28.98732	76.83218	5.47%	78.29473	7.48%	49.8282	-31.60%	76.93271	5.61%
438.963	0.347839	608.7439	82.45104	149.0517	142.6537	49.15588	84.7753	2.82%	87.99788	6.73%	52.06982	-36.85%	84.83986	2.90%
438.963	0.154639	423.668	57.38352	149.0517	142.2117	11.93857	64.3153	12.08%	64.34162	12.13%	48.49261	-15.49%	64.68734	12.73%
438.963	0.307165	559.9805	75.84631	149.0517	142.0495	38.49359	81.02706	6.83%	83.36482	9.91%	50.58094	-33.31%	81.09958	6.93%
438.963	0.221079	520.0502	70.43797	149.0517	141.26	21.34153	72.42732	2.82%	73.16636	3.87%	48.49114	-31.16%	72.55733	3.01%
438.963	0.181085	474.1218	64.21721	149.0517	141.1914	15.34133	67.78117	5.55%	68.0129	5.91%	47.91032	-25.39%	67.98928	5.87%
438.963	0.264262	533.8588	72.30826	149.0517	141.1896	29.13803	76.90774	6.36%	78.3846	8.40%	48.94349	-32.31%	76.99113	6.48%
444.7319	0.445297	691.0607	93.31086	148.3173	144.6782	86.05459	94.44933	1.22%	99.92409	7.09%	60.67129	-34.98%	94.56172	1.34%
444.7319	0.219326	505.1098	68.20274	148.3173	142.2322	21.46198	72.65491	6.53%	73.49507	7.76%	50.69189	-25.67%	72.85112	6.82%
444.7319	0.418379	630.2774	85.10356	148.3173	141.833	74.42607	91.87266	7.95%	96.7666	13.70%	52.96462	-37.76%	91.90985	8.00%
444.7319	0.376303	609.0584	82.23846	148.3173	141.604	58.98036	87.95003	6.95%	91.91408	11.77%	52.03363	-36.73%	87.99613	7.00%
444.7319	0.246812	548.1573	74.01525	148.3173	141.0862	26.30676	75.59424	2.13%	76.88039	3.87%	49.59838	-32.99%	75.70526	2.28%
444.7319	0.287973	575.0185	77.6422	148.3173	141.0167	34.74897	79.6997	2.65%	81.76296	5.31%	50.04472	-35.54%	79.77532	2.75%
444.7319	0.332225	589.9653	79.6604	148.3173	140.8474	45.69935	83.87824	5.29%	86.87082	9.05%	50.35961	-36.78%	83.92915	5.36%
444.7319	0.3315	590.525	79.73597	148.3173	141.8997	45.50214	83.8109	5.11%	86.78775	8.84%	51.91998	-34.89%	83.88041	5.20%
446.043	0.14173	519.2327	70.50624	149.5824	143.7871	10.56072	63.32327	-10.19%	63.38991	-10.09%	49.68752	-29.53%	63.86242	-9.42%
446.043	0.112381	385.8524	52.39462	149.5824	141.988	7.432923	58.56578	11.78%	58.64948	11.94%	47.54269	-9.26%	59.25586	13.10%
446.043	0.081634	338.1772	45.92085	149.5824	140.8278	4.656777	52.49228	14.31%	52.88332	15.16%	46.52116	1.31%	53.88322	17.34%
446.043	0.0835	370.484	50.30776	149.5824	142.2385	4.810927	52.90407	5.16%	53.26589	5.88%	47.28294	-6.01%	54.41483	8.16%
446.5675	0.356714	647.3941	87.76027	149.0964	145.3608	52.71109	86.68678	-1.22%	90.33577	2.93%	58.56991	-33.26%	86.85712	-1.03%
446.5675	0.331389	598.0154	81.06653	149.0964	142.6421	45.43795	84.34273	4.04%	87.417	7.83%	51.8897	-35.99%	84.40802	4.12%
446.5675	0.142647	411.5376	55.78773	149.0964	142.1074	10.72734	63.41255	13.67%	63.51695	13.85%	48.47494	-13.11%	63.83196	14.42%

446.5675	0.291641	552.7275	74.92733	149.0964	142.0433	35.55101	80.58894	7.56%	82.7984	10.50%	50.4755	-32.63%	80.6635	7.66%
446.5675	0.2485	527.5395	71.51287	149.0964	142.2285	26.60398	76.29262	6.68%	77.65476	8.59%	50.15666	-29.86%	76.40692	6.84%
446.5675	0.249701	524.9827	71.16627	149.0964	141.154	26.83093	76.41687	7.38%	77.80083	9.32%	48.88844	-31.30%	76.50419	7.50%
446.5675	0.207517	505.3028	68.49848	149.0964	141.1513	19.54059	71.83184	4.87%	72.53023	5.89%	48.41545	-29.32%	71.96963	5.07%
446.5675	0.168465	463.4699	62.82764	149.0964	141.1406	13.91816	67.02827	6.69%	67.2844	7.09%	47.95767	-23.67%	67.26027	7.06%
448.403	0.049016	429.3099	57.72431	147.406	142.594	2.316635	43.56033	-24.54%	44.8735	-22.26%	47.69929	-17.37%	49.3437	-14.52%
452.0742	0.283353	715.6186	96.35584	147.7813	143.3799	34.47024	79.93335	-17.04%	82.08614	-14.81%	55.28699	-42.62%	80.13143	-16.84%
452.0742	0.253846	668.7181	90.04084	147.7813	140.9045	28.25563	76.96362	-14.52%	78.55415	-12.76%	50.3298	-44.10%	77.07299	-14.40%
452.0742	0.208309	532.6877	71.72476	147.7813	139.1312	20.11545	72.00829	0.40%	72.86501	1.59%	47.85116	-33.29%	72.1283	0.56%
452.0742	0.161205	464.3799	62.52732	147.7813	137.8462	13.27773	66.11016	5.73%	66.46627	6.30%	46.48161	-25.66%	66.30278	6.04%
452.0742	0.115716	405.6139	54.61467	147.7813	137.1378	7.987769	59.1368	8.28%	59.39671	8.76%	45.85267	-16.04%	59.58559	9.10%
452.0742	0.073342	353.8833	47.64929	147.7813	136.3234	4.10905	50.55332	6.09%	51.27064	7.60%	45.46408	-4.59%	52.07833	9.30%
452.0742	0.16465	*487.32*	*65.61614*	*147.7813*	*138.8313*	*13.72872*	*66.57831*	*1.47%*	*66.95935*	*2.05%*	*47.19509*	*-28.07%*	*66.78859*	*1.79%*
454.172	0.210284	688.6259	92.28142	147.4757	143.9457	20.57459	72.13986	-21.83%	73.20831	-20.67%	55.70455	-39.64%	72.66592	-21.26%
454.172	0.188066	596.2816	79.90655	147.4757	141.5175	17.11058	69.50043	-13.02%	70.28214	-12.04%	50.51138	-36.79%	69.78104	-12.67%
454.172	0.154339	458.299	61.41576	147.4757	140.0847	12.48512	65.06468	5.94%	65.54793	6.73%	48.36386	-21.25%	65.3922	6.47%
454.172	0.119739	404.6132	54.22143	147.4757	138.9356	8.464637	59.73949	10.18%	60.14619	10.93%	47.05105	-13.22%	60.26676	11.15%
454.172	0.085777	356.496	47.77334	147.4757	138.2838	5.180332	53.29848	11.57%	53.95251	12.93%	46.37926	-2.92%	54.49654	14.07%
454.172	0.053734	307.6589	41.22878	147.4757	137.3552	2.667398	45.24952	9.75%	46.58032	12.98%	45.85128	11.21%	48.82929	18.43%
454.172	0.12155	429.708	57.58434	148.8431	141.0898	8.657865	60.04383	4.27%	60.44737	4.97%	48.75005	-15.34%	60.75236	5.50%
463.612	0.232113	556.518	75.33482	148.8819	145.097	24.58399	76.34581	1.34%	77.80391	3.28%	55.95086	-25.73%	76.68033	1.79%
463.612	0.20978	505.8743	68.47929	148.8819	141.8998	20.70541	73.81175	7.79%	74.90369	9.38%	49.96716	-27.03%	73.95959	8.00%
463.612	0.175019	458.2668	62.03474	148.8819	141.3277	15.39281	69.50112	12.04%	70.14748	13.08%	48.96886	-21.06%	69.70787	12.37%
463.612	0.139	421.3025	57.03095	148.6489	140.8574	10.72655	64.36135	12.85%	64.75933	13.55%	48.21549	-15.46%	64.71098	13.47%
463.612	0.138921	425.2612	57.56684	148.8819	140.0953	10.71714	64.34903	11.78%	64.74676	12.47%	47.66448	-17.20%	64.66203	12.33%
463.612	0.102644	386.4025	52.3066	148.8819	139.7478	6.801684	58.09076	11.06%	58.54886	11.93%	47.26046	-9.65%	58.78962	12.39%
463.612	0.06919	335.961	45.47843	148.8819	139.2328	3.847389	50.69166	11.46%	51.61178	13.49%	46.93834	3.21%	52.65886	15.79%
466.2343	0.232826	543.1277	73.33612	148.3227	144.5187	24.96452	76.54276	4.37%	78.06749	6.45%	55.99134	-23.65%	76.8721	4.82%
466.2343	0.211017	492.5348	66.5048	148.3227	141.2832	21.12195	74.0656	11.37%	75.23328	13.12%	49.96946	-24.86%	74.20905	11.58%
466.2343	0.177081	450.2016	60.78873	148.3227	140.7565	15.84375	69.86828	14.94%	70.59594	16.13%	49.03086	-19.34%	70.06807	15.26%
466.2343	0.141792	418.0871	56.45245	148.3227	139.5126	11.17172	64.87499	14.92%	65.34362	15.75%	47.71301	-15.48%	65.16929	15.44%
466.2343	0.106344	380.7953	51.4171	148.3227	139.2078	7.239262	58.86748	14.49%	59.36138	15.45%	47.33125	-7.95%	59.5006	15.72%
466.2343	0.073721	331.1068	44.70789	148.3227	138.7026	4.253599	51.8859	16.06%	52.77039	18.03%	46.9958	5.12%	53.55163	19.78%
466.2343	0.1423	412.344	55.67698	148.3227	140.6636	11.23347	64.95279	16.66%	65.42337	17.51%	48.5874	-12.73%	65.30062	17.28%
468.5943	0.177059	625.04	84.87374	149.5984	146.1227	15.77302	74.67077	-12.02%	76.78717	-9.53%	55.38967	-34.74%	75.03913	-11.59%
468.5943	0.156705	514.6196	69.87982	149.5984	143.2872	12.99445	71.47625	2.28%	73.56424	5.27%	50.25032	-28.09%	71.68434	2.58%
468.5943	0.125408	442.9942	60.15387	149.5984	142.3676	9.223544	66.05351	9.81%	68.1907	13.36%	48.99146	-18.56%	66.37896	10.35%
468.5943	0.093263	390.771	53.06252	149.5984	141.1914	5.944774	59.5039	12.14%	61.87378	16.61%	47.9569	-9.62%	60.15854	13.37%
468.5943	0.061539	346.5697	47.06045	149.5984	140.556	3.278815	51.34626	9.11%	54.23842	15.25%	47.57685	1.10%	53.35039	13.37%
468.5943	0.0945	403.02	54.7258	149.5984	142.1838	6.060199	59.78136	9.24%	62.13768	13.54%	48.54966	-11.29%	60.48856	10.53%
471.741	0.167795	591.7109	80.71322	150.5044	147.0378	14.46553	69.92746	-13.36%	70.58545	-12.55%	55.29713	-31.49%	70.56897	-12.57%
471.741	0.148237	491.3477	67.02303	150.5044	144.1676	11.90773	67.10873	0.13%	67.61073	0.88%	50.32628	-24.91%	67.47701	0.68%
471.741	0.118065	427.0721	58.25541	150.5044	143.2837	8.417171	62.1805	6.74%	62.61441	7.48%	49.2007	-15.54%	62.75425	7.72%

471.741	0.087187	380.1018	51.84836	150.5044	142.2103	5.386932	56.07463	8.15%	56.7253	9.41%	48.32895	-6.79%	57.22964	10.38%
471.741	0.0885	386.232	52.68456	150.5044	143.1155	5.504857	56.36372	6.98%	56.99783	8.19%	48.84381	-7.29%	57.58389	9.30%
471.741	0.05684	334.2438	45.59303	150.5044	141.5487	2.930692	48.30211	5.94%	49.57443	8.73%	48.01823	5.32%	51.61881	13.22%
475.1499	0.070385	457.2271	61.77209	148.4513	144.3057	4.056552	51.7504	-16.22%	52.83227	-14.47%	50.87696	-17.64%	55.01455	-10.94%
475.1499	0.052508	376.0125	50.79987	148.4513	140.8964	2.68544	46.67913	-8.11%	48.22187	-5.07%	48.25722	-5.01%	50.93812	0.27%
475.1499	0.024343	320.2237	43.26272	148.4513	139.1454	0.935426	35.39517	-18.19%	38.18029	-11.75%	47.70749	10.27%	47.94326	10.82%
482.2299	0.106626	455.3985	61.64647	148.9284	146.4203	7.496281	60.4622	-1.92%	61.18566	-0.75%	55.7039	-9.64%	62.71009	1.73%
482.2299	0.094632	385.3335	52.16189	148.9284	143.649	6.290354	58.04633	11.28%	58.85609	12.83%	50.82222	-2.57%	59.42569	13.93%
482.2299	0.055567	304.5505	41.22645	148.9284	141.8784	2.942941			49.74738		49.01631	18.90%	49.01631	18.90%
510.2879	0.277512	805.8447	109.1473	149.041	144.0152	37.24357	86.62297	-20.64%	90.16463	-17.39%	55.0312	-49.58%	86.7153	-20.55%
510.2879	0.247079	686.166	92.93744	149.041	141.6681	30.2437	83.26586	-10.41%	86.10597	-7.35%	51.10129	-45.02%	83.32876	-10.34%
510.2879	0.1573	510.3125	69.11905	149.041	139.6126	14.34201	71.64218	3.65%	73.00282	5.62%	49.08197	-28.99%	71.80372	3.88%
510.2879	0.201087	558.2817	75.61621	149.041	139.5482	21.29533	77.73143	2.80%	79.67572	5.37%	48.94502	-35.27%	77.80725	2.90%
510.2879	0.152622	490.2056	66.39568	149.041	138.2673	13.6803	70.92493	6.82%	72.24373	8.81%	48.27726	-27.29%	71.07493	7.05%
510.2879	0.105844	426.9231	57.82441	149.041	137.4069	7.853918	62.69946	8.43%	63.89469	10.50%	48.34386	-16.40%	63.15022	9.21%
510.2879	0.063404	356.7528	48.32022	149.041	136.7698	3.752099	52.51348	8.68%	54.25714	12.29%	48.8992	1.20%	54.65038	13.10%
511.599	0.212889	673.3064	91.27292	146.4054	141.8205	24.11147	79.86328	-12.50%	82.14319	-10.00%	55.47036	-39.23%	80.06955	-12.27%
511.599	0.187259	563.1294	76.3374	146.4054	138.6705	19.5052	76.50749	0.22%	78.37899	2.67%	50.81005	-33.44%	76.63424	0.39%
511.599	0.1116	435.537	59.04108	146.4054	137.2104	8.746415	64.28678	8.88%	65.6328	11.16%	49.71537	-15.80%	64.76245	9.69%
511.599	0.148146	496.0828	67.24862	146.4054	137.4292	13.44649	70.74103	5.19%	72.18629	7.34%	49.73245	-26.05%	70.94693	5.50%
511.599	0.108568	420.4323	56.99349	146.4054	136.0257	8.39573	63.68649	11.74%	65.0411	14.12%	49.12048	-13.81%	64.14576	12.55%
511.599	0.070366	368.7943	49.99348	146.4054	135.1088	4.477057	54.83054	9.68%	56.59134	13.20%	49.25676	-1.47%	56.46875	12.95%
515.2702	0.208188	687.8456	92.56438	147.574	143.2061	23.04382	78.65541	-15.03%	80.84609	-12.66%	55.48747	-40.06%	78.89228	-14.77%
515.2702	0.184008	582.7089	78.41598	147.574	140.4277	18.80943	75.48254	-3.74%	77.2945	-1.43%	51.08091	-34.86%	75.63322	-3.55%
515.2702	0.1108	444.3485	59.79662	147.574	138.758	8.58536	63.65959	6.46%	64.97913	8.67%	49.64528	-16.98%	64.17041	7.31%
515.2702	0.146506	500.2332	67.31711	147.574	138.8407	13.11254	69.95206	3.91%	71.36366	6.01%	49.60883	-26.31%	70.17397	4.24%
515.2702	0.107194	438.0015	58.9425	147.574	137.5428	8.174104	62.94662	6.79%	64.27704	9.05%	49.01553	-16.84%	63.44445	7.64%
515.2702	0.069019	382.5904	51.48574	147.574	136.7333	4.321563	54.06818	5.02%	55.82016	8.42%	49.14576	-4.54%	55.85811	8.49%
517.8924	0.101128	640.5415	86.70894	148.8623	144.5383	7.467547	62.32578	-28.12%	63.65651	-26.59%	53.78134	-37.97%	63.62375	-26.62%
517.8924	0.081463	537.4701	72.75634	148.8623	142.3177	5.452668	57.85933	-20.48%	59.37671	-18.39%	51.44871	-29.29%	59.4386	-18.30%
517.8924	0.0508	387.984	52.52069	148.8623	139.2845	2.796831	49.02587	-6.65%	51.21946	-2.48%	50.2771	-4.27%	53.25307	1.39%
517.8924	0.017396	318.595	43.12762	148.8623	137.3441	0.648347	33.263	-22.87%	37.05651	-14.08%	50.73587	17.64%	50.80982	17.81%
517.8924	0.02225	382.2446	51.74375	147.4571	139.8722	0.903355	36.40039	-29.65%	39.88091	-22.93%	50.90065	-1.63%	51.07596	-1.29%
521.5635	0.086285	501.8987	67.94111	148.2691	142.4273	5.924374	59.02058	-13.13%	60.47719	-10.99%	51.54248	-24.14%	60.3909	-11.11%
521.5635	0.060867	424.1063	57.41049	148.2691	138.0574	3.602166	52.2616	-8.97%	54.17052	-5.64%	49.74328	-13.36%	54.81159	-4.53%
521.5635	0.022095	333.8651	45.19471	148.2691	135.2166	0.894862	36.30755	-19.66%	39.79758	-11.94%	50.37667	11.47%	50.56401	11.88%
524.1858	0.116699	579.273	77.73573	146.8771	143.7007	9.491749	65.36384	-15.92%	66.83919	-14.02%	56.19565	-27.71%	66.68002	-14.22%
524.1858	0.101914	516.4567	69.30608	146.8771	141.44	7.763116	62.41561	-9.94%	63.93054	-7.76%	52.50994	-24.23%	63.44445	-8.46%
524.1858	0.078976	397.495	53.34197	146.8771	140.0864	5.359934	57.16393	7.17%	58.89815	10.42%	51.23703	-3.95%	58.83822	10.30%
524.1858	0.055162	351.4773	47.16661	146.8771	139.0372	3.224751	50.40407	6.86%	52.63285	11.59%	50.72326	7.54%	54.19522	14.90%
524.1858	0.05565	376.57	50.53394	148.7944	144.0752	3.264738	50.5614	0.05%	52.77663	4.44%	54.43594	7.72%	56.60439	12.01%
528.3814	0.46163	1036.197	140.1891	148.7944	146.063	111.9359	108.1139	-22.88%	117.1609	-16.43%	65.91369	-52.98%	108.1904	-22.83%
528.3814	0.442908	958.2978	129.6499	148.7944	144.754	101.2843	106.0581	-18.20%	114.5983	-11.61%	60.09549	-53.65%	106.0942	-18.17%

528.3814	0.412677	772.026	104.4489	148.7944	143.682	86.01314	102.8267	-1.55%	110.5299	5.82%	56.72218	-45.69%	102.8535	-1.53%
528.3814	0.34624	687.7637	93.04885	148.7944	143.453	59.17768	95.91819	3.08%	101.7553	9.36%	55.50602	-40.35%	95.9585	3.13%
528.3814	0.378693	726.748	98.32311	148.7944	143.3385	71.26491	99.27806	0.97%	106.0258	7.83%	55.59168	-43.46%	99.30811	1.00%
528.3814	0.381	750.3405	101.515	146.8771	141.3144	72.19432	99.51735	-1.97%	106.3301	4.74%	52.08388	-48.69%	99.53268	-1.95%
532.0525	0.29076	712.4331	95.6052	146.8771	143.9573	43.09161	89.87045	-6.00%	94.21018	-1.46%	61.80648	-35.35%	90.08093	-5.78%
532.0525	0.273265	655.8065	88.00618	146.8771	141.7697	38.43708	87.94042	-0.07%	91.85776	4.38%	55.26978	-37.20%	88.02462	0.02%
532.0525	0.138847	383.8901	51.51626	146.8771	141.5166	12.54409			71.69938		53.35245	3.56%	53.35245	3.56%
532.0525	0.244672	624.9224	83.86167	146.8771	141.2083	31.55748	84.66726	0.96%	87.93622	4.86%	53.94399	-35.68%	84.76013	1.07%
532.0525	0.213688	604.0542	81.06125	146.8771	140.6857	25.01767	80.88678	-0.22%	83.53224	3.05%	52.88726	-34.76%	81.00155	-0.07%
532.0525	0.183132	553.4405	74.26914	146.8771	140.5632	19.39684	76.81904	3.43%	78.95899	6.31%	52.51549	-29.29%	76.9886	3.66%
532.0525	0.155787	470.1464	63.09145	146.8771	140.3288	14.99509	72.77805	15.35%	74.5877	18.22%	52.08853	-17.44%	73.03076	15.75%
532.0525	0.215	577.3115	77.47251	146.8771	141.4328	25.27669	81.053	4.62%	83.72282	8.07%	54.02473	-30.27%	81.1922	4.80%
532.3147	0.25222	755.5925	101.9383	148.194	143.3273	33.00428	85.98834	-15.65%	89.45319	-12.25%	55.54826	-45.51%	86.09656	-15.54%
532.3147	0.223539	652.755	88.06432	148.194	140.4981	26.76826	82.56095	-6.25%	85.40316	-3.02%	51.17675	-41.89%	82.62983	-6.17%
532.3147	0.14045	495.5102	66.85015	148.194	138.8654	12.65755	70.705	5.77%	72.36051	8.24%	49.95973	-25.27%	70.92135	6.09%
532.3147	0.180472	538.8282	72.69426	148.194	138.879	18.78056	76.87653	5.75%	78.9623	8.62%	49.74901	-31.56%	76.97497	5.89%
532.3147	0.137003	471.8811	63.6623	148.194	137.7121	12.18381	70.11786	10.14%	71.75226	12.71%	49.308	-22.55%	70.32251	10.46%
532.3147	0.09478	415.4047	56.04297	148.194	136.7315	7.027579	61.87616	10.41%	63.52544	13.35%	49.46957	-11.73%	62.50664	11.53%
532.3147	0.054997	364.3835	49.15962	148.194	136.0445	3.233377	51.17971	4.11%	53.49589	8.82%	50.20015	2.12%	54.35091	10.56%
536.5103	0.251035	766.455	103.3457	147.9635	143.15	33.03073	86.27364	-16.52%	89.81088	-13.10%	55.74231	-46.06%	86.3824	-16.41%
536.5103	0.222573	669.7323	90.304	147.9635	140.4072	26.8153	82.84527	-8.26%	85.76275	-5.03%	51.43426	-43.04%	82.91549	-8.18%
536.5103	0.13985	502.197	67.71422	147.9635	138.7344	12.68976	70.94551	4.77%	72.6778	7.33%	50.17662	-25.90%	71.16462	5.10%
536.5103	0.17985	544.4971	73.4178	147.9635	138.7364	18.84748	77.1621	5.10%	79.32638	8.05%	49.94398	-31.97%	77.26111	5.23%
536.5103	0.136753	474.1813	63.9367	147.9635	137.5344	12.26106	70.41406	10.13%	72.12718	12.81%	49.48933	-22.60%	70.61847	10.45%
536.5103	0.094935	417.586	56.30562	147.9635	136.5791	7.108882	62.20924	10.48%	63.93066	13.54%	49.67568	-11.77%	62.83582	11.60%
536.5103	0.055556	369.4	49.80842	147.9635	135.999	3.309543	51.61015	3.62%	53.97772	8.37%	50.44252	1.27%	54.72082	9.86%
536.7725	0.372358	856.8668	115.764	148.4317	145.5675	70.08133	99.57964	-13.98%	106.3686	-8.12%	63.72075	-44.96%	99.69368	-13.88%
536.7725	0.353536	720.784	97.37903	148.4317	143.5118	62.92608	97.60761	0.23%	103.8646	6.66%	56.65521	-41.82%	97.6499	0.28%
536.7725	0.323778	687.8783	92.93343	148.4317	143.0547	52.7797	94.47476	1.66%	99.90238	7.50%	55.35164	-40.44%	94.51969	1.71%
536.7725	0.259279	628.4453	84.90394	148.4317	142.5975	34.8764	87.40408	2.94%	91.1529	7.36%	53.95614	-36.45%	87.47407	3.03%
536.7725	0.291356	669.8868	90.50275	148.4317	142.5227	43.14781	90.99093	0.54%	95.54717	5.57%	54.07775	-40.25%	91.04083	0.59%
536.7725	0.230775	530.691	71.69718	148.4317	142.3409	28.4415	84.03345	17.21%	87.13114	21.53%	53.35659	-25.58%	84.12252	17.33%
536.7725	0.293	647.3235	87.45441	148.4317	143.3207	43.60375	91.17033	4.25%	95.76961	9.51%	55.59177	-36.43%	91.2349	4.32%
538.6081	0.1235	450.0295	60.83392	148.5496	141.8419	10.49887	68.39297	12.43%	70.07083	15.18%	52.30596	-14.02%	68.84732	13.17%
538.6081	0.197315	600.787	81.21295	148.5496	145.2949	21.91442	79.97976	-1.52%	82.4624	1.54%	58.76122	-27.65%	80.33892	-1.08%
538.6081	0.180082	540.7194	73.09316	148.5496	142.5619	18.88204	77.58721	6.15%	79.78925	9.16%	53.25533	-27.14%	77.76546	6.39%
538.6081	0.152114	513.1811	69.3706	148.5496	141.9034	14.44978	73.34712	5.73%	75.20294	8.41%	52.39067	-24.48%	73.59683	6.09%
538.6081	0.122134	473.6876	64.03196	148.5496	140.9339	10.32432	68.13661	6.41%	69.81134	9.03%	51.56915	-19.46%	68.5456	7.05%
538.6081	0.092578	417.493	56.43571	148.5496	140.5507	6.851242	62.0005	9.86%	63.75458	12.97%	51.499	-8.75%	62.90762	11.47%
542.5415	0.3575	775.261	104.6212	148.1708	142.7696	65.23446	98.64918	-5.71%	105.1824	0.54%	55.71403	-46.75%	98.6817	-5.68%
542.5415	0.4519	1046.756	141.2594	148.1708	145.1451	109.7474	108.8213	-22.96%	118.008	-16.46%	64.40745	-54.40%	108.8786	-22.92%
542.5415	0.430178	950.8091	128.3114	148.1708	143.5412	97.66992	106.4152	-17.06%	115.004	-10.37%	58.33291	-54.54%	106.4413	-17.04%
542.5415	0.262483	611.0152	82.4563	148.1708	143.3211	36.12304	88.31494	7.11%	92.29092	11.93%	55.93269	-32.17%	88.40621	7.22%

542.5415	0.39497	790.3047	106.6514	148.1708	142.3133	80.58588	102.618	-3.78%	110.2159	3.34%	55.11521	-48.32%	102.6384	-3.76%
542.5415	0.318443	695.6011	93.87114	148.1708	141.9889	51.77473	94.50036	0.67%	99.94088	6.47%	53.91908	-42.56%	94.53486	0.71%
542.5415	0.284615	640.7233	86.4654	148.1708	141.9346	41.85824	90.81428	5.03%	95.34913	10.27%	53.60243	-38.01%	90.86078	5.08%
542.5415	0.355837	749.5957	101.1577	148.1708	141.8918	64.61204	98.47347	-2.65%	104.9596	3.76%	54.02032	-46.60%	98.49775	-2.63%
548.0482	0.348994	940.0417	126.1492	146.8789	143.6508	63.36541	98.02634	-22.29%	104.3454	-17.28%	61.94943	-50.89%	98.12549	-22.21%
548.0482	0.327765	829.8735	111.3652	146.8789	141.8223	55.89434	95.74606	-14.03%	101.4895	-8.87%	56.27028	-49.47%	95.79302	-13.98%
548.0482	0.167154	518.302	69.55371	146.8789	141.3393	17.28046	76.02913	9.31%	78.27629	12.54%	53.94937	-22.43%	76.27168	9.66%
548.0482	0.293538	727.4195	97.61631	146.8789	140.6719	45.23626	92.00843	-5.74%	96.84919	-0.79%	53.79586	-44.89%	92.0513	-5.70%
548.0482	0.258	691.725	92.82627	146.8789	141.134	35.7414	87.96912	-5.23%	91.93086	-0.96%	54.30826	-41.49%	88.03961	-5.16%
548.0482	0.219805	625.6042	83.95316	146.8789	140.1871	27.05939	83.3189	-0.76%	86.44178	2.96%	52.69326	-37.23%	83.4038	-0.65%
548.0482	0.18785	558.4798	74.94539	146.8789	140.1649	20.84704	79.05126	5.48%	81.59457	8.87%	52.55916	-29.87%	79.1837	5.66%
548.0482	0.255827	678.8175	91.09415	146.8789	140.102	35.20734	87.71454	-3.71%	91.62518	0.58%	52.73156	-42.11%	87.76847	-3.65%
548.3104	0.262319	832.7691	112.6352	148.6747	145.3786	36.3439	89.11173	-20.88%	93.23655	-17.22%	60.17813	-46.57%	89.28597	-20.73%
548.3104	0.095954	407.7027	55.14334	148.6747	142.3685	7.347202	63.56938	15.28%	65.4562	18.70%	53.12878	-3.65%	64.55471	17.07%
548.3104	0.21095	602.4568	81.48455	148.6747	142.3079	24.92273	82.81811	1.64%	85.77067	5.26%	53.20745	-34.70%	82.9168	1.76%
548.3104	0.178429	555.4404	75.12541	148.6747	141.5879	18.93401	78.33495	4.27%	80.7106	7.43%	52.30747	-30.37%	78.47192	4.45%
548.3104	0.146427	529.2562	71.58391	148.6747	141.5371	13.86091	73.34294	2.46%	75.32831	5.23%	52.30125	-26.94%	73.5886	2.80%
548.3104	0.116051	487.0147	65.87058	148.6747	141.1753	9.732148	67.82445	2.97%	69.65794	5.75%	52.13028	-20.86%	68.29734	3.68%
548.3104	0.17935	583.74	78.95304	148.6747	141.7954	19.09173	78.46914	-0.61%	80.85889	2.41%	52.52921	-33.47%	78.60982	-0.43%
553.8171	0.117523	503.2538	67.83767	147.9564	141.8802	10.07419	68.33766	0.74%	70.29607	3.62%	53.44309	-21.22%	68.90105	1.57%
553.8171	0.091856	453.6727	61.15423	147.9564	140.9936	7.00281	62.82542	2.73%	64.85997	6.06%	52.77839	-13.70%	63.84718	4.40%
553.8171	0.066588	417.411	56.26623	147.9564	140.7895	4.413956	56.18576	-0.14%	58.56123	4.08%	52.8554	-6.06%	58.67552	4.28%
553.8171	0.04339	348.2617	46.94502	147.9564	140.1328	2.426023	48.27847	2.84%	51.2942	9.26%	52.89631	12.68%	54.7108	16.54%
553.8171	0.0926	471.8335	63.60227	147.9564	141.7567	7.085514	62.99981	-0.95%	65.02873	2.24%	53.34091	-16.13%	64.10167	0.79%
561.1594	0.086022	608.9312	80.85699	144.4506	142.3801	6.62898	60.99252	-24.57%	63.31171		59.17559	-26.81%	64.46251	-20.28%
561.1594	0.076795	481.18	63.89353	144.4506	140.3449	5.630425	58.63597	-8.23%	61.06469	-4.43%	54.98515	-13.94%	61.1665	-4.27%
561.1594	0.06213	392.0479	52.05812	144.4506	139.542	4.167159	54.44064	4.58%	57.12939	9.74%	53.95503	3.64%	58.09305	11.59%
561.1594	0.04655	365.815	48.57478	144.4506	139.8644	2.783982	49.143	1.17%	52.24941	7.56%	53.9875	11.14%	55.79716	14.87%

APPENDIX C

CORRELATION COMPARISON

In order to assess experiment data, some well-known condensation heat transfer correlations were referred to and compared. Because of the different condensation mechanisms involved, two categories of correlations were selected. For the high mass flux data, the annular flow type correlation of Akers et al. [2], Azer [5], Cavallini et al. [13], Shah [47], Chen [15], Dobson et al. [21], and Traviss et al. [58] were chosen. The film condensation correlation of Chato [14], and Jaster et al. [31] were used in the low mass flux, wavy flow.

C.1 Annular Flow Correlation

As pointed out in the chapter two, three types of approaches were encompassed in those correlations. Akers, Cavallini, Shah, and Dobson's were two-phase multiplier type. Azers used boundary layer analysis to develop a correlation. And a shear-based correlation was proposed by Chen.

The predictions of the Akers correlation are shown in Figures 4.25 and 4.26. An equivalent Reynolds number with the same wall shear stress as the two-phase flow is introduced in Figure 4.26. The correlation provides good agreement with the experimental data, with a mean deviation of 15.2%. Most data (83.7%) were predicted within +/-25%. The correlation tended to over-predict data at high mass fluxes with lower quality. On the other hand, it seemed to underestimate data with low mass flux, where wavy flow pattern prevailed. In general, the Akers correlation covered extended ranges of flow conditions with fairly satisfactory predictions.

The Chen correlation is compared to experimental data in Figure C.1. The prediction agrees well with the data, with a mean deviation of 17.4%. Almost all of the data were predicted within +/-50%, and nearly ¾ of data were within +/-25%. The most significant deviations occurred at low mass fluxes with wavy-annular flow patterns, and at some high flux, high quality data. In general, the Chen correlation under-predicted for Nusselt numbers less than 50; however, the prediction tended to be high for data with larger Nusselt numbers.

In Figure C.2, the prediction of the Azer correlation was compared with the experimental data. The mean deviation of the prediction is 21.6%. As for the Chen correlation in Figure C.1, the Azer correlation under-predicted the data at low Nusselt numbers, but over predicted the data at high Nusselt numbers.

The prediction of Cavallini is displayed in Figure C.3. The predictions overestimated all the data with a mean deviation of 25.0%. Figure C.4 is the comparison of Shah correlation with experimental data. The mean deviation of the correlation and data is 14.0%. The prediction of Dobson is plotted as Figure C.5 for which the mean deviation is 15.9%. Figure C.6 shows the comparison of the Traviss correlation with the data, where the mean deviation is 20.1%. These four correlations tended to over-predict the experimental data, pronouncedly in the high quality region.

A tabular comparison of the previous six annular flow condensation correlations is listed in Table C.1.

Correlation	Mean Deviation	Percentage of data within +/- 10%	Percentage of data within +/- 25%	Percentage of data within +/- 50%
Akers	15.2%	41.2%	83.7%	100%
Chen	17.4%	32.4%	74.7%	97.1%
Azer	21.6%	23.4%	49.5%	82.5%
Shah	14.0%	1.4%	8.5%	51.3%
Cavallini	25.0%	0.0%	6.2%	22.9%
Traviss	20.1%	6.8%	16.3%	47.5%
Dobson	15.9%	4.8%	16.2%	58.0%

Table C.1 Comparison of various annular heat transfer correlation of literature

C.2 Gravity-dominated correlation

The prediction of the Chato correlation is plotted against the experimental data in Figure C.7. There is a mean deviation of 25.4% between 260 experimental data points with vapor Reynolds number less than 35000 recommended by the Chato correlation for stratified flow. More than half of the data was predicted within +/- 25%. The major drawback of the Chato correlation was the neglect of quality variation, which was only valid for the wavy flow pattern.

Figure 4.27 displays the prediction of the Jaster correlation. By taking the void fraction into consideration, Jaster and Kosky accounted for the liquid pool depth and quality variation. The prediction was much improved over the Chato correlation and agreed well with the experimental data. The mean deviation between the experimental data and predicted values is 16.3%, and most are within +/-25%. Table C.2 is the summary of each gravity-dominated correlation in predicting the experimental data.

Correlation	Mean Deviation	Percentage of data within +/- 10%	Percentage of data within +/- 25%	Percentage of data within +/- 50%
Chato	25.4%	20.0%	51.8%	85.5%
Jaster	16.0%	34.5%	80.4%	100.0%

Table C.2 Comparison of film-wise condensation correlation to data.

C.3 Discussion

The correlation of Chato and Jaster were capable of predicting the experimental data at lower mass fluxes. However, the Chato correlation was not able to describe the offset of the quality on the heat transfer. On the other hand, the Jaster correlation accounted for the void fraction; therefore, the prediction agreed more with the trend of data. For the data at low mass fluxes, the Jaster correlation under-predicted the data for quality less then 15%, but over-predicted the data with quality more than 25%, as shown in Figure C.8. As mass fluxes increased to around 185 klb/ft^{2}hr, the Jaster correlation over-predicted data with intermediate quality from 25% to 50%, which was the wavy-annular flow pattern, as shown at Figure C.9. As mass fluxes approached 280 klb/ft^{2}hr, the Jaster correlation under-predicted the data over the entire quality range as shown in Figure C.10 where the annular flow mechanism was more dominant.

Both correlations did not account for the heat transfer in the bottom liquid pool. A superposition model accounting for both mechanisms of film wise condensation and forced convection heat transfer may describe the actual behavior more closely.

Among the annular flow correlations, the simple form of Akers correlation had the most accurate prediction. Most data were predicted within +/-25%. Both Chen and Azer's correlations had reasonable agreement within the experimental data. However, other correlations by Shah, Cavallini, Dobson, and Traviss overestimated most of the data.

In order to verify the applicability of each correlation, the deviation of the data was plotted against the quality. The distribution of Akers correlation is shown in Figure C.11, which overestimated the data when the quality was less than 15%, the wavy-annular flow regime. The same discrepancies are shown in Figures C.12 and C.13 for the Chen and Azer correlation, but they were underestimation instead of over-predictions. All three correlations have better agreements in the intermediate ranges of quality, where the annular flow patterns persisted. As quality increased beyond 80%, the consistency between predictions and experimental data fell again. This is where the annular-mist flow pattern could occur.

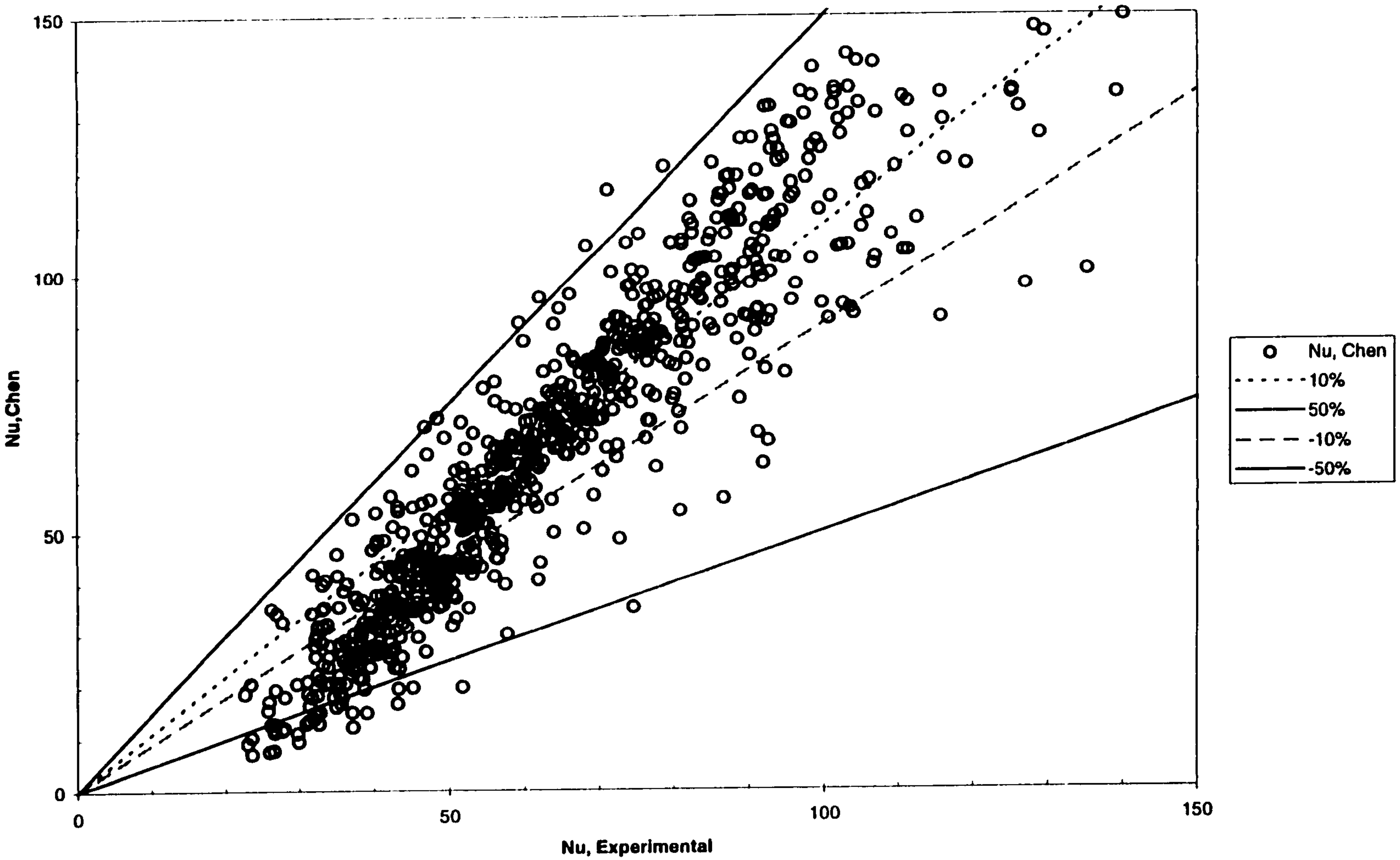

Figure C.1 Comparison of experimental data with prediction of Chen correlation

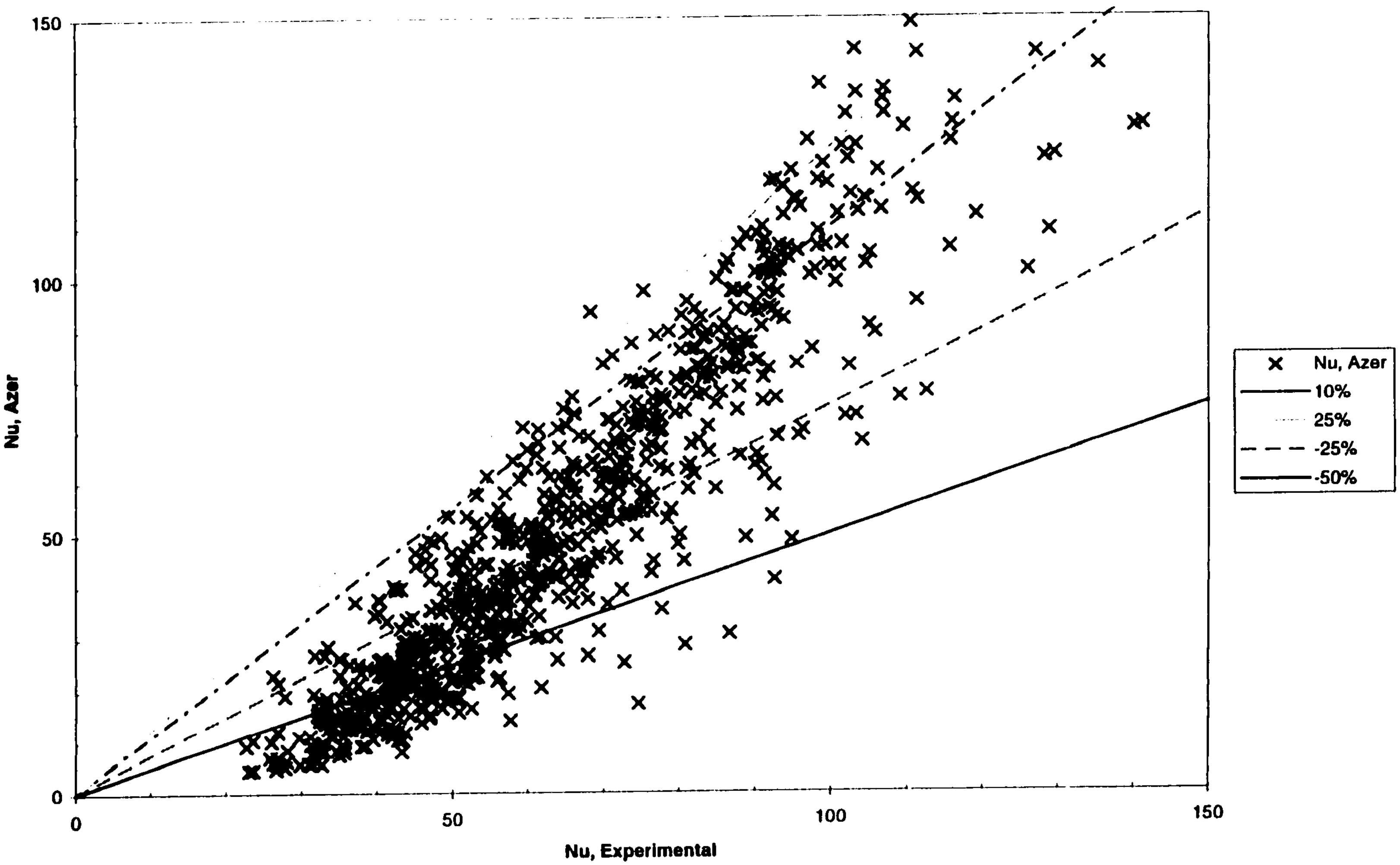

Figure C.2 Comparison of experimental data with prediction of Azer correlation

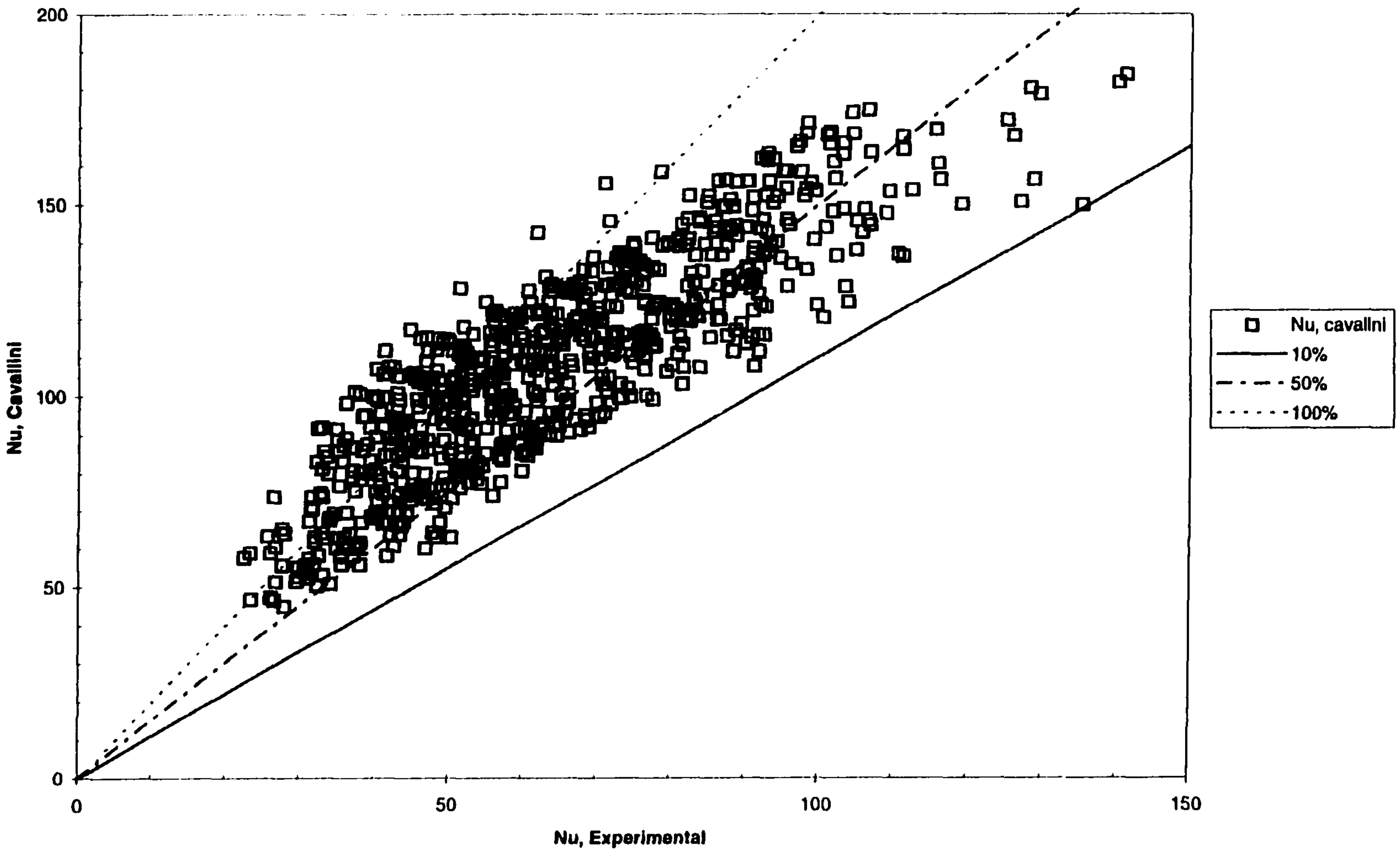

Figure C.3 Comparison of experimental data with prediction of Cavallni correlation

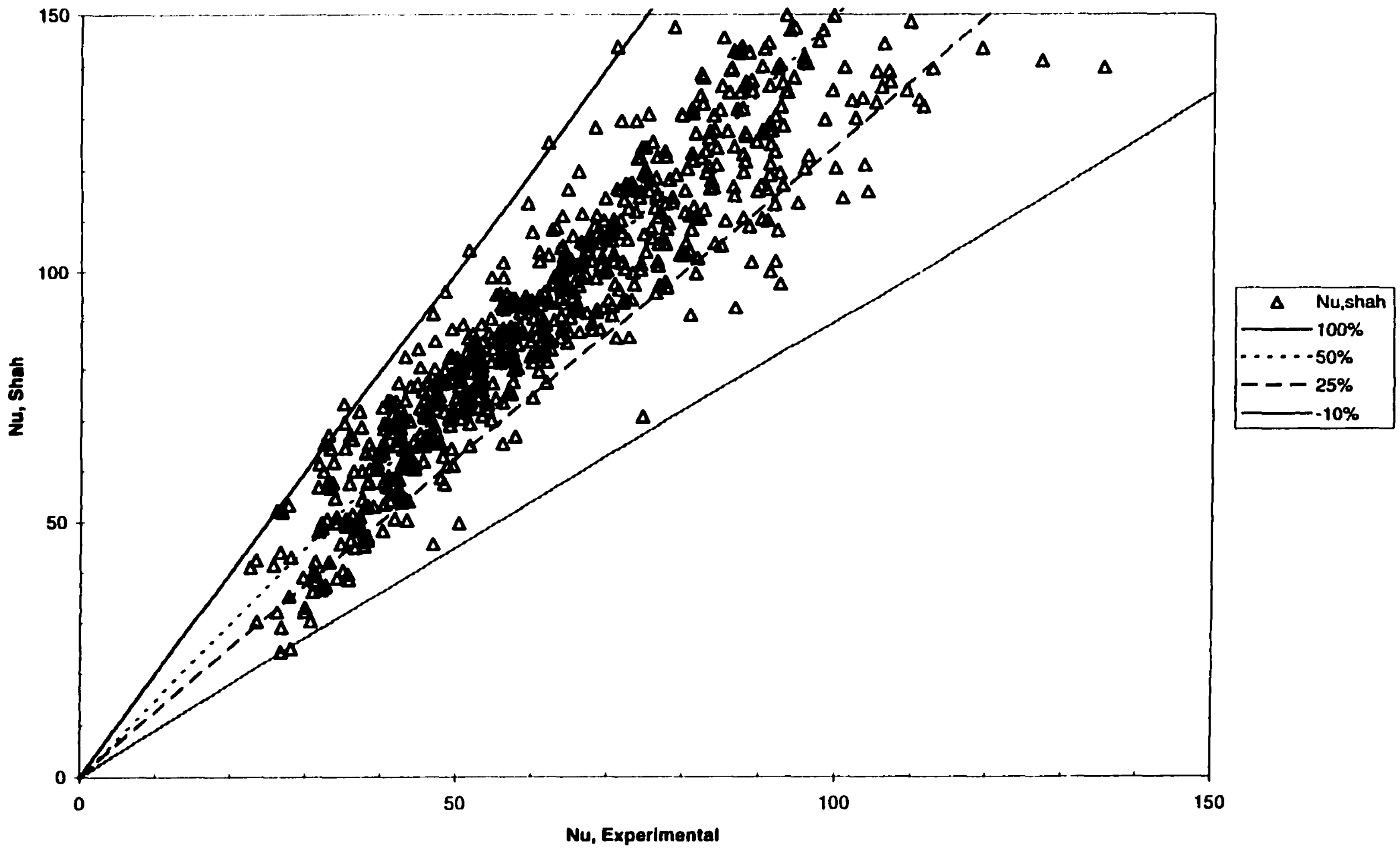

Figure C.4 Comparison of experimental data with prediction of Shah correlation

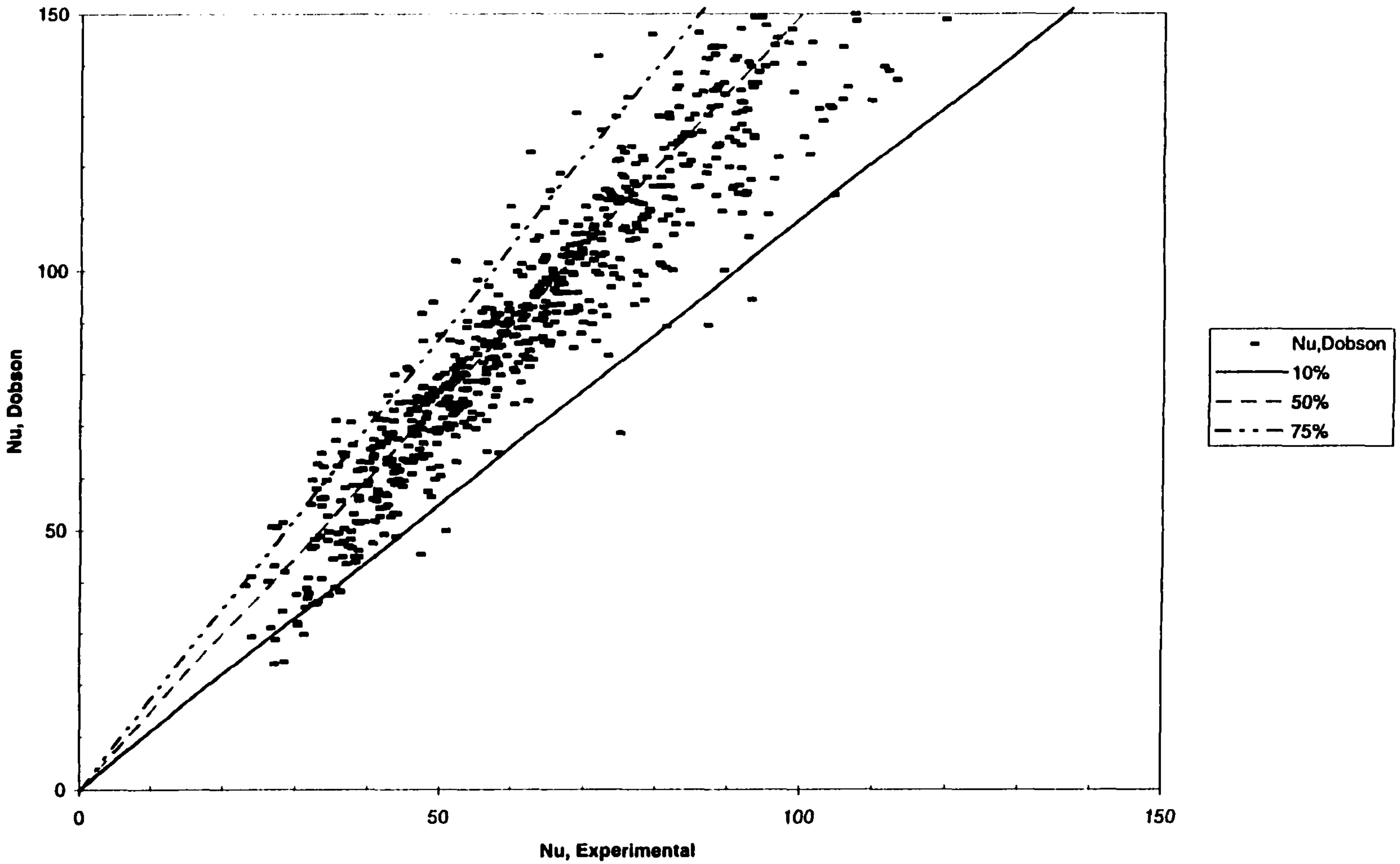

Figure C.5 Comparison of experimental data with prediction of Dobson correlation

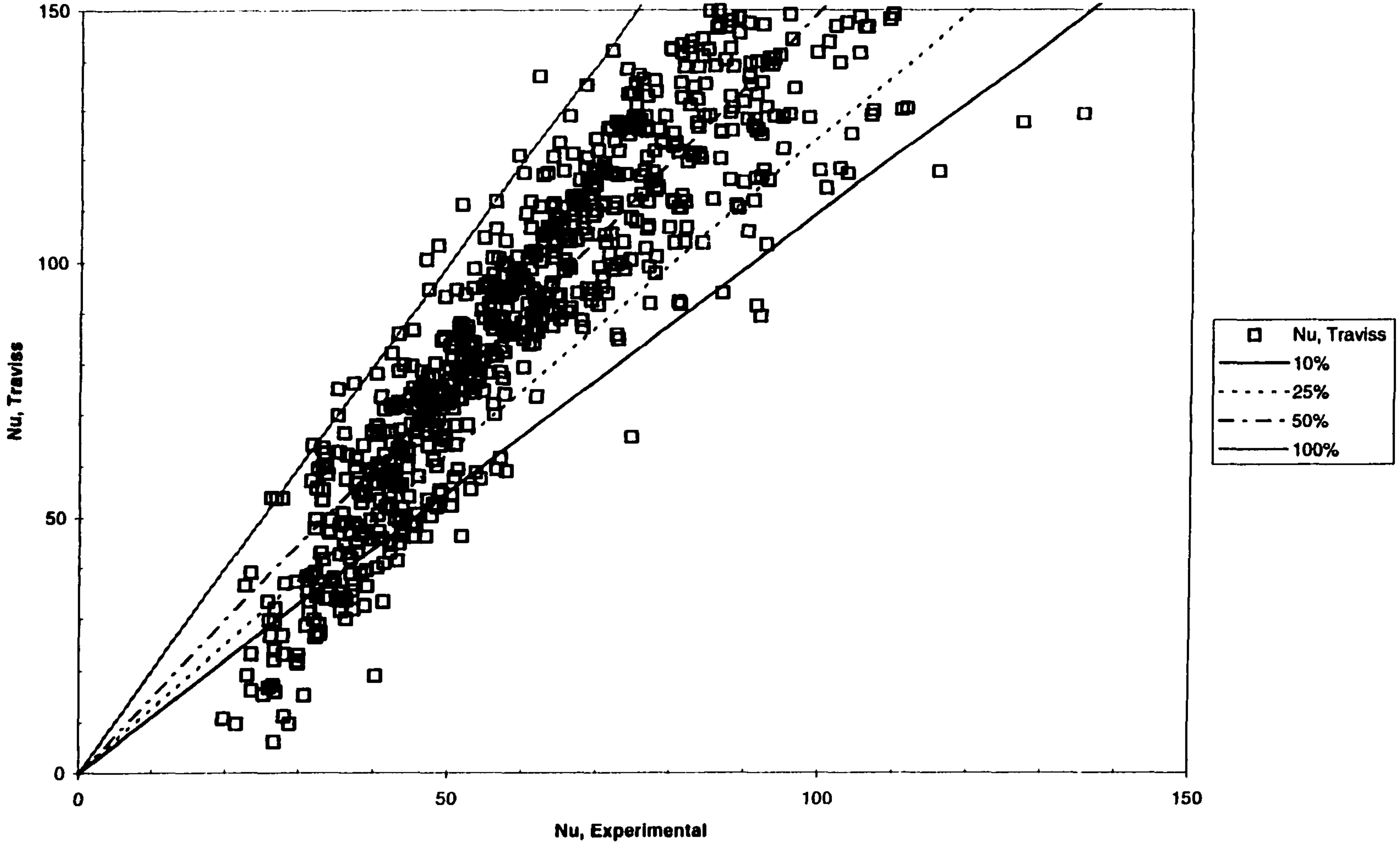

Figure C.6 Comparison of experimental data with prediction of Traviss correlation

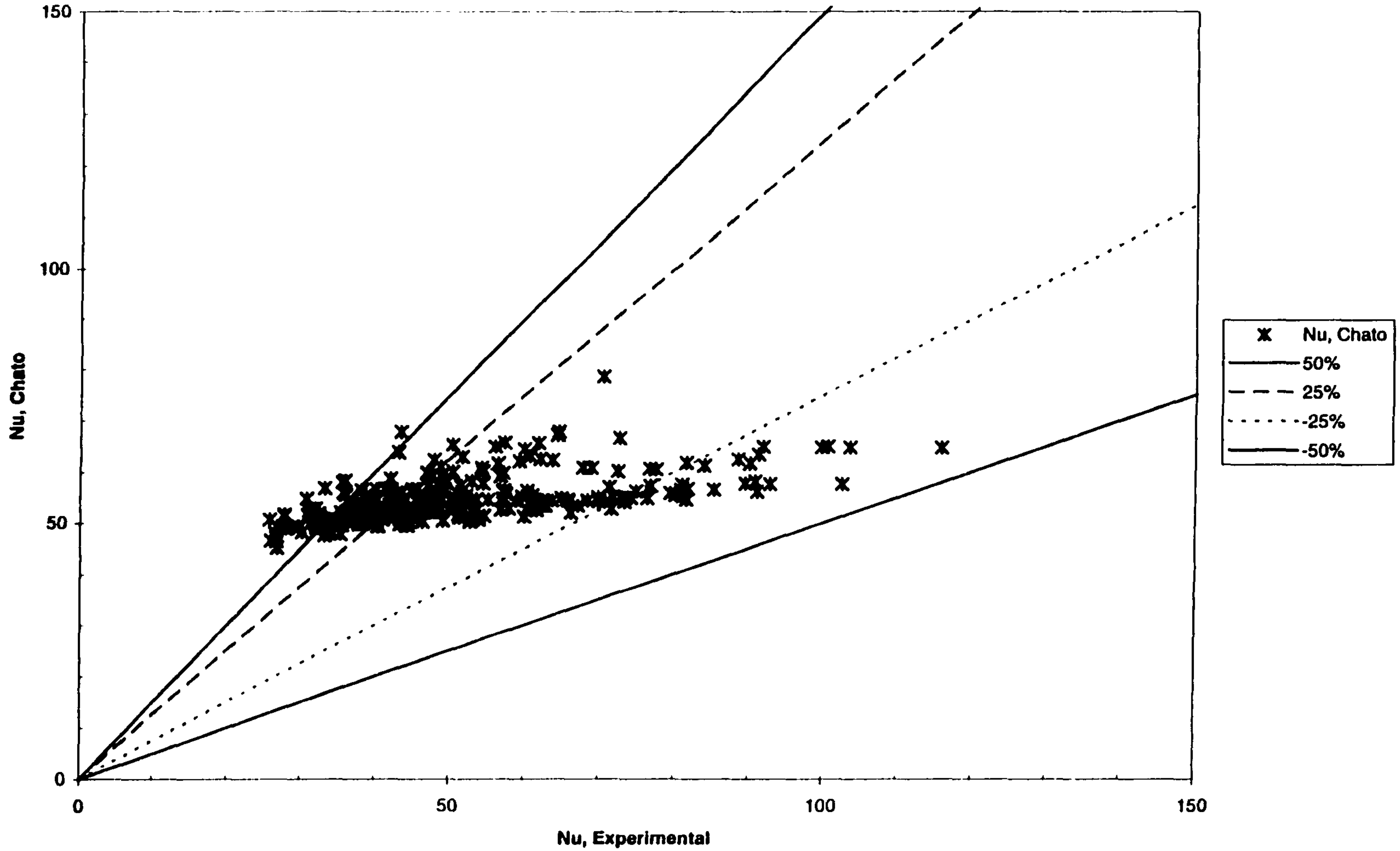

Figure C.7 Comparison of experimental data with prediction of Chato correlation

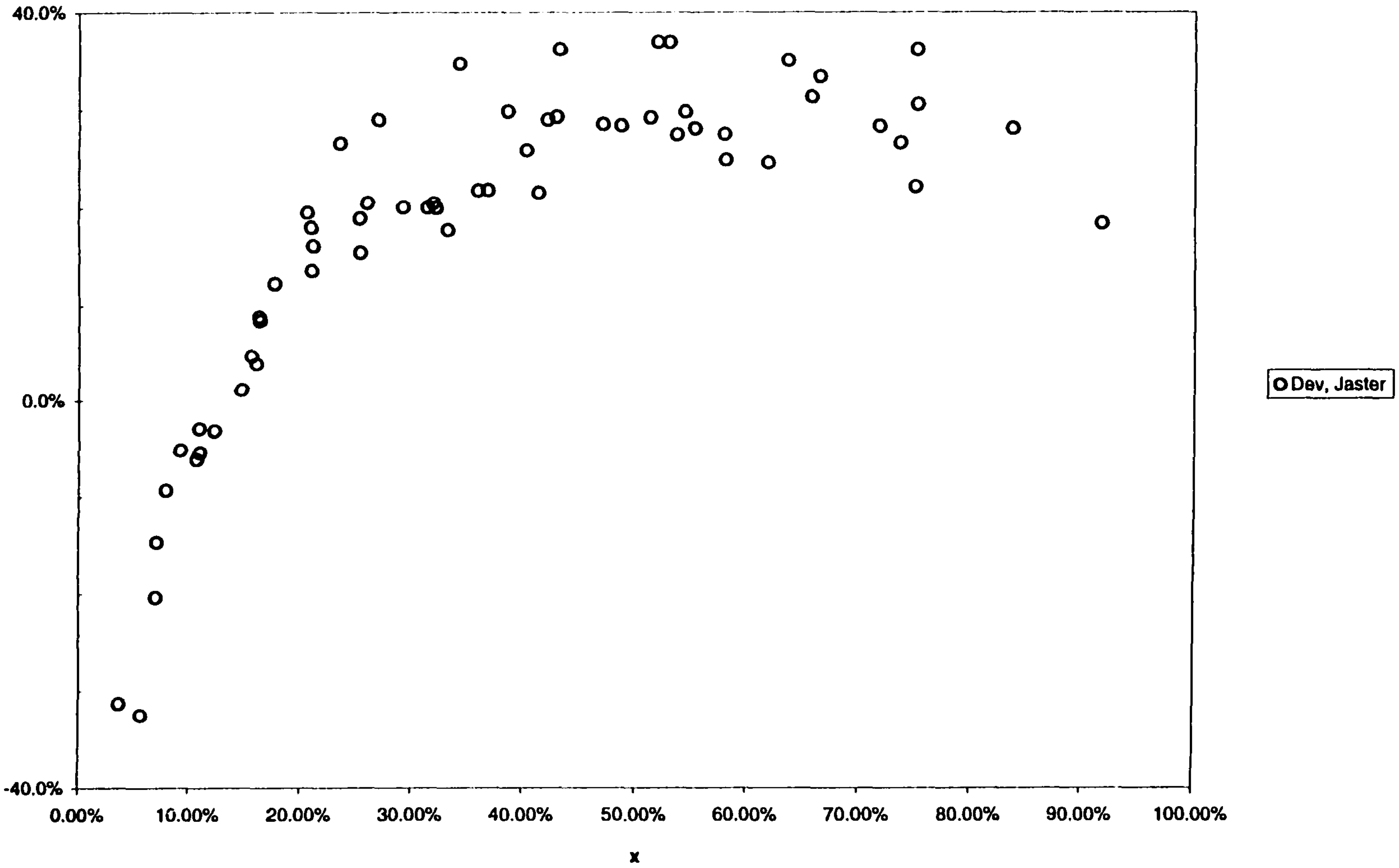

Figure C.8 Deviation of Jaster Correlation against Quality for G = 60 ~100 klb/ft^{2}hr

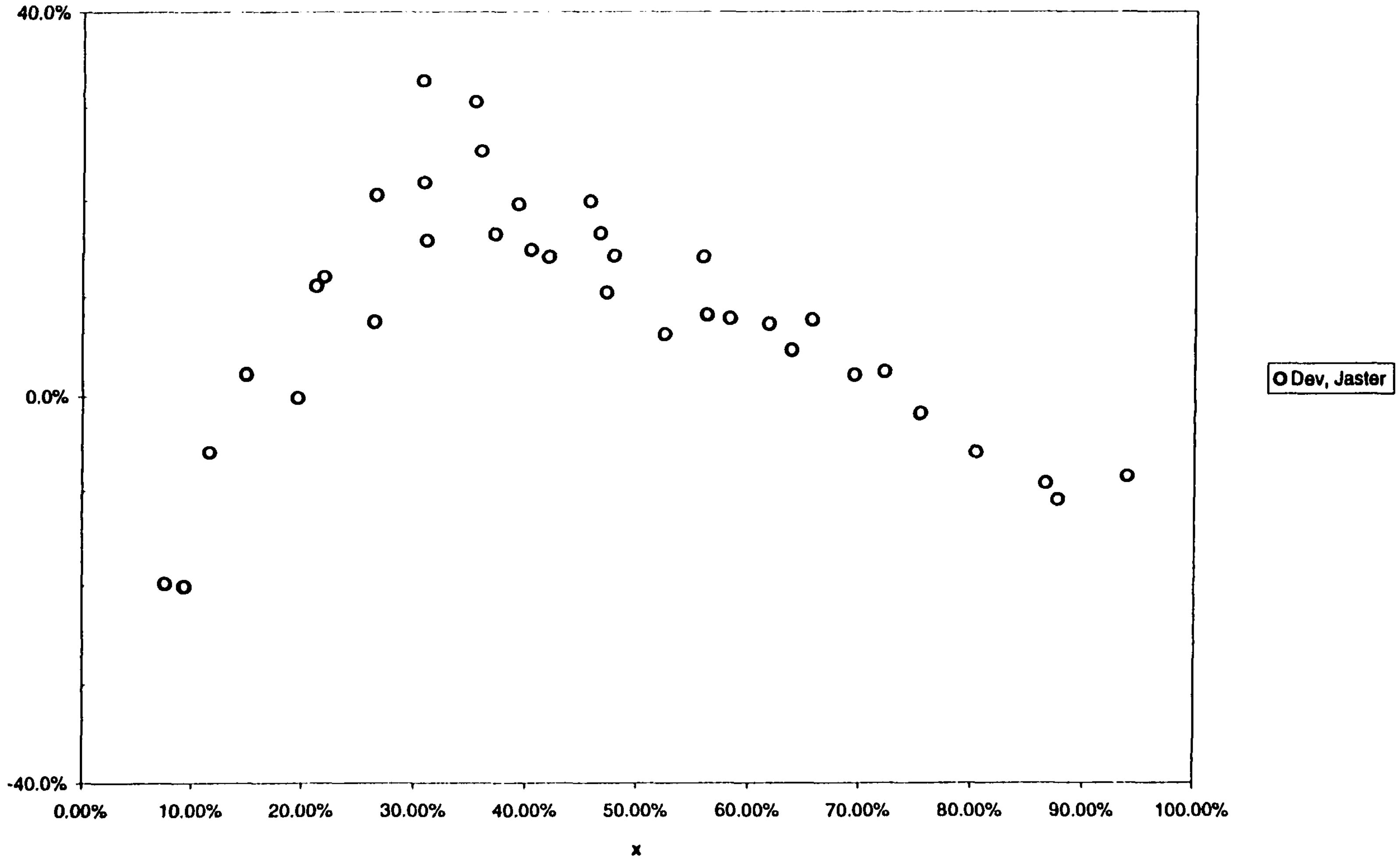

Figure C.9 Deviation of Jaster Correlation against Quality for
G = 180 ~ 190 klb/ft^{2}hr

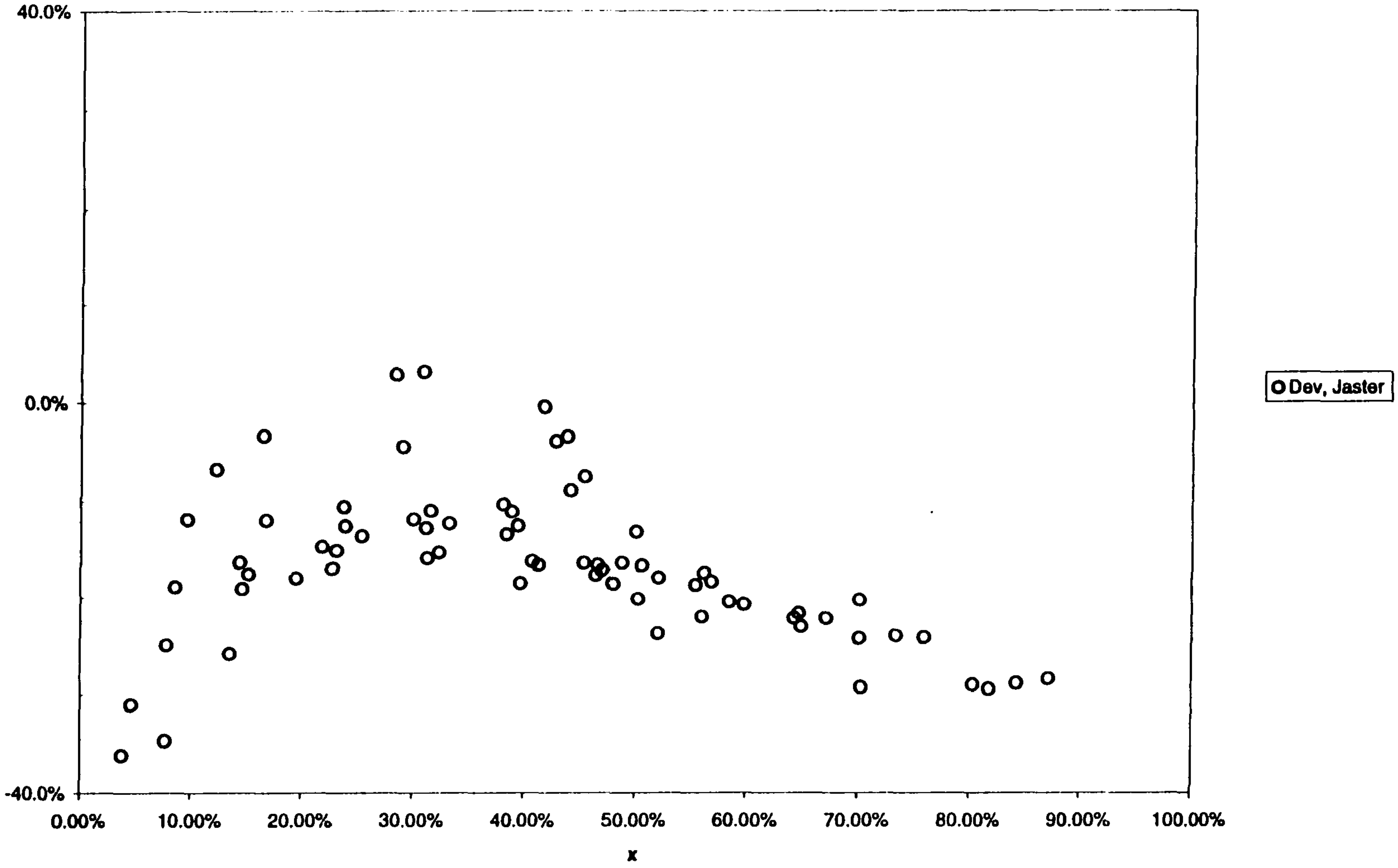

Figure C.10 Deviation of Jaster Correlation against Quality for $G = 260 \sim 290\ klb/ft^2hr$

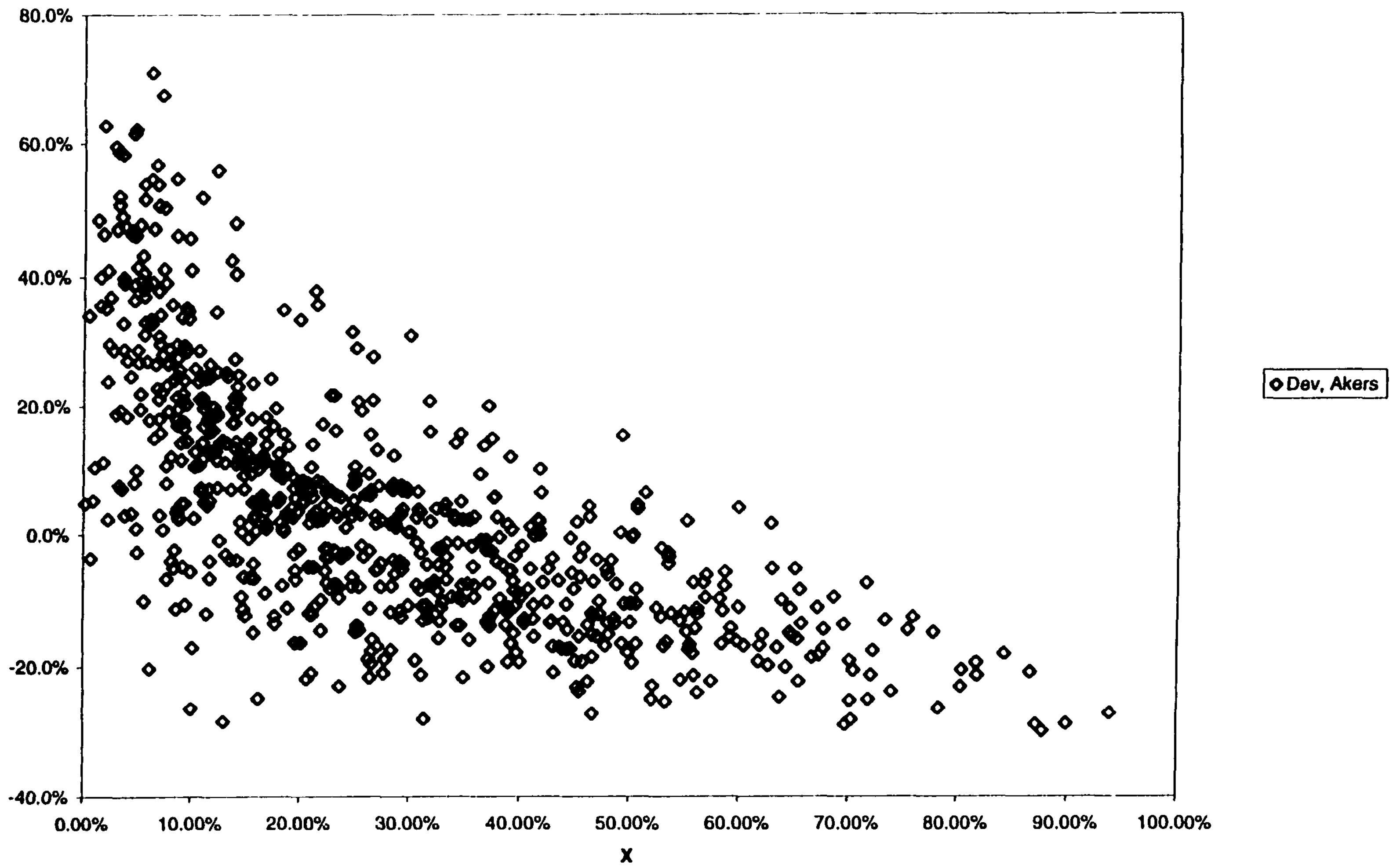

Figure C.11 Deviation of Akers Correlation against Quality

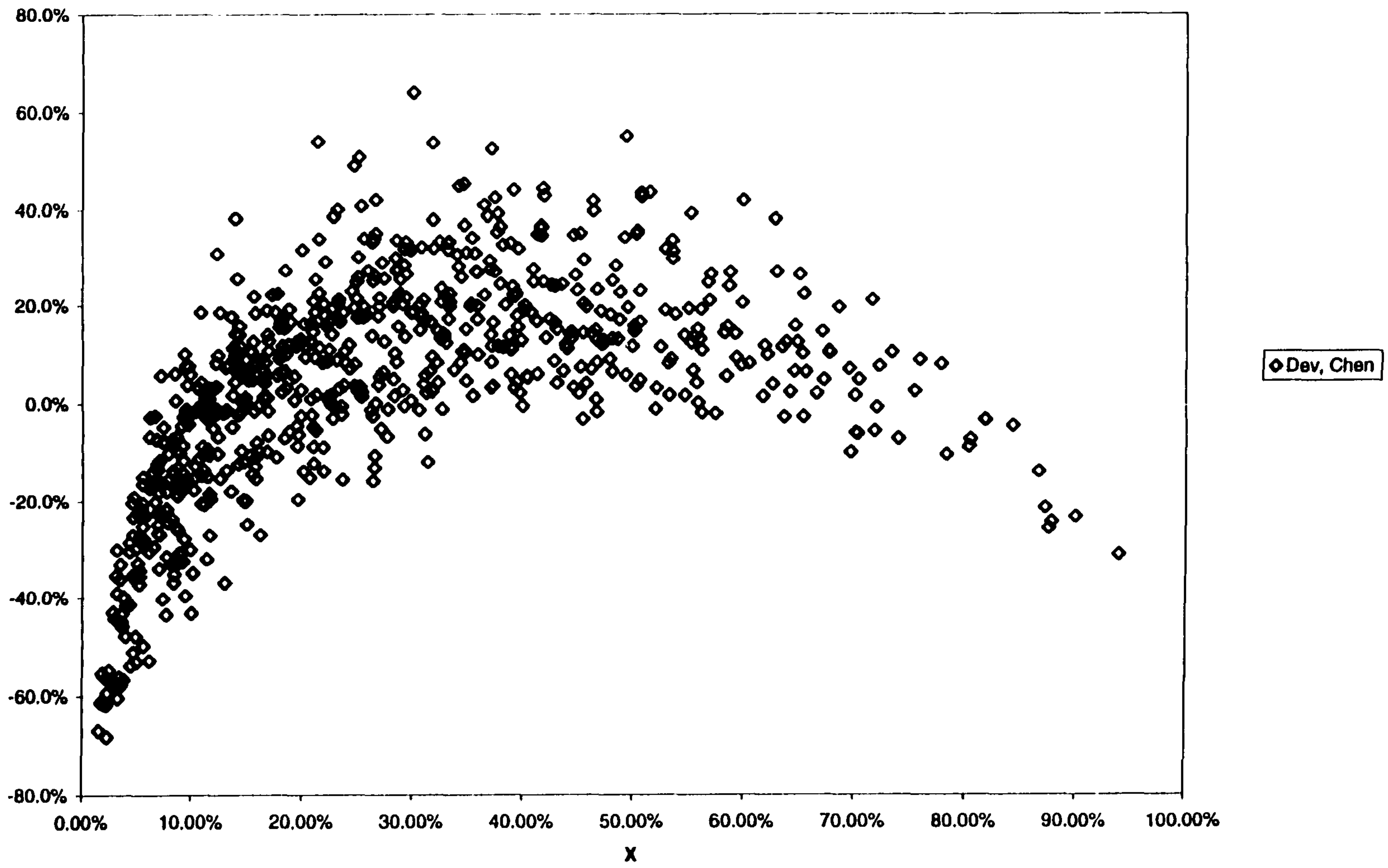

Figure C.12 Deviation of Chen Correlation against Quality

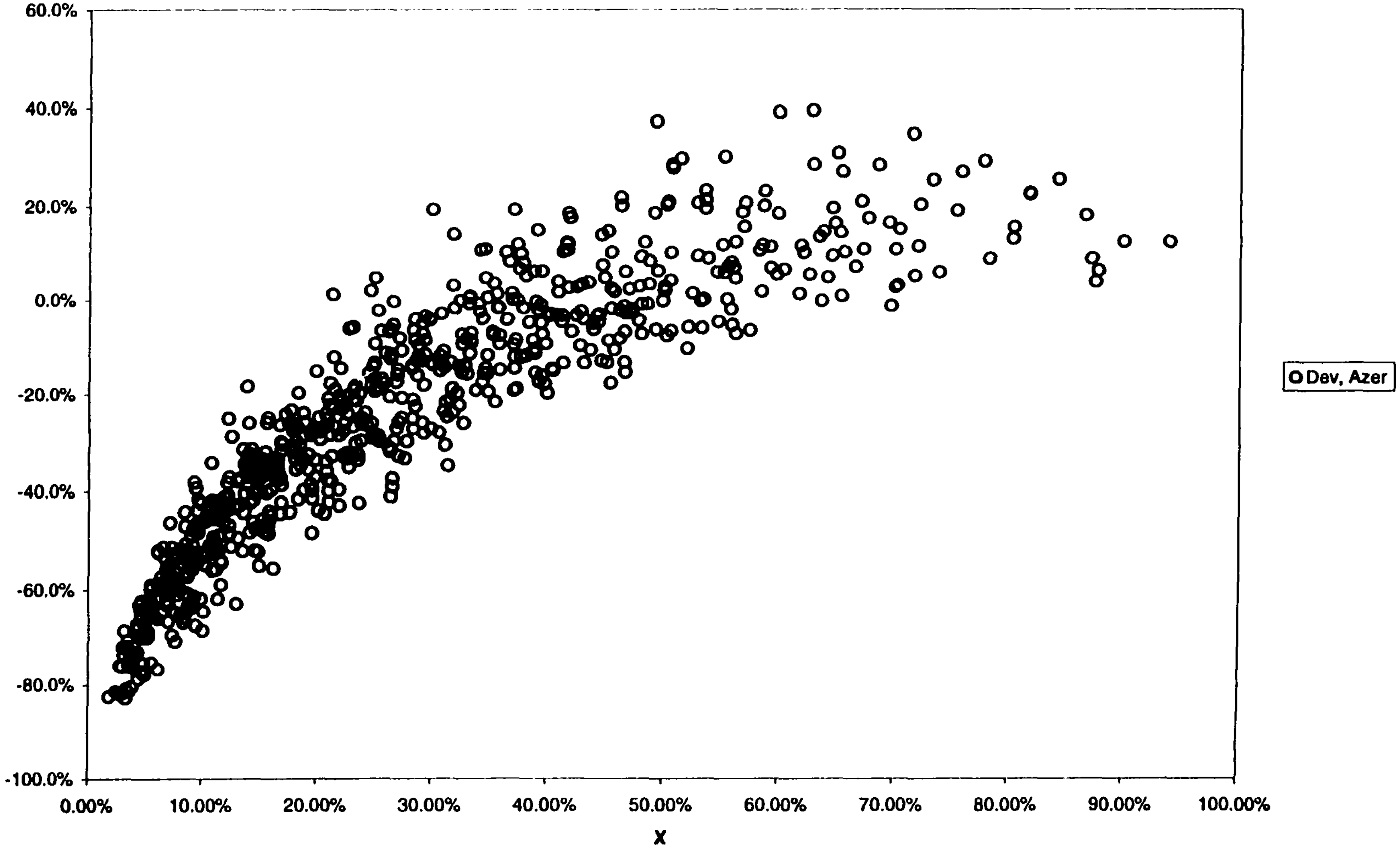

Figure C.13 Deviation of Azer Correlation against Quality

APPENDIX D

FLOW REGIME MAPS COMPARISONS

Condensation heat transfer is closely related to flow patterns while different condensation mechanisms take place. Predicting flow patterns correctly is the key to a satisfactory heat transfer correlation. Verifying various predicting flow maps from literature for the innovative microchannel tubing provided precious information for future applications without the expense of repeated flow visualization testing. Various maps including works from Mandhane [43], Taitel and Dukler [64], Breber [9] and Soliman [56], [57], [58] were evaluated.

D.1 Mandhane map

Based on superficial vapor and liquid velocities, the corresponding Mandhane map was plotted as Figure D.1 for various mass fluxes ranging from 55 klb/ft^{2}hr to 300 klb/ft^{2}hr. Most of data were predicted as slug flow patterns, and none were within the annular flow regime. In reality, annular flow did exist for high flux and high quality conditions. In other words, boundaries on the Mandhane map needed to be modified to be able to describe the real situation. The property differences between air and refrigerant may be accounted for the disagreement predicting the flow patterns of the refrigerants. Therefore, a modified superficial vapor velocity was introduced as,

$$j_{v,mod} = \sqrt{\frac{\rho_v}{\rho_{air}}} \cdot j_v$$

By using the new coordinate, a modified Mandhane map was plotted at Figure D.2. After conversion, agreement between prediction and observation was improved. Most data were predicted among the slug and annular flow regimes.

D.2 Taitel-Dukler map

The condensation data based on the Taitel-Dukler map are shown in Figure D.3. Almost all data were predicted among the annular regime. The absence of wavy and wavy-annular flows on the Taitel-Dukler map was caused by the small diameter of the microchannel. The parameter, F_{td}, predicting the transition between the wavy and annular or slug flow is proportional to $D_h^{-0.5}$; therefore, the transition happens at lower mass flux. In other words, the annular flow pattern occurs easier in compact tubing with a smaller diameter.

Figure D.4 is another way of presenting the Taitel-Dukler map, based on the quality and mass flux. Stratified and wavy flows are predicted at low mass fluxes across most of the quality range. Slug flow is shown at higher mass fluxes with qualities less than 16%. Flow with quality more than 16% is predicted as annular flow.

Because of terminology, the transition between wavy, slug and annular flow was not so clear and easy to define. The intermittent pattern described by Taitel and Dukler was a better terminology to describe the transition flow pattern, instead of defining it as slug flow or wavy-annular flow. In the literature, Nicholson et al. [43] used proto-slug flow, Barnea et al. [7] used wavy-annular flow, and Lin and Hanratty[39] used pseudo-slug to label the transition.

D.3 Breber map

Based on the dimension-less vapor velocity and Martinelli parameter, the prediction of the Breber map is shown in Figure 5.5. Modifying the Taitel and Dukler map, accounting for transitions between flow patterns and broadening the wavy region produced predictions on the Breber map that more clearly defined the flow pattern categories. Furthermore, the uncertainty of terminology as discussed in the previous section was reduced.

D.4 Soliman transitions

There were two transitions proposed by Soliman [54], [56], defining boundaries between wavy/slug flow and annular flow, and between annular and mist flow. As shown in Figure 5.6, based on the mass flux and quality, there was some agreement between the Soliman transitions and the observed transitions. The transition between wavy and annular flow at a quality higher than 30% was well predicted. For a quality less than 30%, the Soliman transition extended to higher mass flux regions where slug flow was identified on the Taitel-Dukler map, because both wavy and slug flow patterns were included in the same regime by Soliman. Unlike the Taitel-Dukler map, the Soliman transition between slug and annular flow is not fixed at a specified quality, which is closed to the observation. As the mass flux decreases, the boundary of the transition extends to higher quality, where wavy/slug-annular flow may persist.

There is also a transition between the mist and annular flow predicted on the Soliman map. The mist or spray flow is a regime where entrained droplets form a core flow with an unstable film along the wall. Based on the Soliman transition, no mist flow occurred at a mass flux less than 300 klb/ft^{2}hr. Neither should mist flow be seen at 550 klb/ft^{2}hr for a quality less than 45%. Because of the requirement of high mass flux and high quality, mist flow was not easily obtained or observed. The minute diameter of the microchannel tube is the reason attributed to the delay of mist flow. The liquid film on the wall was stabilized by the micro channel and sustained to higher quality and mass flux.

D.5 Conclusion of Flow Regime Observation

There were various flow patterns observed in the condensation of R-134a inside the microchannel tube. As the quality increased, the flow pattern changed from plug/slug to slug/wavy, then became wavy/annular, and finally annular. Both a transition prediction map and a flow regime map are developed from the observation of the microchannel tube.

To verify the flow regime visualization, four flow maps were cited. Because of the definition of flow pattern, terminology, and the subjectivity of visualized determination, both agreements and discrepancies were shown.

By accounting for the variation of vapor density between the refrigerant and air, the modified Mandhane map provided a good prediction of flow regimes. Only slug and annular flows were predicted on the Mandhane map. The small diameter of the microchannel tube was not accounted for in the prediction of the Mandhane map.

The Taitel-Dukler map included the diameter effect and provided a prediction similar to the Mandhane map. Because of the terminology, there is no transition between the wavy and annular flow on the Taitel-Dukler map.

By including transition zones, the Breber map provided more detailed predictions. The transition between the wavy and annular flow accounted for data with intermediate mass flux and high quality. Compared to the flow visualization results shown in Figure 5.5, the Breber's map predicted well for the wavy and slug flows. The annular flow occurs at 0.8 ft/s superficial vapor velocity, j_v^*, instead of 1.5 ft/s predicted by the Breber map.

The Soliman map included two transitions and was divided into three flow regimes: wavy/slug, annular, and mist flow pattern. Combined with slug, stratified and wavy flow, a broadening regime was predicted over the low mass flux or high mass flux with low quality. The surface tension over the micro-channel stabilized the annular-mist flow; therefore, the onset of the mist was extended to the high flux with high quality regions.

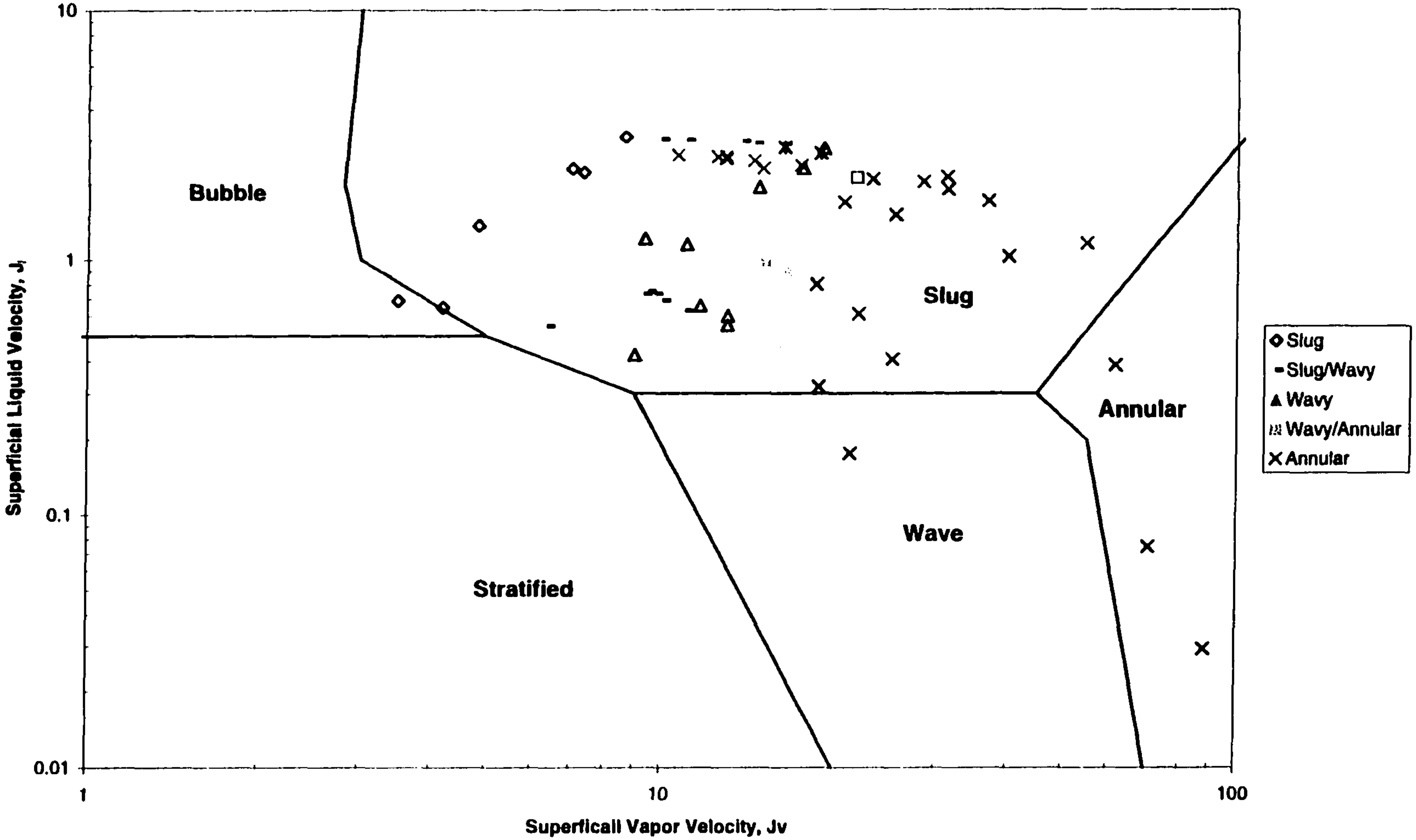

Figure D.1 Flow map based on the Mandhane map

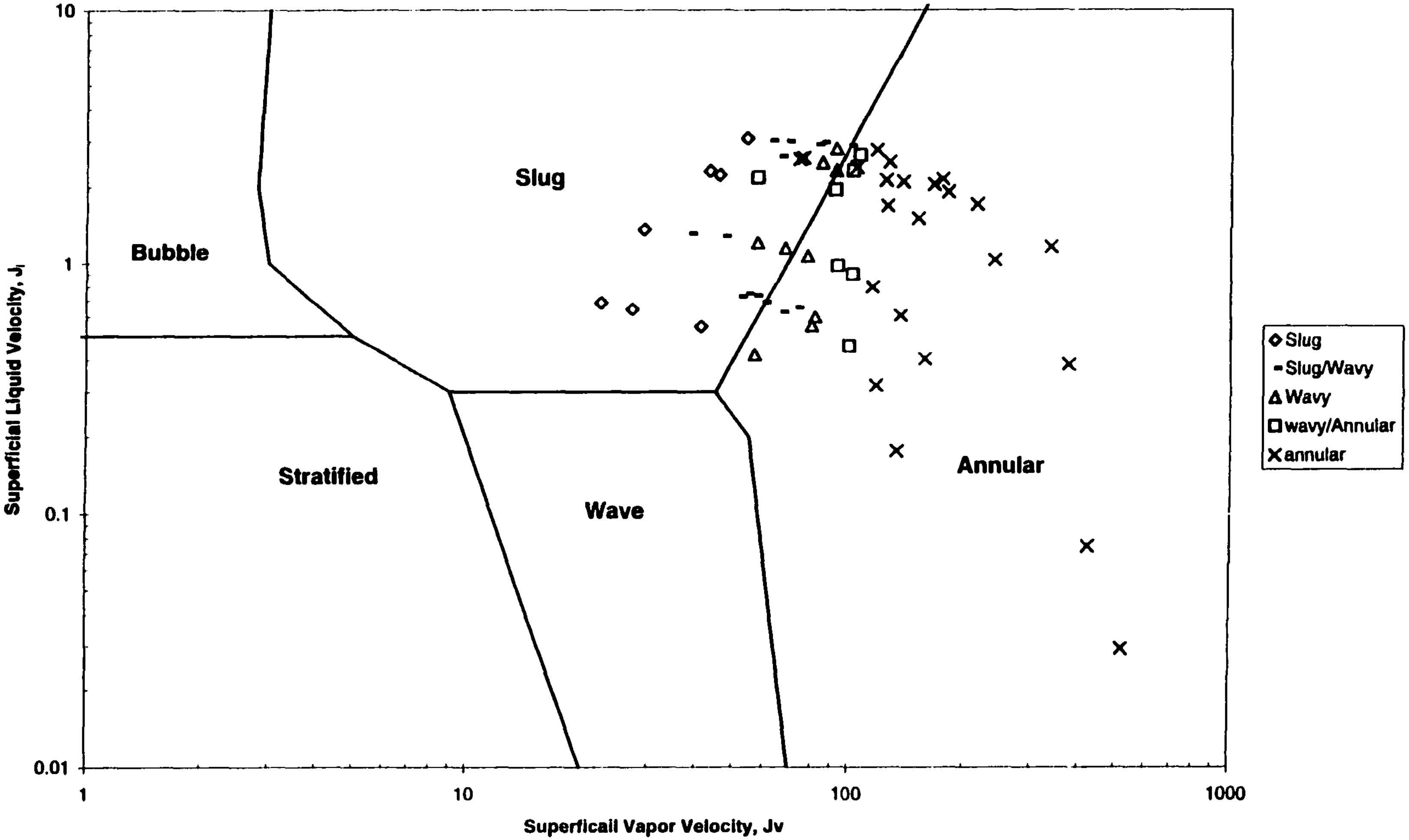

Figure D.2 Flow map based on the Modified Mandhane map

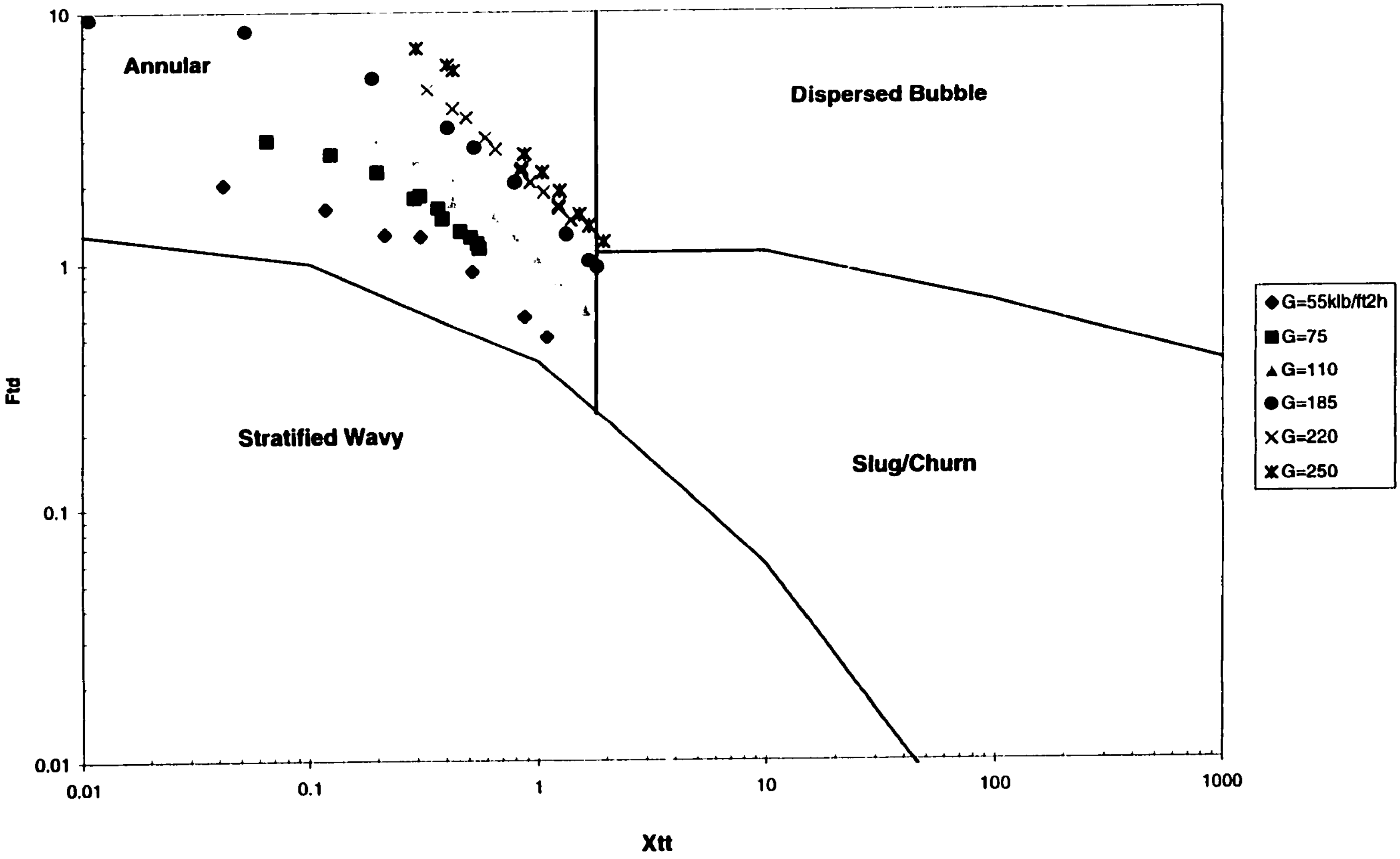

Figure D.3 Flow map based on the Taitel-Dukler map

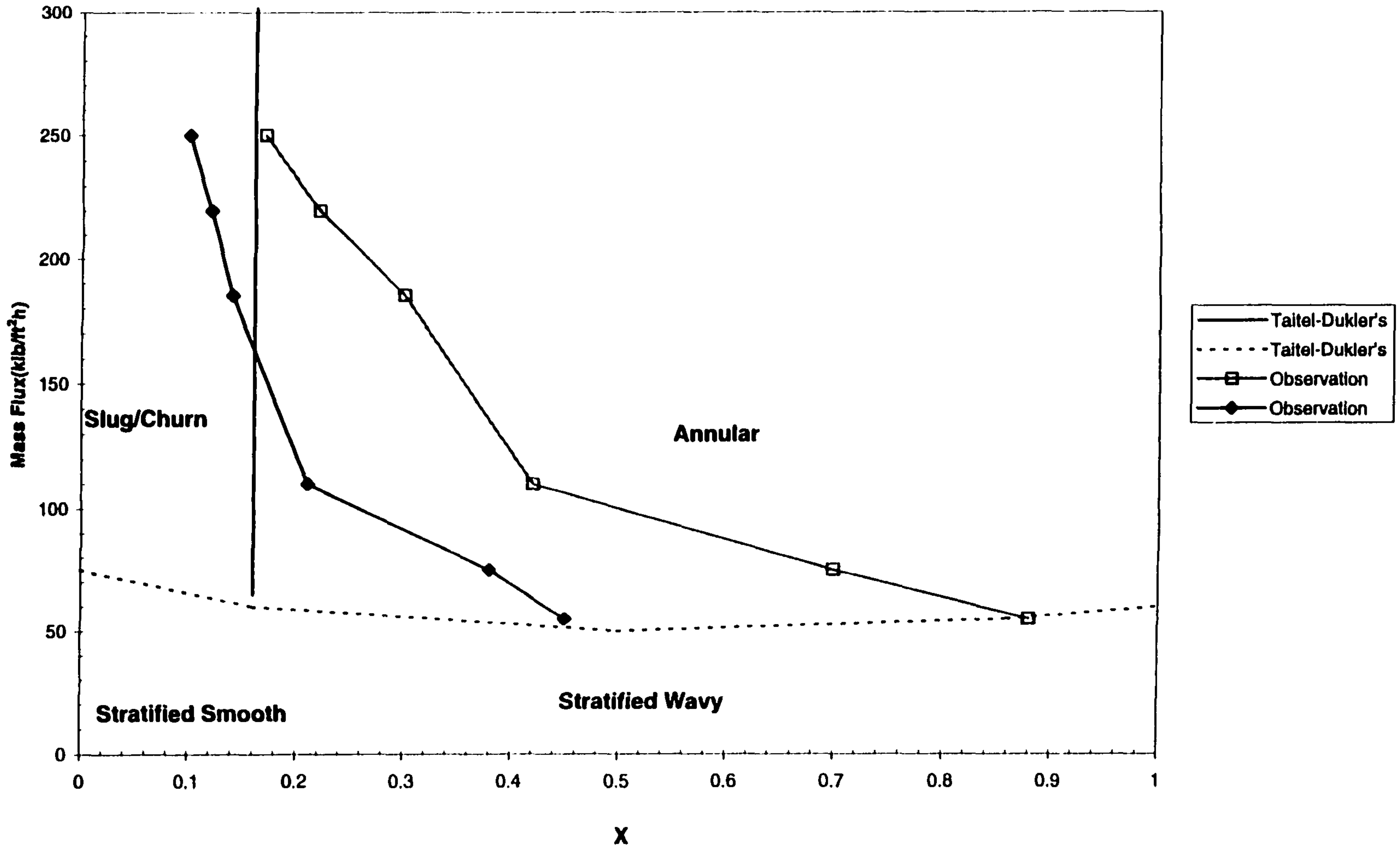

Figure D.4 Flow map based on the Taitel-Dukler map for mass flux vs. quality

Figure E.1 Slug/Plug flow patterns

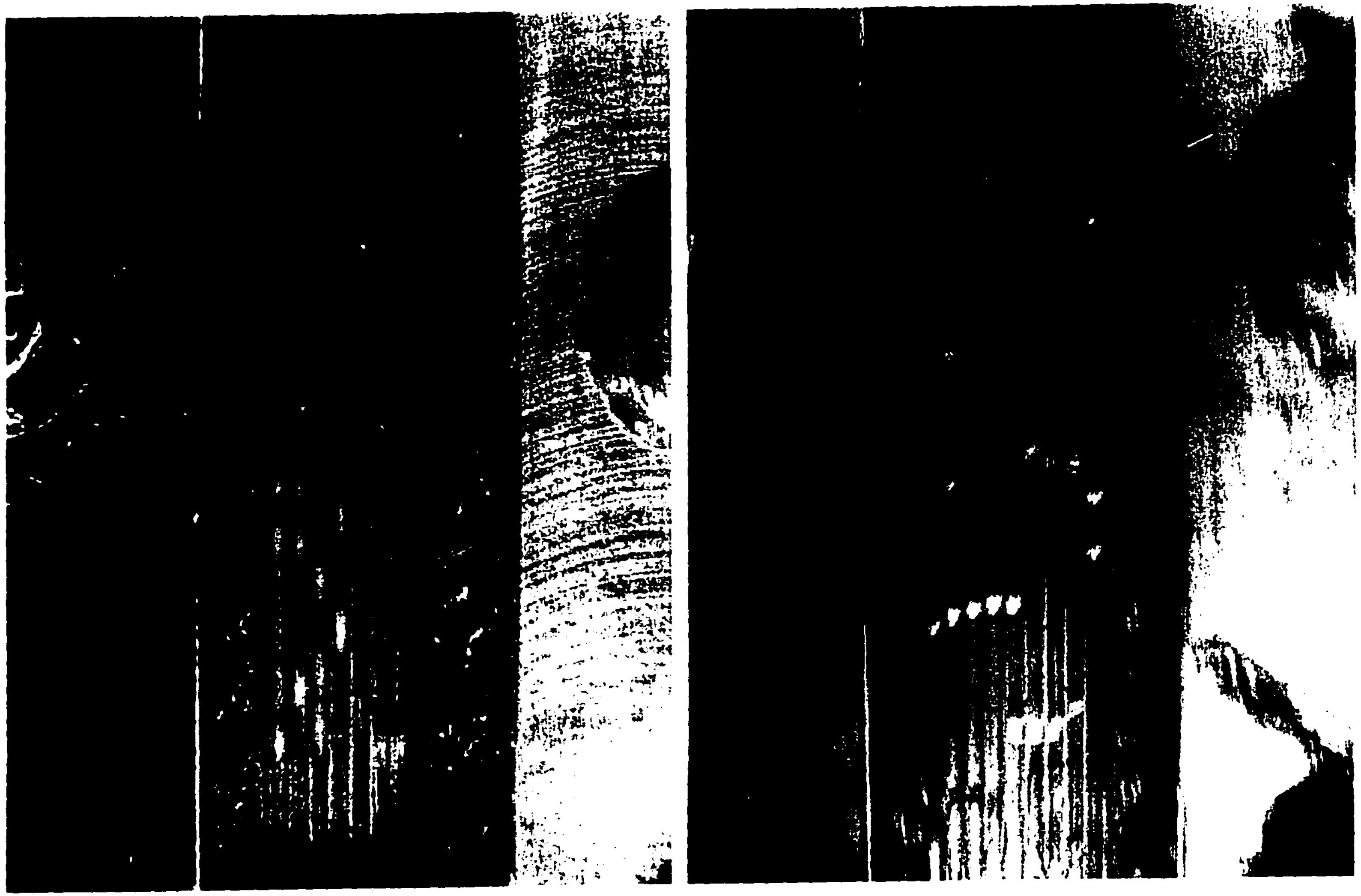

Figure E.2 Wavy/Slug flow patterns

Wavy/Slug flow patterns

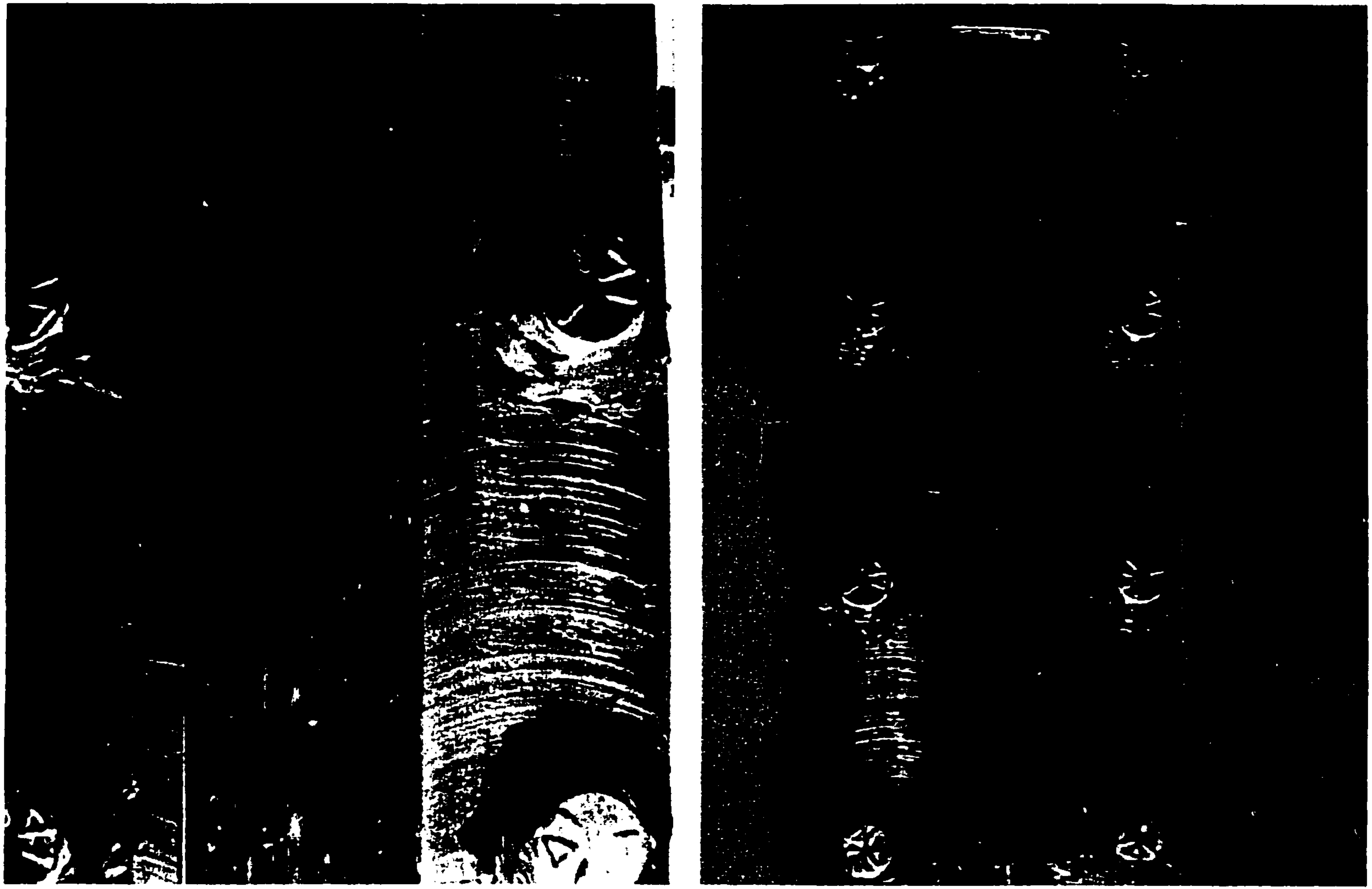

Figure E.3 Wavy/Annular flow patterns

Experiment apparatus of flow visualization

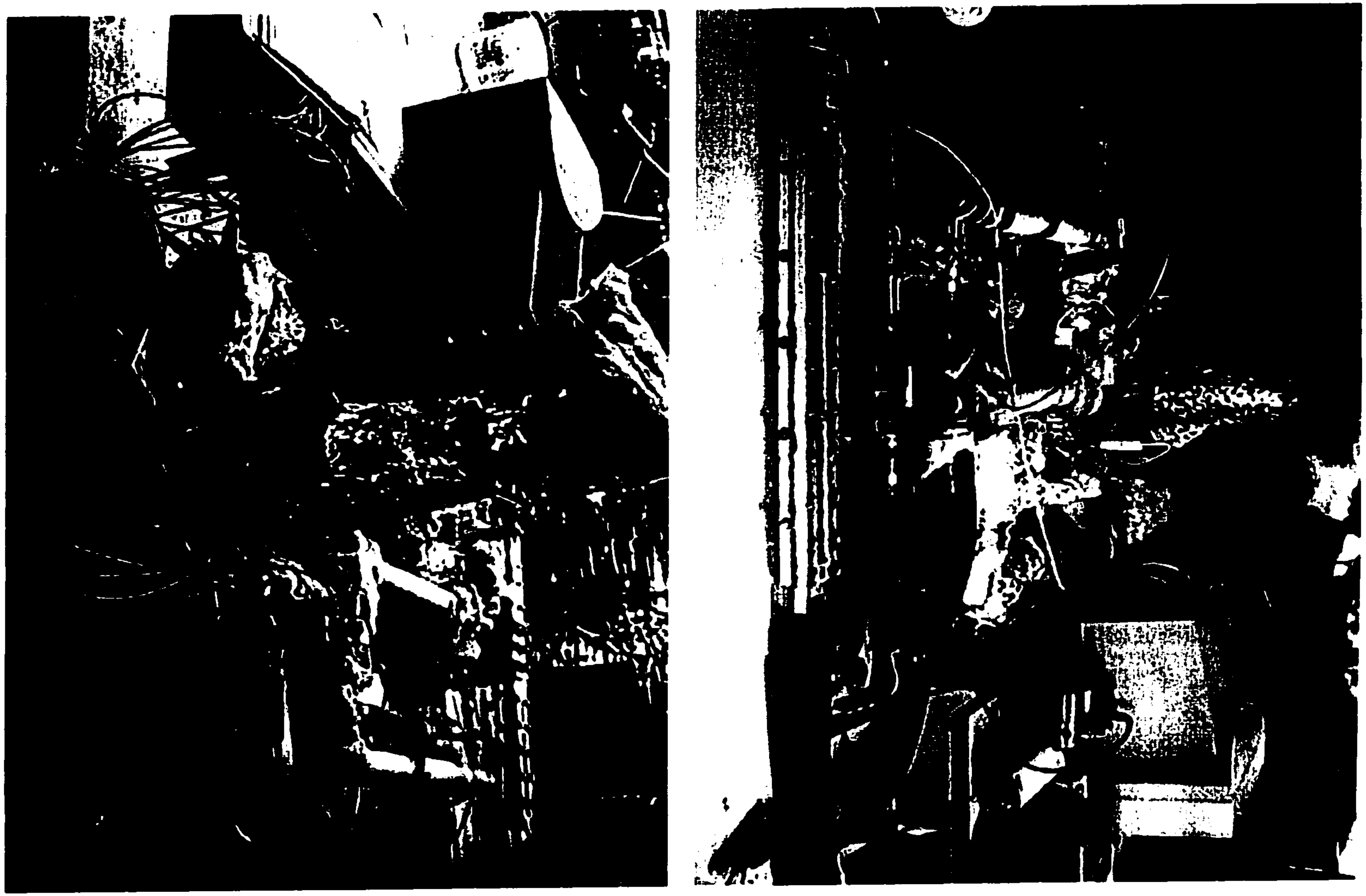

Figure E.4 Experiment apparatus of flow visualization